Analysis of Genetic and Protein interactions associated with mutant Huntingtin-induced degeneration.

A thesis submitted for the degree of Doctor of Philosophy

At

Cardiff University

School of Biosciences

Rachel Marie Spicer

September 2024

Acknowledgements

Firstly, I would like to thank the Biotechnology and Biological Sciences Research Council-funded SWBio DTP for funding the research project, and for supporting me throughout my PhD project. I would also like to extend my gratitude to my supervisors, Dr Michael Taylor, Professor Anne Rosser and Dr Mariah Lelos, for giving me the unprecedented opportunity of completing this PhD project with them. I am very grateful for the continued support, guidance and advice that you so generously gave me throughout the last four years.

I would also like to thank every member of the Brain Repair Group and the Cardiff Fly Group for all the love and support I've received during this time. In your own way, every one of you helped and guided me both in my research studies and personal life. A big thanks specifically to Dr Sophie Rowlands and Anne-Marie for your patience and love with every complaint and personal difficulty that you've had to endure hearing about. A special thanks to Masters students Laura Clark and Lucy Cowton, for your help in staining and analysing some of the experimental tissue.

I would also like to thank the members of Dr Michael Taylors' fly lab, in particular Rob Mitchell, and Cristina Newnes, for the daily Greggs Coffee runs, the pick me ups when experiments didn't work for the 10th time, and endless chats over hours of Fly flipping.

I also have to thank my wonderful family! To my Mum and Dad, Anna and David, who have supported me every step of the way, showing me how to keep faithful in God's plan; To my brother, Michael, and sister, Michaela, who always know how to make me laugh; To my second mother, Cathy, for being a continued rock of patience and love. To my in-laws, Keith and Katy, for the endless supply of coffee, and English language lessons; And to my wonderful Nan who I wish could be here today. I feel your love every day, and I'm so grateful for the years I got to spend with you.

And finally, to my wonderful Husband, without whom I probably wouldn't have made it. Tyler, your love and support through every high and low over the last four years has been incredible. Your unwavering support, patience, and smile got me to where I am today, and I am so grateful to God for you. Here's to our next chapter.

Thesis Summary

FoxP1 and *Mef2C* are two genes important for mouse striatal development, the brain region that is most vulnerable the effects of the mutated protein responsible for Huntington's Disease (HD), Huntingtin (HTT). Using *Drosophila* and mouse models of HD, I have investigated the effects of manipulating these two genes and showed that they can suppress mutant HTT (mHTT)-induced degeneration.

Prior to this project, studies had shown that a *Mef2* isoform, *Mef2D*, could physically interact with mHTT and that a chromosomal deficiency, which included the single *Drosophila Mef2* gene, could suppress whole-eye mHTT-induced degeneration. However, research had not investigated whether the *Mef2* gene was responsible for this observation, or how this might be translated to the human HD condition. Utilising the Gal4/UAS system, I showed that downregulating the *Drosophila Mef2* gene can suppress mHTT-induced degeneration in a whole-eye and pan-neuronal model of HD. I also showed that over-expressing the N-terminal fragment of *FoxP1* in a *Drosophila* HD model can suppress mHTT-induced degeneration.

I generated a novel mouse line which expressed that R6/1 transgene with striatal knockout of *Mef2C*, a concept that had not been investigated prior to this project. I showed that striatal *Mef2C knockout* in the R6/1 brain significantly reduces the number of mHTT inclusions in the striatum. These mice also performed better on the balance beam task.

Finally, using the Gal80^{ts}Gal4/UAS system, I show that pre-exposure of neurons to mHTT during development of the Drosophila eye leads to enhanced vulnerability and early cell death of photoreceptor neurons, which is not seen when inducing mHTT in the fully developed eye.

In this work, I utilised *Drosophila* HD models to further our understanding of the role of *Mef2C* and *FoxP1* in mHTT-induced degeneration and translated this research into a novel mouse model to investigate *Mef2C* downregulation in a complex mammalian model.

Abbreviations

AAV: adeno-associated virus

ASO: Antisense oligonucleotide

BAC: Bacterial artificial chromosome

BDNF: brain-derived neurotrophic factor

CC: Cone cell

CNS: Central nervous system

CTIP2: COUP-TF interacting protein 2

D1R: Dopamine D1 receptor

D2R: Dopamine D2 receptor

DARPP32: Dopamine and cyclic AMP-regulated phosphoprotein

FD: Forkhead domain

FoxP1: Forkhead box protein P1

GABA: Gamma-aminobutyric acid

GPe: Globus pallidus externus

GPi: Globus pallidus internus

GS1: Glutamine Synthetase 1

HD: Huntington's Disease

HJURP-C: Holliday junction recognition protein C-terminal

HTT: Huntingtin

IHC: Immunohistochemistry

iPSC: induced pluripotent stem cells

L3: 3rd instar Larvae

LGE: Lateral ganglionic eminence

lhRNA: Long hairpin RNA

LMC: Laminar monopolar cell

LZ: Leucine zipper domain

Mef2C: Myocyte enhancer factor 2

MF: Morphogenetic Furrow

mHTT: Mutant Huntingtin

MMR: DNA mismatch repair pathway

mRNA: Messenger ribonucleic acid

MSH2: MutS Homolog 2

MSN: Medium spiny neurons

NLS: Nuclear localisation site

O.D: Optical Density

PMS1: Postmeiotic segregation increased 1

PolQ: Polyglutamine

PPC: Primary pigment cell

PR: Photoreceptor

RNAi: Ribonucleic acid interference

shRNA: short-hairpin RNA

SNr: Substantia nigra pars reticulata

SPC: Secondary pigment cell

TAD: Transcriptional activation domain

TrkB: Tropomyosin receptor kinase B

UAS: Upstream activator sequence

WT: wild type

Y2H: Yeast-2-hybrid

ZF: Zinc finger domain

Table of Contents

Table of Figures

List of Tables

Chapter 1: General Introduction

1.1 Introduction

The focus of the work presented in this thesis is to explore whether two genes, FoxP1 and Mef2C, are implicated in the pathological process underlying Huntington's Disease (HD). HD is a condition caused by the presence of the mutant huntingtin (mHTT) protein, and experiments aim to determine whether manipulating these genes might impact mHTT-induced degeneration. Only a few therapeutic options, of limited benefit, are available to treat the symptoms associated with HD disease progression, and there is currently no disease-modifying treatment available. Understanding how these genes interact with the complex molecular pathways that are dysregulated in the HD brain may facilitate the development of more effective therapies.

Medium spiny neurons (MSNs) comprise 90-95% of all neurons in the striatum. It is degeneration of these MSNs that are the earliest and most prominent cells to degenerate in HD. A microarray analysis of mouse striatal development (over the period of peak striatal neurogenesis) undertaken in the host lab, identified Forkhead box protein P1 (FoxP1) and Myocyte enhancer factor C (Mef2C) to be highly up regulated during this period. Subsequent research has shown that both FoxP1 and Mef2C are involved in aspects of striatal development, the former of which, has been shown to be significantly reduced in the HD striatum (Hodges et al., 2006; Precious et al., 2016).

In this thesis, I have used Drosophila and mouse models of HD to investigate the effects of manipulating FoxP1 and Mef2C in mHTT-induced models of degeneration. Each model has a unique set of attributes that, when combined, can uncover novel gene associations and how manipulating them may be beneficial. In particular, Drosophila melanogaster are cost effective animals that have a rapid generation time and can be easily manipulated genetically (Tolwinski, 2017). Furthermore, 75% of genes implicated in human diseases have been identified to have functional homologs in the Drosophila genome (Rubin et al., 2000; Verheyen, 2022). However, these animals do not provide a complex biological system that is comparative

to the human body. Mouse models provide a step toward the complexity of a human and can therefore be used to enhance our understanding of the data derived from the Drosophila models.

1.2 Huntington's Disease

HD was discovered by George Huntington in 1872, who described a hereditary chorea, given the name due to the dancing propensities of those it affected (Bhattacharyya, 2016; McColgan & Tabrizi, 2018b). It wasn't until a century later, due to a collaborative international effort, involving the study of large families affected by the disease, that the genetic cause and location of the HTT gene was identified (Wexler et al., 2016; Wexler et al., 2004). Over the last 40 years, research has started to unravel the complex molecular pathways through which the presence of the mHTT protein leads to impaired function and cell loss (Jurcau, 2022). Whilst current disease management includes treating the symptoms associated with the disorder, there is no disease-modifying treatment to suppress or reverse disease progression.

1.2.1 Aetiology and Epidemiology

HD is a rare neurological disorder, with a reported global prevalence of 4.88 per 100,000 in 2022, having risen from 2.71 per 100,000 in 2010 (Medina et al., 2022). Characterised by progressive cognitive decline, motor impairment, and psychiatric symptoms, diagnosis is confirmed by the presence of an autosomal dominant mHTT protein (Jimenez-Sanchez et al., 2017). The toxic gain-of-function mHTT protein is encoded by a CAG polyglutamine (polyQ)-repeat expansion in the N-terminal first exon of the wild-type HTT gene on chromosome 4 (Jimenez-Sanchez et al., 2017; Tabrizi et al., 2022). Wild-type HTT alleles contain up to 35 CAG repeats, whereas HD carriers carry expansions of 36 repeats, or more, with an inverse correlation found between the length of CAG expansion and the age at symptom onset (Rubinsztein et al., 1996; Ruocco et al., 2006).

1.2.2 HD and striatal degeneration

The mHTT protein is ubiquitously expressed throughout the body, however the most vulnerable and prominent cells to degenerate are the inhibitory Gamma-aminobutyric acid (GABA)-ergic medium spiny neurons (MSNs) of the striatum (McColgan & Tabrizi, 2018a). The striatum is the main input structure of the basal ganglia and is involved in motor, cognitive and emotional control (Ali, 2022; Bamford & Bamford, 2019). The striatum integrates thalamic and neocortical glutamatergic inputs and midbrain dopaminergic inputs, in turn, sending

inhibitory GABA-ergic outputs to target nuclei. This facilitates its role in processing motor and cognitive-related function (Morigaki & Goto, 2017). The GABA-ergic MSNs account for ~90-95% of all striatal neurons and give rise to two distinct pathways: the direct and indirect pathway (Barry et al., 2018; Ehrlich, 2012). MSNs of the direct pathway express dopamine D1 receptors (D1R) and project their axons to the substantia nigra pars reticulata (SNr) and Globus pallidus internus (GBi) (Ehrlich, 2012; Peak et al., 2020) MSNs of the indirect pathway express dopamine D2 receptors (D2R) and project axons to the globus pallidus externus (GPe) (Barry et al., 2018). Electrophysiological studies using HD mouse models have shown that indirect pathway communication with the direct pathway in the HD brain is increased, and that reduced levels of BDNF (brain-derived neurotrophic factor), an important neuromodulator in the cortex, can induce neuronal degeneration of indirect-pathway striatal MSNs (Barry et al., 2018; Morigaki & Goto, 2017). Striatal degeneration and subsequently impaired cortical and basal ganglia circuits significantly contribute to the impaired cognitive and motor symptoms observed in HD patients (Blumenstock & Dudanova, 2020).

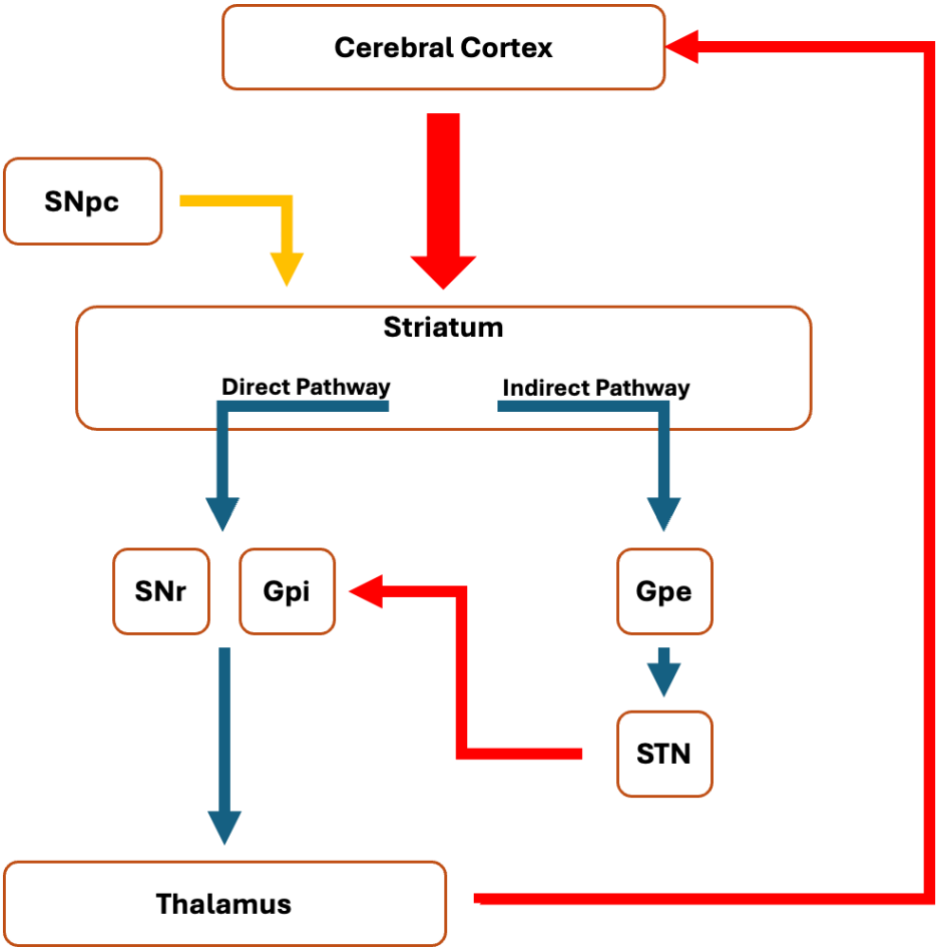

Figure 1.1 Schematic diagram of the direct and indirect pathways of the striatum.
Schematic diagram to show the direct and indirect pathways of the striatum. SNpc/SNr: Substantia Nigra pars compacta/reticulata, GPi/e: Globus pallidus internus/externus, STN: subthalamic nucleus. Red arrows represent excitatory glutamatergic neurons. Blue arrows represent inhibitory GABAergic neurons. Orange arrows represent dopaminergic neurons. Adapted from (Ali, 2022; Roshan et al., 2016).

1.2.3 Pathogenesis

The pathogenesis of HD involves the presence of a toxic gain-of-function mHTT protein and the loss of normal HTT function, which together, contribute to neurodegeneration (Jimenez-Sanchez et al., 2017). For decades, it has been known that the presence of the polyQ repeat expanded region contributes to abnormal folding and aggregate accumulation, leading to the subsequent impairment of a multitude of cellular processes and complex pathways. Most noteworthy is the presence of abnormal mHTT and aggregate formation in the brain which leads to significant neuronal loss and gliosis (McColgan & Tabrizi, 2018a). Increasing evidence indicates that the presence of the N-terminal fragment of the HTT protein, comprising only exon 1 of the protein, produces toxic nuclear aggregates (Landles et al., 2010; Sogorb-

Gonzalez et al., 2024; Vieweg et al., 2021). For example, a recent study showed that the first 17 amino acids of the HTT protein (Nt17) modulates the aggregation propensity of exon 1, and that removal of the Nt17 region can reduce inclusion formation (Vieweg et al., 2021). Additionally, researchers showed that disrupting the conformation of Nt17 in a HD cell model system could reduce the number of aggregates by 50% (Vieweg et al., 2021). Further investigations into the production of exon 1 aggregates has shown that alternative processing of HTT pre-mRNA (messenger ribonucleic acid) can lead to the production of an HTT1α transcript, subsequently encoding the exon 1 protein (Sathasivam et al., 2013; Sogorb-Gonzalez et al., 2024). N-terminal fragments are present in postmortem HD brain tissue, and the sole presence of the exon 1 fragment causes highly progressive pathological phenotypes in mouse and *Drosophila* model systems (Barbaro et al., 2015; Mangiarini et al., 1996). For example, the R6/2 mouse model has the earliest and most progressive phenotype onset and only expresses the human exon 1 HTT transgene (Ghosh et al., 2020; Mangiarini et al., 1996). Additionally, a comparative study of seven HTT fragments commonly used in *Drosophila* studies showed that the presence of exon 1 led to drastic degeneration of photoreceptor (PR) neurons, deficits in climbing and reduced longevity (Barbaro et al., 2015). These results were not replicated in *Drosophila* expressing larger proportions of the HTT protein (Barbaro et al., 2015). Overall, there is accumulating evidence that exon 1 of the HTT protein plays a role in HD pathogenesis, and studies in models with this fragment can recapitulate human disease pathology.

It should be noted that there are additional factors that contribute to the rate of HD pathogenesis. One such factor is that the polyQ region of HTT is subject to somatic expansion. (Monckton, 2021). Somatic expansion refers to the elongation of the polyQ domain of HTT in somatic tissues, such as the brain, often producing repeats of over 100, in contrast to other components such as blood, where polyQ expansion is less observed (Kacher et al., 2021). This discovery was made in 1993 and is thought to explain, at least in part, some of the variability of onset seen between patients (Gusella et al., 2014; Monckton, 2021). Studies of postmortem HD brains has shown that longer somatic expansions are associated with earlier symptom onset, and that disease progression may correlate more closely with CAG somatic expansion in patient blood as opposed to the size length of the polyQ that is encoded (Monckton, 2021). Studies using HD mouse models have shown that genes involved in the DNA mismatch repair

(MMR) pathway are pivotal to driving this somatic expansion (Roy et al., 2021). In 1997, Schweitzer and Livingston used yeast to study the instability of CAG repeats, and showed that CAG repeats were destabilised by mutations in MSH2 (MutS Homolog 2) and PMS1 (postmeiotic segregation increased) (Schweitzer & Livingston, 1997). Since then, several studies have shown that other genes involved in the DNA MMR pathway, such as MLH1 and MLH3 are genetic modifiers of CAG instability, and may drive somatic expansions (Loupe et al., 2020; Pinto et al., 2013; Roy et al., 2021). As a result, suppressing somatic expansion has become an attractive target for the development of new therapeutics. For example, splice redirection of the MLH3 gene to a protein isoform that does not include the endonuclease domain, was able to significantly reduce CAG expansion in a HdhQ111 mouse model of HD, and in patient-derived primary fibroblasts (Roy et al., 2021). Furthermore, treatment of patient-derived induced pluripotent stem cells (iPSC) with a single-stranded RNA interference (RNAi) antisense oligonucleotide to restrict MSH3 expression, could slow somatic expansion in a dose-dependent manner (Amartumur et al., 2024; Bunting et al., 2022)

One of the major pathogenic mechanisms associated with HD pathogenesis and loss of neurons are gene expression changes, including transcriptional dysregulation (Jimenez-Sanchez et al., 2017). Several studies have reported progressive gene expression changes in the human HD brain as well as in disease models of the disorder (Hodges et al., 2008; Hodges et al., 2006; Kaltenbach et al., 2007; Luthi-Carter et al., 2000; Seredenina & Luthi-Carter, 2012). For example, post-mortem studies have shown that levels of BDNF are reduced by 50-80% in the HD caudate and putamen compared with control brains (Ferrer et al., 2000; Speidell et al., 2023). Additionally, in vitro studies have shown that cells expressing mHTT secrete >50% less BDNF compared with cells that do not express mHTT (Zuccato et al., 2001). BDNF is required for the survival and differentiation of striatal neurons, and has been shown to protect MSNs from excitotoxin-induced degeneration (Canals et al., 2001). It is thought that the presence of mHTT disrupts the transcription of BDNF, subsequently impairing its transport to the striatum, and subsequent interaction with other genes, such as TrkB (Tropomyosin receptor kinase B) (Plinta et al., 2021; Zuccato et al., 2008). Mechanisms by which these gene expression changes occur may include sequestration of the protein by mHTT, and abnormal protein binding that perturbs the genes' function and downstream pathways (Tong et al.,

2024). Understanding these abnormal interactions has become a large focus of research in the field of HD.

1.2.3 Current research into disease-modifying treatments for HD

There are currently no disease-modifying therapies for the treatment of HD. However, there are several potential therapeutic approaches progressing through pre-clinical and clinical trials. One of the most promising strategies at present, is lowering the levels of HTT gene products, including the mHTT protein (Tabrizi et al., 2022). One such approach for lowering HTT is through the use of antisense oligonucleotides (ASO). ASOs are synthetic single-stranded oligodeoxynucleotides that can target pre-mRNA or mRNA, preventing the translation of mRNA to protein (Rinaldi & Wood, 2018). Tominersen was the first ASO administered to patients with HD, and targets exon 36 of the human HTT mRNA (McColgan et al., 2023). Binding of Tominersen to the mRNA results in degradation of the mutant and wild-type transcripts, by RNase H. Results from phase I/2a clinical trials showed dose-dependent reduction in mHTT levels, as measured in the cerebral spinal fluid (CSF) of HD patients (Kordasiewicz et al., 2012; McColgan et al., 2023). Following these promising results, a multinational phase 3 clinical trial began – GENERATION HD1, and although there were dose-dependent decreases of mHTT in the CSF, unfortunately dosing was halted due to the observation of severe adverse events, such as increased white blood cell count, indicative of an inflammatory reaction (McColgan et al., 2023; Tabrizi et al., 2022). GENERATION-HD2 is now underway and hopes to determine a safe and optimum dose for Tominersen in younger participants, who have lower disease burden and more resilient brains (Tabrizi et al., 2022). Another example is the clinical trial VO659-CT01, which involves intrathecal administration of VO659, an ASO that targets the RNA produced from CAG repeats in DNA (Estevez-Fraga et al., 2024). Studies have shown that VO659 can reduce levels of soluble mHTT and aggregates in the R6/2 and Q175 mouse models of HD. Additionally, VO659 increased mRNA levels of the striatal marker DARPP-32, and improved motor performance, compared with untreated HD mice (Datson et al., 2017). Phase 1/2a trials aim to recruit patients with SCA (Spinocerebellar ataxia) type 1 and SCA type 3, followed by the addition of a third, HD cohort. However, there is a lack of sensitivity against other CAG-repeat containing genes, so close monitoring is required (Estevez-Fraga et al., 2024).

Other therapeutic approaches include adeno-associated virus (AAV)-mediated micro-RNA (miRNA) therapies, such as AMT-130 (Tabrizi et al., 2022). AMT-130 is a miRNA that silences the human HTT gene. The molecule is delivered in an AAV5 plasmid, via stereotaxic infusion to the striatum and is currently in phase 1/2 clinical trials (Cheng et al., 2024). Animal studies have shown wide-spread distribution of the AAV5-miRNA in the minipig, with sustained huntingtin lowering in both the minipig and Hu128/21 HD mouse model, and improvements in motor coordination of the R6/2 mouse (Caron et al., 2020; Cheng et al., 2024; Evers et al., 2018). Together, these results indicate the potential for the translation of this therapy to the clinic. However, as with other huntingtin lowering therapies, it is important to consider that the wild-type HTT protein is likely affected in addition to the mutant protein. It remains unclear as to the impact that long-term suppression may have on the roles of wild-type HTT in HD patients, and the continued development of other therapeutic angles is important (Caron et al., 2020).

1.3 Modelling HD in research

The use of animals in research is an integral part of understanding the development and progression of human disease, whilst providing considerable insight into the effectiveness of therapeutic targets (Mukherjee et al., 2022). Mammalian models have been used frequently in biological research due to their anatomical and physiological similarities, and mammalian models can be affected by a number of diseases that are seen in humans. For example, 90% of drugs used in the veterinarian clinic are either identical or very similar to those used for the treatment of human conditions (Barré-Sinoussi & Montagutelli, 2015). In the context of HD, the pathological symptoms and molecular hallmarks of the disease, including cognitive an behavioural deficits and the presence of mHTT aggregates have been reproduced in mammalian and *Drosophila* HD models, and understanding the effectiveness of targeted therapeutics have been better understood using these models (Rana et al., 2024).

1.3.1 In vitro models of HD

In vitro approaches have been developed as a way of understanding the pathogenesis and aetiology of neurodegenerative diseases, including HD (Slanzi et al., 2020). The use of human

embryonic stem cells (hESCs) generated from embryos affected with HD have been utilised (Akimov et al., 2021). In recent years, patient-derived human iPSCs generated from adult somatic cells have become a powerful way of understanding mechanisms of cell degeneration in the human HD condition (Le Cann et al., 2021). Somatic cells can be reprogrammed using specific transcription factors to develop iPSC lines with the same genotype, and specific differentiations of these cells can yield models in multiple cell types that carry the mutated gene. These can then be used to investigate the effects of mHTT in these specific cell types (Akimov et al., 2021). For example, a recent study showed that dysfunction in a HD-iPSC line of microglia (with 109 CAG repeats) led to increased pro-inflammatory cytokine production in the absence of immune stimulation, and showed that mHTT expression in microglia function is cell-autonomous (Stöberl et al., 2023).

With major advances in technology, such as CRISPR gene editing and 3D bioprinting, the use of in vitro cell cultures provide promising tools for understanding gene function on a cell-by-cell basis (Zhao, 2023). However, these protocols are often complicated, and lead to variable cell phenotypes. Additionally, these cell cultures cannot recapitulate the authentic interactions between cells that would occur in a 3D biological system (Slanzi et al., 2020).

1.3.2 In vivo models of HD

1.3.2.1 Summary of in vivo models of HD

In vivo models overcome the limitations of cell cultures, providing a 3D system for exploring the underpinnings of human disease processes. These models also play a crucial role in understanding interactions of genes and associated proteins that may lead to the development of therapeutics (Dhapola et al., 2023). In vivo models of HD include simple whole systems such as Caenorhabditis elegans (C. elegans) and *Drosophila melanogaster,* as well as more complex mammalian models such as mice, rats, pigs, sheep, and the rhesus macaque (Ardan et al., 2019; Morton, 2018; Ramaswamy et al., 2007; Slanzi et al., 2020; Weiss et al., 2022). Simple models such as C. elegans provide a transparent, free-living, self-fertile whole system and are an attractive model for early identification of disease modifiers due to the ease of genetic manipulation (Chauhan et al., 2022; Van Pelt & Truttmann, 2020). Since the N-

terminal HTT protein (150 CAG repeats) was first expressed in the C. elegans in 1999, studies have shown that mHTT in C. elegans neurons and muscle cells leads to aggregation and cellular toxicity in a CAG repeat length-dependent manner and can be used to investigate disease pathogenesis (Faber et al., 1999; Lee et al., 2017; Wang et al., 2006). Furthermore, C. elegans have been used to identify potential neuroprotective effects that can be followed up with mammalian studies for therapeutic avenues. For example, in 2021, it was demonstrated that the up-regulation of the stress resistance modulator, DAF-16, is able to reduce polyQ-induced death of neurons (Cordeiro et al., 2022). However, C. elegans have a very simple anatomy and do not possess many vital mammalian organs and tissues, such as lungs, liver, and blood transport systems (Ha et al., 2022), so other complex animals should be considered alongside these to fully understand the complex nature of disease progression and the effect of disease modifiers in a biological system.

More complex mammalian models such as rodents and the rhesus macaque have been vital for enhancing our understanding of HTT-mediated disease pathology and the development of disease-modifying treatment (Weiss et al., 2022). Second to the mouse (which will be commented on in detail below), rat models are the most used species for laboratory studies (Hickman et al., 2016). Due to their larger brain size and reduced tissue damage upon surgical intervention, rats are often used in lesion and transplantation studies (Aggleton et al., 2010; Lelos et al., 2016; Torres & Dunnett, 2012). However, continued development of molecular technology has enabled the development of genetic rat models in an attempt to capture the heritable nature of HD (Ramaswamy et al., 2007). The first transgenic rat model of HD (TgHD) was generated in 2003, carrying the N-terminal HTT cDNA with 51 CAG repeats (von Hörsten et al., 2003). These rats developed adult-onset symptoms such as cognitive impairment and motor dysfunction from 10-months of age with the accumulation of mHTT inclusions and striatal shrinkage from 12-months of age (von Hörsten et al., 2003). Since then, optimisation of this line has included the generation of a congenic F344tgHD rat model that has been derived by crossing rats from the TgHD colony to rats of an F344 genetic background (Plank et al., 2018). A rat model expressing a bacterial artificial chromosome (BAC) containing the full-length HTT sequence with 97 CAG repeats has also been established (Nittari et al., 2023; Yu-Taeger et al., 2012).

Other animal models such as the pig and sheep, have larger brains and are longer-lived, making them a potentially desirable model for pre-clinical testing (Morton, 2018). The developmental pattern of the basal ganglia and cortex in sheep is similar to the pattern seen in the human brain (Jacobsen et al., 2010). As a result, the OVT73 transgenic sheep expressing the full-length human HTT cDNA with 73 CAG repeats, was generated (Jacobsen et al., 2010). This model has been used to investigate the most effective AAV serotypes for neuronal uptake and distribution of miRNAs, as well as the safe AAV-mediated administration of human HTT miRNA in large brain models (Mondo et al., 2018; Pfister et al., 2018). Other large animals such as the Libechov transgenic minipig model of HD which contains the N-terminal human HTT fragment and 124 CAG/CAA repeats, have proven useful models for pre-clinical testing of human HTT-lowering therapies (Ardan et al., 2019). For example, following initial studies in mice, an AAV5-miHTT ASO was tested in the minipig model, and showed widespread distribution as well as mHTT lowering, supporting the translation of this therapy to the clinic (Evers et al., 2018; Southwell et al., 2017). These studies are also extended into rhesus macaques and may be used for developing disease biomarkers and the screening of future therapeutics (Weiss et al., 2022).

1.3.2.2 Drosophila models of HD

For over a century, *Drosophila melanogaster* have been used to define gene roles in biological processes and disease progression (Jennings, 2011). Their low cost and ability to be manipulated via many genetic tools, has made the *Drosophila* a prime model system for basic research (Tolwinski, 2017). Additionally, with a life cycle from embryo to adult of as little as 10 days, which can be influenced slightly by temperature changes, and a lifespan of 60-80 days, *Drosophila* are an effective model for obtaining quick and accurate results (Fernández-Moreno et al., 2007) (Figure 1.2). In 1995, Christiane Nusslein-Volhard, Ed Lewis and Eric Wieschaus won the Nobel Prize for their research in understanding genetic control of embryonic development using the *Drosophila*, and since then, many of these genes have been identified to play pivotal roles in mammalian development (Jennings, 2011). Furthermore, 75% of genes implicated in human disease have been identified to have functional homologs in the *Drosophila* genome (Rubin et al., 2000; Verheyen, 2022). One of the advantages of using

simpler in vivo models such as *Drosophila* is the ability to focus on identifying new gene and protein interactions and/or functions, that may provide insight into underlying molecular mechanisms in disease processes. For example, research using *Drosophila* models of Parkinson's' Disease (PD) uncovered p21-activated kinase 4 as a novel gene implicated in the progression of PD. Further research using *Drosophila* found that the *Drosophila* homolog, Mushroom bodies tiny was required to prevent age-dependent loss of locomotor activity via its presence in dopamine neurons (Pütz et al., 2021; Verheyen, 2022).

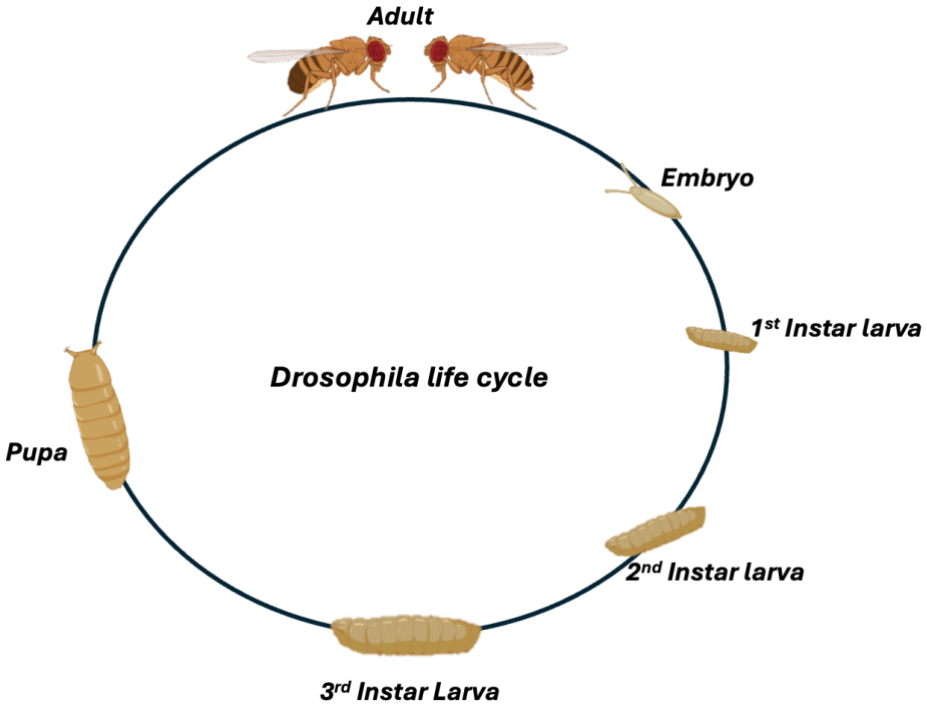

Figure 1.2 Diagram to show the life cycle of a Drosophila.
Schematic diagram to show the lifecycle of *Drosophila melanogaster* from embryo to adult. Adapted from (Fernández-Moreno et al., 2007).

Since the *Drosophila* HTT protein does not have an expanded CAG repeat region like that which is responsible for HD, many *Drosophila* models of HD transgenically introduce a mutant human gene (Bolus et al., 2020). For the majority of research conducted using *Drosophila*, studies either express fragments of the gene such as exon 1 only, or encode the entire protein, with various CAG repeat lengths (Babcock & Ganetzky, 2015; Kaltenbach et al., 2007; Kazantsev et al., 2002; O'Rourke et al., 2013; Steffan et al., 2001; Zhang et al., 2010). Table 1.1 outlines different constructs for expressing mHTT in *Drosophila*. These mHTT fragments are

expressed in a tissue-specific pattern using the Gal4-UAS system and display motor deficits, reduced fly survival, and neurodegeneration as measured by loss of compound eye structure and loss of rhabdomeres of the eye (Marsh et al., 2003; Raamsdonk et al., 2005). In the Gal4/UAS system, genes are fused to an upstream activator sequence (UAS) and integrated into the *Drosophila* genome via injection into embryos. This produces a transgenic line carrying a UAS>transgene (Marsh et al., 2003). 'Driver lines' contain the GAL4 protein that can be placed under the control of a specific promoter to drive tissue-specific expression (Sonnenfeld, 2009). By crossing 'driver lines' to transgenic lines, the GAL4 protein binds to the 17 base-pair UAS, driving tissue-specific expression of the transgene. This thesis uses mHTT models containing the N-terminal exon 1 fragment with 93 and 120 CAG repeats.

In the context of HD, *Drosophila* research tends to use the whole-eye driver, GMR-Gal4 to investigate mHTT-induced whole eye degeneration, or the pan-neuronal driver Elav^{c155}Gal4, to quantify loss of rhabdomeres of the eye (Lobato et al., 2024; O'Rourke et al., 2013; Steffan et al., 2001; Zhang et al., 2010). Using GMR-Gal4, research has shown that whole-eye induction of mHTT leads to retinal shortening and detachment, the presence of large vacuoles in the retina, cell loss and reduced pigmentation (Kaltenbach et al., 2007; Rai & Tapadia, 2022; Vernizzi et al., 2020). Since the GMR-Gal4 driver induces expression of mHTT in all cells of the eye, a pan-neuronal driver can be used to exclusively express mHTT in the neurons. Pan-neuronal expression of mHTT using Elav^{c155}Gal4 leads to progressive neuronal degeneration, decline in motor performance and premature death (Marsh & Thompson, 2004; Song et al., 2013). Additionally, neurotoxicity of mHTT leads to loss of PR neurons which can be quantified by counting the number of 'intact' rhabdomeres that autofluoresce when eyes are visualised under a light microscope (Song et al., 2013) (Figure 1.3).

Table 1.1 Table outlining mHTT constructs used to study HD in *Drosophila*

Fly Model	CAG repeat length	Huntingtin fragment	Observations (Gal4 driver)	References
HttQ128	128	First 12 exons of the human HTT gene.	Presence of HTT aggregates in CNS axons and photoreceptor growth cones (GMR-Gal4).	(Krench & Littleton, 2013)
128Qhtt^{FL}	128	Full length human HTT	Cytoplasmic aggregate accumulation (GMR-Gal4). No diffuse axonal aggregates, loss of rhabdomeres at 20 days, severe flight impairment at 25 days, abnormal motor behaviour, premature death (Elav-Gal4). Reduced lifespan and locomotor deficits (C164-Gal4).	(Lewis & Smith, 2016; Romero et al., 2008)
128Qhtt$^{1-548}$	128	N-terminal human HTT (1-548 amino acids)	Large huntingtin and synaptotagmin I axonal aggregates (Elav-Gal4).	(Romero et al., 2008)
HttQ93^{ex1}	93	N-terminal exon 1 human HTT	Accumulation of organelles and proteins across the axon, neuronal apoptosis (d42-Gal4). locomotion deficits in larvae, loss of rhabdomeres, loss of ability in the climbing assay, 70% lethality, premature death (Elav-Gal4). Loss of α' and β' lobes of the mushroom body, reduced Kenyon cell number (OK107-Gal4).	(Agrawal et al., 2005; Krench & Littleton, 2013; Marsh et al., 2003; Sinadinos et al., 2009)
HttQ200	200	Full-length human HTT	Progressive locomotor decline in adult flies (Elav-Gal4).	(Rosas-Arellano et al., 2018)
HttQ120^{ex1}	120	N-terminal exon 1 human HTT	Progressive degeneration of rhabdomeres (Elav-Gal4). Progressive degeneration of the eye (GMR-Gal4	(Jackson et al., 1998; Lewis & Smith, 2016; Shiraishi et al., 2014)
Htt 103Q	103	Full-length human HTT	Normal glial morphology, reduced lifespan, abnormal motor activities (Repo-Gal4). Reduced eclosion rate, reduced lifespan (gcm-Gal4). Reduced climbing ability (Cha-Gal4).	(Shiraishi et al., 2014; Tamura et al., 2009)

GMR-hHTTex1.Q120	120	N-terminal exon 1 human HTT under the GMR eye promoter	Retinal degeneration, reduced phototaxis performance, severe photoreceptor degeneration.	(Jackson et al., 1998; Louis Sam Titus et al., 2017)

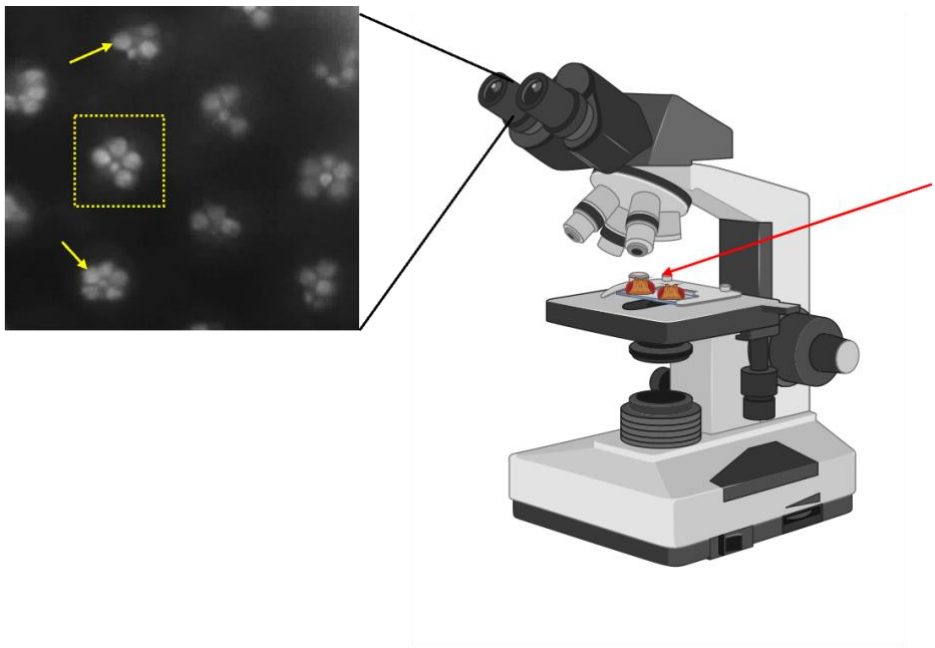

Figure 1.3 Image to show method for rhabdomere quantification.
Fly heads were mounted in parallel with a microscope slide, using clear nail varnish (red arrow). Oil was added to the fly eye and stage moved towards a 40X magnification objective. Concentrated light through a condenser allowed rhabdomeres to be visualised and quantified in real time. Each cluster of rhabdomeres (yellow arrow) made up one ommatidium (yellow dashed box).

Drosophila models of HD have also been used to investigate genes associated with disease progression and potential therapeutics. For example, Glutamine Synthetase-1 (GS1) has been shown to be reduced in the post-mortem brain of HD patients (Behrens et al., 2002). A *Drosophila* model of HD expressing the human HTT gene with 93 CAG repeats (Htt-Q93), was used to investigate the contribution of GS1 in HD. Research showed that co-expression of GS1 with human HTT with 93 CAG repeats in the neurons could significantly rescue neuronal loss and improve animal motility (Vernizzi et al., 2020). Another study used human HTT exon 1 with 72 CAG repeats (Htt-Q72) to investigate its effects on peripheral function (Roth et al., 2023). Pan-neuronal expression of Htt-Q72 led to age-dependent aggregation of mHTT in the brain, and loss of synapsin, which was reduced using the Target of Rapamycin signalling pathway inhibitor, Rapamycin (Roth et al., 2023). *Drosophila* models of HD are an effective system for identifying genetic interactions that may modulate disease progression and identify possible treatment pathways. However, the major limitation of these models are the large physiological and biological differences compared with humans.

1.3.2.3 Mouse models of HD

Over recent years, rodents have been the most commonly used models for answering biological questions associated with disease progression (Ramaswamy et al., 2007). Logistically, rodents can be used in research due to their short gestation and relatively large litters, and the relatively small space required for their maintenance (Bryda, 2013). Genetic studies have shown that rats, mice and humans share approximately 95% of the 30,000 genes throughout the genome (Bryda, 2013), and as a result, provide an opportunity to use these models for research. Additionally, genetic tools have been used to create transgenic, knock-in and knock-out models that can contribute to the understanding of human biology and disease (Perlman, 2016).

The R6 transgenic mouse models were the first mutant lines to model HD (Brooks, Jones, et al., 2012; Mangiarini et al., 1996). These models were generated to address the large differences in cell death that were found to occur in diseases that all have CAG mutations, including HD, SCA1, and Spinal and bulbar atrophy (SBMA). The R6/1 and R6/2 transgenic mouse lines express the 1.9kb human N-terminal HTT exon 1 fragment with a CAG repeat length of roughly 115 and 150, respectively (Mangiarini et al., 1996; Naver, Stub, Moller, et al., 2003; Zhiqiang Zheng & Marc I. Diamond, 2012). Unexpectedly, it was found that the N-terminal fragment of HTT was sufficient to generate the progressive phenotype, observed in the human HD disorder, including molecular, motor and behavioural disturbances (Mangiarini et al., 1996; Naver, Stub, Møller, et al., 2003).

The knock-in HD mouse lines are considered more genetically accurate in that these mice exhibit copies of the HTT gene that are under the control of the mouse HTT promoter (Ramaswamy et al., 2007). The mutation is inserted directly into the mouse genome, and can be homozygous or heterozygous (Menalled, 2005). These knock-in lines have anything between 40 and 200 CAG repeats and show an inverse correlation between repeat length and symptom onset, as is seen in the human condition. This makes them a useful tool for evaluating how potential treatments can delay the onset of early abnormalities (Menalled, 2005). Table 1.2 outlines knock-in and transgenic models of HD that are used in research,

including their CAG repeat length, age of behavioural phenotype as well as cellular and molecular manifestations (Table 1.2).

Table 1.2. Table outlining different transgenic and knock-in models used to study HD.

Mouse model	Knock-in or Transgenic	CAG repeat length	Construct	Behavioural Phenotype (earliest reported age of onset)	Pathology (earliest reported age of onset)	References.
R6/1	Transgenic	115	Exon 1 HTT containing genomic fragment	Impulsive-behaviour (4-weeks), deficits in balance beam and rotarod (8-weeks), sniffling and rearing (26-weeks), anxiety-like phenotype (26-weeks).	Presence of mHTT inclusions (8-weeks), abnormal axonal connectivity (11-weeks), increased presence of astrocytes and glia (11-weeks), reduced MSN number (16-weeks), reduced BDNF expression (20-weeks), reduced whole-brain volume (30-weeks).	(Angeles-López et al., 2021; Bolivar et al., 2004; Brooks, Janghra, et al., 2012; Clifford et al., 2002; Desplats et al., 2006; Gatto et al., 2021; Hodges et al., 2008; Naver, Stub, Moller, et al., 2003)
R6/2	Transgenic	150	Exon 1 HTT containing genomic fragment	Dyskinesia in the limbs (4-weeks), deficits in balance beam (5-weeks), deficits in swimming (5-weeks), deficits in rotarod (6-weeks), altered walking pattern (9-weeks), reduced whisker movements (18-weeks). Early death (10-15 weeks).	Decreased soluble HTT protein (4-weeks), presence of mHTT aggregates (4-weeks), abnormal neuronal morphology (6-weeks), decreased brain volume (10-weeks), significant loss and shrinkage of striatal neurons (12-weels).	(Cowin et al., 2011; Gourfinkel-An et al., 2003; Klapstein et al., 2001; Mangiarini et al., 1996; Nittari et al., 2023; Rossignol et al., 2015)
N171-82Q	Transgenic	82	The first 181 amino acids of human HTT	Hypokinesia and coordination deficits (10-weeks), gait deficits (10-weeks), resting tremor, and abnormal hind-limb clasping (11-weeks), early death (6-months).	Wide-spread mHTT inclusions (3-months), increased striatal cell volume (4-months), gliosis (4-months), apoptotic neuronal degeneration in the cortex and striatum (4.5-months).	(Farshim & Bates, 2018; Harper et al., 2005; William Yang & Gray, 2011)
N586-82Q	Transgenic	82	N-terminal mHTT fragment	Moderate rotarod deficits (3-months), abnormal gait (4-months), dyskinesia (8-months)	Cytoplasmic inclusions and cerebellar degeneration (8-months).	(Nittari et al., 2023; Tebbenkamp et al., 2011)

YAC 128	Transgenic	125	Full length human HTT, duplicated 4 times.	Hyperactivity (3-months), motor deficits (3-months), deficits on rotarod (6-months), deficits on rotarod (6-months), hypoactivity (12-months).	Decreased striatal volume (9-months), reduced MSN cell number (9-months), decreased cortical volume (12-months), nuclear aggregates (12-months), presence of inclusions (18-months)	(Nittari et al., 2023; Slow et al., 2003)
BACHD	Transgenic	97	Human HTT exon 1	Decreased rotarod performance (2-months), weight gain (2-6 months), deficits in forced swim test (4-months), open field deficits (6-months), anxiety-like phenotypes (6-months).	Presence of mHTT aggregates (6-months), educed cortical and striatal volume (12-months), presence of nuclear inclusions (12-months),	(Gray et al., 2008; Nittari et al., 2023; William Yang & Gray, 2011)
BAC225Q	Transgenic	225	Full length human HTT	Reduced body weight (1-months), chorea-like movements (12-weeks), circling behaviour (14-weeks), deficits in balance and coordination (4-months).	Presence of mHTT inclusions (4-months), 31% reduction in striatal volume (11-months). Reduced MSN count (11-months), 80% increase in reactive gliosis (11-months)	(Nittari et al., 2023; Shenoy et al., 2022)
HdhQ111/+	Knock-in	111	Chimeric human exon 1/mouse exon 1	Deficits on rotarod (6-months), deficits on balance beam (9-months), decreased locomotion (40-weeks), abnormal gait (46-weeks), reduced body weight (11-months),	Reduced striatal volume (10-months), reduced cortical thickness (10-months), decreased intensity of DARPP-32 immunostaining (18-months), reduced synapse density (18-months).	(Hölter et al., 2013; Kovalenko et al., 2018; Yhnell et al., 2016)
CAGQ140	Knock-in	146	Chimeric human exon 1/mouse exon 1	Decreased rearing (1-month), increased locomotor activity (1-month), decreased locomotor activity (4-months), abnormal gait (12-months).	Presence of mHTT aggregates in the striatum and cortex (4-months), Widespread neuropil aggregates (4-months).	(Menalled et al., 2003)

HdhQ150 (CHL2)	Knock-in	150	Expanded CAG in exon 1 of mouse HTT	Abnormal gait (40-weeks), rotarod deficits (40-weeks), reduced hind-limb drag (50-weeks), exploratory behaviour (70-weeks), deficits on balance beam (70-weeks), clasping behaviour (70-weeks).	Presence of mHTT aggregates in the striatum (5-months), increased GFAP staining (21-months), reduced dopamine transported binding (100-weeks), reduced neuronal count (100-weeks), reduced striatal volume (100-weeks),	(Bayram-Weston et al., 2012; Farshim & Bates, 2018; Heng et al., 2007; William Yang & Gray, 2011)
zQ175	Knock-in	198	Chimeric human exon 1/mouse exon 1	Reduced muscle strength (4-weeks), decreased movement and rearing (8-weeks), rotarod deficits (30-weeks), body tremor and lower body temperature (33-weeks), decreased climbing activity (33-weeks), deficits on swim tasks (58-weeks), abnormal gait and hunching (93-weeks), early death (104-weeks).	Reduced mRNA expression of DARPP32, Drd2, Cnr1, and PDE10a (41 weeks).	(Farshim & Bates, 2018; Koch et al., 2024; Menalled et al., 2012; Nittari et al., 2023)

The mouse experiments conducted in this thesis use the R6/1 transgenic mouse line. R6/1 mice exhibit a rapidly progressive neurological phenotype with symptoms appearing from ~5 weeks of age (Zhiqiang Zheng & Marc I. Diamond, 2012). Due to the slower progression of the R6/1 compared with the R6/2 mouse, and the longer lifespan, it is considered a more suitable model for investigating the potential long-term effects of new treatments. Behaviourally, R6/1 mice exhibit significant increases in impulsive-like behaviour from 4 weeks-of-age and changes in exploratory behaviour from 7 weeks-of-age (Bolivar et al., 2004; Rodríguez-Urgellés et al., 2022). Some studies have reported motor deficits on the balance beam and rotarod from 8 weeks-of-age, however others have not reported these findings until 5 months (Brooks, Jones, et al., 2012; Spires et al., 2004). More subtle behavioural traits such as sniffing and rearing, and anxiety-like phenotypes have not been observed until 26-30 weeks of age (Angeles-López et al., 2021; Clifford et al., 2002; Naver, Stub, Moller, et al., 2003).

Morphological changes of brain structure and volume have been investigated using multiple imaging approaches, including diffusion tensor imaging (DTI) and magnetic resonance imaging (MRI). MRI has been used to detect structural brain changes, and significantly reduced whole-brain volume has been reported in 30-week manifest R6/1 mouse brain compared with wild-type mouse brains, which was not seen in 11-week pre-manifest R6/1 mouse brain (Gatto et al., 2021). Further analysis revealed significant reduction in white-matter and grey-matter regions, including the corpus collosum and striatum, respectively (Gatto et al., 2021). DTI can capture microstructural changes in the R6/1 mouse brain and showed significant changes to the fractional anisotropy measure in the 11-week pre-manifest brain, indicating abnormalities in axonal connectivity (Gatto et al., 2021; Johnson & Gregory, 2019; Z. Zheng & M. I. Diamond, 2012). Additional pathology and longitudinal MRI studies have reported widespread increases in axon density at 16-weeks of age, significant atrophy of grey matter regions by 17-weeks of age, and 17% reduction in striatal volume by 18-weeks of age (Casella et al., 2023; Hansson et al., 1999; Rattray et al., 2013).

The presence of neuronal inclusions and loss of MSNs are pathological hallmarks of the human condition. Neuronal inclusions and aggregates of mHTT are present in the R6/1 mouse striatum from 8 weeks-of-age (Gatto et al., 2021; Li et al., 2005; Naver, Stub, Møller, et al., 2003). With respect to MSN cell loss, PCR amplification indicated a loss in *FoxP1* gene

expression in the 24-week R6/1 striatum compared with the wild-type striatum, and reduced DARPP-32 positive nuclei in the 16-week-old R6/1 striatum as seen by immunohistochemistry (Desplats et al., 2006; Naver, Stub, Møller, et al., 2003). Additionally, BDNF is significantly reduced in the 20-week-old R6/1 striatum (Hodges et al., 2008). Analysis of other markers such as those for glial cells, have shown an increase in GFAP-immunopositive astrocytes and Iba1-positive microglia in the cortex, striatum, hippocampus, and corpus collosum of R6/1 mice from 11-weeks of age (Angeles-López et al., 2021; Gatto et al., 2021).

The need for accurate models of human disease is imperative for a fuller understanding of mechanisms associated with disease progression, and the subsequent development of therapeutics. Whilst many in vivo models recapitulate the hallmarks of HD with regard to motor and cognitive deficits and the presence of mHTT inclusions, each model may only mimic parts of the HD phenotype seen in the human condition. (Li et al., 2005). It is important to evaluate each model in detail and if necessary, use more than one model to address research questions.

In this thesis, mouse models of HD were used to assess some of the findings obtained using *Drosophila* models, the latter being more powerful for conducting precise and rapid molecular genetic interaction studies (Tolwinski, 2017). Previously, a microarray analysis was performed in the lab to identify genes important for striatal development (Jeyasingham, PhD Thesis; Precious et al., 2016), and subsequently, genes that might be implicated in HD. In this analysis, *Mef2C* and *FoxP1* were identified to be highly upregulated during this process.

1.4 Mef2

1.4.1 Mef2 overview

In 1989, a myocyte-specific enhancer-binding factor, *Mef2*, was first identified in mammalian cell culture as a protein activator that bound to a DNA sequence, leading to the expression of the muscle creatine kinase (McK) gene in muscle differentiation (Gossett et al., 1989; Taylor & Hughes, 2017). Subsequent cloning of *Mef2* revealed that the gene was part of the MADS-box family of transcription factors, which share the highly conserved MADS-box domain

(minichromosome maintenance genes (MCM1), agamous (AG), deficiens (DEFA), and serum response factor (SRF)) (X. Chen et al., 2017; M. Lisek et al., 2023; Taylor & Hughes, 2017). In the early 1990s, significant progress was made regarding the role of *Mef2* in skeletal muscle differentiation (Yu et al., 1992), followed by evidence of critical roles in the development and function of the heart with loss of specific *Mef2* isoforms leading to embryonic lethality due to cardiac defects (Black & Cripps, 2010; Filomena & Bang, 2018). *Mef2* has since been implicated in several neuronal processes, including neurotransmitter release, synaptic transmission, and neuronal maturation (Adachi et al., 2016; M. Lisek et al., 2023; Lyons et al., 1995). In particular, the *Mef2C* gene has been implicated in the differentiation of postmitotic neurons, growth and pruning of axons, maintenance of neuronal and synaptic function, as well as microglial function and mediation of the immune response (Assali et al., 2019; Neely et al., 2009; Zhang & Zhao, 2022).

1.4.2 The Mef2 gene

The Mef2 proteins are a highly conserved family of transcription factors. *Drosophilae* possess a single *Mef2* gene, whereas vertebrates have four highly conserved genes, *Mef2A-D* (M. Lisek et al., 2023; Matthew J. Potthoff & Eric N. Olson, 2007; Yu et al., 1992). The N-terminal region is highly conserved across species with a 57-amino acid MADS-box domain, and an immediately adjacent 29 amino-acid MEF2 motif (Black & Olson, 1998; Matthew J. Potthoff & Eric N. Olson, 2007). Together, they enable homo- and heterodimersation via recognition and binding to the consensus DNA sequence CTA(A/T)$_4$TAG/A, and mediate DNA binding and co-factor interactions (W. Wu et al., 2011). There is 90-95% conservation across *Drosophila Mef2* and all mammalian *Mef2* isoforms in this region (Matthew J. Potthoff & Eric N. Olson, 2007) (Figure 1.3). The C-terminus is subject to a high degree of variability due to alternative splicing and contains two transcriptional activation domains: TAD1 and TAD2. Along with the holliday junction recognition protein C-terminal (HJURP-C) domain, these regions aid in the activation of transcriptional processes (Chaudhary et al., 2021). The nuclear localisation site (NLS) regulates the translocation of proteins in the nucleus (Borghi et al., 2001) (Figure 1.4).

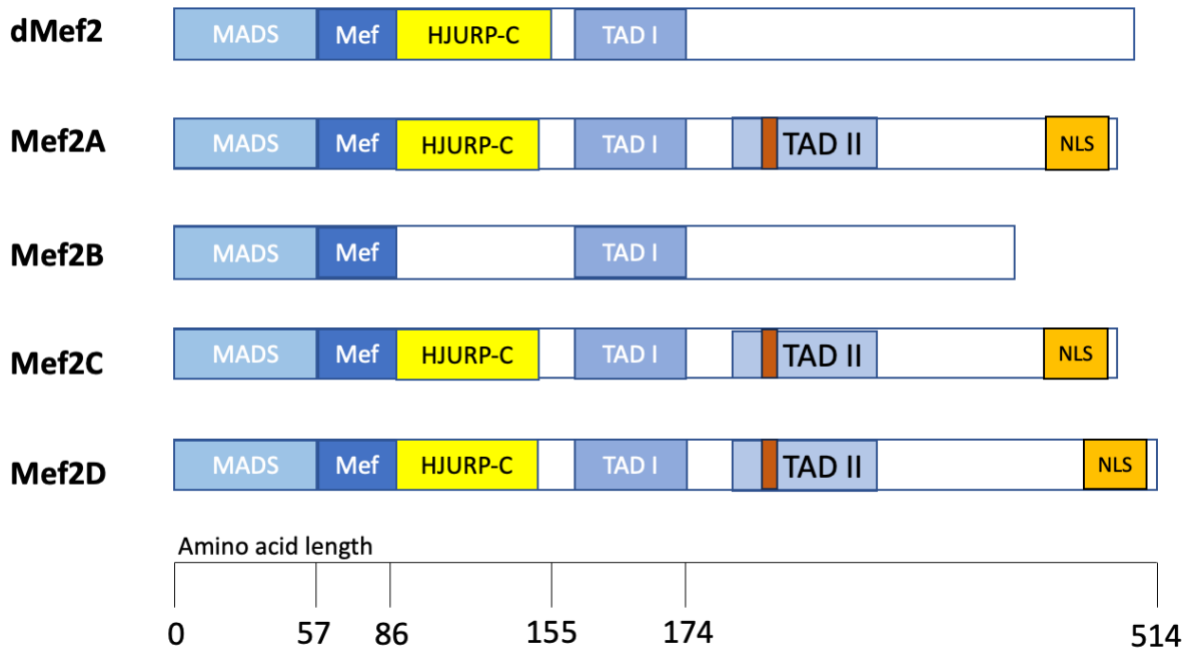

Figure 1.4. Schematic drawing of Mef2 isoforms and conserved domains.
Schematic drawing to show conservation and differences between the single *Drosophila Mef2* (dMef2) and four mammalian *Mef2* genes, *Mef2A-D.* MADS: MADS-Box domain, Mef: Mef2 motif, HJURP-C: Holliday junction recognition protein C-terminal domain. TAD: Transactivation domain. NLS: Nuclear Localisation Signal. Red Box: Beta domain. Adapted from (Xiao Chen et al., 2017).

1.4.3 The Mef2C gene

Mef2C is the first of the *Mef2* genes to be expressed in the mammalian central nervous system (CNS) and is expressed in a tissue-specific manner with restrictions to the brain, skeletal and cardiac tissue (Assali et al., 2019; A. C. Barbosa et al., 2008; Infantino et al., 2013). Knockout studies of *Mef2A* and *Mef2D* have shown that these genes are implicated in processes related to hippocampal learning and memory through suppression of excitatory synapse and dendritic spine formation (Carmichael et al., 2018; Cole et al., 2012; Pon & Marra, 2016). Outside the CNS, *Mef2A* has been highly associated with cell proliferation and survival, and inflammation throughout the cardiovascular system (M. J. Potthoff & E. N. Olson, 2007; Xiong et al., 2019). By contrast to the other *Mef2* genes, *Mef2B* is the least studied and has no clear role in neuronal development, but has been implicated in ovarian cancer signalling, hepatic cell activation, and de-differentiation of vascular smooth muscle cells (Assali et al., 2019; Estrella et al., 2015; Pon & Marra, 2016).

The *Mef2C* gene consists of 9 conventional exons and 3 sites specific for alternative splicing: the mutually exclusive exon α1 and α2 that lie immediately adjacent to the MEF2 domain; the cassette skipping/inclusion exon β located within TADII; and the 3' splice site γ region located in the terminal coding exon of the *Mef2C* gene (Figure 1.5)(Assali et al., 2019; Infantino et al., 2013; Zhang et al., 2015). Alternative splicing can play a role in regulation and localisation of proteins, and their ability to interact with ligands and other proteins. It has also emerged as a central element in gene regulation and the diversity of transcriptional activity (Kelemen et al., 2013). Within the mammalian *Mef2C* gene, six isoforms are generated, and expressed in a tissue-specific manner (Sekiyama et al., 2012). *Mef2C* isoforms containing α1 have been found in cardiac muscle tissue and neurons, whilst those containing α2 have high potency for myogenic activity and is required for the efficient differentiation of skeletal muscle cells (McDermott et al., 1993; Zhang et al., 2015). *Mef2C* mRNA transcripts lacking the α exons show increased transcriptional activity compared with those that do not lack these exons (Infantino et al., 2013). *Mef2C* isoforms including exon β are expressed specifically in the brain of neural tissues (Hakim et al., 2010) whilst absence of exon β is expressed in non-neural tissue (Sekiyama et al., 2012). *Mef2C* isoforms containing the γ region is ubiquitously expressed and is thought to encode a phosphoserine-dependent transrepressor domain and isoforms lacking the γ region show enhanced interactions (Sekiyama et al., 2012; Zhu et al., 2005).

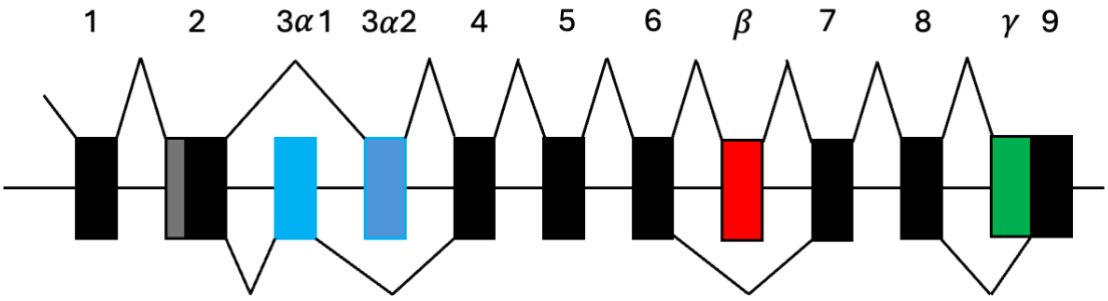

Figure 1.5 Schematic of Mef2C gene.
Schematic representation of *Mef2C* showing 9 conventional exons and 3 alternatively spliced exons: mutually exclusive exon α1 and α2 (blue), the cassette skipping/inclusion exon β, (red) and the 3' splice site γ exon (green). Adapted from (Zhu et al., 2005).

1.4.5 Mef2C protein structure

The human Mef2C (hMef2C) protein contains 5 core domains that are consistent across the four isoforms: MADS domain, MEF2 domain, TAD1, TAD2, and the NLS (Figure 1.3). The N-terminal region including the MADS and MEF2 domains are highly conserved across invertebrates and mammalian orthologs and together, are known for mediating DNA binding and dimerisation amongst Mef2 isoforms (Molkentin et al., 1996). Together, these regions interact with co-factors and function in complexes with various other proteins, regulating gene expression and modulating transcriptional function within cells (Wu et al., 2010). The C-terminal region of Mef2 isoforms is considerably divergent, but shares commonality, in that they all function as transcriptional activation regions (Wu et al., 2010). TAD1 and TAD2 are transcriptional activation domains that have been reported to promote signal transduction and regulation of gene transcription (Chaudhary et al., 2021; Wenwu Wu et al., 2011). The NLS is required for efficient localisation of proteins to the nucleus and subsequent nuclear retention and has been shown to interact with HDAC4, a mainly cytoplasmic-located protein, to provide translocation to the nucleus (Borghi et al., 2001) (Figure 1.3).

1.4.6 Expression and role of Mef2C in the brain

In the early 1990s, *Mef2C* was highlighted as a potentially important gene associated with the developing CNS due to the presence of specific isoforms found exclusively within the brain (Leifer et al., 1993). In situ hybridisation studies of the developing human brain indicated that *Mef2C* is expressed from as early as 14 weeks in the developing foetal cerebral cortical plate, with minimal expression in the subventricular and ventricular zones. Interestingly, expression was limited to the cell nuclei of neurons within the outer layers of the neocortex with a more apparent bilaminate pattern later in gestation (16-27 weeks) (Leifer et al., 1994a; Leifer et al., 1993). These findings have implicated *Mef2C* in orchestration of neuronal differentiation and survival, as well as synapse formation in the cerebral cortex, and to an extent, the hippocampus (Kamath & Chen, 2019; Hao Li et al., 2008). More recent studies have investigated the spatio-temporal expression profile of Mef2C RNA and protein in the developing mouse cerebellum and have found it to be restricted to the Purkinje cell layer, unlike Mef2A and Mef2D where expression is also detected in the molecular cell layer (Kamath & Chen, 2019). Limited expression has also been observed in the thalamus, basal forebrain,

globus pallidus, brainstem and spinal cord (Leifer et al., 1994a). With respect to studying how *Mef2C* might be implicated in HD, it is important to be aware of the normal expression pattern of *Mef2C* in the striatum. Previous work in the host lab investigated the expression profile of *Mef2C* throughout mouse brain development, into adulthood (Ali, 2022). Highest expression of the *Mef2C* gene was reported between embryonic day 14 (E14) and postnatal day 14 (P14), with peak expression at P0 (Ali, 2022). The initial observation of *Mef2C* expression at E14 was consistent with peak neurogenesis of matrix MSNs and expression was restricted to the lateral aspects of the mantle zone, indicating that *Mef2C* might be specific to postmitotic cells (Ali, 2022). Studies of the neocortex have also shown that deletion of *Mef2C* in neural progenitor cells leads to reduced numbers of mature neurons, and reduced brain mass which may indicate an additional role in neuronal maturation (H. Li et al., 2008). In the E16 mouse striatum, Mef2C mRNA expression was tripled compared with the E14 brain, and Mef2C-expressing cells became more distributed throughout the ventral and medial mantle zone (Ali, 2022). Further investigations of *Mef2C* striatal knockout throughout development led to a 15-20% reduction in neuronal cell count in the P14, 3- and 12-month striatum, compared with the wild-type brain, and fewer FoxP1-positive and Ctip2 (COUP-TF1 interacting protein 2)-positive cells (Ali, 2022). Mef2C co-localisation with Ctip2, a regulator of MSN differentiation, provided more evidence that *Mef2C* might play a role in MSN development (Ali, 2022; Arlotta et al., 2008).

Complete knockout of *Mef2C* was embryonic lethal by E10.5 due to severe cardiac defects (Hao Li et al., 2008; Lin et al., 1997). Therefore, studies investigating the role of *Mef2C* in the brain require conditional knockdown. Brain-wide deletion of *Mef2C* during the course of development was reported to increase dendritic spine density, whilst deletion of *Mef2C* in the embryonic neural stem cells of mice, using nestin-cre, caused deficits in cortical neuron migration and transcription of excitatory synapses (Harrington et al., 2016; H. Li et al., 2008). Other studies have shown that mice lacking *Mef2C* in the neural crest can survive to birth, however 100% die within an hour due to upper airway obstruction (Verzi et al., 2007). In the hippocampus, heterozygous knockdown of *Mef2C* has resulted in increased hippocampal network activity and reduced neurogenesis (Tu et al., 2017). Additionally, the presence of *Mef2C* in hippocampal neurons can provide a level of resistance to ischemia, suggesting a role for *Mef2C* in protection from ischemic events (Janson et al., 2001). Conversely, over-

expression of *Mef2C* in an embryonic stem cell line led to significant upregulation of mature and immature neuronal markers, implicating *Mef2C* in neuronal lineage specification (Z. Li et al., 2008). Phenotypically, mice with conditional *Mef2C* knockout appear to exhibit behavioural deficits similar to those reported in patients with Rett Syndrome and Autism Spectrum Disorder (ASD) (Bai et al., 2020). Combined, the literature makes a compelling case that *Mef2C* is particularly important for the development and maintenance of neurons, and the relationship and function of *Mef2C* in neurons may be an important consideration when studying neurodegenerative disorders.

1.4.7 *Mef2C* in neurological disease

Mutations within the *Mef2C* gene have been shown to be involved in multiple neurodevelopmental and neuropsychiatric disorders such as ASD, bipolar, depression, and attention deficit hyperactivity disorder (Zhou et al., 2019). Patients with microdeletions in the *Mef2C* gene are diagnosed with *Mef2C* haploinsufficiency syndrome, and present with autism-like symptoms in addition to presenting with mental retardation, epileptic seizures and cerebral malformations (Le Meur et al., 2010; Vrečar et al., 2017). High expression of *Mef2C* in brain regions associated with learning and memory, such as the frontal and entorhinal cortex, hippocampus and amygdala, has also suggested a role for *Mef2C* in Alzheimer's Disease (AD)(Hassan et al., 2021; Ren et al., 2022). Moreover, more study identified that the presence of a single-nucleotide polymorphism, rs190982, near the *Mef2C* region increased the risk of late-onset AD disease (Chaudhary et al., 2021; Lambert et al., 2013; Zhang & Zhao, 2022). In 2022, Ren and colleagues (2022) reported reduced Mef2C mRNA in the blood of AD patients, and Mef2C protein was reduced in the temporal and frontal lobes of AD patients compared with normal controls (Ren et al., 2022). Further research showed that knocking down *Mef2C* increased deposition of amyloid-β (Aβ) in the cortex of the APP/PS1_DT (APPswe/PSEN1dE9 double transgenic) mouse model of AD as well as their learning and memory ability (Ren et al., 2022). With respect to HD, *Mef2C* was reported to be reduced in the hippocampus of R6/1 and $Hdh^{Q7/Q111}$ mice at the onset of cognitive dysfunction (Vidal-Sancho et al., 2020). Furthermore, treatment of the R6/1 mice with BML-210, which activates Mef2 transcriptional activity, led to improved cognitive performance and increased activity of Mef2-dependent memory-related genes, including BDNF and Arc (Vidal-Sancho et al., 2020).

Additionally, treatment of BML-210 in R6/1 hippocampal cultures led to increased neurite growth (Vidal-Sancho et al., 2020). Table 1.3 outlines research that has mentioned *Mef2C* expression in HD. Interestingly, a study of skeletal atrophy in polyQ models of HD, including the R6/2, reported that muscle-specific deletion of *Mef2C* led to rapid deterioration of myofibers and that mHTT was able to sequester *Mef2* in skeletal muscle, decreasing *Mef2* gene expression (Nath et al., 2020). Researchers also showed that restoring *Mef2* activity could rescue muscle atrophy in the AR113Q model of SBMA (Nath et al., 2020). *Mef2C* may be interacting with multiple complex pathways in a tissue- and region-specific manner. In this thesis, I aim to investigate how *Drosophila Mef2* and human *Mef2C* influence mHTT-induced degeneration.

Table 1.3 Research that has reported Mef2C expression in the context of HD models.

Model	Region	Age	Gene/Protein/ mRNA	Observation	Log2 Fold Change	P value	Method of study	Reference
$Hdh^{Q111/Q7}$	Hippocampus	3 months	Protein	No change			Western Blot	(Vidal-Sancho et al., 2020)
		6 months	Protein	Reduced		<0.05	Western Blot	
		17 months	Protein	Reduced		<0.05	Western Blot	
		3 months	Gene	No change			RT-PCR	
		6 months	Gene	No change			RT-PCR	
		17 months	Gene	No change			RT-PCR	
Hdh^{Q150}	Striatum	6 months	mRNA	No change	-0.155	0.62	Microarray	Brooks et al, unpublished
		12 months	mRNA	No change	1.298	0.0993	Microarray	
		18 months	mRNA	No change	-1.04	0.9096	Microarray	
Hdh^{Q140}	Striatum	6 months	mRNA	No change	1.1796	0.862	Microarray	Brooks et al, unpublished
		14 months	mRNA	No change	0.0046	0.998	Microarray	
		18 months	mRNA	No change	-1.933	0.905	Microarray	
Hdh^{Q175}	Striatum	3 months	mRNA	No change	1.193	0.999	Microarray	Brooks et al, unpublished
		6 months	mRNA	No change	1.196	0.985	Microarray	
		12 months	mRNA	No change	-0.432	0.471	Microarray	
R6/1	Striatum	2 months	mRNA	No change	1.213	0.748	Microarray	Brooks et al, unpublished
		4 months	mRNA	Increased	2.049	0.039	Microarray	
		6 months	mRNA	No change	1.169	0.622	Microarray	
	Hippocampus	8 weeks	protein	No change				(Vidal-Sancho et al., 2020)
		12 weeks	protein	Reduced		<0.01	Western Blot	
		20 weeks	protein	Reduced		<0.05	Western Blot	
		30 weeks	protein	Reduced		<0.05	Western Blot	

		8 weeks	gene	No change			RT-PCR	
		12 weeks	gene	No change			RT-PCR	
		20 weeks	gene	No change			RT-PCR	
		30 weeks	gene					
YAC 128	Striatum	6 months	mRNA	No change	-1.049	0.999	Microarray	Brooks et al,
		12 months	mRNA	No change	-0.104	0.999	Microarray	unpublished
		18 months	mRNA	No change	-0.325	0.954	Microarray	

1.5 FoxP1

1.5.1 FoxP overview

The Forkhead Box P (FOXP) subfamily of transcription factors is encoded by the FOX gene family (Feng et al., 2010). In 2001, *FoxP1* was first identified and characterised in the lungs of mice and recognised as a tumour suppressor in breast cancer (Kim et al., 2019; W. Shu et al., 2001). In 2004, the importance of *FoxP1* in development became apparent when a conventional knockout of *FoxP1* in mouse was found to be embryonically lethal at E14 due to cardiac defects (B. Wang et al., 2004). It has since been implicated in a range of non-neuronal processes such as in the regulation of B cell development and myocyte proliferation (Bacon et al., 2015; Hu et al., 2006; B. Wang et al., 2004) but, is now widely known to be involved in regulating the development of spinal motor neurons and neurons of the brain (Reymundo Lozano et al., 2021). *FoxP1* binds a 7-nucleotide consensus sequence, TATTT(G/A)T, and represses transcription at target locations, including SV40 (simian virus 40) and IL-2 (Interleukin-2) promoters, and directly regulates the expression of genes important for neurogenesis (Johnson et al., 2018).

1.5.2 The *FoxP* gene

The forkhead domain was defined in 1990 by the homology between the *Drosophila* forkhead gene and the DNA-binding domain of hepatocyte nuclear factor-3. This first indicated conservation of transcription factors between *Drosophila* and mammals (Tamura et al., 2004a). The *FoxP* gene itself, first arose in eukaryotic unicellular organisms, and following multiple gene duplications, led to the generation of four members of the subfamily in vertebrates (*FoxP1-4*) (Lawton et al., 2014; M. Emília Santos et al., 2011). These genes are characterised on the basis that they contain a C_2H_2-type zinc finger domain, a leucine zipper motif, and a forkhead domain at the C-terminus, and are important for DNA-binding and dimerisation (Takahashi et al., 2009). *Drosophila FoxP* and the human isoforms show a large degree of conservation in these functional domains (Lawton et al., 2014) (Figure 1.6).

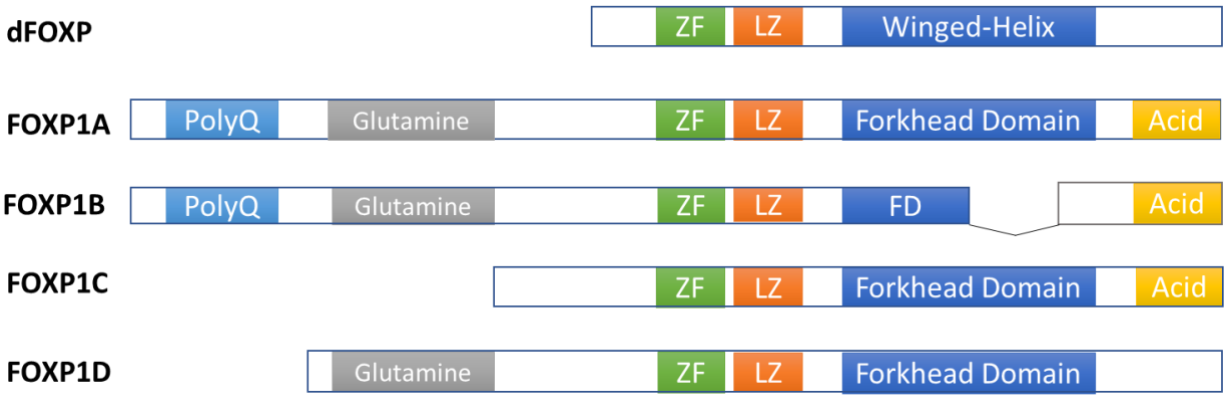

Figure 1.6 Schematic of Drosophila FoxP1 and FoxP1 protein isoforms
Schematic diagram of the single FoxP gene in *Drosophila* and the four FoxP1 alternatively spliced isoforms. Adapted from (B. Wang et al., 2003).

The *Drosophila FoxP* gene is comprised of 7 exons, of which, exons 1 and 2 encode the zinc finger domain, and exons 6 and 7 encode the C-terminal conserved forkhead domain (M. E. Santos et al., 2011) (Figure 1.7). Whilst the *Drosophila FoxP* gene is conserved in its' C-terminus amongst mammalian *FoxP1* genes, it does not contain the N-terminal fragment of the mammalian gene and associated protein which explains the low number of exons compared with the mammalian orthologs. The human *FoxP1* gene consists of 21 exons across 586kb within chromosome 3p14.1. The zinc finger domain is encoded by exons 12 and 13, the leucine zipper domain by exons 13 and 14, and the forkhead domain by exons 16 through 19 (Gabut et al., 2011; Vernes et al., 2009) (Figure 1.7) The mouse gene consists of 19 exons however, sequences across these regions show >95% conservation to the human gene (Gabut et al., 2011; Bin Wang et al., 2003).

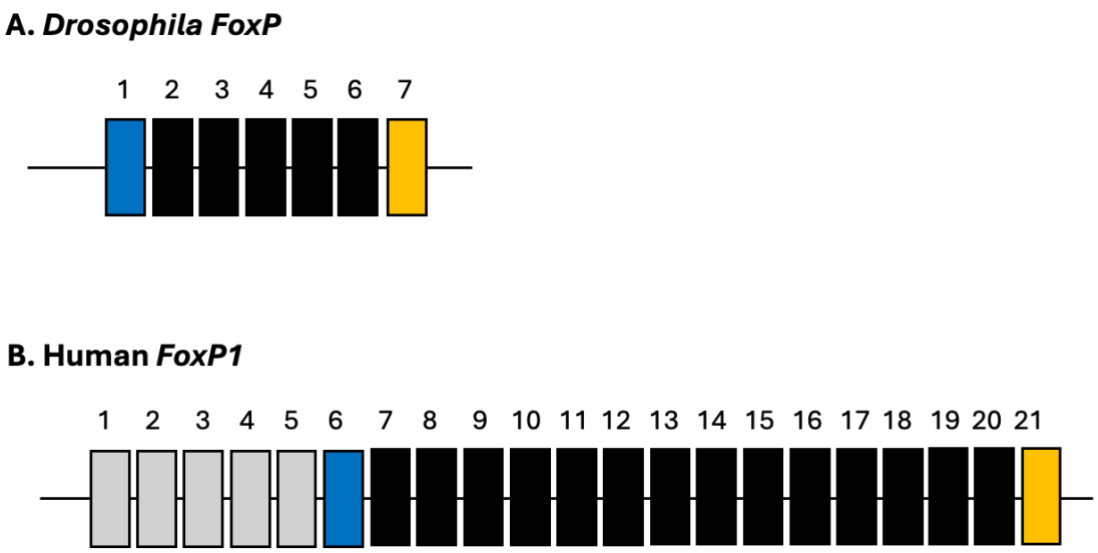

Figure 1.7 Schematic of exons of the FoxP gene
A) Exons of the *Drosophila FoxP* gene, and B) Exons of the human *FoxP1* gene. Grey: non-coding exons, black: coding exons, blue: START codon, red: STOP codon. Adapted from (Brown et al., 2008; Castells-Nobau et al., 2019).

1.5.3 The FoxP1 protein

Through alternative splicing, *FoxP1* forms four distinct protein isoforms, most distinctively, the truncated *FoxP1-D* isoform which contains a unique 5'-untranslated exon (exon 2b) in addition to two in-frame stop codons at the beginning of exon 3 (Bin Wang et al., 2003). *FoxP1-A* refers to the canonical full-length form of the FoxP1 protein, and FoxP1-C results from a splicing event that leads to a truncated N-terminal region. FoxP1-B (also known as ES-FOXP1 for its precise expression in embryonic stem cells) forms via exit splicing of exons 13 and 14, which leads to a truncated forkhead domain (Louis Sam Titus et al., 2017; Weiguo Shu et al., 2001). The N-terminal region of FoxP1 is a DNA binding-dependent transcriptional repression domain, contributing to protein-protein interactions (PPI) via the presence of the zinc finger and leucine zipper domain, which together are often referred to as subdomain 1 (Johnson et al., 2018; Li et al., 2004). Through these domains, all FoxP proteins (and the FoxP1 protein variants) can homo- and heterodimerise with subfamily members. Research has shown that mutations in the leucine zipper and/or zinc finger domain significantly reduces the capability of *FoxP1* to repress transcription (Li et al., 2004).

1.5.4 Expression and role of *FoxP1* in the brain

FoxP1 is expressed throughout the body and has been associated with a vast array of biological processes such as B cell activation and macrophage development, and is an important regulator of lung, heart, kidney and gut development (Bacon et al., 2015; Barrans et al., 2004; M. E. Santos et al., 2011; B. Wang et al., 2003). More recently, *FoxP1* has become of significant interest regarding its' expression profile in the brain (Louis Sam Titus et al., 2017; Precious et al., 2016; Tamura et al., 2004b). In the mouse brain, the FoxP1 protein is highly expressed in the postmitotic neurons of cervical and lumbar spinal regions from as early as E9.5, with mRNA expression in the marginal zone of the lateral ganglionic eminence (LGE) from as early as E12 (Ferland et al., 2003; Tamura et al., 2003). High mRNA expression levels are observed in the striatum from E13.5, with expression also being reported in the substantia nigra, hippocampus, thalamic nuclei, amygdala and hypothalamus (Ferland et al., 2003; Tamura et al., 2003). FoxP1 is also reported at high levels in cortical layers 3-5, with migration to layer 6 in adulthood and has implicated *FoxP1* in axonal growth and neuronal migration (Ferland et al., 2003; Li et al., 2015).

FoxP1 null mice are embryonic lethal at E14.5 due to severe cardiac defects (Bin Wang et al., 2004). Therefore, to study the importance of *FoxP1* in brain function, conditional knock-out models have been generated to specifically delete *FoxP1* in the brain. Bacon and colleagues (2015) generated Nestin-Cre$^{FoxP1-/-}$ mice to knockdown *FoxP1* in the embryonic neural stem cells, and observed reduced total striatal volume and significantly enlarged ventricles in postnatal day 1 (P1) mice, compared with wild-type littermates, which became more prominent in adulthood (Bacon et al., 2015). Surprisingly, there was no change to the total striatal volume at E18 which may indicate the significance of *FoxP1* in processes during late embryonic development and adulthood (Bacon et al., 2015). Electrophysiological analysis of the P18 and P25 CA1 hippocampal region showed significantly reduced excitability in the hippocampal pyramidal neurons and increased dendritic branching in the primary striatal neurons. Behaviourally, adult Nestin-Cre$^{FoxP1-/-}$ mice showed reduced anxiety and hyperexcitability, reduced exploratory behaviour and impaired short-term memory. (Bacon et al., 2015).

In another study, forebrain knockdown of *FoxP1* using *Emx1.Cre* led to mice with decreased sociability and hyperexcitability in addition to impaired spatial learning and memory (Araujo et al., 2017). MRI showed a 12% decrease in the overall brain volume of mice with forebrain *FoxP1* knockdown compared with wild-type littermates, with the most affected region being the hippocampus (Araujo et al., 2017).

In 2003, Ferland and colleagues conducted histological staining of the wild-type mouse brain and In situ hybridisation to uncover the expression profile of FoxP1 mRNA and protein in the developing and adult brain (Ferland et al., 2003). In the adult brain, *FoxP1* expression is abundant in cells of cortical layers 3-5 with scattered expression in cells of layers 2 and 6. As the brain ages, FoxP1-positive cells become more apparent in layer 6 of the cortex, and the increased presence of FoxP1 protein in this layer may implicate the protein in late neuronal migration, indicating its involvement in neuronal differentiation (Ferland et al., 2003). Hippocampal localisation persists throughout development and adulthood, and was the brain region with the greatest level of FoxP1 protein expression in the mature basal ganglia (Ferland et al., 2003). In the striatum, FoxP1 has been shown to co-localise with the MSN markers, DARPP-32 and CTIP2 (Arlotta et al., 2008; Precious et al., 2016). Interestingly, western blot analysis of the 4 FoxP1 isoforms revealed specific patterns of expression. FoxP1-B is not expressed in the adult brain, whilst FoxP1-A is ubiquitously expressed throughout, with highest expression in the striatum and cortex (Louis Sam Titus et al., 2017; Tang et al., 2012). FoxP1-C is expressed at low levels in the hippocampus and striatum, whilst FoxP1-D is specific to the cortex and striatum (Louis Sam Titus et al., 2017). This may also indicate that isoform-specific FoxP1 proteins play different roles in developing and maintenance of neurons in the brain.

1.5.5 FoxP1 in neurological disease

Mutations and/or deletions in the *FoxP1* gene have been attributed to several neurodevelopmental disorders, where symptoms include intellectual disability, language and speech impairments, and developmental delay 'with or without autistic features' (R. Lozano et al., 2021). Research has identified *FoxP1* as one of the top five ASD risk genes. However, whilst some studies have shown that *FoxP1* is significantly up-regulated in the hippocampus and striatum of some ASD patients, (Zhou et al., 2022) others have reported ASD patients with

FoxP1 loss-of-function variants (Chien et al., 2013; Zhou et al., 2022). Additionally, a de novo heterozygous nonsense mutation in *FoxP1*, R525X, that subsequently leads to a truncated FoxP1 protein, led to delayed migration and altered dendritic morphology in cortical neurons (Li et al., 2019). This indicated a potential novel mechanism for development of ASD (Li et al., 2019). With regard to HD, Desplats and colleagues were the first to report changes in FoxP1 mRNA levels in the 6-month-old R6/1 striatum (Desplats et al., 2006). Since then, other researchers have reported reduced FoxP1 mRNA and protein in the striatum and cortex of knock-in and transgenic models of HD, indicating the importance of *FoxP1* dysregulation in HD pathogenesis (Table 1.4). Interestingly, reports have not mentioned that changes to FoxP1 in the cortex and striatum tend to appear comparable to that of wild-type tissue at earlier, pre-manifest timepoints, which is then followed by a reduction in FoxP1 mRNA and protein at later timepoints. Understanding the full time-course of FoxP1 expression, and how the expression of FoxP1 changes throughout pre-manifest and manifest stages in mouse models, may provide additional input into mechanisms associated with these changes. In turn, this may influence how researchers develop further therapeutics.

Table 1.4. Research conducted that has reported FoxP1 changes in the HD models

Model	Region	Age	Gene/ Protein/ mRNA	Observation	Log2 Fold Change	P Value	Method of Study	References
Human	Caudate	Grade 0-2	mRNA	No change	-0.578		RNA Seq	(Hodges et al., 2006)
		Grade 2-4	mRNA	Reduced				
	Cingulate Cortex	Grade 0-2	mRNA	Reduced				
		Grade 2-4	mRNA	Reduced				
R6/1	Striatum	10 weeks	mRNA	Reduced	-0.345		Real-time	(Desplats et al., 2006)
	Striatum	6 months	mRNA	Reduced	-1.152	0.0017	PCR analysis	
R6/2	Striatum	2 weeks	Protein	No change			Western Blot	(Louis Sam Titus et al., 2017)
		6 weeks	Protein	Reduced				
	Cortex	2 weeks	Protein	No change			Western Blot	
		6 weeks	Protein	Reduced				
	Cerebellum	12 weeks	Protein	No change			Western Blot	
R6/2-Q150	Striatum	12 weeks	mRNA	Reduced	-0.775		Differential GO	(Kuhn et al., 2007)
	Striatum	12 weeks	Gene	Reduced	-0.304		Microarray Analysis	(Tang et al., 2011)
Hdh^{Q92}	Striatum	18-months	mRNA	Reduced	-1.737		Differential GO	(Kuhn et al., 2007)
Hdh^{Q100}	Striatum	No data	Protein	Reduced		<0.01	Western Blot	(Louis Sam Titus et al., 2017)
	Cortex	No data	Protein	No change			Western Blot	

Hdh^{Q140}	Striatum	6 months	mRNA	No change	-1.621	0.581	Microarray	Brooks et al., unpublished
		14 months	mRNA	No change	-0.435	0.923	Microarray	
		18 months	mRNA	No change	-2.144	0.452	Microarray	
Hdh^{Q150}	Striatum	6 months	mRNA	No change	-0.151	0.501	Microarray	Brooks et al., unpublished
		12 months	mRNA	Reduced	-1.42	0.003		
Hdh^{Q175}	Striatum	3 months	mRNA	No change	-1.0295	0.999	Microarray	Brooks et al., unpublished
		6 months	mRNA	No change	-1.353	0.963	Microarray	
		12 months	mRNA	No change	-0.082	0.807	Microarray	
Hdh^{Q200}	Striatum	No data	Protein	Reduced		<0.001	Western Blot	(Louis Sam Titus et al., 2017)
	Cortex	No data	Protein	No change			Western Blot	
Yac128	Striatum	12 months	mRNA	Reduced	-0.403		Differential GO	(Kuhn et al., 2007)
	Striatum	6 months	mRNA	No change	-1.252	0.999	Microarray	
	Striatum	12 months	mRNA	No change	0.034	0.999	Microarray	Brooks et al., unpublished
	Striatum	18 months	mRNA	No change	-0.44	0.933	Microarray	
CHL2 Hdh^{Q150}	Striatum	22 months	mRNA	Reduced	-0.979		Differential GO	(Kuhn et al., 2007)
Het-KI-Q111	Striatum	10 months	mRNA	Reduced	-0.222		RNA Sequencing and proteomics	(Langfelder et al., 2016)
Het-KI-Q140	Striatum	10 months	mRNA	Reduced	-0.341		RNA Sequencing and proteomics	(Langfelder et al., 2016)
Het-KI-Q175	Striatum	10 months	mRNA	Reduced	-0.341		RNA Sequencing and proteomics	(Langfelder et al., 2016)
Primary cortical neurons	Transfection of Q138 into cell line.	-	Protein	Reduced	-1.732		Quantified cells.	(Louis Sam Titus et al., 2017)

N2A neuroblastoma cells	Transfection of Q138 into cell line	-	Protein	Reduced	-1.358		Quantified cells.	(Louis Sam Titus et al., 2017)
Transgenic Rat model (Q51)	Whole Brain	12 months	Gene & Protein	Upregulated		0.02	Microarray analysis and Western Blot	(Nguyen et al., 2008)

1.6 The *Drosophila* eye as an in vivo test tube for disease progression

As mentioned in section 1.3.2.2, one of the advantages of using *Drosophila* as a model of degeneration is the ability to identify potential disease modifiers and the roles these modifiers play in disease progression. A commonly used structure to study neurodegenerative disease in *Drosophila* is the compound eye (Cutler et al., 2015; Krench & Littleton, 2013; Treisman, 1999). The adult compound eye comprises ~800 identical structures called ommatidia (Figure 1.8). Each ommatidium consists of 8 PR cells surrounded by pigment and support cells (Cagan & Ready, 1989; Cutler et al., 2015). Using the Gal4/UAS system to induce expression of foreign genes in the developing eye provides an opportunity to identify how expression of these genes leads to loss of PR cells, degeneration of the eye, and subsequently, how one might rescue this phenotype. To fully understand the mechanisms associated with expression of genes in the *Drosophila* eye, and identify mechanisms associated with disease progression, it is important to fully understand development of this structure.

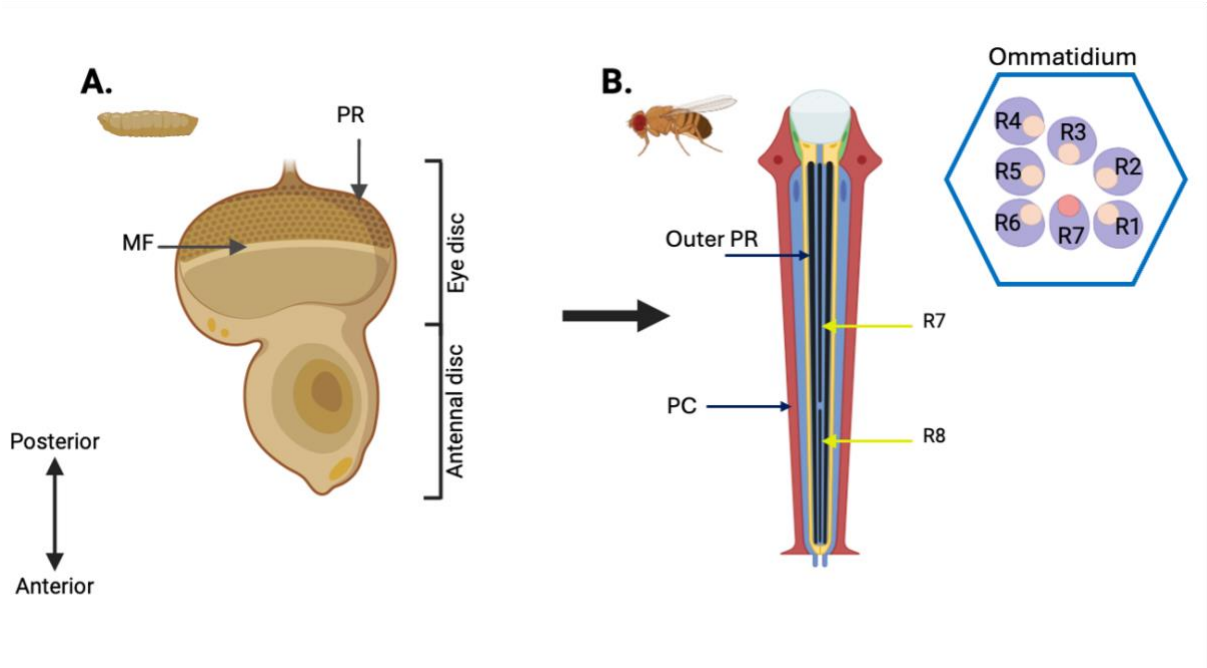

Figure 1.8 Schematic of the developing and adult eye structure.
A) Diagram of the eye-antennal imaginal disc seen in the larvae and early pupa. B). Diagram of the adult eye, to show the organisation of rhabdomeres in an ommatidium. MF: Morphogenetic furrow, PR: photoreceptor. R1-8: Rhabdomere 1-8. PC: Pigment Cell. Outer PR refer to R1-R6. Adapted from (Bostock et al., 2020; Mishra & Sprecher, 2023). Made using Biorender.

1.6.1 Development of the *Drosophila* eye

Differentiation of the adult compound eye begins from a monolayer of epithelium, termed the eye-antennal imaginal disc (Treisman & Heberlein, 1998). The imaginal disc originates from a cluster of cells with no region identity, and these cells begin to proliferate during the first instar larval stage (Figure 1.2), with segregation of the eye and antenna during the second larval instar stage (Mishra & Sprecher, 2023). During the second larval instar, the eye field is marked by expression of retinal determining genes (RDGs), most prominently eyeless (ey) and twin-of-eyeless (toy), whose pathways signal induction of the developing eye disc (Bonini et al., 1993; Braid & Verheyen, 2008; Mishra & Sprecher, 2023). These RDGs control cell proliferation, ommatidial patterning, and apoptosis, promoting and inhibiting eye development processes depending on their spatiotemporal appearance (Kumar & Moses, 2001). At the eye-antennal field interface, a gradient of Epidermal Growth Factor Receptor (EGFR) EGFR and Notch signalling antagonises antennal expression within the eye field whilst promoting development of the eye within the eye field (Baonza & Freeman, 2002; Kumar & Moses, 2001; Mishra & Sprecher, 2023). During the mid-third larval instar stage, retinal pattern formation begins to occur via the morphogenetic furrow (MF) (Baonza & Freeman, 2002). Marked by a dorsoventral indentation at the posterior end of the eye disc, the MF passes anteriorly, transforming unpatterned and undifferentiated cells into organised ommatidial clusters (Mishra & Sprecher, 2023). As the MF passes over the cells, cells will exist the cell cycle and the presence of molecular signals such as *Hedgehog* and *Senseless* will initiate the formation of PR, rhabdomeres, cone and pigment cells, and cells of the bristle complex (Chanut & Heberlein, 1997; Mishra & Sprecher, 2023). It is during this stage, that these currently undifferentiated cells, will change their thickness, morphology, and expression profile (Sahin & Çelik, 2013). A new column of ommatidial clusters arises every 2 hours, and by the end of the third larval instar, ~26 rows have emerged with the specification of the R8 founder cell. R8 specification is critical, since without it, no other PR precursors can develop (Hsiung & Moses, 2002). Following R8 specification, recruitment of R2/R5 and R3/R4 occurs, forming a five-cell pre-cluster, followed by recruitment of R1/R6 and R7, and other accessory cells that occur via a second mitotic wave of post-MF proliferation (Mishra & Sprecher, 2023).

During the first 10 hours of pupation, the final 10 ommatidial rows are generated, and the eye-imaginal disc everts, allowing adult eye formation to begin. In the 10 hours that follow,

four glial-like cone cells (CCs) are recruited to each ommatidial cluster, in addition to two additional glial-like primary pigment cells (PPCs), completing the 14-cell ommatidial core (Cagan, 2009). By 30 hours post-pupation formation, the PPCs encounter each other, and a translucent eye patch is now visible in the eye region of the pupa, and secondary pigment cells (SPCs) begin to appear. It is also during this time that bristles begin their final divisions, and the eye experiences maximal cell death of unrequired, undifferentiated cells (Cagan & Ready, 1989). Between 40- and 50-hours after the commencement of pupation, there is a visible indication of rhabdomere formation due to apparent 'bubbling' of the membrane, and the surviving cells are organised into the precise hexagonal lattice. From 60-hours, subsequent stages of development focus on cell specialisation and ommatidia function (Cagan, 2009; Cagan & Ready, 1989). At this timepoint, the retina deepens from 30-120μm, and microvilli folds at the apical membrane of the PRs form the rhabdomeres. It is these stacks of membrane that are packed with phototransduction machinery and light-sensing rhodopsins which are visible under light microscopy (Cagan & Ready, 1989).

70-hours after the initiation of pupation, CCs accumulate ommachrome-containing pigment granules at the base of the eye, whilst the microvilli of these cells begin secreting a lightly staining material onto the apical surface. Within a few hours, the microvilli of SPCs begin secreting darkly staining lens material. (Cagan & Ready, 1989). By 110 hours, the secondary and tertiary pigment cells elongate to form a membrane at the base of the PR and CCs, defining the floor of the retina. Along with the basal lamina neurons, the retinal floor forms a fenestrated membrane, and it is through this membrane that the PR axons pass through to reach their synaptic targets in the optic lobe. By 130 hours, lens formation is complete and by 140 hours, retina formation is complete and the adult eye is fully formed (Cagan & Ready, 1989).

1.6.2 Identifying genetic modifiers of HD using *Drosophila*

Protein interaction assays and genetic screens are effective ways to identify potential gene interactions associated with disease progression. For example, human tissues or tissues from mouse models of diseases can be processed to identify patterns of gene expression changes due to the presence of a particular mutations and/or disease phenotypes (Louis Sam Titus et

al., 2017; Malaiya et al., 2021). In one study, single-nucleotide RNA-Seq analysis of 14-month-old striatal cells from a mouse model of HD with 175 CAG repeats, was able to separate expression profiles of genes related to D1R and D2R MSNs, and further comparative analysis suggested that partial loss-of-function of polycomb repressive complex 2 (PPRC2) may lead to dysregulation in cell identity in the adult HD striatum (Malaiya et al., 2021). In another study, yeast-2-hybrid and mass spectrometry were used to identify novel wild-type and mutant HTT-fragment-interacting proteins (Kaltenbach et al., 2007). In this study, orthologs of 35 of the genes that were identified to have physical interactions with HTT were then tested for genetic interactions using a *Drosophila* model of HD (Kaltenbach et al., 2007). These unbiased approaches can reveal novel genes and potential pathways involved in disease progression, which can be followed up using in vivo systems.

1.7 Aims and Objectives of this thesis

This chapter highlights some of the key pathways that might be impaired in the HD brain due to the presence of mHTT, and that using multiple model organisms to study these differences can provide valuable insight into therapeutic treatment pathways. As mentioned above, results from the microarray analysis performed in the host lab identified *FoxP1* and *Mef2C* as two highly up-regulated transcription factors during embryonic striatal development. However, how they are implicated in neurodegenerative diseases, specifically HD, is largely unexplored. Whilst *FoxP1* has been shown to be reduced in the HD mouse and post-mortem striatum, there is very little literature regarding *Mef2C* changes in the HD brain. The literature discussed in this chapter show that *FoxP1* and *Mef2C* play important roles in neuron development and differentiation, and that manipulation of these genes may impact disease progression. Therefore, it is plausible that these genes may be implicated in the HD brain, and manipulating them, may suppress disease phenotypes and the presence of disease pathology, including mHTT inclusions.

The aim of this thesis was to investigate how manipulating these genes in a *Drosophila* model of HD might impact mHTT-induced degeneration. Furthermore, the generation of a novel HD mouse line with striatal knockout of *Mef2C* provided an opportunity *t*o investigate how removing *Mef2C* from the striatum of an R6/1 HD model might impact behavioural and

pathological changes observed in these mice. Understanding how manipulating *FoxP1* and *Mef2C* in the HD brain will provide valuable insight into potential mechanisms implicated in progression of the disease which could be targeted when developing new therapeutics.

Specific objectives and predicted outcomes.

1. To test how manipulating *Drosophila Mef2* and *hMef2C* affects mHTT-induced degeneration in a *Drosophila* model of HD, using the eye as an *in vivo* test tube. Based on previous literature, the hypothesis is that downregulation of *Mef2* and *Mef2C* in a mHTT-induced *Drosophila* model of HD will suppress mHTT-induced degeneration.
2. To test how manipulating *Drosophila Mef2* and human *Mef2C* in the developing and fully developed PRs can rescue mHTT-induced degeneration in a *Drosophila* model of HD. Due to the large body of evidence that shows *Mef2C* to be involved in developmental processes, it is thought that early knockdown of *Mef2C* would be required to suppress mHTT-induced degeneration.
3. To investigate the potential physical interactions that accompany any genetic interactions that occur between the Mef2C and HTT protein. Previous literature indicates that Mef2 isoforms can physically interact with HTT, and thus Mef2C may also physically interact.
4. To investigate how striatal knockout of *Mef2C* in a HD mouse model effects the deficits on behavioural tasks that are seen in the HD mouse model, and to assess whether striatal knockout of *Mef2C i*n a HD mouse model effects volume, the total MSN and neuronal cell number, and the presence of mHTT inclusions in the diseased striatum. To do this the R6/1 mouse model of HD will be used to generate a novel HD mouse line with striatal *Mef2C* knockout. Predicted outcomes are that striatal *Mef2C* knockout will reduce the presence of mHTT inclusions and reduce loss of MSNs. This may also lead to reduced behavioural deficits that are reported in the R6/1 mouse.
5. To investigate the timeline of FoxP1 protein loss in a transgenic and knock-in mouse line of HD. Previous literature indicates that FoxP1 protein expression may be comparable to that of the wild-type brain at early timepoints which may provide insight into how FoxP1 protein is lost, and how elevating FoxP1 protein expression might suppress mHTT-induced degeneration.

6. To test how manipulating human F*oxP1* affects mHTT-induced degeneration in a *Drosophila* model of HD. Previous literature studies indicate that over-expressing *FoxP1* in the whole-eye of a *Drosophila* model of HD, can rescue mHTT-induced degeneration. Rescuing mHTT-induced degeneration in the neurons of these flies may indicate a potential avenue for suppress MSN loss in the mammalian brain.
7. To investigate any potential physical interactions that accompany the genetic interactions that occur between the FoxP1 and HTT protein. Whether FoxP1 and HTT proteins interact will provide insight into how FoxP1 protein is lost in the HD brain, and how elevating FoxP1 protein levels may suppress degeneration.

Chapter 2: Materials and Methods

2.1 *Drosophila* Melanogaster

2.1.1 Fly Husbandry

2.1.1.1 Fly food

All fly lines were maintained in plastic vials on a standard cornmeal media. For every 50L, 345g of agar is added to 1.8kg maize, 1.875kg dextrose, 875g yeast and 6L of distilled H_2O, in a 70°C cooker containing 40L of distilled H_2O. Food is stirred frequently and a further 2L of distilled H_2O added, heating food to 95°C for 20 minutes. Following heating, an additional 1.5L of distilled H_2O is added with 111g nipagin (Hydroxybenzoic acid methyl ester) dissolved in 1.3L of absolute ethanol and 175ml propionic acid. Once food is roughly 75°C, food is dispensed into plastic vials of 8cm in length and 2.5cm in diameter. Food is dispensed to roughly one-third the height of the vials.

2.1.1.2 Standard fly housing conditions

Fly stocks were kept in an 18°C temperature-controlled room unless otherwise stated. Experimental flies were kept in temperature-controlled incubators depending on the experimental requirements, which are detailed in specific experiments, below. When collecting and sorting fly lines for experimental crosses, flies were immobilised using CO_2 anaesthesia pads, under a dissecting microscope. Experimental fly crosses were transferred into fresh food vials every 2-3 days.

2.1.2 Fly stocks

A variety of fly stocks were used in this thesis. Table 2.1 outlines the genotypes and sources of the stocks used. Targeted gene expression was achieved using the Gal4/UAS binary and $GAL80^{ts}$Gal4/UAS system, and each experiment will be outlined in more detail, in the methodology below.

Table 2.1. Fly stocks used in this thesis.

Fly line (chromosome)	Full genotype	Description	Original source (stock number)
	Gal4 Driver		
GMR-Gal4 (II)	P{GMR-GAL4.w[-]}2	Expresses GAL4 in the eye.	Bloomington (#9146)
Elav-^{c155}Gal4 (x)	{GawB}elav[C155]	Expresses GAL4 in neurons.	Bloomington (#458)
Appl-Gal4 (x)	P{Appl-GAL4.G1a}1	Expresses GAL4 in the larval nervous system under the control of APPL.	Bloomington (#32040)
	UAS transgene		
UAS-hHTTex1.Q20 (III)	W[*]; P{w[+mC]=UAS-HTT.ex1.Q20}111F1L	Expresses human HTT exon 1 with 20 CAG repeats.	Bloomington (#68412)
UAS-hHTTex1.Q50 (III)	W[*]; P{w[+mC]=UAS-HTT.ex1.Q50}Y4	Expresses human HTT exon 1 with 50 CAG repeats.	Bloomington (#68413)
UAS-hHTTex1.Q93 (III)	W[*]; P{w[+mC]=UAS-HTT.ex1.Q93}4F1	Expresses human HTT exon 1 with 93 CAG repeats.	Bloomington (#68418)
UAS-hHTTex1.Q120 (II)	W[*]; M{RFP[3xP3.PB]w[+mC]=UAS-HTT.ex1.Q120}ZH-51D	Expresses human HTT exon 1 with 120 CAG repeats.	Bloomington (#68408)
UAS-Q93/CyO (II)		Expresses human HTT exon 1 with 93 CAG repeats.	Dr Susanna Campesan - University of Leicester
UAS-hFoxP1 (II)	Y[1] w[*]; PBac{y[+mC]=UAS-hFOXP1.HA}VK00037	Expresses HA-tagged human FOXP1 under control of UAS.	Bloomington (#77992)
UAS-hFoxP1-FL (II)		Full length human FoxP1 cDNA in a pUASt vector.	Made in the host lab.

UAS-hFoxP1-FL(FLAG) (II)		Full length human FoxP1 cDNA with 3xFLAG tag on the C-terminus, in a pUASt vector.	Made in the host lab.
UAS-hMef2C (II)		Full length human Mef2C cDNA in a pUASt vector.	Made in the host lab.
UAS-dFoxP		*Drosophila* FoxP isoform 2	Gift from Annette Schenck's lab.
UAS-Mef2-10t4A		*Drosophila* Mef2 isoform 3 cDNA in a pUASt vector	Made in the host lab.
	RNAi lines		
UAS-Mef2RNAi (II)	Y[1] sc[*] v[1] sev[21]; P{y[+t7.7] v[+t1.8]= TRiP.HMS01691}attP40	Expresses dsRNA for RNAi of Mef2 under UAS control in the VALIUM20 vector	Bloomington (#38247)
UAS-Mef2RNAi (III)		Expresses GD long hairpin (lh) RNA for Mef2	VDRC (15550)
UAS-Mef2RNAi (III)		Expresses GD long hairpin (lh) RNA for Mef2	VDRC (1429R1)
	Other lines		
GMR-hHTT.Q120 (II)	Y[1] w[118]; P{w[+mC]=GMR-HTT.Q120}2.4	Drives expression of human huntingtin with Q120 CAG repeats in the eye.	Bloomington (#8533)
GMR-hHTT.Q120 (III)	W[118]; wg[Sp-1]/CyO; P{w[+mC]=GMR-HTT.Q120}4.62/TM6B, Tb[1]	Drives expression of human huntingtin with Q120 CAG repeats in the eye.	Bloomington (#8534)

Gal80^{ts}	P{TubP-GAL80[ts]}20	Expresses the temperature-sensitive GAL80 under the control of the alphaTub84B promoter	Bloomington (#7019)

2.1.3 Vector cloning

2.1.3.1 Genomic DNA (gDNA) Extraction

Extraction of gDNA from *Drosophila melanogaster* was conducted using the Invitrogen ChargeSwitch gDNA micro-tissue kit (Thermo-fisher, Massachusetts, USA). A lysis mix containing 0.5mL Lysis Buffer (L15) and 5µL Proteinase K per sample was prepared. 3-5 flies, containing the required UAS construct, are cooled on ice for 5-10 minutes, transferred to a 1.5mL Eppendorf and crushed with ~150µL of lysis mix using a sterile pipette tip, before adding the remaining lysis mix. The mix was inverted a few times before incubating at 55°C for two hours. Following incubation, 2.5µL RNase A was pipetted into the lysis mix, homogenised, and incubated at room temperature for 5 minutes. 20µL of ChargeSwitch magnetic beads were added to 100µL of Purification Buffer (N5) and the lysis mix, and pipetted up and down 5 times, before incubating for 1 minute at room temperature. The Eppendorf containing the mix is placed into a magnetic rack for 1 minute before removing supernatant with a pipette. The tube was then removed from the magnetic rack, and 0.5mL of Wash Buffer (W12) is added to resuspend the beads. The tube is then placed into the magnetic rack for 1 minute before removing and discarding any supernatant. This washing step is then repeated. The tube is removed from the magnetic rack and 100uL Elution Buffer (E5- Tris-HCl pH8.5 10mM) added, before pipetting up and down 10 times to resuspend the beads. The mix is incubated at room temperature for 5 minutes, agitating halfway through, before being placed in the magnetic rack for 1 minutes. After this, the eluate containing purified gDNA is removed and stored at -20°C until required.

2.1.3.2 Plasmid preparation for cloning.

For cloning of cDNA fragments of interest into vectors, a circular plasmid must be cut with two restriction digestion enzymes that are complimentary to those of the cDNA insert. To do this, a double digest reaction is set up in a PCR tube, including 2μg vector DNA, 5μl 10x CutSmart Buffer, 1μl XhoI, 1μl Xbal, made up to a 50μl solution with nuclease-free water. The reaction mixture was incubated at 37°C for 3 hours. 1μl Calf-intestinal Phosphatase (CIP) was added to the pUASt-attB prep, only, for 30 minutes at 37°C to dephosphorylate the 5' DNA ends. Reaction enzymes were then heat-inactivated at 65°C for 20 minutes.

2.1.3.3 PCR amplification of cDNA and plasmid fragments

PCR amplification was conducted using the Q5 High-Fidelity 2x Master Mix, following a protocol from New England Biolabs (https://neb.com). In a 100μl PCR tube, the following were assembled to make the PCR reaction mix: 25μl Q5 High-Fidelity 2x Master Mix, 2.5μl forward primer (10μM), 2.5μl reverse primer, template DNA at the concentration of 1μg from gDNA and 10ng for plasmid DNA, made up to 50μl with nuclease-free water. Table 2.2 outlines primers used for PCR in this thesis. The reaction mix was transferred to a thermocycler for routine PCR. The initial denaturation was conducted at 98°C for 30 seconds, followed by 30 cycles of denaturation (98°C for 10s), annealing (50-72°C for 30s) extension (72°C for 20-30s per 1kb). The temperature for annealing was calculated using the NEB Tm calculator. A final extension at 72°C for 2 minutes was completed before samples were stored at 4°C until required.

Table 2.2 Primer design for vector cloning

aa: amino acids; FWD: forward primer; REV: reverse primer. WT HTT: wild-type huntingtin, mHTT: mutant huntingtin.

Plasmid	Insert	Primer sequence	Digestive Enzyme
pB27	WT HTT 1-450aa	FWD: CTAGTGAATTCATGGCGACCCTGGAAA	ECoR1
		REV: TCATAGCGGCCGCTTCTTCTCCTAAGAGCA	Not1
pB27	mHTT 1-450aa	FWD: CTAGTGAATTCATGGCGACCCTGGAAA	ECoR1
		REV: TGTCGACTAGTGCAATACTCCCACTACGG	Spe1

pP6	FoxP1 1-300aa	FWD: CCAGGTGCACTAGTATGCAAGAATCTGGGACT	Spe1
		REV: TCTTAGGATCCAGGATGGCTATGGGGGT	BamH1
pP6	FoxP1 301-580aa	FWD: GCCTACGGATCCCTCTATGGACATGGTG	BamH1
		REV: GCTAGGCTCGAGACTATTCTCAGCCATT	XhoI
pP6	FoxP1 301-463aa	FWD: TCATAGCGGCCGCATATGGACATGGTGTAT	XhoI
		REV: GCGCACTCGAGAACTTCTGCGTTCTTATAAA	NotI
pP6	FoxP 464-580aa	FWD: TGGCACGGATCCTTAGACCACCATTTACATATGC	BamHi
		REV: ACGAGCTCGAGACTATTCTCAGCCATTG	XhoI
pP6	Mef2D 1-134aa	FWD: CTGCGACTAGTGATGGGGAGGAAAAGATT	SpeI
		REV: TATGACTCGAGCTTGTCCTCCAGCAGGGG	XhoI
pP6	Mef2D 1-350aa	FWD: CTGCGACTAGTGATGGGGAGGAAAAGATT	SpeI
		REV: ATTGCGGATCCCAAAGGCTGGTAAGGAGGA	XhoI
pP6	Mef2D 134-514aa	FWD: GAATCGAATTCGTCCCGGCCCCAACTT	ECoR1
		REV: TACTAGCGGCCGCTCACTTTAATGTCCAGG	NotI
pP6	Mef2C 1-134aa	FWD: CTGACGGATCCTTATGGGGAGAAAAAG	BamH1
		REV: CACTGCTCGAGACACAATCTTTGCCTG	XhoI
pP6	Mef2C 1-350aa	FWD: CTGACGGATCCTTATGGGGAGAAAAAG	BamH1
		REV: GACGTCTCGAGCCAGCCAGTTACTGAACCAA	XhoI
pP6	Mef2C 134-455aa	FWD: ACTATGGATCCTTGCTGTTCCACCTCCCA	BamH1
		REV: CGTATCTCGAGTCATGTTGCCCATCCTTC	XhoI
pUASt		FWD: CAACTACTGAAATCTGCCAAG	
		REV: CTCTGTAGGTAGTTTGTC	
PUASt	FoxP1-FL	FWD: TTACGCTCGAGATGCATCGGATACAT	XhoI
		REV: ACGGCTCTAGATTTGAGACCCACATAC	Xbal
pB27		FWD: CCAATTGTCGTTGACCTTCG	
		REV: AGCAACCTGACCTACAGG	
pP6		FWD: GACGGACCAAACTGCGTA	
		REV: AGCAACCTGACCTACAGG	

2.1.3.4 Gel extraction protocol (QIAGEN)

To gel extract cDNA fragments and cut plasmid preps, 10µl 6x purple loading dye was added to the 50µl reaction and loaded onto a 0.8% agarose Tris-borate-EDTA (TBE) gel. The gel was run in an electrophoresis tank for 1 hour at 75V. Upon completion, the cDNA band was visualised on a blue light box, cut from the gel using a scalpel, and placed into a 1.5ml Eppendorf tube for purification using the Qiagen gel extraction kit (QIAquick®). Buffer QG was

added at a ratio of 3:1 based on gel weight (μg) and incubated at 50°C for 10 minutes, or until the gel had fully dissolved. 1 gel volume of isopropanol was added to the solution and passed through a QIAquick spin column to adhere the cDNA to the resin within the column. 500μl buffer QG was passed through the spin column followed by 750μl buffer PE for washing. DNA was then eluted in 50μl of buffer EB.

2.1.3.5 PCR Purification

PCR purification was conducted using the standard QIAquick PCR purification kit protocol. 5 volumes of buffer PB was added to 1 volume of the PCR sample and placed in a QIAquick spin column and centrifuged for 1 minute. Waste was collected in a 2ml collection tube and flow-through was discarded. DNA was bound to the spin column and washed with 750μl buffer PE. Following centrifugation, flow-through was discarded, and the spin column was placed into a clean 1.5ml microcentrifuge tube. DNA was eluted in 50μl buffer EB (10mM Tris-Cl, pH 8.5). Purified DNA was analysed on a gel to determine concentration of the product and length of the DNA.

2.1.3.6 DNA ligation and transformation

Ligation of a pUASt attB plasmid prep and insert cDNA was conducted using the NEB ligation protocol (https://interantional.neb.com). Using the NEB ligation calculator, 20ng pUASt-attB and a concentration of cDNA insert or PCR product, as calculated at a 1:5 ratio, was added to a 20μl reaction mixture, including 2μl 10X T4 ligase bugger, 1μl T4 DNA ligase, made up to 20μl by adding nuclease-free water. The reaction mixture was incubated at room temperature for 1 hour followed by heat inactivation at 65°C for 10 minutes. 3-5μl of the ligation reaction mixture was transformed into 50μl DH5α competent cells and spread onto the LB agar plates with the appropriate antibiotic resistance.

2.1.3.6 Miniprep procedure (QIAGEN)

Following transformation of the ligation mix onto LB agar plates, single colonies are picked using a sterile pipette tip, placed into a 15ml falcon tube with 2ml LB broth (with the appropriate antibiotic resistance), and incubated in at 37°C overnight at 2-300 rotations per

minute (rpm). Following overnight incubation, bacterial cells are harvested by centrifugation at 6800xg in a table-top microcentrifuge for 3 minutes, at room temperature. The supernatant is removed, and bacterial cells are resuspended in 250μl Buffer P1. The resuspended cells are transferred to a 1.5ml microcentrifuge tube and 250μl Buffer P2 is added. 350μl Buffer N3 is also added to the microcentrifuge tube, and the mixture is immediately and thoroughly mixed by inverting the tube 4-6 times. The mixture is centrifuged for 10 minutes at 13,000rpm and 800μl of the supernatant is added to a QIAprep 2.0 spin column. Following centrifugation for 60s, the QIAprep column is washed by adding 0.5ml Buffer PB, followed by centrifugation for 60s and addition of 750μl Buffer PE. The spin column should then be centrifuged for 60s, twice, to ensure removal of all residual wash buffer. The DNA is then eluted in 50μl Buffer EB into a clean 1.5ml microcentrifuge tube. All plasmid minipreps are stored at -20°C.

2.1.4 Experiments using the Gal4/UAS system

2.1.4.1 Whole-eye expression of transgenes

To drive expression of transgenes in the whole-eye, the whole-eye driver, GMR-Gal4 is used. 10-15 virgin female GMR-Gal4 flies were crossed with male flies expressing the UAS-construct of interest and kept at 25°C throughout the entire experiment. At 0, 5, 7, 10, 12, and 15 days post-eclosion, unless otherwise stated in each chapter, the progeny were immobilised using CO_2 and orientated under a Leica MZFLIII microscope for visualisation and imaging. Images were taken at 10x magnification using a Nikon Coolpix 4500 (2002) and zoomed in electronically to produce better quality images. Progeny from fly crosses that showed significant results in terms of their effect on mHTT-induced neurodegeneration were collected and frozen at -20°C at 15 days post-eclosion for imaging using confocal microscopy. To drive expression of transgenes in the GMR-hHTTex1.Q120 line, an additional stock carrying the GMR-hHTTex1.Q120 and the Gal4 line (Elav^{c155}Gal4 or Appl-Gal4) were generated (Appl-Gal4; GMR-hHTTex1.Q120 or Elav^{c155}Gal4; GMR-hHTTex1.Q120). 10-15 females carrying the UAS construct of interest were taken and crossed with 3-5 males of the generated line. Crosses were maintained at 25°C throughout the entire experiment.

2.1.4.2 Pan-neuronal expression of transgenes

Pan-neuronal overexpression of transgenes was used to drive expression in the neurons for quantification of mHTT-induced neurodegeneration. To do this, the pan-neuronal Gal4 driver lines, Elav^{c155}Gal4 or Appl-Gal4 were used. 10-15 virgin females from the UAS transgenic lines were crossed with 5 males from the Elav^{c155}Gal4 stock, and crosses maintained at 21°C to increase the likelihood of flies eclosing. Upon eclosion, male and female progeny were collected in separate vials and maintained at 25°C to enhance transgene expression. At 2- and 1- one day prior to eclosion, and 0, 5, 7, 10, 12, and 15 days post-eclosion (unless otherwise states), flies were taken for quantification of rhabdomeres, using the protocol outlined by Song and colleagues (Song et al., 2013). Since Elav^{c155}Gal4 and Appl-Gal4 are located on the X chromosome, males from the progeny were used as an internal control.

2.1.5 Gal80^{ts}Gal4/UAS system for temporal control of transgene expression

In these experiments the Gal80^{ts} line (BL7019) was crossed with Elav^{c155}Gal4 flies to generate the fly line Elav^{c155}Gal4; Gal80^{ts}. Males from this stock were crossed with 10-15 virgin females with the desired UAS construct and maintained at 19°C. At these low temperatures, the flies develop normally and the GAL80 protein prevents Gal4/UAS expression, and the flies can develop normally (see Figure 3.5). To induce transgene expression, flies were placed at 30°C. Larval and pupa were removed from the side of the vials, into a fresh food vial, and placed in the 30°C incubator. Eclosed flies were separated into males and females and placed in the 30°C incubator. Flies were taken at 2 days and 1 day prior to eclosion, and 0, 5, 7, 10, and 12 days post-eclosion unless otherwise stated. Rhabdomeres were quantified using the method outlined by Song and colleagues (Song et al., 2013) (outlined in section 2.1.8).

2.1.6 Longevity assay

10-15 female flies expressing the UAS-transgene of interest were crossed with 3-5 male flies from the Elav^{c155}Gal4 stock and maintained at 21°C until eclosion. Upon eclosion, virgin female flies were housed at 25°C in vials containing a maximum of 10 flies. Flies were transferred to fresh food vials every 2-3 days, and the number of surviving flies recorded. An average of 100 flies per genotype were housed, overall. Survival results for each genotype were plotted using

the Online Application for Survival Analyses (OASIS) (Yang et al., 2011). This included the generation of a Kaplan-Meier plot and statistical analyses among survival datasets to determine significance. Longevity was carried out to determine survival of the following fly lines:

Elav>UAS-hHTTex1.Q93,

Elav>UAS-mCherry; hHTTex1.Q93,

Elav>UAS-hFoxP1; hHTTex1.Q93,

Elav>UAS-Mef2RNAi (BL38247); hHTTex1.Q93,

Elav>UAS-Q93-II,

Elav>UASQ93-II; Mef2RNAi (15550), and

Elav>Q93-II; Mef2RNAi(1429R1).

2.1.7 Whole-eye imaging

To obtain high quality images of the *Drosophila* whole-eye, flies were frozen on ice and stored at -20°C until required. When required, flies were defrosted under an LED light and stuck to a piece of double-sided tape, so that their body and wings were parallel with the surface of the slide. This allowed imaging of one eye per fly. Once orientated, the slide was placed under a confocal microscope, with a home-made LED ring surrounding the samples. This ensured that light was being projected from all angles of the fly and provided sufficient illumination for imaging. Eyes were imaged using a Yokogawa CSU-1X spinning disk confocal head which was attached to a Zeiss Axio Examiner upright microscope, fitted with a Zeiss Axiocam 712 Colour CMOS and Zeiss Axiocam 503 Mono CCD camera. Images were taken using a 10x objective lens with an eye-piece objective of 10x magnification, and 5μm sections were taken to produce a Z-stack, processed to a single composite image using the “Extended depth of focus” tool from Zen Blue Microscopy Software.

2.1.8 Pseudopupil image analysis

2.1.8.1 Quantifying rhabdomeres in the adult fly eye

The "pseudopupil" assay allows the quantification of degeneration, by visually quantifying the number of rhabdomeres in the *Drosophila* eye. Aged flies were immobilised on ice for 10 minutes and the flies were decapitated using microdissection scissors. Using forceps to grab the proboscis, the fly head was mounted onto a slide, into a blob of clear nail varnish to avoid movement. The head is positioned so that the eye is as close to parallel with the surface of the slide (see Figure 1.1). To visualise the rhabdomeres, the microscope slide was placed onto the stage of an Olympus BX50 microscope, with a condenser between the main light source and stage, concentrating the light through the eye of the fly. A drop of oil was added to the fly eye and the stage was slowly moved towards the 40x magnification objective, with an eye piece objective of 10x magnification. Closing the iris diaphragm to the approximate diameter of the size of the head allowed the light to focus through the objective, visualising the rhabdomeres. Looking down the light microscope allowed quantification of the rhabdomeres at the time of visualisation down the microscope. Any rhabdomere that was not seen as an intact circle was regarded as degenerated (Song et al., 2013). For each fly head, 20-30 ommatidia were counted and at least 10 fly heads were scored for each genotype. Following rhabdomere quantification, the sum of the total number of ommatidia with varying numbers of rhabdomeres was used to obtain an average for each condition and timepoint.

2.1.8.1 Quantifying rhabdomeres in the developing fly eye

Rhabdomeres are visible under a light microscope due to their ability to autofluorescence. In the eyes of flies that are two days prior to eclosion, and younger, it is not possible to visualise the rhabdomeres in this way. Instead, fly heads were bisected and fixed in 3.7% formaldehyde for 25-30 minutes at room temperature, before being washed 3 times in 0.5% PBTx, and 3 times in 1x PBS. Sample components outlined in Table 2.3. Fixed samples were mounted in O.C.T medium and frozen in liquid nitrogen. Samples were stored at -80°C until ready for use. Samples were sectioned to 10μm thickness using the Cryostat Bright OTF500 and mounted onto Super Frost microscope slides. Sections were washed in 0.5% PBTx for 3 minutes,

followed by a 30-minute incubation and 3x 5-minute washes. Sections were then incubated for 30 minutes in 3% Bovine Serum Albumin (BSA) (in 0.5% PBTx).

Primary antibodies were prepared by dilution into 3% BSA (150µl per slide) (Figure 2.4) Coverslips were placed on top of the primary antibody solution and incubated in a humidity chamber at room temperature, overnight. Following overnight incubation, coverslips were removed, and sections were washed in 0.5% PBTx and coverslips removed. Secondary antibodies were then prepared in 3% BSA and added to the sections (Table 2.4). Coverslips were placed on top of the secondary antibody and incubated in the dark for 2 hours in a room temperature humidity chamber. Following incubation, coverslips were removed, and sections were washed for 5-minutes in 0.5% PBTx and 5-minutes in 1x PBS. Slides were air-dried and sections mounted with 100µl mounting media (50% glycerol in 1x PBS). Sections are cover slipped, sealed with nail varnish, and stored in the fridge (covered), prior to imaging.

Sections were imaged using an LSM800 confocal microscope. Rhabdomeres were visualised using a 40X oil objective lens for counting of rhabdomeres. Any images taken were taken under the same 40X oil objective and 1.5µm sections were taken to produce a Z-stack.

Table 2.3 Contents of buffer solutions required for cryosection of fly heads.

Buffer	Components
3.7% Formaldehyde	1ml 37% formaldehyde, 9ml 0.5% PBTx
1 x PBS	100 ml 10x Phosphate Buffer Saline, 900ml distilled H2O
0.5% PBTx	25ml Triton, 475ml 1x PBS
3% BSA	3g Bovine Serum Albumin, 100ml 0.5% PBTx
O.C.T.	Optimum Cutting Temperature Embedding Medium

Table 2.4. Antibodies used in immunostaining of *Drosophila*.

Antibody	Species	Concentration	Supplier	Catalogue number
Anti-GFP	Chicken (IgY)	1:500	Abcam	EPR14104
Anti-Elav	Rat (IgG)	1:20 Larvae 1:100 pupa/adults	DSHB	7E8A10
Phalloidin-555	-	1:140	Cytoskeleton	029
DAPI	-	1:1,000	Thermofisher	YK4113231
Alexafluor-488	Anti-chicken (IgY)	1:400	Jackson Immunoresearch	162189
Alexafluor-594	Anti-Rat (IgG)	1:400	Invitrogen	A-11007
Hoerchst	-	1:3,000	Abcam	33258

2.1.9 Fly eye-brain complex dissection

2.1.9.1 larval eye-brain complex dissection

3rd instar larvae (L3) are transferred from a vial into ice cold 1x PBS and dissected with guidance from already-published protocols (Hafer & Schedl, 2006). The larval body is torn in half with forceps, and the posterior portion discarded. The anterior portion of the larvae is moved 'inside-out' to expose the remaining CNS, including the eye-antennal imaginal disc and the larval brain. Any cuticle and remaining fat are removed.

2.1.9.2 pupa and adult eye-brain complex dissection

Pupal and adult eye-brain complexes were dissected in 1x PBS using a published protocol (Williamson & Hiesinger, 2010). For adult dissections, flies were immobilised on ice for 10 minutes, whilst for pupal dissections, pupa are removed from the vial using forceps and placed onto a dish under a dissecting microscope. The head is removed from the body, and the head submerged in 1x PBS. The connective tissue between the proboscis and eyes of the fly head as well as the retinal tissue and cuticle is removed. Once the eye-brain complex is visible, the

remaining trachea and cuticle can be removed, and the now fully exposed eye-brain sample is ready for fixation and staining.

2.1.9.3 Immunostaining of eye-brain complexes

The staining protocol for larval, pupal, and adult eye-brain complexes was provided by Ines Do Lago E Baldaia at University College London. Eye-brain complexes were fixed in 4% formaldehyde for 20-25 minutes at room temperature and rinsed 3x in 0.5% PBTx followed by incubation in 0.5% PBTx for more than 1 hour. Eye-brain complexes were then transferred into primary antibodies, diluted in 5% donkey serum in 0.5% PBTx and incubated for two nights, at 4°C. Primary antibodies include anti-GFP (1:500) and anti-Elav (1:20 pupa and adult complexes, 1:100 larval brains) (Table 2.4). Following primary antibody incubation, eye-brain complexes were rinsed three times in 0.5% PBTx, incubated in 0.5% PBTx for more than 1 hour at room temperature. 0.5% PBTx is then removed, and eye-brain complexes are then incubated in secondary antibody, diluted in 5% donkey serum in 0.5% PBTx, for two nights, at 4°C. Secondary antibodies include Alexafluor-488 and Alexafluor-594 (Table 2.4). Samples were also stained with DAPI (1:1,000) or Hoerchst (1:3,000), diluted in 5% donkey serum in 0.5% PBTx for visualising cell nuclei. Finally, eye-brain complexes were rinsed in 0.5% PBTx at room temperature, left to rest in 0.5% PBTx for over an hour, and then rinsed and stored in 1x PBS prior to mounting. Samples are then removed from 1x PBS, mounted in VectorShield and oriented prior to coverslipping. Clear nail varnish is used to prevent removal of the coverslip.

2.2 Yeast-2-Hybrid

Yeast stocks were stored indefinitely at -80°C, in a 30% glycerol stock. To refresh these stocks, yeast was streaked onto YPD agar (Foremedium, CCM0102) in a 90mm petri dish using a sterile inoculating loop and grown at 30°C for 2-3 days.

The haploid L40ΔGal4 (MATahis3-$\Delta 200$ trp1-901 leu2-2,122 ade2 lys2-801 am-gal4::LanMX6 LYS2::(LexAop)4-HIS3 URA3::(LexAop)8-LacZ) yeast cells were grown on YPD agar for 48 hours at 30°C. Once grown, a single colony was picked using a sterile inoculating loop, and added to 15ml of YPAD broth (Foremedium, CCM1002) in a 50ml falcon tube. A control sample of 15ml YPAD (no yeast) was also made. The screwcap is left loosely to allow aeration into the tube

and placed into a 30°C agitation incubator at 200rpm for 12-16 hours. Following incubation, a spectrophotometer is used to determine the concentration of the culture. The optical density at 600 (OD_{600}) of each sample is calculated by subtracting the value of the control culture from that of the yeast culture. An OD_{600} of 0.1 corresponding to ~$1x10^6$ cells/ml. The culture was then diluted back to a $2.5x10^6$ cells/ml concentration in a glass conical flask containing 50ml of YPAD and incubated at for 4-4.5 hours in a 30°C agitation incubator at 200rpm. Following this incubation, the concentration of the culture is determined. The culture is centrifuged in a 50ml falcon tube for 5 minutes (3000g) and the resulting pellet of cells is washed twice in 2ml of 1x TE (1:10 dilution of 10xTE, Fisher, BP2475-100). After each wash, the culture is centrifuged at 3000g for 3 minutes. The washed pellet of cells is suspended into LA (LiOAc, pH7.5 (Sigma –Aldrich, L4158-100G) at a resulting concentration of $2x10^9$ cells/ml.

A 2ml Eppendorf tube is set up for each construct to be transformed, including a negative control that contains no plasmid. Each Eppendorf tube contains the following, in order: 200µl cells, 20µl of 10 mg/ml denatured salmon sperm carrier DNA, 4µl 5x TE/LA, 2.2µg plasmid DNA to be transformed, and 1.2ml LAP (10xTE in 50% w/v polyethylene Glycol 3350 (Sigma-Aldrich, 2022444-250G) in distilled water). The transformation mixture is incubated at 30°C in an agitation incubator at 150-160rpm for 30 minutes. Following incubation, 140µl Dimethyl sulfoxide (DMSO) (Sigma, D8418-50ML) is added to each tube, and heat shocked at 42°C for 15 minutes. Each tube is inverted 4-5 times every 5 minutes. Following heat shock, each tube is immediately placed on ice for 2 minutes, then placed in a microcentrifuge at 10,000rpm for 60s. The resulting pellet of cells is re-suspended in 200µl 1xTE and 50µl of cells is pipetted and spread using sterile glass rods onto the appropriate agar plates (Table 2.5) Plates were incubated at 30°C for 2-3 days (YPD plates) or 3-4 days (drop-out plates) to allow for slower growth due to lack of amino acids (Table 2.6).

This method was used repeatedly to transform bait and prey proteins into L40ΔGal4 yeast cells in a sequential manner. Firstly, the bait proteins were transformed into yeast cells and grown on DO1-tryptophan plates. Following this, prey proteins were transformed into an L40ΔGal4-bait-colony, and grown on DO2 (-leucine, -tryptophan) plates to select yeast colonies containing both plasmids. Table 2.6 outlines plasmid preps used to test in the yeast-

2-hybrid assays. Yeast colonies from DO2 plates were then streaked onto DO3 (-leucine, -tryptophan, -histidine) plates to test for physical protein interactions. The transformation was undertaken according to the protocol below. It was important that before use, any glassware used for incubating yeast cultures was washed and rinsed for 1 hour in Decon 90 detergent. Following this, glassware was rinsed 5x with tap water and 3x with distilled water prior to autoclaving with 100ml distilled H2O for >15 minutes at 121°C. The full protocol is outlined below.

Table 2.5. Plates made for testing yeasts-2-hybrid interactions.

Plate type	Contents	Experimental outcome
YPD	70g YPD Agar (Foremedium, CCM0102) in 1L distilled H2O.	Growth on YPD confirms presence of yeast cells.
DO-1 Trp	6.9g Yeast nitrogen base without amino acids (Foremedium, CYN0401), in 1L distilled water. 740mg drop-out -tryptophan (Foremedium DCS0141), 2% Agar (Foremedium, AGA02) and 2% filter-sterilised D-glucose (Foremedium, GLU2).	Growth on DO-1 -Trp confirms the presence of pB27 plasmid.
DO-1 -Leu	6.9g Yeast nitrogen base without amino acids in 1L distilled water. 590mg drop-out -leucine (Foremedium, DCS0091), 2% Agar and 2% filter-sterilised D-glucose	Growth on DO-1 -Leu confirms the presence of pP6 plasmid
DO-2	6.9g Yeast nitrogen base without amino acids in 1L distilled H20. 1546mg Kaiser drop-out 2 (Foremedium, DSK172), 2% Agar, 2% filter-sterilised D-glucose.	Growth on DO-2 confirms the presence of pB27 and pP6 plasmid.
DO-3	6.9g Yeast nitrogen base without amino acids in 1L distilled H20. Kaiser drop-out 3(Foremedium, DSCK424), 2% Agar, 2% filter-sterilised D-glucose.	Growth on DO-3 confirms a protein-protein interaction.

Table 2.6. Plasmids generated to test for yeast-2-hybrid protein-protein interactions.

Plasmid	Protein	Species	Fragment Size (amino acids)	Source of the protein
pB27	Mutant Huntingtin (Q51)	Human	1-450	Addgene (#111734)
pB27	Wild-type Huntingtin (Q23)	Human	1-450	Addgene (#111723)
pP6	Mef2C	Mouse	1-350	Host laboratory.
pP6	Mef2C	Human	1-350	Mef2C cDNA clone from Genscript (#0060600485)
pP6	Mef2C	Human	134-455	Mef2C cDNA clone from Genscript (#0060600485)
pP6	Mef2C	Human	1-134	Mef2C cDNA clone from Genscript (#0060600485)
pP6	Mef2D	Human	1-350	Mef2C cDNA clone from Genscript (#0060600485)
pP6	Mef2D	Human	134-515	UAS-Mef2D fly line (gDNA extraction)
pP6	Mef2D	Human	1-134	UAS-Mef2D fly line (gDNA extraction)
pP6	Foxp1	Human	1-301	UAS-Mef2D fly line (gDNA extraction)
pP6	FoxP1	Human	301-580	Addgene (#153145)
pP6	FoxP1	Human	301-463	Addgene (#153145)
pP6	FoxP1	Human	464-580	Addgene (#153145)

2.3 Mouse

2.3.1 Mouse husbandry

All mouse experiments were conducted in compliance with the UK Animals (Scientific Procedures) Act 1986 under Home Office Licence Project No. PP7595333, with the approval

of the local Cardiff University Ethics Review Committee. All mice were housed in standard cages, in holding rooms under a 07:00 – 19:00 light-dark cycle in an ambient room temperature of 24 ± 2°C, and a humidity of 55%. Mice had ad libitum access to food and water, and were weighed and health-checked weekly, with more frequent monitoring during testing.

2.3.2 Mouse lines

The R6/1 (B6.Cg-Tg(HDexon1)61Gpb/J) mouse line was obtained from Charles River, UK, and is the primary Huntington's Disease mouse line used in all behavioural experiments within the project. The HdhQ150 mouse was also obtained from Charles River UK, and brain tissue available in the host laboratory was used for histological analysis. The Gsx2-Cre^{+} Mef2C$^{fl/fl}$ (B6;CBA-Tg(Gsx2-icre)1Kess/J Mef2Ctm1Jjs/J) mouse line was generated by previous PhD student, Dr Ali (Ali, 2022).

2.3.2.1 Mef2C floxed mouse line

The Mef2C loxP/loxP (Mef2C$^{fl/fl}$) mouse line was a gift from Eric Olson's lab at the University of Texas. In this line, the two loxP sites are oriented in the same direction and flank the *Mef2C* coding exon 2. This means that following cre recombination, exon 2 of the gene is excised.

2.3.2.2 Gsx2-cre mouse line

The Gsx2-cre line was originally generated by (Kessaris et al., 2006). Gsx2, formally Gsh2, is expressed in multiple regions along the anterior-posterior axis of the CNS, earliest in the telencephalon at E9.5, and is critical in establishing LGE identity (Deacon et al., 1994; Qin et al., 2016). Gsx2 expression was found to be required for striatal neurogenesis between E11-E16, and is expressed in the ventricular zone progenitors of the LGE and MGE in a high-dorsal to low-ventral gradient manner (Ali, 2022; Kessaris et al., 2006). The Cre line was generated using P1 artificial chromosome (PAC) transgenic mice that expresses a cre recombinase under the control of Gsx2, using 110kb of genomic DNA (Fogarty et al., 2005; Kessaris et al., 2006).

2.3.2.3 Breeding strategy to generate R6/1Gsx2-Cre^{+} Mef2C$^{fl/fl}$ line

The *Mef2C* conditional knockout mouse colony was generated by a previous PhD student in the laboratory, methods of which are detailed in her PhD thesis (Ali, 2022). First, Gsx2-Cre^{-}

Mef2C$^{fl/fl}$ females were crossed with males, positive for the R6/1 transgene, to generate litters that were all heterozygous for the Mef2C floxed allele (Mef2C$^{fl/+}$), negative for the Gsx2-Cre and positive or negative for the R6/1 transgene. An R6/1Gsx2Cre^{-}Mef2C$^{fl/+}$ male was then crossed to a Gsx2-Cre^{+}Mef2C$^{fl/fl}$ female to generate litters with different combinations of Gsx2-Cre presence, Mef2C$^{fl/fl}$, Mef2C$^{fl/+}$ alleles, positive or negative for the R6/1 transgene (Table 2.7).

2.3.2.4 Breeding strategy to maintain R6/1 Gsx2-Cre^{+} Mef2C$^{fl/fl}$ line

To maintain the colony, R6/1Gsx2Cre^{-}Mef2C$^{fl/fl}$ or R6/1Gsx2-Cre^{-}Mef2C$^{fl/+}$ mice were crossed with Gsx2-Cre^{+} Mef2C(fl/fl) or Gsx2-Cre^{+}Mef2C$^{fl/fl}$ mice. It is important that male mice were negative for cre recombinase to avoid deletion of Gsx2 from the testes. Table 2.7 outlines the mouse lines and experimental groups used in this project.

Table 2.7. Mouse lines used in this thesis.

fl/fl = homozygous for the Mef2C LoxP sites. fl/+ = heterozygous for the Mef2C LoxP sites.

Experimental Group	Presence of Cre	Presence of R6/1 transgene	Presence of Mef2C LoxP sites
Wild type	-	-	fl/fl or fl/+
R6/1	-	+	fl/fl or fl/+
R6/1Cre^{+}Mef2C$^{fl/fl}$	+	+	fl/fl
Cre^{+}Mef2C$^{fl/fl}$	+	-	fl/fl

2.3.2.5 Genotyping

Mice were weaned at 21-28 days of age and genotyped by taking an ear notch sample. Samples were placed in a 96-wellplate, provided by Transnetyx, which were sent to Transnetyx for genotyping (https://www.transnetyx.com).

2.3.3 Behavioural testing

All behavioural tests were carried out at 6-, 8-, 12- and 16-weeks of age.

2.3.3.1 Balance beam

The balance beam allows for testing fine motor coordination and balance (Luong et al., 2011). The beam is 100cm long with a flat surface that is 12mm in width at the bottom, and 6mm at the top, to increase difficulty. A black box is placed at the end of the beam, acting as the endpoint of the experiment and has nesting material from the mouse cage to attract the mouse to this point. The beam is placed ~50cm above a tabletop with soft bedding towels overlaying the area. A video camera is set up to record the performance so that further analysis can be completed following the experiment. Prior to testing at 6 weeks of age, the mice are allowed to acclimatise to the room and the beam, by placing them at the top of the beam, encouraging them to enter the black box. Once the mouse has clearly identified the black box as a 'safe zone', the mouse is placed further away and encouraged to make their way to the endpoint of the beam. Following training, and at each testing timepoint, mice are subject to three trials. At the beginning of each trial, the mouse is placed facing away from the black box, and the time taken to turn is measured. At this time, the timer is reset, and the time taken to reach the end of the beam is measured. During this time, the number of forelimb and hindlimb foot slips is counted. The apparatus is cleaned of mouse droppings and wiped with 70% ethanol before the next experiment begins. The time taken to reach the black box is measured, and in the case of a failed trial, i.e. not reaching the end of the box within 2 minutes, the length at which the mouse traversed, is noted.

2.3.3.2 Rotarod

The rotarod test is often used in testing of mouse models of neurodegeneration to detect deficits in motor coordination and balance (Hamm et al., 1994; Wagner et al., 2008). The rotarod was set at two different settings to text the ability of the mice to move at an increasing speed and at a fixed speed. In the accelerating rotarod, the moving cylindrical platform (Ugo Basile, Varese, Italy) rotates at a gradually accelerating speed (5-40 rpm over 300 seconds). On the first day of testing (at 6 weeks), mice were allowed to acclimatise to the equipment before completing two successive trials per day, over three days. The latency for mice to fall off the rotarod was measured. In the fixed rotarod, the cylindrical platform rotates at a constant speed of 12rpm for 300 seconds. The latency for the mice to fall in the first 60 seconds was noted, as well as the number of times the mouse falls from the rotarod over the

300 second period. Again, this experiment was over three days, with two successive trials on each day.

2.3.3.3 Inverted grip strength test

This test is used to measure the strength of the fore- and hind-limbs (Deacon, 2013) by calculating the time the mouse can grasp onto the under-surface of a metal grid without falling. The metal grid was inverted and placed over a 30cm height with bedding towels placed beneath to soften any falls. The latency to fall within one-minute was recorded.

2.3.3.4 Vertical Pole

The vertical pole is another test of fine motor movement and tests the mice ability to travel down a 30cm vertical pole (Fleming & Chesselet, 2005). Mice were subject to a training trial at 6 weeks, followed by two test trials at each experimental age, which were averaged.

2.3.3.5 Open Field

Open Field is one of the most commonly used platforms to measure normal activity of animal models (Seibenhener & Wooten, 2015), and uses an overhead video tracking software, Ethovision (Noldus), to record a number of exploratory parameters. The open field arena is 80 x 80cm and mice were allowed to explore the arena during a 5-minute test period. Data were collected automatically via the Ethovision software for later analysis. Parameters analysed included: total distance moved (cm); mean velocity (cm/s); total duration of movement (s); and frequency of rearing.

2.3.4 Histological analysis

2.3.4.1 Perfusion

At 16 weeks of age, all mice were terminally anesthetised via intraperitoneal (i.p) administration of 0.3ml of 0.2mg/ml sodium pentobarbital (Dolethal), and subsequently, transcardially perfused to obtain adult mouse tissue for histological analysis. To do this, mice were perfused with ice-cold pre-wash solution (di-sodium hydrogen phosphate (dihydrate)

and sodium chloride in distilled water, pH7.3) for 2 minutes, followed by 6 minutes of 4% paraformaldehyde (PFA in pre-wash solution, pH7.3) (Table 2.8). Whole brain tissue was removed and post-fixed in 4% PFA for 4 hours and preserved at room temperature in 25% sucrose solution in pre-wash (Table 2.8). Brains were cut coronally in 30μm sections on a freezing sledge microtome (Leitz, Wetzlar), in a 1:12 series and stored indefinitely at -20℃ in a 48-wellplate with antifreeze (sodium dihydrogen phosphate, di-sodium hydrogen orthophosphate anhydrous, ethylene glycol and glycerol in distilled water).

2.3.4.2 Free-floating Immunohistochemistry (IHC)

One well of brain sections from each 1:12 series (per animal) is placed into individual pots and washed in tris-buffered saline (TBS) to remove the antifreeze (Tris-base and sodium chloride in distilled water, pH7.4). To allow for good antigen retrieval of the tissue, sections were treated with citrate buffer (pH 6.0) in a 70°C water bath for 30 minutes (Table 2.8). Once cooled, the sections were then washed in TBS and transferred to a quenching solution for 5 minutes (30% hydrogen peroxide H_2O_2, 10% methanol in distilled water) to reduce endogenous peroxidase activity. During all incubation periods, pots were placed on an orbital shaker to allow full access of the solutions to the tissue. Sections were then washed 3 times in TBS, for 10 minutes. To block non-specific binding, sections were incubated in a blocking solution of 3% normal serum (NS) in TXTBS (0.2% Triton-X-100 in TBS) for 1 hour, prior to overnight primary antibody incubation in 10% NS in TXTBS at room temperature (Table 2.9). Triton-X-100 was added to PBS to allow for good permeabilisation. On the following day, sections were washed 3 times in TBS, for 10 minutes at room temperature, before being placed in a secondary antibody solution (1% NS in TBS) for 3 hours. (Table 2.10). Following 3x10 minute washes in TBS, an avidin-biotin complex (Vectastain ABC HRP kit, PL-4000) kit (1:200 concentration) was placed on the sections for 2 hours; the kit was premixed according to the manufacturer's instructions 30 minutes prior to application to allow binding of the complex. Sections were then washed 3x 10 minutes in TBS followed by 2x10 minutes in TRIS non-saline (TNS) followed by overnight storage at 4°C in TNS (Trisma-base in distilled water, pH7.4). Immuno-positive cells were made visible via incubation of chromogen 3-3'-diaminobenzadine (DAB, Sigma) solution. 2mL DAB was made up in 40ml TNS and further

diluted to a 1:5 concentration in fresh TNS and 12µl 30% H_2O_2 which was placed onto sections for 10-30 minutes, depending on the intensity of the staining. The time of required DAB incubation required was noted and maintained for each primary antibody for consistency. To stop the reaction, sections were washed thoroughly in TNS, followed by TBS, and kept in TBZ (TBS with 0.02% sodium azide) until mounted. All sections were mounted onto double-subbed 1% gelatinised slides (Thermo Scientific, Menzel Gläser) and air-dried overnight. The following day, air-dried slides were dehydrated in an industrial methylated spirit (IMS) ethanol ladder of increasing concentration (70%, 95%, 100%), prior to clearing in xylene solution to remove fat cells in the tissue. Slides were then cover slipped using distyrene plasticiser and xylene mounting medium (DPX) and dried for at least 24 hours in a fume hood, before storing.

Table 2.8 Buffers and their components for storage and staining of mouse tissue

Buffer	Components
0.1M Phosphate Buffered Saline (Pre-wash)	90g Di-sodium hydrogen orthophosphate, 45g Sodium Chloride, 5L distilled H2O, pH 7.3 with Orthophosphoric acid.
4% paraformaldehyde (PFA)	40g Paraformaldehyde powder, 1L pre-wash, dissolved for 2-3 hours on a heated stirrer, and overnight at room temperature. pH 7.3, with NaOH/orthophosphoric acid.
25% Sucrose	22.92g Di-sodium hydrogen phosphate dihydrate, 18g Sodium Chloride, 250g sucrose, 950ml distilled H2O. pH 7.4
Citrate Buffer	58.8gm/1 Sodium citrate, 42.02 gm/1 citric acid. pH 3-6.2.
4x Tris Buffered Saline (TBS)	96g TRIS base, 72g Sodium Chloride, 2L distilled H2O, pH 7.3
1x TBS	500ml 4xTBS, 1.5L distilled H2O. pH 7.3
0.05M Tris non saline (TNS)	6g TRIS base, 1L distilled H2O, pH 7.4 with HCL
Tris Buffered Saline + Sodium Azide (TBZ)	2.5ml 5% Sodium azide stock solution, 500ml 1x TBS
Anti-freeze	5.4g di-sodium hydrogen orthophosphate anhydrous, 1.57g Sodium dihydrogen phosphate, 400ml distilled H2O, pH 7.3. 300ml Ethylene glycol, 300ml glycerol.

Table 2.9. Primary antibodies used for mouse immunohistochemical staining

Primary Antibody	Species	Concentration	Serum	Supplier	Catalogue Number
FoxP1	*Rabbit*	*1:500*	*Goat*	*Abcam*	*AB16645*
NeuN	*Mouse*	*1:2,000*	*Horse*	*Millipore*	*MAB377*
DARPP-32	*Mouse*	*1:1,000*	*Horse*	*Santa Cruz*	*SC271111*
MW8	Mouse	1:1,000	Horse	DHBS	MW8

Table 2.10. Secondary antibodies used for mouse immunohistochemical staining.

Secondary Antibody	Species	Concentration	Serum	Supplier	Catalogue Number
SB3	Anti-Mouse (Rat absorbed) IgG biotinylated	1:200	Horse	VectorLabs	BA2001
SB7	Anti-Rabbit IgG biotinylated	1:200	Goat	VectorLabs	BA1000

2.3.5 Imaging and quantification of histology

2.3.5.1 Stereological analysis

Cell counts were obtained from the entire striatum via stereological sampling, using the Visiopharm integrator system (VIS, version 4.4.6.9). Whole slides were imaged and a SuperImage captured at 1.25X objective lens using a Leica DFC520 Camera using the Leica Application Core V3.6 software, which was attached to a Leica DM6b microscope. The auto-sampling module with field correction using this software allowed for regions of interest (ROIs) to be defined by manually drawing around the entire striatum in each brain section. The striatal sections were randomly sampled from a grid using a consistent step length, with cells counted manually under 20X objective lens and 10x eye-piece objective. A 1,000μm^2 counting frame was used with cells being counted if they sat within the frame or touched the green lines. Those touching the red lines or sitting outside the frame were excluded (Figure 2.1).

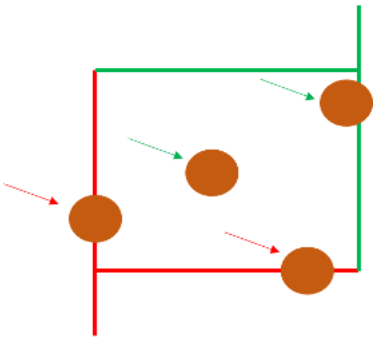

Figure 2.1. Stereological sampling method.
Illustration of cells that are included or excluded from 1,000μm^2 counting frame. The red arrows indicate cells that would be rejected; green arrows indicate those that are accepted.

The total number of cells (C) for each striatal section was calculated using the following formula: $C = (\sum c \times (\sum n \times a)) \times f$,

Where:

C = estimated total number of cells

$\sum c$ = total number of cells counted

$\sum A$ = sum of all striatal areas

$\sum n$ = total number of frames allocated to the included striatal area

a = area of sampling user grid (1,000μm^2)

f = frequency of sectioning (6)

x = multiplication

To determine an estimate for the total striatal volume of R6/1 and HdhQ150 mice, as well as their wild-type littermates, the striatal area was manually drawn around using the SuperImage generated using the Leica Application Core V3.6 software microscope. Five anatomically matched striatal sections from rostral to caudal were analysed and the striatal volume was calculated using the formula: $V = (\Sigma a * M)/f$

Where:

V = Volume,

a = area (mm2),

M = section thickness (40µm)

f = frequency of sampled sections (1:6)

2.3.5.2 Manual cell counting using ImageJ

Manual cell counting was conducted using ImageJ Software (http://imagej.nih.gov). Three images of the lateral, medial, and ventral regions of the striatum were taken at 10x magnification and uploaded to the ImageJ Software. Using the cell counter plugin, individual cells were selected, and the Software kept a record of the total number of cells.

2.3.5.3. Automated cell counting using ImageJ

Automated cell counting was conducted using the ImageJ Software (http://imagej.nih.gov/ij/download/html). Three images of the lateral, medial, and ventral regions of the striatum were taken at 10x magnification and uploaded to the ImageJ Software. Images were converted to 16-bit greyscale, and threshold adjusted to highlight all cells (Figure 2.3). Once all cells were highlighted, application of the threshold created a binary version of the image with two-pixel intensities: black = 0 and white = 255. Where multiple cells were merged, it was possible to accurately cut within 1 pixel thickness for counting (Process → Binary → Watershed). Upon completion, analysis was conducted using the 'Analyse Particles' tab, to obtain a total number of cells within the image. For MW8 immunostaining, 20x total magnification images were taken but the same process applied (Figure 2.2).

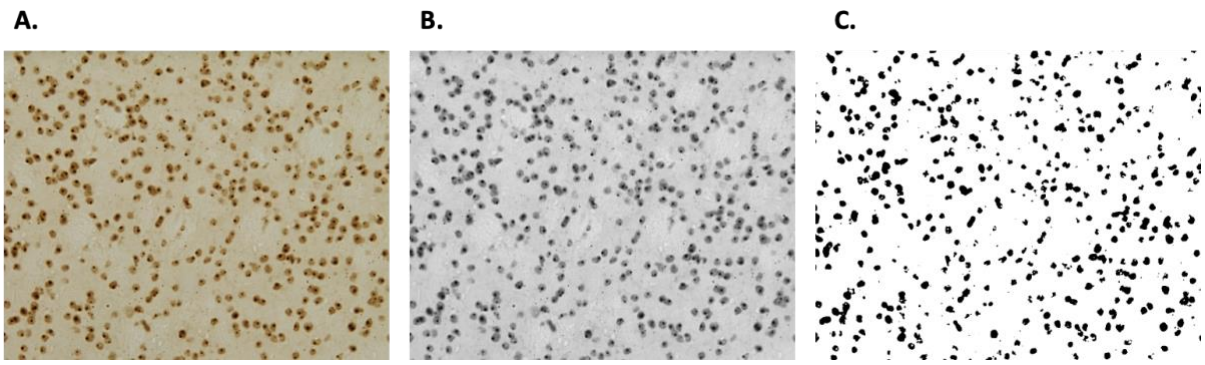

Figure 2.2 Automated cell counting using ImageJ.
A) Original 20X magnification image of MW8 staining in R6/1 striatum. B). Images are converted to 16-bit greyscale, and C) threshold applied to create a binary version of the image for cell quantification.

2.3.5.4 Optical density for protein expression quantification

Optical Density (O.D.) measures were used to determine protein expression of FoxP1 positive nuclei using the ImageJ Software (https://imagej.nih.gov/ij/download.html). 20x magnification images were taken of the lateral, ventral and medial sections of the striatum (Figure 2.4). Mean grey values were measured for 8 FoxP1-positive nuclei and 3 background (control) areas on each striatal image where there are no stained cells (Figure 2.3). An average cumulative mean grey value was calculated for the FoxP1-positive nuclei, and an average value calculated for the background. A final O.D. value was calculated for wild-type and R6/1 mice by subtracting the average background value from the average FoxP1-positive value.

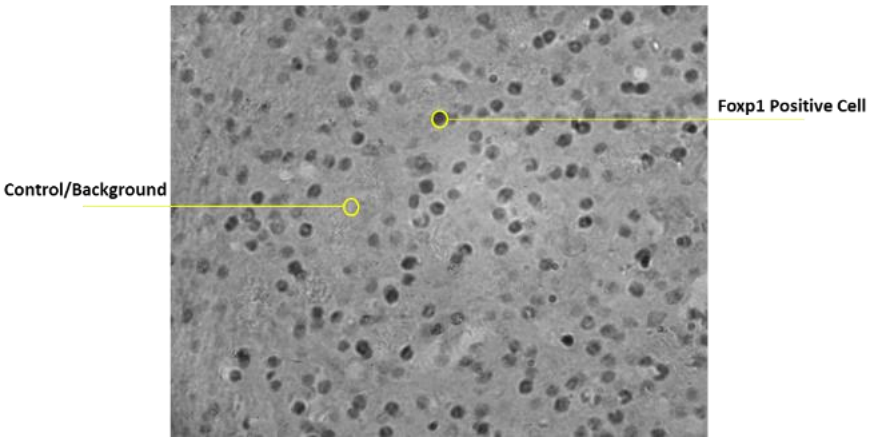

Figure 2.3. Optical density measures of FoxP1 positive nuclei
20x magnification image of the striatum to show method for optical density measures of FoxP1 positive nuclei. FoxP1 positive nuclei can be identified as dark, circular regions. Control regions were chosen based on lack of stained nuclei.

2.4 Statistical analysis

SPSS V 29.0.2.0 and RStudio were used to carry out statistical analysis of all data. For analysis of rhabdomere counts in *Drosophila*, multivariate analysis was used to determine significant effects of genotype and time with regard to rhabdomere loss. For fly survival analysis, the log rank test was used to determine statistical significance between genotypes. For mouse experiments, G*Power v3.1.9.4 was used to conduct a power analysis for determination of sample number. To do this, data was taken from the results of rotarod behaviour of $Cre^{+}Mef2C^{fl/fl}$ mice compared with wild-type littermates (Ali, 2022). Specifically, the mean and standard deviation for each genotype was used to determine Cohen's D (1.64133) which was subsequently used with and α probability of 0.05, power of 0.95, and an allocation ratio of 1/1 to determine the sample number required in the experiment. Sample size required in each group came to 11. For statistical analysis of mouse behavioural data, a univariate ANOVA was used with Genotype as a factor and Sex as a co-variate. Bonferroni was used to correct for multiple comparisons. For histological analyses, an independent samples t-test was used. In all cases, significance was assumed if $p<0.05$.

Chapter 3: Downregulation of *Mef2* in a *Drosophila* model of Huntington's Disease (HD) can suppress mHTT-induced degeneration.

3.1 Introduction

The *Drosophila* melanogaster is an effective model system for studying the mechanisms associated with neurodegenerative disease and has been a long established model of HD (Lin et al., 2019). As discussed in Section 1.3.2.2, the binary Gal4/UAS system can be used to modulate gene expression with spatial and temporal specificity, to investigate molecular interactions within subpopulations of cells, which in turn, can provide insight into the mechanisms associated with gene interactions in disease (Krench & Littleton, 2013). With regard to HD, the *Drosophila* eye can has been used to show that expression of mHTT leads to progressive mHTT-induced degeneration of the eye, which can be visualised under light microscopy and quantified statistically (Bilen & Bonini, 2005; O'Rourke et al., 2013; Zhang et al., 2009). Additionally, the tissue-specific expression of genes has allowed for studying the effects of mHTT in other cells, and identifying potential disease modifiers for suppression of disease progression (Kaltenbach et al., 2007; Lin et al., 2019; Warrick et al., 1999).

In 2007, Kaltenbach and colleagues conducted an extensive yeast-2-hybrid (Y2H) screen to investigate potential HTT protein interactors and explore whether any of these interactants may be genetic modifiers of HD degeneration (Kaltenbach et al., 2007). Amongst these physical interactants, *Mef2D* was identified as a physical interactor with the first 450 amino acids (aa) of wild-type and mutant HTT (mHTT) protein. Kaltenbach and colleagues then used a *Drosophila* model of HD to investigate whether any interactors could suppress disease progression. The whole-eye driver, GMR-Gal4 was used to induce expression of the N-terminal HTT fragment, with 128 CAG repeats (GMR>UAS128Qhtt), and expression of Df(2R)X1, which has a chromosomal deletion of the 46C1-7 region: this region includes the single *Drosophila Mef2* gene. Deletion of this chromosomal region in a model of whole-eye mHTT expression partially rescued a degenerative phenotype, showing increased retinal thickness and decreased vacuolisation, compared with HTT expression, alone (Kaltenbach et al., 2007).

Mammalian *Mef2C* has been identified as an essential gene implicated in brain development and biological processes of the CNS. This includes its role in protecting neurons from apoptotic cell death in addition to controlling synapse formation which has been implicated in hippocampal-dependent learning and memory (Assali et al., 2019; Barbaro et al., 2015; Ana C. Barbosa et al., 2008a, 2008b; A. C. Barbosa et al., 2008; Li et al., 2024; Okamoto et al., 2000). As a result, *Mef2C* is of particular interest to this project. There is 90-98% and 70-90% conservation in the N-terminal MADS and MEF2 domains, respectively, of the 4 mammalian Mef2 proteins and the *Drosophila* Mef2 protein. Thus, using the *Drosophila* to explore how manipulating *Mef2* and *Mef2C* in a mHTT-induced model of HD may provide an insight into their roles in this process, both in terms of development of neurons, and degeneration of cells (Malwina Lisek et al., 2023) (Figure 1.4).

Whilst Kaltenbach and colleagues were able to show that removing the chromosomal region 46C1-7 from the *Drosophila* genome which includes the *Mef2* gene, is sufficient to suppress a mHTT-induced whole-eye phenotype, there isn't any published research that has specifically knocked down only *Mef2*. Neither is there much information regarding *Mef2* expression in the developing and adult eye-brain complex, which would provide further understanding on where *Mef2* is being downregulated. In this chapter, I will first establish a baseline for phenotypes associated with mHTT-induced degeneration before investigating whether knocking down the endogenous *Mef2* gene in these *Drosophila* models of HD is responsible for suppressing the mHTT-induced phenotype. I will achieve this by using the whole-eye driver GMR-Gal4, and pan-neuronal driver, ELAV^{C155}-Gal4. I will also use this method to over-express *Drosophila Mef2*, and human *Mef2C* to investigate whether these proteins can independently affect mHTT-induced degeneration. Additionally, I want to investigate the potential developmental effects of *Drosophila* with expression of mHTT. I will use the GAL80-Gal4/UAS system to drive expression of mHTT before and after PR development, to understand the extent of mHTT-induced degeneration, before unpicking whether *Mef2* may impact on these processes. Finally, I will explore the *Mef2* expression profile in the *Drosophila* larval and pupal eye-brain complex, in addition to conducting Y2H experiments to start to unpick potential mechanisms for the role *Mef2* might play in mHTT-induced degeneration.

3.2 Methods

3.2.1 Experimental Design

The first experiment aimed to investigate the extent of degeneration in a whole-eye and pan-neuronal model of HD. To do this, the whole-eye driver, GMR-Gal4, and the pan-neuronal driver, ELAV^{C155}-Gal4 were used to induce expression of mHTT with 93 (Q93) and 120 (Q120) CAG repeats in the whole-eye and neurons, respectively. Since the ELAV^{C155}-Gal4 driver is on the X-chromosome, virgin females carrying the UAS-constructs were used which meant that male progeny could serve as controls in the experiment. For the full experimental method, refer to Section 2.1.4. Additionally, the Gal80^{ts}Gal4/UAS system was used to investigate the effect of inducing mHTT at various times throughout development of the eye, and in the fully developed eye.

Following this, RNAi lines for *Mef2* knockdown were used to investigate the effect of downregulating *Mef2* in a whole-eye (GMR>Mef2RNAi; hHTTex1.Q93) and pan-neuronal (Elav>Mef2RNAi; hHTTex1.Q93) model of HD. Additionally, constructs expressing *Mef2* and human *Mef2C* were used to investigate the effects of over-expressing *Drosophila Mef2* or human *Mef2C* on whole-eye and pan-neuronal mHTT-induced degeneration. As an extension of this work, the Gal80^{ts}Gal4/UAS system was used to determine whether *Mef2* downregulation at different timepoints during eye development could influence mHTT-induced degeneration. In this work a multiple comparisons analysis was used to determine any statistically significant changes in rhabdomere counts under different conditions. Statistical significance was reported when $p<0.05$.

To fully understand any effects from *Mef2* manipulation in a mHTT-induced model, the next experiment looked to investigate the pattern of *Mef2* expression in the developing eye-brain complex, including the PRs. To do this, the Mef2GFP line was used to immunostain whole mount eye-brain complexes for the presence of *Mef2*. Anti-GFP was used to stain for the GFP tag that is present on the endogenous *Mef2* C-terminus. Flies were taken at L3 larval and early-, mid- and late-pupal stages, to determine the presence of *Mef2* in the brain, and developing

PRs of the *Drosophila* eye. Furthermore, Y2H assays were used to investigate potential physical interactions between *Mef2C* and HTT.

3.3 Results

3.3.1 Whole-eye expression of mHTT induces a degenerative phenotype

This section aims to determine the degenerative phenotype seen in flies with expression of mHTT. Previous studies have reported degeneration in these models using the eye (Kaltenbach et al., 2007; Louis Sam Titus et al., 2017; Warrick et al., 1999). Prior to moving on to new analysis, it is important to establish the mHTT lines used in this thesis, in these experimental assays. To do this, the first approach was to use the whole-eye driver, GMR-Gal4, to induce expression of the human HTT exon 1 fragment with 93 CAG repeats (Q93), in all cells of the eye (Li et al., 2012). Flies were assessed every day post-eclosion to determine a phenotype. In flies expressing Q93, there was visible degeneration of the eye compared with the control eye, which was clear by 15 days post eclosion. This was imaged using confocal microscopy (Figure 3.1A/B). To test the effect of whole-eye degeneration on a more aggressive HD model, GMR-Gal4 was used to drive expression of the human HTT exon 1 fragment with 120 CAG repeats (Q120). At 15 days, there was more visible degeneration compared with the degeneration seen when Q93 was expressed in all eye cells (Figure 3.1C). To conclude, expressing mHTT in the whole-eye can induce a degenerative phenotype, that is visible under confocal microscopy.

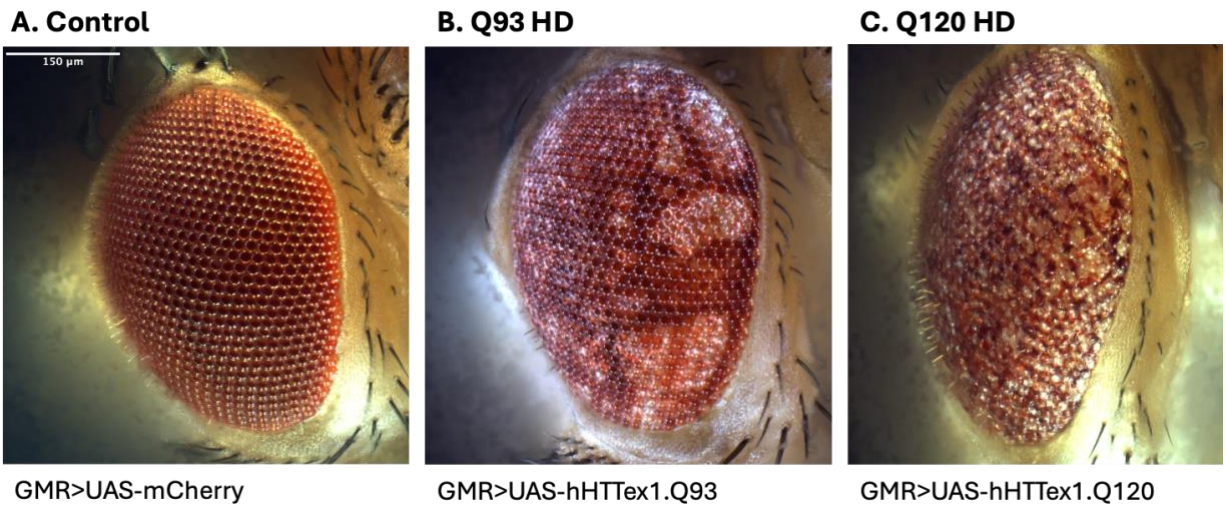

Figure 3.1 whole-eye expression of mHTT shows a degenerative phenotype.
Representative confocal microscopy images of flies expressing GMR-Gal4. A) Image of a control eye with whole-eye expression of mCherry. B) Whole-eye expression of mHTT with 93 CAG repeats showed degeneration of the eye. C) Whole-eye expression of mHTT with 120 CAG repeats showing a greater amount of degeneration. Scale bar: 150µm.

3.3.2 Pan-neuronal expression of mHTT results in loss of rhabdomeres

The previous experiment used the whole-eye driver, GMR-Gal4, to induce expression of mHTT in all cells of the eye, including neurons, support cells, and glia (Mishra & Sprecher, 2023). Neural degeneration is the main documented effect of expanded CAG repeats in human HD (Jurcau, 2022), so the next experiment focused on assays that affect mHTT in neurons of the *Drosophila* eye model system. To do this, the pan-neuronal driver ELAV^{C155}-Gal4 was used to induced Q93 expression only in the neurons. To assess the extent of degeneration in this, and subsequent genetic interaction experiments, it was important to have a quantifiable assay. This was to count the number of rhabdomeres seen under light microscopy (Figure 3.2A; Section 2.4.3 for methodology). Rhabdomere counts were taken from the day of eclosion, through to 15 days post-eclosion. There were significantly fewer rhabdomeres in the flies expressing Q93 compared with control flies (Group*Time $F_{5,95}$ = 13.022, p<0.001) (Figure 3.2Bi). Upon eclosion, the average rhabdomere count of Q93 expressing flies was 5.5, compared with 6.9 in the control flies (p<0.001). By 15 days post-eclosion, rhabdomere counts had reduced to 4.4 compared with 7.0 in the control flies (p<0.001) (Figure 3.2Bi). Another mHTT line with 93 CAG repeats (Q93-II) was also used. Pan-neuronal expression of Q93-II also

showed significantly reduced rhabdomeres in the eye compared with the control flies (Genotype*Time: $F_{5,73}$ = 8.646, p<0.001) (Figure 3.2Bii). Upon eclosion, the average rhabdomere count of flies expressing Q93-II was 6.1, and by 15 days post-eclosion, had reduced to 4.6 rhabdomeres. To conclude, these experiments show that pan-neuronal mHTT expression leads to significantly fewer rhabdomeres in the eye, compared with control flies.

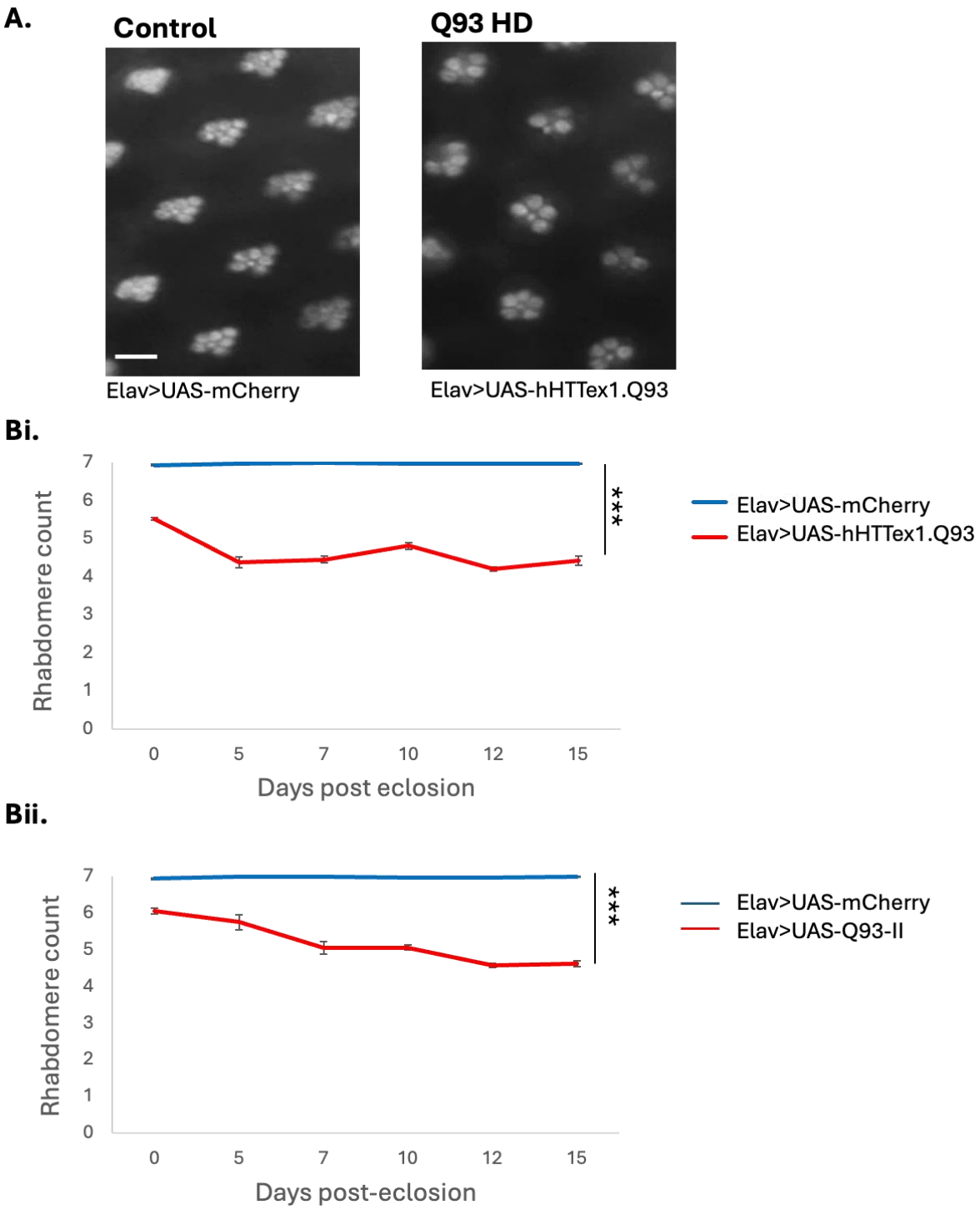

Figure 3.2. Pan-neuronal expression of mHTT leads to significant rhabdomere loss.
A). Images taken under light microscopy to show the extent of rhabdomere loss at 15 days post eclosion. Pan-neuronal expression of mHTT (Q93) using ELAV^{C155}-Gal4, led to significantly fewer rhabdomeres, which was quantified using pseudopupil analysis (B). Rhabdomeres were counted from the day of eclosion, to 15 days post-eclosion. There were significantly fewer rhabdomeres in flies expressing Q93 (Bi) and flies expressing Q93-II (Bii) compared with control flies (Q93, Genotype*Time: $F_{5,95}$ = 13.022, p<0.001, Q93-II, Genotype*Time: $F_{5,73}$ = 8.646, p<0.001). ***p<0.001. Scale bar in (A) = 10μm.

3.3.3 Pan-neuronal expression of mHTT reduces fly survival

The next question was to determine whether pan-neuronal expression of mHTT influenced fly survival. To do this, longevity assays were performed. The ELAV^{C155}-Gal4 driver was used to induce expression of mHTT. Upon eclosion, flies were placed into fresh food vials every two days, and the number of surviving flies recorded. Pan-neuronal expression of mHTT using the Q93 (UAS-hHTTex1.Q93) model led to significantly reduced fly survival compared with control flies (Log rank test: t-ratio$_{252}$ = -0.693, p<0.001) (Figure 3.3A). Pan-neuronal expression of mHTT using another mHTT line with 93 CAG repeats (Q93-II) also significantly reduced fly survival (Log rank test: t-ratio$_{271}$ = 11.892, p<0.001) (Figure 3.3B).

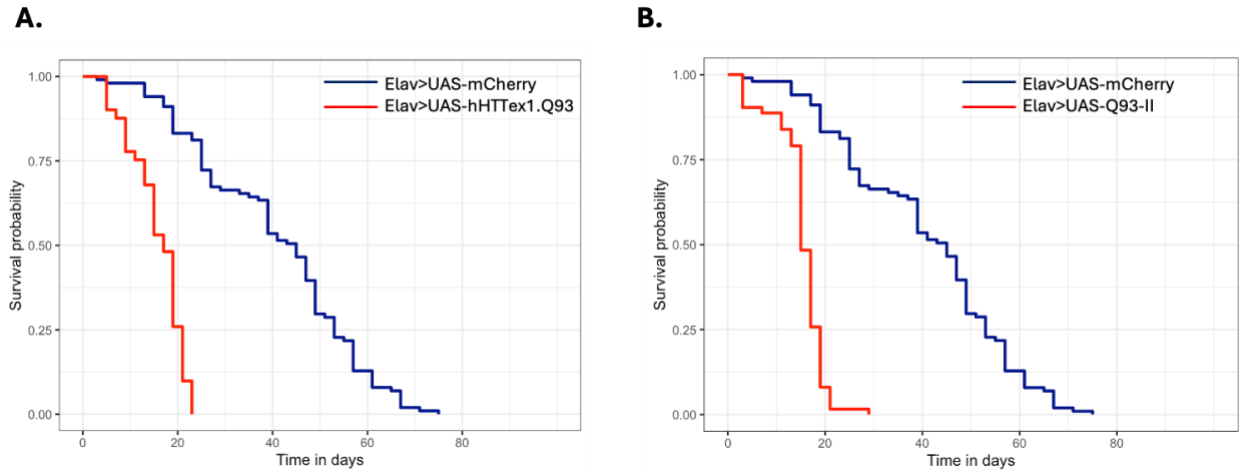

Figure 3.3 Pan-neuronal expression of mHTT reduces fly survival.
Kaplan Maier plots to show the survival of flies expressing mHTT, compared with control flies. A). Pan-neuronal expression of mHTT using the Q93 (UAS-hHTTex1.Q93) model led to significantly reduced fly survival compared with control flies (Log rank test: Q93, t-ratio$_{252}$ = -0.693, p<0.001) B) Pan-neuronal expression of mHTT using another mHTT line with 93 CAG repeats (93-II) significantly reduced fly survival (Log rank test: t-ratio$_{271}$ = 11.892, p<0.001).

3.3.4 In the presence of mHTT, rhabdomeres develop but subsequently degenerate

In the previous section, it was shown that there is already a significant loss of rhabdomeres in the Q93-expressing flies, compared with wild-type flies at the time of eclosion (p<0.001). This is a common observation in the literature but is not commented on (Kaltenbach et al., 2007; Louis Sam Titus et al., 2017; O'Rourke et al., 2013; Song et al., 2013). A possible explanation

is that the rhabdomeres develop normally, but they quickly degeneration in pupal life, prior to eclosion. Alternatively, the rhabdomeres do no develop in the first place. The literature states that by 100 hours from formation of the prepupa (day -2), the retinal lattice has been established and photoreceptors that the rhabdomeres equate to begin to project their axons toward the optic lobe. By 130 hours (day -1), lens and retina formation is considered to be complete (Cagan & Ready, 1989) (Table 3.1).

To investigate whether the rhabdomeres develop, flies were removed from the pupal case at 2- and 1-day prior to eclosion for rhabdomere quantification in the same pan-neuronal ELAV^{C155}-Gal4 Q93 model. At day -2, it was not possible to count rhabdomeres using the light microscope "pseudopupil" method due to the lack of autofluorescence to clearly see the rhabdomeres. Therefore, for day -1 flies, rhabdomeres were quantified using light microscopy, but phalloidin staining of cryosections had to be used to quantify the rhabdomeres at day -2 (Figure 3.4). At day -2, the rhabdomeres were clearly visible, and appeared to look fully developed with a compact complement of 7 rhabdomeres (Figure 3.4A). This correlated with what was seen in the wild-type day -2 eye (Figure 3.4A). At day -1, rhabdomeres were larger than those visualised at day -2 in both genotypes and had 7 rhabdomeres. However, the rhabdomeres in flies expressing Q93 appeared slightly less organised (Figure 3.4, yellow arrow) compared with the wild-type fly eye (Figure 3.4A, red arrow). When quantified, there was no difference in rhabdomere number between flies expressing Q93 and control flies at day -2 (Q93 = 6.9 +/- 0.04, control = 6.9 +/- 0.02, p=1.00). However, at day -1, there were significantly fewer rhabdomeres in the Q93 expressing flies, compared with control flies (Q93: 6.4 +/- 0.1, control = 6.9 +/- 0.04, p=0.009) (Figure 3.4B). This section has shown that the normal number and arrangement of rhabdomeres develop in the Q93-expressing flies, but subsequently there is degeneration.

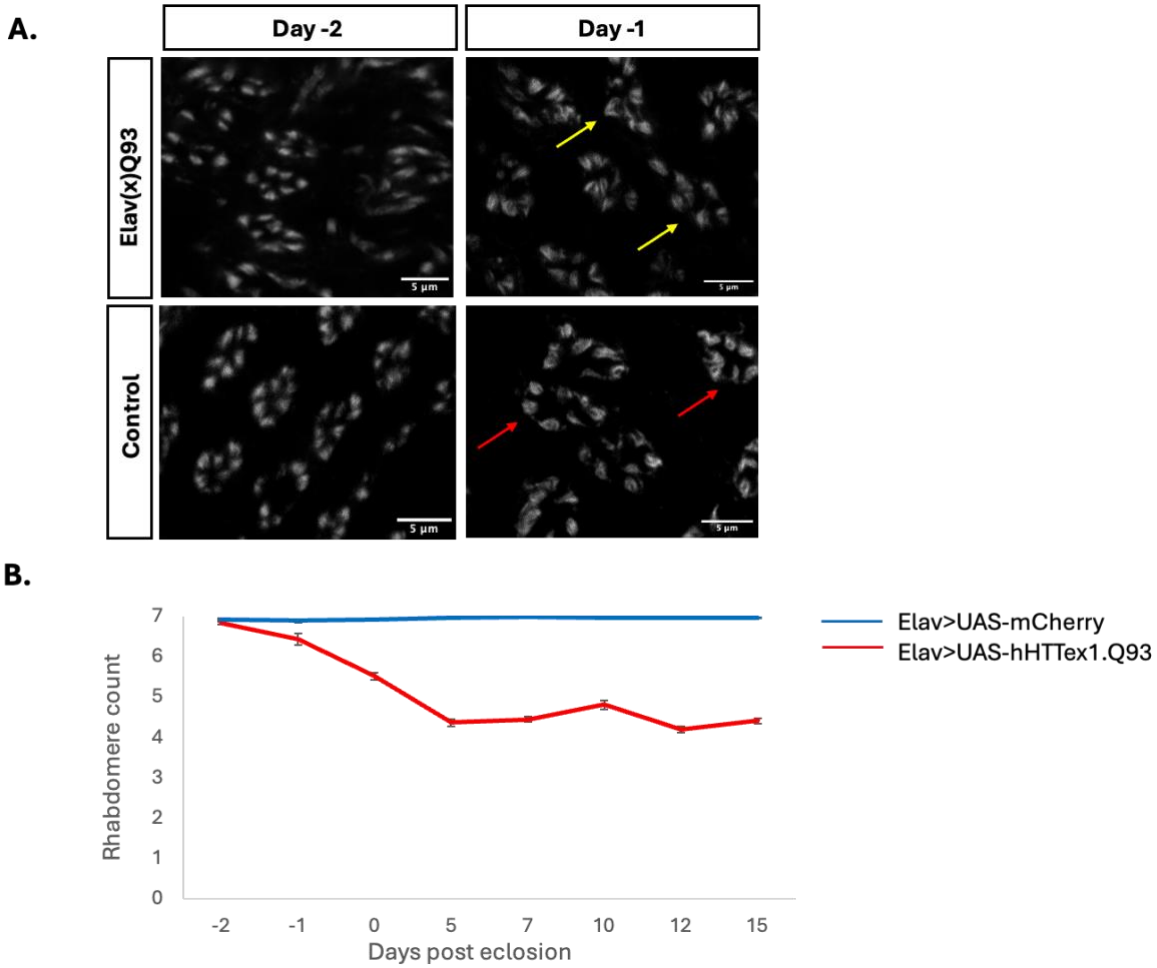

Figure 3.4. Flies expressing mHTT develop the wild-type number of rhabdomeres.
Image panel showing rhabdomeres of control and Q93 mHTT-expressing flies as imaged using phalloidin staining. At day -2, the rhabdomeres of wild-type and Q93-expressing flies look similar and appear to be fully developed. At the day -1, the rhabdomeres expressing Q93 look less organised (yellow arrow) than control rhabdomeres (red arrow) but appear to have 7. B) Graph representing the average rhabdomere counts from figure 3.2 with the addition of day -2 and day-1 post-eclosion. At day -2, Q93-expressing flies have the same number of rhabdomeres compared with control flies. At day -1, Q93-expressing flies have significantly fewer rhabdomeres than control flies. Data in this graph is the same as in Figure 3.2 with the addition of timepoint day -1 and day -2.

3.3.5 Early mHTT expression leads to increased mHTT-induced degeneration.

The previous section showed that rhabdomeres expressing mHTT do develop but begin to degenerate prior to eclosion. The next question was to ask whether inducing mHTT expression at later timepoints would lead to wild-type numbers of rhabdomeres at eclosion, which would

subsequently degenerate. To do this, one can manipulate the GAL4/UAS system used in previous experiments by introducing the temperature inducible GAL80^{ts} to temporally control the Gal4-induced transgene expression (Barwell et al., 2023; Matsumoto et al., 1978). In this system, at low temperatures (19°C) the GAL80 protein is bound to GAL4, inhibiting transgene expression, but at the permissive temperature of 29°C or above, GAL80 unbinds due to instability of the protein, repression is relieved, and the UAS target gene can be expressed (Figure 3.5).

In this experiment, flies expressing Q93 (Elav; Gal80^{ts}>UAS-hHTTex1.Q93) were kept at 19°C until ready for induction of Q93 expression. Flies were transferred to 30°C at the L3 larval stage (L3), prepupa (PP), three-days prior to eclosion (D-3), two-days prior to eclosion (D-2), one-day prior to eclosion (D-1), on the day of eclosion (D0), and one-day post-eclosion (D1). Temperature affects the activity of the Gal4/UAS system, independently of any Gal80^{ts} or similar component. Therefore, to compare these Gal80^{ts} experiments with the pan-neuronal Q93 expression from the embryo stage onwards that was used in previous experiments, these control flies were kept in the same temperature regime: flies were kept at 19°C then moved to 30°C at the time of eclosion. Table 3.1 outlines these timepoints. Rhabdomere counts were made from 1-day prior to eclosion, to 12-days post eclosion, except for L3 and PP flies, where counts were taken to 10-days post eclosion, due to early fly death.

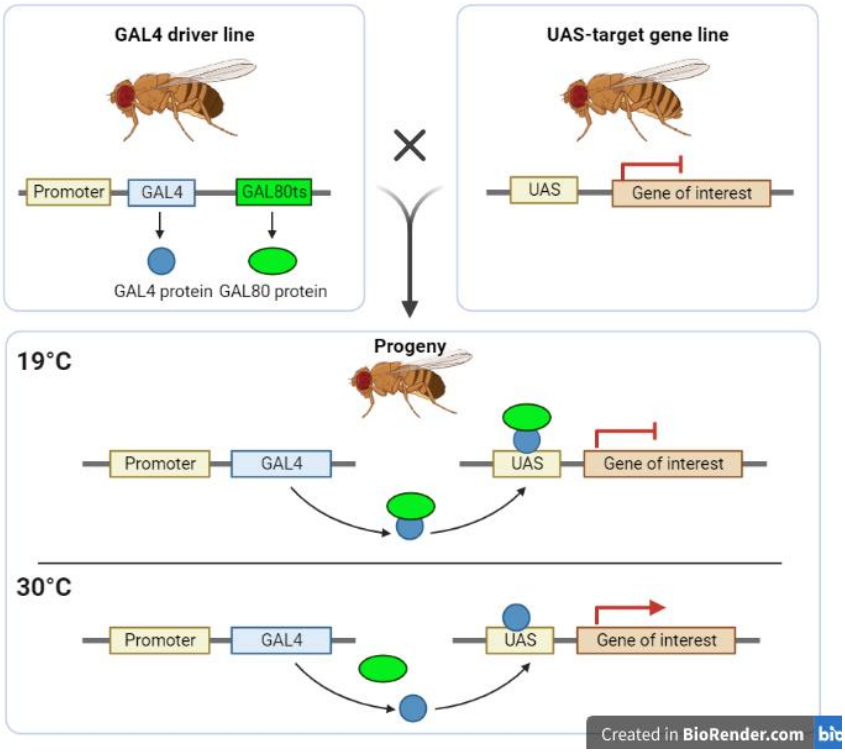

Figure 3.5. Schematic diagram of the temperature inducible GAL80ts, Gal4/UAS system.
At low temperatures, the GAL80 protein is bound to GAL4, inhibiting transgene expression. At temperatures above 29°C or above, the GAL80 protein unbinds, allowing GAL4-UAS binding and subsequent transgene expression. This schematic was made using biorender.

Table 3.1. Stages of eye development that expression of mHTT is induced.

Table outlining the various timepoints that mHTT expression is induced and how far through eye development this equates.

Labelled timepoint	***Hours from formation of prepupa***	***Percentage through pupal development (%)***	***Stage of eye/rhabdomere development***
L3 larvae (L3)	-48	-	~26 rows of ommatidia have emerged with a full complement of photoreceptors.
Prepupa (PP)	0	0	Midway through morphogenetic furrow (MF). By hour 10, the MF is complete.
Day -3 (D-3)	50	31.25	The cellular architecture of the eye is complete and the hexagonal lattice of ommatidia has emerged.
Day -2 (D-2)	100	62.5	The retinal lattice has been established, the rhabdomeres have formed, and the axons of photoreceptors are about to migrate through to the optic lobe.

Day -1 (D-1)	130	81	Lens formation is complete and the pseudocone begins to form. By this timepoint the retina is virtually complete.
Day 0 (D0)	160-180	>100	The eye is fully formed, and the fly has eclosed from the pupal case. Adult: 0 days old.
Day 1 (D1)	185-200	>100	Fully formed adult fly.

Strikingly, induction of pan-neuronal expression of Q93 at D0 (eclosion) led to significantly less rhabdomere degeneration compared with Q93-induced expression throughout development of the fly (Elav>UAS-hHTTex1.Q93) (Genotype*Time $F_{4,110}$ = 5.614, p<0.001) (Figure 3.6A). With this crossing regime, rhabdomeres had already begun to degenerate by the time of eclosion (Elav>UAS-hHTTex1.Q93: 6.0 +/- 0.1, Elav; Gal80ts>UAS-hHTTex1.Q93(D0): 7.0 +/- 0.01, p<0.001), and continued to degenerate to 4.7 by 12-days post-eclosion (p<0.001). This indicates that mHTT expression in the neurons of the fully formed, young adult fly results in limited rhabdomere loss. However, by contrast, inducing Q93 expression at the PP stage resulted in a pattern of degeneration similar to that of the control Elav>UAS-hHTTex1.Q93 fly line. There was a small, but significant difference between the two genotypes (Genotype*Time $F_{4,72}$ = 4.253, p=0.004) (Figure 3.6B) Post hoc analysis revealed that at eclosion and 5 days post-eclosion, flies expressing Q93 at PP timepoints had fewer rhabdomeres compared with the flies with Q93 expression throughout development (p<0.001) (Figure 3.6B).

When comparing onset of mHTT expression from L3 to Day 1, there was a significant difference in rhabdomere number between genotypes (Genotype*Time $F_{32,379}$ = 6.025, p<0.001). Interestingly, the rate of degeneration appears to increase when neurons are pre-exposed to mHTT at earlier timepoints (Figure 3.7). Post-hoc analysis revealed that there was no difference in rhabdomere counts of flies where mHTT was expressed at L3 or PP stages (p>1.00). Flies in these two experimental categories had significantly more rhabdomere degeneration compared with flies where mHTT was expressed at D-3, D-2, D-1, D0 and D1, from the day of eclosion (p<0.001) (Figure 3.7). To conclude, this section has shown that expressing mHTT in the young adult fly results in relatively little rhabdomere loss, but that

early pre-exposure to mHTT has a significant impact and increase vulnerability to mHTT-induced rhabdomere loss that occurs around the time of eclosion.

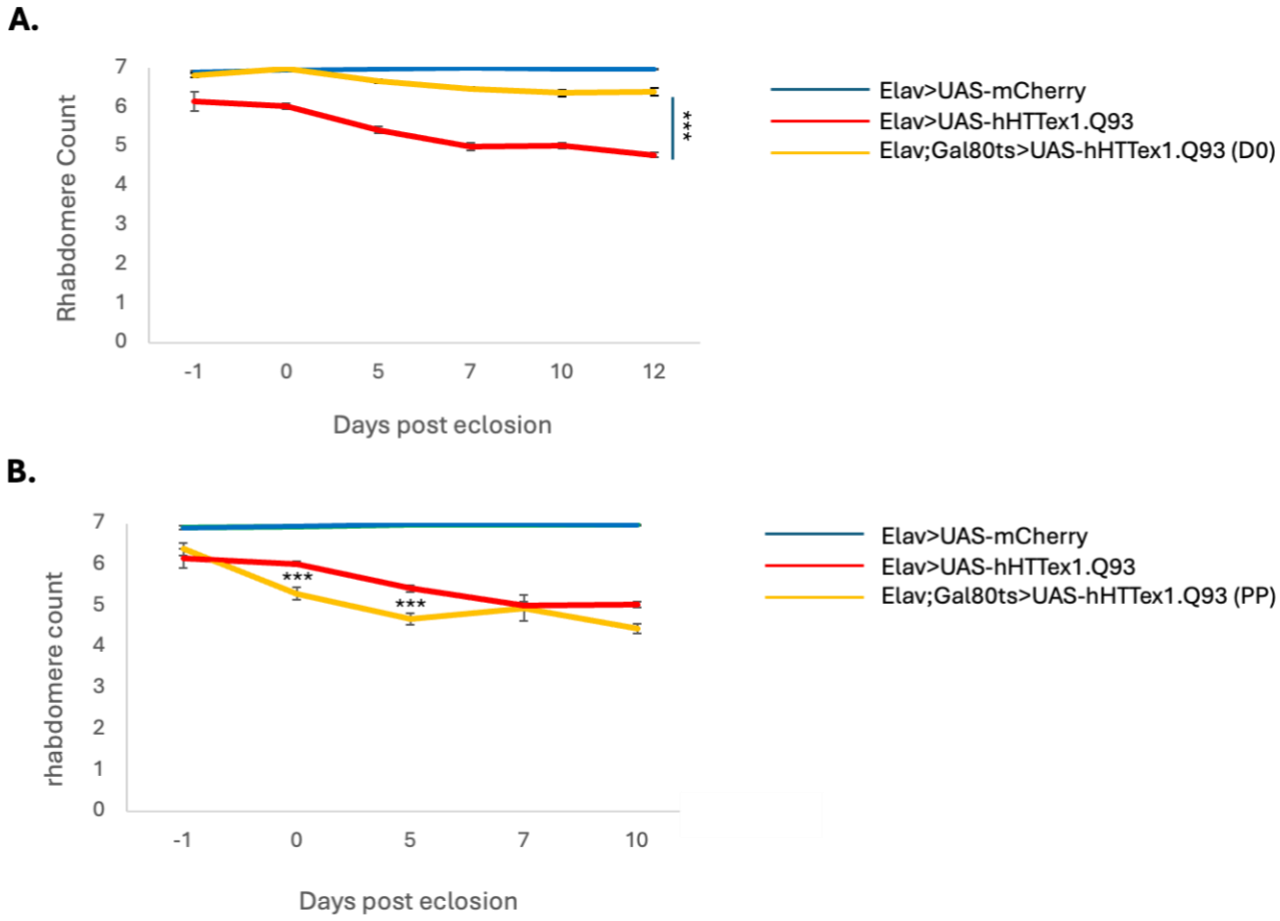

Figure 3.6. Early pre-exposure to mHTT increases rhabdomere degeneration.
A) Graph to show that induction of mHTT expression on the day of eclosion, using ElavGal4; Gal80ts driving UAS-hHTTex1.Q93, shows relatively little degeneration across time, and this is significantly less compared with when mHTT is expressed throughout development of the fly (Genotype*Time $F_{4,110}$ = 5.614, p<0.001). B) Graph representing the change in rhabdomere count across time, when mHTT is induced at prepupa (PP) compared with expression via the pan-neuronal ELAV^{C155}-Gal4. There is a difference between the two genotypes across time (Genotype*Time $F_{32,379}$ = 6.025, p<0.001), and flies with mHTT expression at PP, have significantly fewer rhabdomeres at day 0 and day 5. **p<0.01, ***p<0.001.

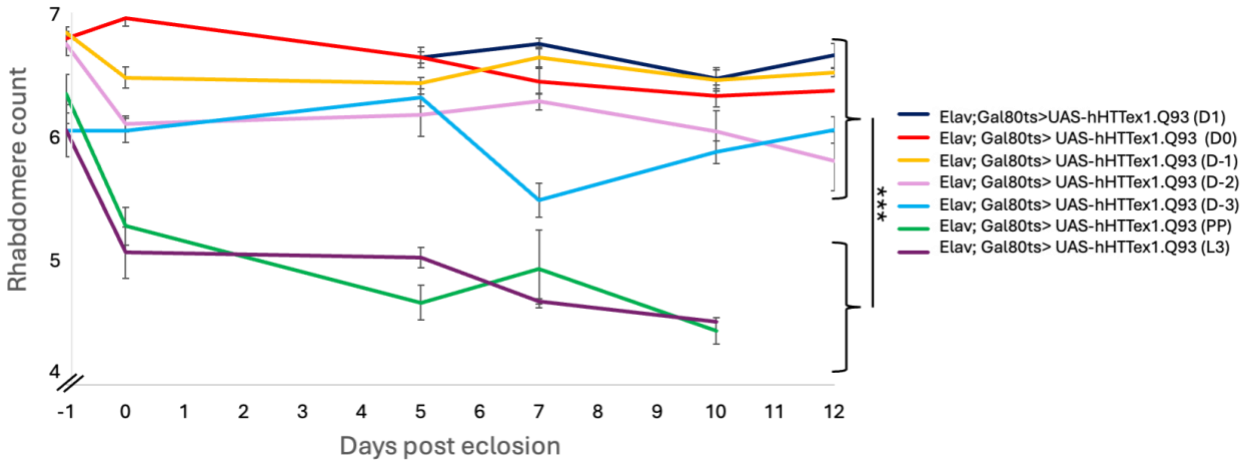

Figure 3.7. The time of induction of mHTT expression alters the amount of rhabdomere degeneration.

Graph to show mHTT expression at different timepoints throughout eye development. Flies were crossed at 19°C until the appropriate time to induce expression, when flies were placed at 30°C. Rhabdomeres were counted between one-day prior to eclosion, and 12 days post-eclosion, except those where mHTT was expressed at prepupal (PP) or L3 larval stages, where rhabdomeres were counted to 10 days post eclosion. There was a significant difference in rhabdomere counts between experimental groups (Genotype*Time $F_{32,379}$ = 6.025, p<0.001). Flies expressing mHTT from L3 and PP stages had significantly fewer rhabdomeres than flies expressing mHTT from D-3 through D1 (p<0.001). Data points with error bars indicate where counts were taken. Error bars = SEM.

3.3.6 Downregulation of *Mef2* suppresses mHTT-induced degeneration in the whole-eye

This section aimed to determine how downregulating *Mef2* impacts the whole-eye mHTT phenotype seen in the mHTT-induced model of HD. To do this, GMR-Gal4 was used to drive expression of Q93 and Mef2RNAi (BL38247) in all cells of the eye (Li et al., 2012). At 15 days post-eclosion, flies were imaged using confocal microscopy. This showed more uniform pigmentation and less degeneration compared with the Q93 flies, alone, and was comparable to that seen in the 15-day wild-type fly eye (Figure 3.8A). To test the strength of the effect that *Mef2* downregulation has on mHTT-induced whole-eye degeneration, *Mef2* was downregulated in a mHTT model with 120 CAG repeats (GMR>UAS-hHTTex1.Q120), which gives a stronger degenerative phenotype. To do this, GMR-Gal4 was used to drive expression of Mef2RNAi (15550) and Q120. At 15 days post-eclosion, there was less degeneration of the whole-eye compared with the whole-eye expressing Q120 flies, alone (Figure 3.8B).

To conclude, whole-eye downregulation of *Mef2* in a whole-eye degenerative model of HD can suppress the mHTT-induced whole-eye phenotype.

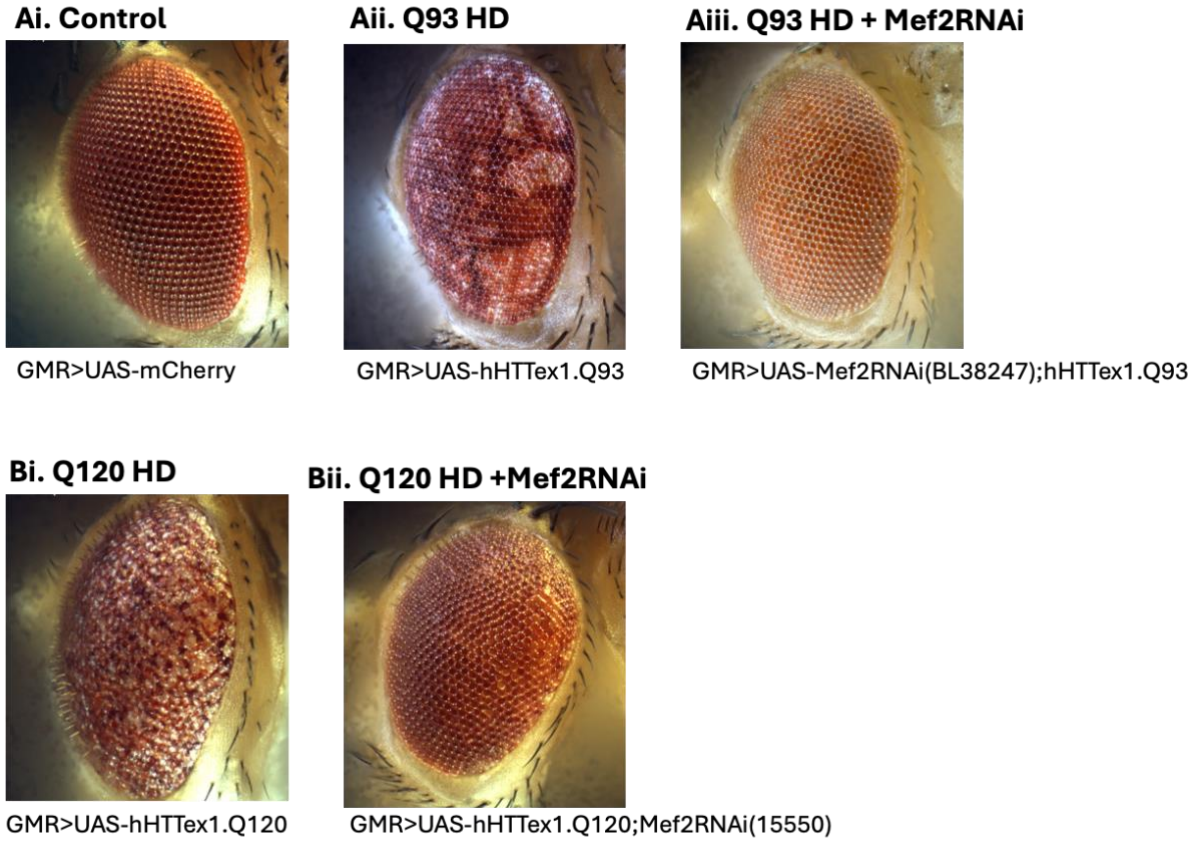

Figure 3.8. Whole-eye downregulation of Drosophila Mef2 suppresses mHTT-induced degeneration in a mHTT-induced degenerative model of HD.

A) Confocal microscopy to show the uniform pigmentation of the whole-eye in a control fly, and degeneration that appears due to whole-eye expression of the human mutant huntingtin fragment with 93 CAG repeats (GMR>hHTTex1.Q93). Whole-eye downregulation of the *Mef2* using BL38247 (GMR>BL38247; hHTTex1.Q93), suppresses the degenerative phenotype seen in Q93 fly line. B). Confocal imaging of the whole eye, showing degeneration of the whole-eye in a model expressing mHTT with 120 CAG repeats. Whole-eye downregulation of *Mef2*, using 15550, (GMR>hHTTex1.Q120; 15550) is also able to suppress the degenerative phenotype.

3.3.7 Downregulation of *Mef2* suppresses mHTT-induced degeneration in neurons.

This section aimed to investigate the effect of downregulating *Mef2* in mHTT-induced neurons. To do this, the pan-neuronal driver ELAV^{C155}-Gal4 was used to induce mHTT (Q93) and BL38247 in the neurons. Rhabdomere counts were taken at 2 days prior to eclosion, through

to 15 days post-eclosion. An additional line expressing Q93 and mCherry was added to control for any results influenced by the presence of an additional UAS construct in the genome (Elav>mCherry; hHTTex1.Q93). Analysis compared rhabdomere counts between flies expressing Q93 and mCherry, with those expressing Q93 and BL38247. Downregulation of *Mef2* in the Q93 model significantly suppressed mHTT-induced loss of rhabdomeres (Genotype*Time $F_{12,119}$ = 3.649, p<0.001) (Figure 3.9A). Post-hoc analysis revealed that there was no difference between the two genotypes at the day prior to eclosion (Elav>UAS-mCherry; hHTTex1.Q93 6.7 rhabdomeres +/- 0.1, Elav>UAS-Mef2RNAi; hHTTex1.Q93 6.9 rhabdomeres +/- 0.02, p=0.875). At eclosion, Q93-expressing flies with *Mef2* downregulation using BL38247 had more rhabdomeres that flies expressing Q93, only (Elav>UAS-mCherry; hHTTex1.Q93 day 0 = 5.6 +/- 0.04, Elav>UAS-Mef2RNAi(BL38247); hHTTex1.Q93 = 6.05 +/- 0.08, p=0.004) and was maintained until 15 days post-eclosion which was the last timepoint analysed in this experiment (Elav>UAS-mCherry; hHTTex1.Q93 4.5 rhabdomeres +/- 0.1, Elav>UAS-Mef2RNAi(BL38247); hHTTex1.Q93 5.4 rhabdomeres +/- 0.3, p=0.013) (Figure 3.9A). At day 12, whilst there were fewer rhabdomeres in the Q93 expressing flies compared to the flies expressing Q93 and Mef2RNAi, this was not significant (Elav>UAS-mCherry; hHTTex1.Q93 4.5 rhabdomeres +/- 0.1, Elav>UAS-Mef2RNAi (BL38247); hHTTex1.Q93, 4.7 rhabdomeres +/- 0.1, p=0.061). However, due to time constraints, the number of flies expressing Q93 and mCherry was small and may contribute to this (n=3).

To further confirm the effect of *Mef2* downregulation, the 15550 RNAi line was used to downregulate *Mef2* in another model of mHTT containing 93 CAG repeats (Q93-II) This UAS construct is present on the 2nd chromosome and expresses the same human exon 1 sequence with 93 CAG repeats, which is expressed in the UAS-Q93 line on the 3rd chromosome. To control for the addition of another UAS construct, another fly line was generated, expressing the Val20GFP construct and Q93-II (Elav>UAS-Q93-II; UAS-Val20GFP). Due to time constraints, rhabdomere counts were unable to be conducted to 15 days post-eclosion. Therefore, analysis compared flies expressing Q93-II, and flies expressing Q93-II and 15550. However, fly counts for flies expressing Val20GFP and Q93-II were added to the graph to show that adding a second UAS construct does not appear to influence rhabdomere counts up between the day of eclosion and 10 days post-eclosion (Figure 3.9B, yellow). Pan-neuronal downregulation of *Mef2* using 15550, significantly suppressed mHTT-induced rhabdomere degeneration

(Genotype*Time $F_{5,113}$ = 5.345, p<0.001) (Figure 3.9B). Upon the day of eclosion, there was no significant difference in rhabdomere number compared with pan-neuronal mHTT expression alone (Q93-II = 6.05 +/- 0.08, Q93-II;15550 = 5.95 +/- 0.06, p=0.654). However, as flies aged, rhabdomere loss was suppressed and by 10 days post-eclosion, rhabdomere count in Q93-II flies with *Mef2* downregulation, was significantly higher compared with Q93-II expression alone (Q93-II = 4.62 +/- 0.08, Q93-II ;15550 = 5.74 +/- 0.23, p<0.001) (Figure 3.9B). This was maintained at 12- and 15-days post-eclosion (p<0.001).

To test the pattern changes with downregulation of *Mef2* using two different RNAi lines and two different mHTT models, I repeated the experiment using a third RNAi line for *Mef2*, 1429R1. Using 1429R1, there was no significant difference in the rhabdomere counts between the Q93-expressing flies and the Q93 flies with *Mef2* downregulation (Genotype*Time $F_{4,56}$ = 0.148, p=0.963). However, it should be noted that there appears to be a trend by which the flies with downregulation of *Mef2* using 1429R1 do have slightly more rhabdomeres at each timepoint, and this data is preliminary, with low sample number at each timepoint (n=3) (Figure 3.9C). To conclude, downregulating *Mef2* in a pan-neuronal model of HD can suppress mHTT-induced loss of rhabdomeres.

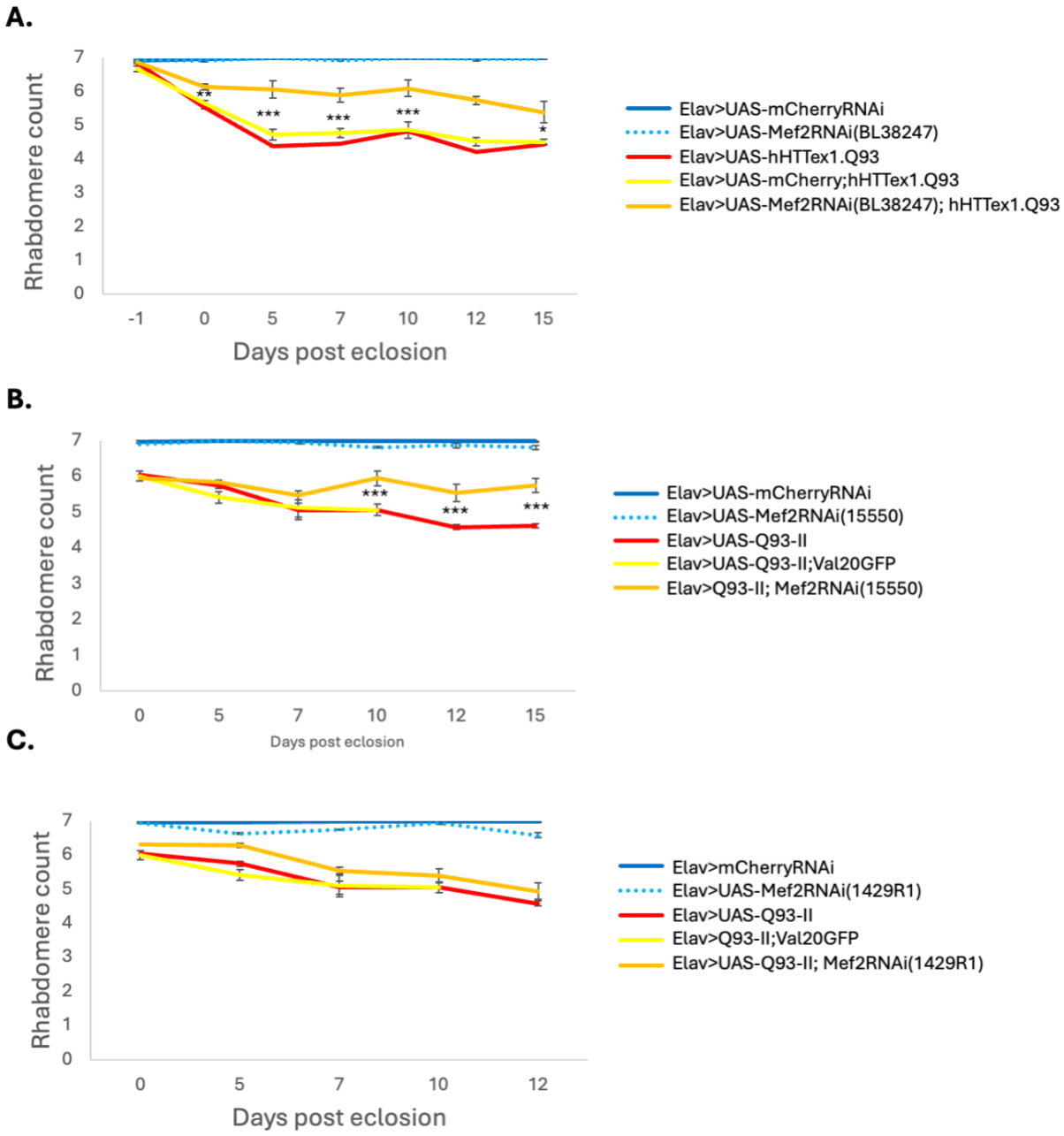

Figure 3.9. Pan-neuronal downregulation of Mef2 suppresses mHTT-induced degeneration.
A) Graphical representation of the effect of *Mef2* downregulation in a mHTT-induced fly model of HD with 93 CAG repeats (Q93). Rhabdomere counts were taken from 1 day prior to eclosion to 15 days post eclosion. Downregulation of *Mef2* using BL38247, significantly suppresses rhabdomere cell loss compared with the Q93-expressing flies (Genotype*Time $F_{12,119}$ = 3.649, p<0.001) B) Graphical representation of the effect of downregulation *Mef2* using 15550, in another Q93 model of mHTT-induced degeneration (Q93-II). Pan-neuronal downregulation of endogenous *Mef2* using 15550 significantly suppressed mHTT-induced degeneration (Genotype*Time $F_{5,113}$ = 5.345, p<0.001) *** p<0.001, ** p<0.01, *p<0.05. Error bars = SEM. C) Graph to show the effect of downregulation *Mef2* with 1429R1. Rhabdomere counts taken at 1 day prior to eclosion, to 12 days post-eclosion. There was no difference in rhabdomere counts between Q93-expressing flies and Q93 flies with *Mef2* downregulation (Genotype*Time $F_{4,56}$ = 0.148, p=0.963).

3.3.8 Downregulation of *Mef2* in a mHTT-induced model can prolong fly survival

The previous sections have shown that downregulating *Mef2* in a whole-eye and pan-neuronal model of HD can suppress a mHTT-induced phenotype. The next question to ask was whether pan-neuronal downregulation of *Mef2* in the mHTT model could increase fly survival. To do this, a longevity assay was conducted. mHTT was expressed in the neurons of flies (using ELAV^{C155}-Gal4) and from eclosion, flies were housed in vials at 25°C. Every two days, the flies were flipped into fresh food and the number of surviving flies counted. To account for the additional UAS construct present in the flies expressing Q93 and BL39247, survival analysis was also conducted for flies expressing Q93 and mCherry. Due to time constraints, this data was not available for flies expressing Val20GFP and Q93-II, therefore, analysis compared longevity of flies expressing Q93-II and either 15550 or 1429R1, with flies expressing only Q93-II. Downregulation of *Mef2* using BL38247 in Q93-expressing flies, did not influence fly survival compared with flies expressing Q93 and mCherry (Log rank test: t_{252} = 0.580, P=0.938) (Figure 3.10A). Pan-neuronal downregulation of *Mef2* using 15550 in the Q93-II line significantly prolonged survival (Log rank test: t_{271}= -8.076, P<0.001) (Figure 3.10B). Similarly, downregulation using 1429R1 significantly prolonged survival compared with Q93-II-expressing flies (Log rank test: t_{182} = 9.907, p<0.001) (Figure 3.10C). To conclude, downregulating *Mef2* in a pan-neuronal model of mHTT expression can prolong fly survival.

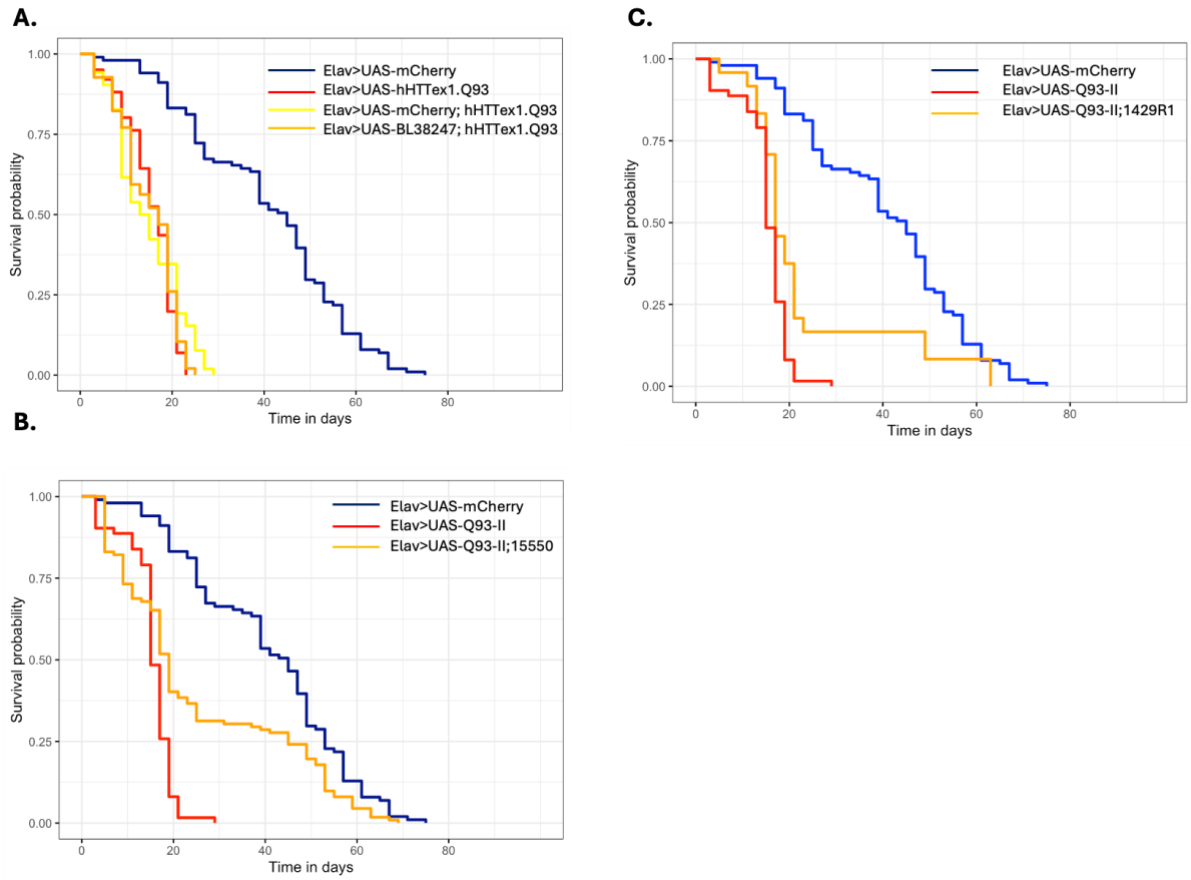

Figure 3.10. Mef2 downregulation can prolong survival in flies expressing mHTT.
Kaplan Meier plots to show survival of flies expressing mHTT and how downregulation of *Mef2* effects this survival. A) Pan-neuronal downregulation of *Mef2* using UAS-Mef2RNAi (BL38247) does not significantly increase survival of the flies (Log rank test: t_{345} = 0.580, p=0.9380). B) Pan-neuronal downregulation of *Mef2* using UAS-Mef2RNAi (15550) can significantly prolong fly survival (Log rank test: t_{271}= -8.076, p<0.001). C) Pan-neuronal downregulation of *Mef2* using UAS-Mef2RNAi (1429R1) can significantly prolong fly survival (Log rank test: t_{182} = 9.907, p<0.001).

3.3.9 *Mef2* downregulation in fully developed photoreceptors can rescue mHTT-induced degeneration.

Section 3.3.5 showed that pre-exposure of neurons to mHTT leads to increased loss of rhabdomeres, compared with the neurons where mHTT is expressed after eye development is complete (Figure 3.6/3.7). Therefore, the next experiment aimed to determine whether downregulating *Mef2* in the developed PR neurons of the eye have any impact on mHTT expression at this time. The GAL80^{ts}Gal4/UAS system was used to induce pan-neuronal downregulation of *Mef2* (using BL38247) and pan-neuronal expression of mHTT (Q93) one day prior to eclosion (D-1), since at this timepoint, eye development is complete (Cagan & Ready, 1989). Rhabdomere counts were taken from one day prior to eclosion, to 12 days post-

eclosion. There was not an effect between the two genotypes across time, however there was an overall effect of genotype (Genotype*Time $F_{5,127}$ = 1.015, p=0.412, Effect of Genotype: $F_{6,127}$ = 5.694, p<0.001) (Figure 3.11). Post hoc analysis revealed that on the day of eclosion, Q93-expressing flies with downregulation of *Mef2* had more rhabdomeres than Q93 flies, alone (Elav; Gal80ts>Q93, 6.51 +/- 0.09, Elav; Gal80ts>BL38247; Q93, 6.76 +/- 0.04, p<0.001). This was also true at 5 days post-eclosion (Elav; Gal80ts>BL38247; Q93 6.78 +/- 0.02, Elav; Gal80ts> Q93, 6.46 +/- 0.04, p<0.001). Interestingly, this was not maintained, and at 7 days post-eclosion, there was no difference in rhabdomere counts between the two genotypes (Gal80ts; Q93, 6.67 +/- 0.08, Gal80ts; Mef2RNAi; Q93, 6.80 +/- 0.02 p=0.106) (Figure 3.16). To conclude, this experiment shows that onset of mHTT with *Mef2* downregulation in the developed eye can suppress rhabdomere loss in the young adult fly, compared with flies expressing mHTT, alone, in the developed eye.

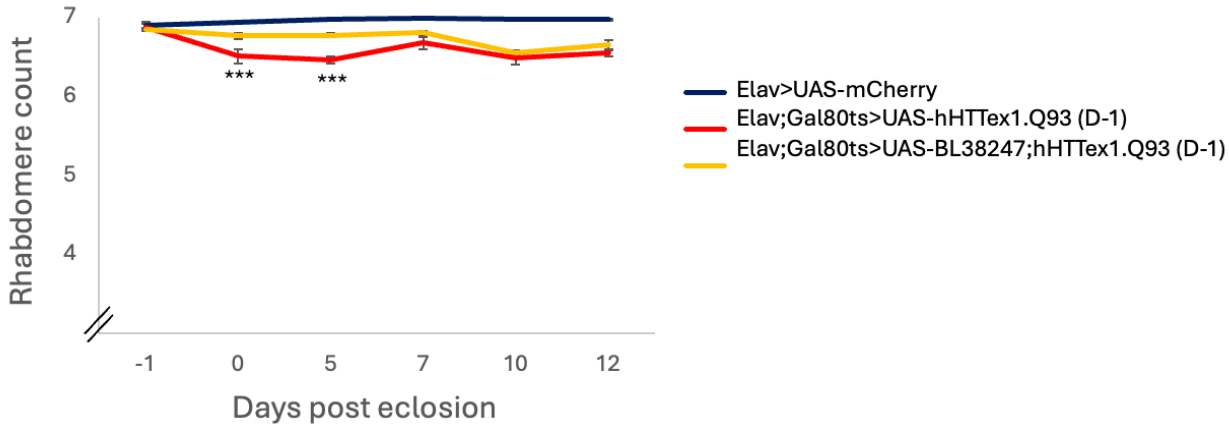

Figure 3.11. mHTT-induced degeneration in developed photoreceptors can be suppressed by downregulation of Mef2.
A graph showing the rhabdomere counts of flies expressing mHTT in the neurons from one-day prior to eclosion (D-1), and flies with mHTT and downregulation of the endogenous *Mef2*. Rhabdomere counts were taken from 1 day prior to eclosion, to 12 days post eclosion. There was an overall effect of Genotype ($F_{6,127}$ = 5.694, p<0.001), which showed that 0- and 5-days post eclosion, mHTT flies with *Mef2* downregulation had more rhabdomeres compared with mHTT flies, alone. ***p<0.001.

3.3.10 *Mef2* downregulation in developing photoreceptors does not influence mHTT-induced degeneration.

The next experiment aimed to investigate the effect that downregulating *Mef2* (BL38247) has on rhabdomeres where mHTT is induced in the developing eye. To do this, the Gal80^{ts}Gal4/UAS system was used to induce pan-neuronal mHTT expression and pan-neuronal downregulation of *Mef2* at the PP stage. Rhabdomeres were counted between one day prior to eclosion and 7 days post-eclosion. There was no significant difference between flies expressing Q93 and BL38247, compared with flies expressing Q93, alone (Genotype*Time $F_{3,50}$ = 2.740, p=0.053) (Figure 3.12). It should be noted that the sample number at each timepoint is small in the Elav; Gal80ts>UAS-BL38247; Q93 line may impact these results (At day 7, n=2. At day 1 and -1, n=3. At day 5, n= 9).

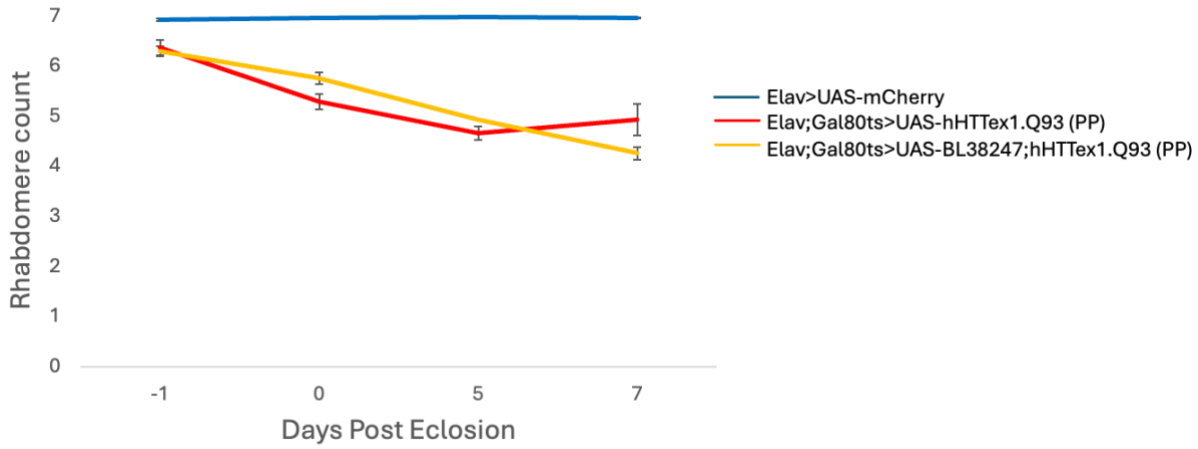

Figure 3.12. Mef2 downregulation in developing photoreceptors does not influence mHTT-induced degeneration.
Graphical representation to show rhabdomere loss in flies where pan-neuronal mHTT expression is induced at pupation (PP), and the extent of rhabdomere loss when *Mef2* is downregulated in these fly neurons. Rhabdomere counts were taken from one day prior to eclosion, to 10 days post-eclosion. There was no significant difference between the two genotypes (Genotype*Time $F_{3,50}$ = 2.740, p=0.053)

3.3.11 Whole-eye over-expression of *Drosophila Mef2* exacerbates mHTT-induced degeneration.

In the previous sections of this chapter, *Mef2* knockdown in a whole-eye and pan-neuronal model of mHTT has been shown to suppress mHTT-induced eye degeneration and rhabdomere loss, respectively. This implies a potential genetic interaction between *Mef2* and mHTT. Therefore, this experiment aimed to investigate whether over-expressing *Drosophila Mef2* influences mHTT-induced rhabdomere loss. To do this, the whole-eye driver GMR-Gal4 was used to over-express *Drosophila Mef2* in the mHTT-induced eye model with 93 CAG repeats (GMR>UAS-Mef2; hHTTex1.Q93). On the day of eclosion, there was visibly worse degeneration in the Q93-expressing flies with *Mef2* over-expression, compared with flies expressing Q93, only (Figure 3.11Aii/Aiii). In these flies there was no red pigmentation, and only the bristles on the exterior of the eye were present (Figure 3.11Aiii).

There is also evidence from other disease models that over-expression of mammalian *Mef2* isoforms, including *Mef2C*, is beneficial to degenerative disease processes (Ren et al., 2022). Therefore, using the Gal4/UAS system, one can over-express the human *Mef2C* (*hMef2C*) gene to assess whether this gene functions similarly to *Drosophila* Mef2 in a whole-eye mHTT-model. Whole eye over-expression of *hMef2C* in the Q93 model led to significantly worse degeneration at eclosion, compared with flies expressing Q93, only (Figure 3.11Aiv). *hMef2C* was over-expressed in a whole eye mHTT model with 120 CAG repeats (Q120). Interestingly, upon eclosion, Q120 flies with *hMef2C* over-expression has reduced pigmentation compared with Q120-expressing flies, alone, however, this did not worsen with age (Figure 3.11Bi/ii). Even more interestingly, there appears to be a gradient of degeneration, antero-posteriorly, with gradual loss of pigmentation throughout the eye. To conclude, over-expression of *Drosophila Mef2* and *hMef2C* in a model of mHTT, exacerbates the whole-eye degenerative phenotype.

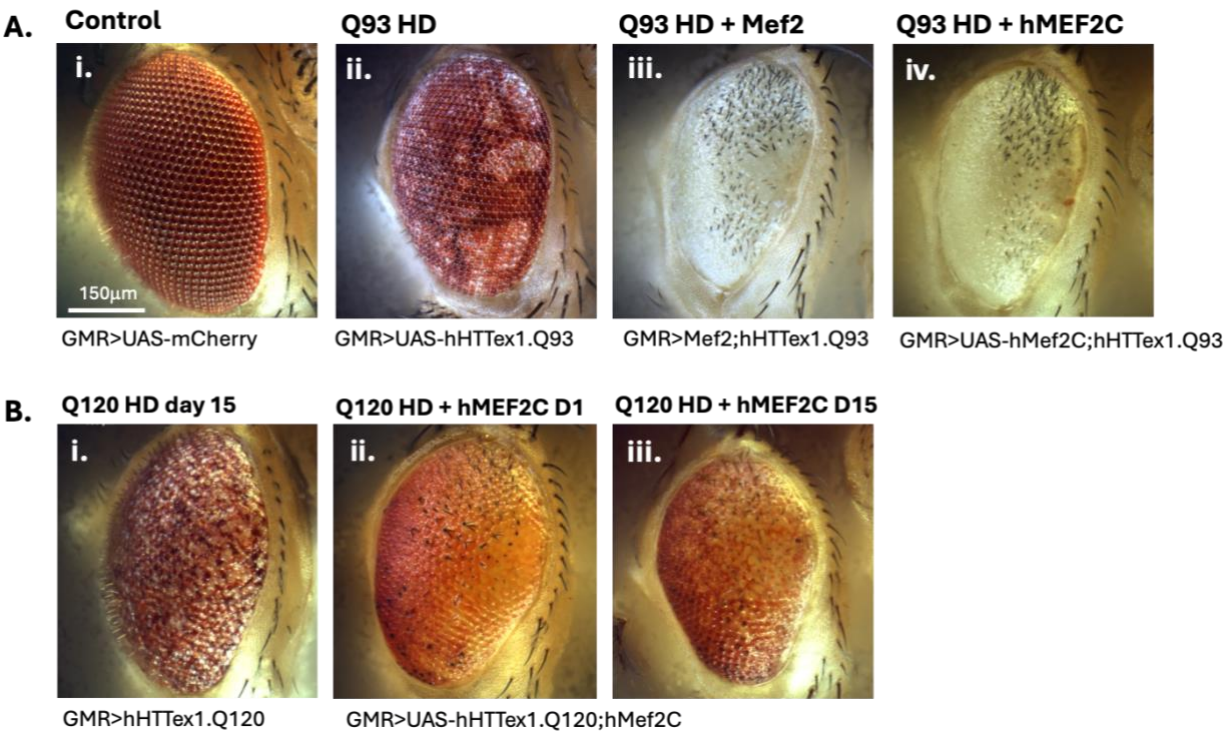

Figure 3.13. Over-expression of Drosophila Mef2 and human Mef2C (hMef2C) exacerbates whole eye degeneration.

A) Representative confocal images of the effect of whole-eye over-expression of *Drosophila Mef2* (Aiii) and human *Mef2C* (*hMef2C*) (Aiv) in a mHTT model with 93 CAG repeats (Aii). Over-expression of *Mef2* and *hMef2C* exacerbates the mHTT-induced whole-eye phenotype compared with the HD fly, alone. B) Representative confocal images to show that over-expression of *hMef2C* in a mHTT-induced fly model, containing 120 CAG repeats, exacerbates the mHTT-induced phenotype.

3.3.12 Pan-neuronal over-expression of *Drosophila Mef2* does not influence mHTT-induced degeneration, whilst over-expression of *hMef2C* is lethal.

Whole-eye over-expression of *Drosophila Mef2* and *hMef2C* exacerbated mHTT-induced eye degeneration. The next experiment investigated whether over-expression in mHTT-induced neurons would lead to further loss of rhabdomeres. To do this, ELAV^{C155}-Gal4 was used to drive expression of *Drosophila Mef2* or *hMef2C* in a pan-neuronal model of mHTT. Rhabdomere counts were taken from 2 days prior to eclosion, to 15 days post-eclosion. Pan-neuronal over-expression of *Drosophila Mef2* in the Q93-expressing flies resulted in no difference in rhabdomere count compared with Q93-expressing flies, alone (Genotype*Time $F_{7,141} = 1.375$, p=0.220) (Figure 3.12). By contrast, pan-neuronal over-expression of *hMef2C* in the same Q93 model was lethal. Since *hMef2C* over-expression in wild-type *Drosophila* led to rhabdomere counts comparable with wild-type flies (Genotype*Time: $F_{5,36} = 0.716$, p=0.616) (Figure 3.15), the hMef2C-Q93 interaction is causing lethality. To conclude, pan-neuronal over-

expression of *Drosophila Mef2* has no effect on mHTT-induced loss of rhabdomeres, however *hMef2C* over-expression in this mHTT model is lethal. Therefore, is not possible to determine whether *hMef2C* has any impact on rhabdomere degeneration.

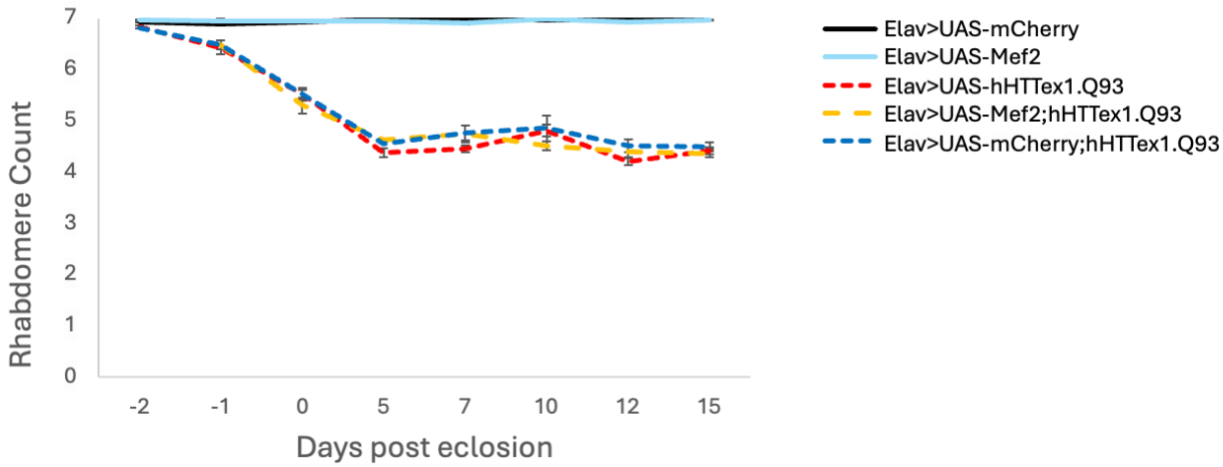

Figure 3.14. Pan-neuronal over-expression of Mef2 has no effect on mHTT-induced degeneration.
Graph showing average rhabdomere loss from 2 days prior to eclosion, to 15-day-old flies. Pan-neuronal over-expression of endogenous *Mef2*, using ELAV^{C155}Gal4 showed no difference in rhabdomere loss, compared with mHTT-induced degeneration from expression of mHTT, alone (Genotype*Time $F_{7,141}$ = 1.375, p=0.220). Pan-neuronal over-expression of mCherry was used as a control to show that control flies show no rhabdomere degeneration, and pan-neuronal over-expression of *Drosophila Mef2* have does not induce any rhabdomere loss. Error bars = SEM.

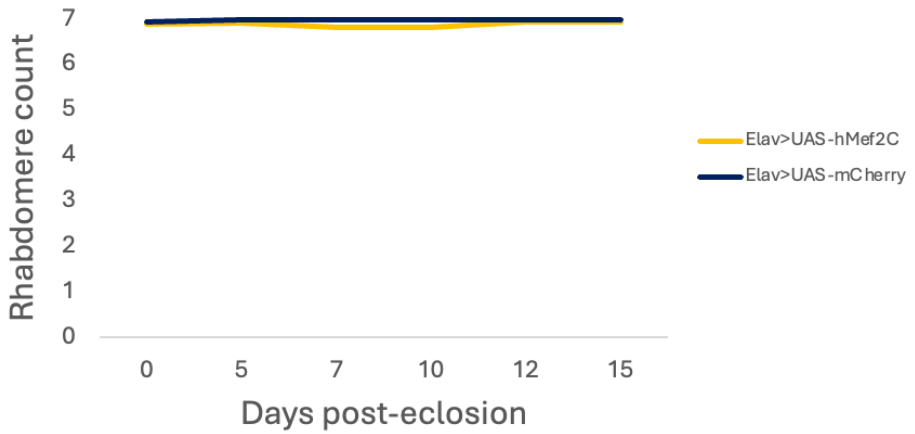

Figure 3.15. Pan-neuronal over-expression of hMef2C does not induce a phenotype.
Graph to show representative rhabdomere counts in flies expressing human *Mef2C* (*hMef2C*) in the neurons (Elav>UAS-hMef2C). Counts were taken at 0 to 15-days post eclosion. Over-expression of *hMef2C* had no impact on rhabdomere counts compared with wild-type flies (Genotype*Time: $F_{5,36}$ = 0.716, p=0.616).

3.3.13 Over-expression of *hMef2C* in fully developed photoreceptors has no effect on mHTT-induced degeneration

The previous experiment showed that over-expression of *hMef2C* in a pan-neuronal model of mHTT-induced degeneration is lethal. It is well established that *Mef2* is a key regulator in cardiovascular development, and repressing overall *Mef2* activity may, in part, aid in treatment of cardiac hypertrophy (Cornwell & McDermott, 2023). Therefore, it is possible that lethality in these flies is due to other complications during development, and that over-expression of *hMef2C* and its interaction with mHTT in other parts of the nervous system, plays a role in lethality of the flies prior to adulthood. Therefore, the next experiment aimed to induce over-expression of *hMef2C* following development of these major structures, and the eye. To do this, the GAL80^{ts}Gal4/UAS system was used to induce pan-neuronal over-expression of *hMef2C* and pan-neuronal expression of mHTT (Q93) one day prior to eclosion (D-1). Rhabdomere counts were taken from one day prior to eclosion, to 12 days post-eclosion. There was no difference between the rhabdomere counts with Q93 at D-1, compared with Q93-expressing and over-expression of *hMef2C* (Genotype*Time $F_{5,101}$ = 2.053, p=0.077) (Figure 3.16). To conclude, over-expressing *hMEf2C* in flies expressing Q93 the day prior to eclosion had no effect on mHTT-induced degeneration at D-1.

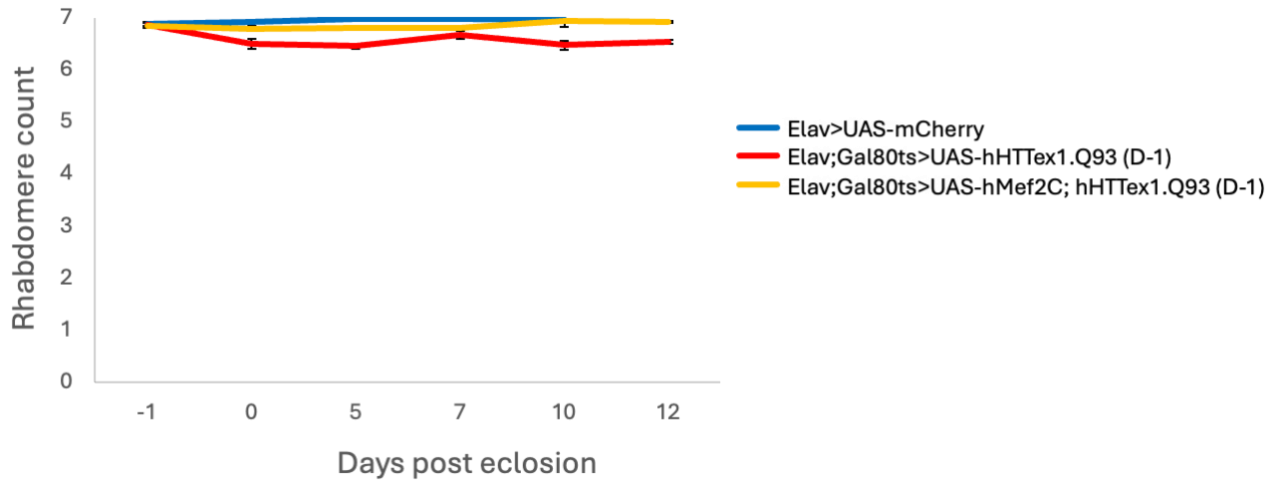

Figure 3.16. Over-expression of hMef2C in developed photoreceptors has no effect on mHTT-induced degeneration.

A graph to show the rhabdomere counts of flies expressing mHTT (Q93) in the neurons from one day prior to eclosion (D-1), and flies expressing mHTT and over-expression of *hMef2C*. Rhabdomere counts were taken from one day prior to eclosion, to 12 days post eclosion. There was no difference in the rhabdomere counts with *hMef2C* over-expression in Q93-expressing flies, compared with those expressing Q93, alone (Genotype*Time $F_{5,101}$ = 2.053, p=0.077).

3.3.14 *Mef2* is expressed in the developing eye-brain complex

The previous experiments have shown that downregulating *Mef2 i*n a whole-eye and pan-neuronal of mHTT can suppress mHTT-induced eye and rhabdomere degeneration, respectively. Experiments have also shown that over-expressing *Mef2* and *hMef2C* in a whole-eye model of mHTT can exacerbate whole-eye mHTT degeneration. Therefore, the next question aimed to address why and how these changes come about. In 1996, Schulz and colleagues observed that *Mef2* is expressed in embryonic and larval Kenyon cells; the neurons that make up the adult mushroom body, the brain region in *Drosophila* known to function in learning and memory (Schulz et al., 1996). Since then, studies have reported seeing *Mef2* expression in the photoreceptors of the adult fly (Crittenden et al., 2018; Hall et al., 2017), however little is known about *Mef2* expression in the developing eye-brain complex.

The next experiment aimed to investigate where *Mef2* is expressed in the developing eye-brain complex. To do this, a Mef2-GFP line generated in the host lab was used to visualise endogenous *Mef2* expression. The Mef2-GFP line was generated using CRISPR-Cas9, to directly tag the endogenous Mef2 protein at its C-terminus (Hubbert, 2023). The line is

homozygous viable, with no phenotype, and expression has been verified in the host laboratory using immunohistochemistry and live imaging to extensively study the expression profile in the fly embryo, wing imaginal disc, and the dorsal longitudinal muscles (DLMs) of the adult muscle (Hubbert, 2023).

Whole eye-brain complexes from Mef2-GFP L3 larvae, early (50hr post prepupa formation (ppf), mid (100hr ppf), and late (130hr ppf) pupae, and early adult (1 day post eclosion) flies. Eye-antennal imaginal discs from the L3 larvae were also dissected. Imaginal discs and eye-brain complexes were stained for Mef2 (anti-GFP), neurons (anti-elav) and cell nuclei (Hoechst). See Section 2.1.9 for full methods. There was no evidence of Mef2 expression in the L3 eye-antennal imaginal disc (Figure 3.17), however two concentrated populations of Mef2 positive cells were observed in the central brain lobes of the L3 larval brain (Li et al., 2014) (Figure 3.18Bi).

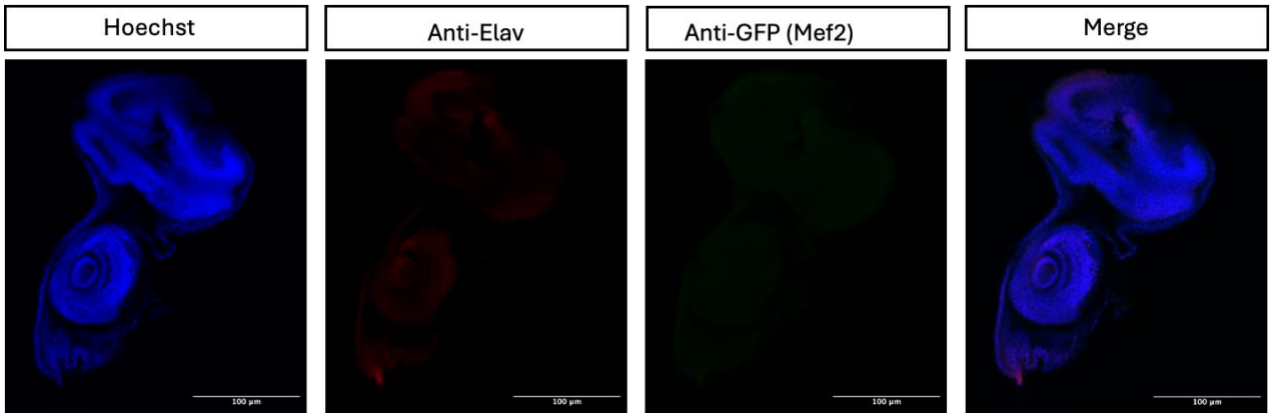

Figure 3.17. Mef2 is not expressed in the eye-antennal disc.
Confocal imaging to show that *Mef2* is not expressed in the developing eye disc of L3 larvae. Hoechst was used to stain nuclei (blue), anti-elav for neuronal staining, and anti-GFP to stain *Mef2*. Scale bar: 100μm.

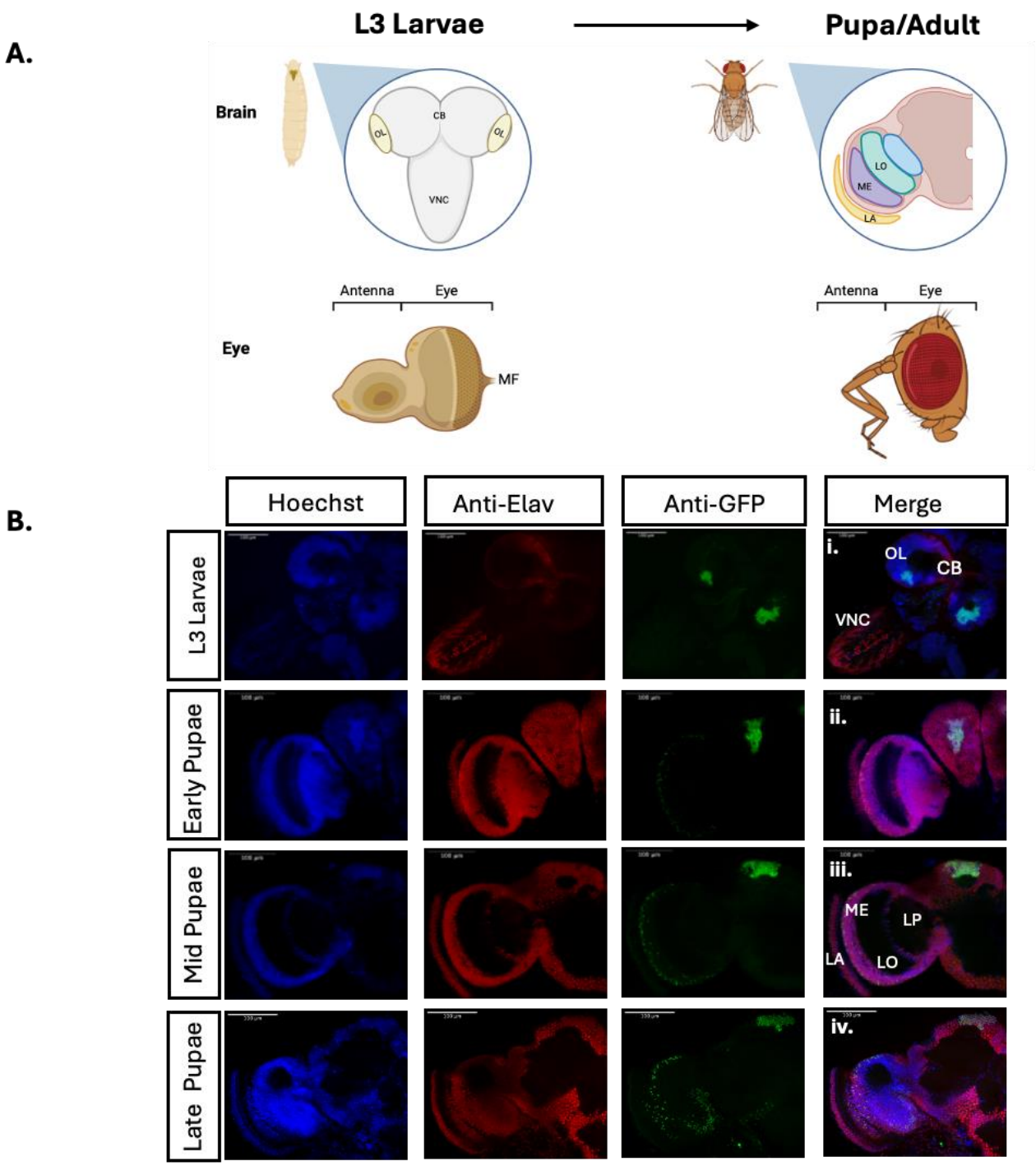

Figure 3.18. Mef2 expression in the developing eye-brain complex.

A). Schematic of the developing antenna-eye disc, and developing larval brain, to the adult eye-brain complex and compound eye. VNC: Ventral Nerve Cord, OL: Optic Lobe, CB: Central Brain, MF: Morphogenetic Furrow, LA: Lamina, ME: Medulla, LO: Lobula, LP: Lobula Plate. Made using biorender. B). Panel to show Mef2 expression in the developing eye-brain complex. Mef2 is expressed in L3 central brain, and an additional population of Mef2-expressing cells populate the lateral aspect of the optic lobe, neurons of which, connect to the developing eye.

In the early pupal eye-brain complex, a concentrated population of Mef2 positive cells was observed at the rostral end of the central brain (Figure 3.18 Bii). In the mid-stage pupal eye-brain complex, Mef2 positive cells are in an area surrounding, but not in, the mushroom body, and in nuclei of cells on the lateral surface of the optic lobe medulla (Figure 3.18 Biii). In the late pupal eye-brain complex, Mef2 positive cells were again, observed in an area surrounding, but not in, the mushroom body, and more Mef2 positive nuclei appear on the lateral surface of the optic lobe medulla (Figure 3.18Biv). To conclude, Mef2 is expressed in the developing eye-brain complex. Mef2 expression appears as a concentrated population of cells in the central brain, and a sub-population of nuclei on the lateral aspect of the optic lobe medulla are Mef2 positive.

3.3.15 Mef2 is not expressed in the adult *Drosophila* Photoreceptors

From dissection and immunostaining of whole eye-brain complexes, it was difficult to determine whether Mef2 is expressed in the PRs because these neurons are often damaged in the dissection process. Therefore, in this experiment, heads of one-day-old flies from the Mef2-GFP fly line were cryosectioned and phalloidin used to visualise the PRs. See Section 2.1.9 for methods. Sections of muscle were used as a positive control to ensure that the staining was successful (Figure 3.19). Imaging of 10μM sections containing rhabdomeres showed that Mef2 is not expressed in the nuclei of the photoreceptors or the projecting axons. However, there was a subset of Mef2-positive nuclei on the boundary between the medulla and lamina of the optic lobe, which corresponds to the population of cells seen in Figure 3.18 Biv (Figure 3.20). To conclude, Mef2 is not expressed in the photoreceptors of one-day-old adult flies but is expressed in a sub-population of nuclei on the lateral aspect of the optic lobe medulla.

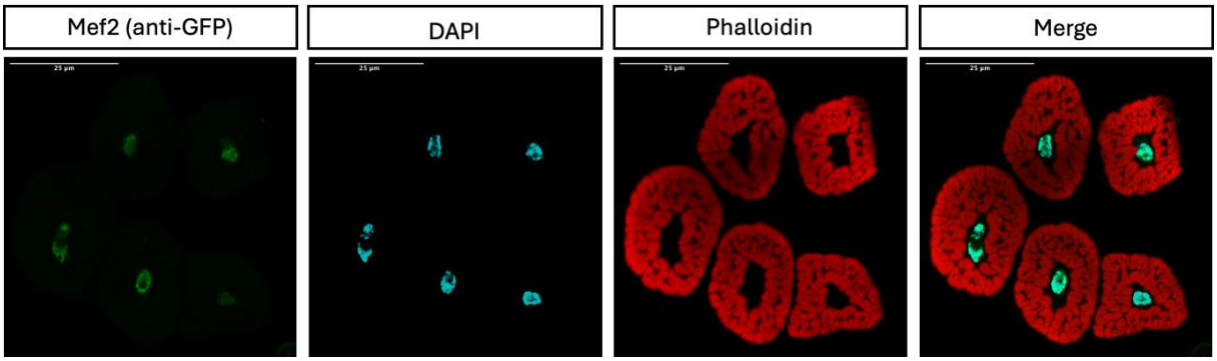

Figure 3.19 Mef2 is expressed in muscles of the Drosophila head.
Positive anti-GFP staining shows Mef2 expression in the head muscle of *Drosophila*. Images taken at 63X magnification.

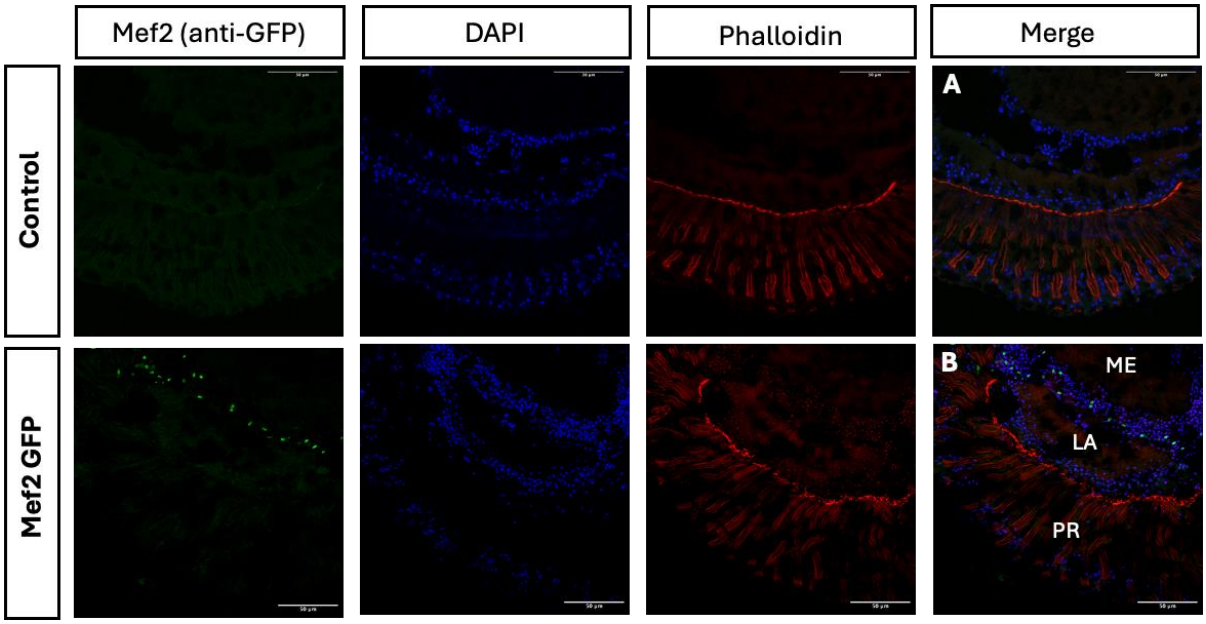

Figure 3.20. Mef2 is not expressed in the rhabdomeres and projecting photoreceptor axons of one-day-old adult flies.
Anti-GFP staining of flies with GFP-tagged endogenous Mef2, did not produce positive staining for Mef2 in the photoreceptors, indicating that there are no Mef2-positive cells in the rhabdomeres. However, there is positive staining for Mef2 in a subset of nuclei that sit at the border between the medulla and lamina of the optic lobe. PR: photoreceptors. LA: Lamina. ME: Medulla. A) Control to show Mef2 autofluorescence, and B) to show positive staining of Mef2. Images taken at 40X magnification.

3.3.16 N-terminal Mef2C physically interacts with wild-type and mHTT.

The previous experiment showed that Mef2 is expressed in the developing eye-brain complex but is not expressed in the photoreceptors. This may imply an indirect pathway for Mef2 effecting mHTT-induced degeneration of rhabdomeres. To more fully understand a potential mechanism for this effect, the next question to ask is whether there is a physical interaction between Mef2 and mHTT. To do this, the Y2H assay was used. In this assay, fragments of interest were cloned into bait (pP6) and prey (pB27) protein plasmids and amplified in yeast cells. Cells were then spread onto plates lacking specific nutrients, and those that physically interact, lead to cell growth. Plates with no cell growth indicates a lack of physical interaction between the two tested proteins (see section 2.6 for specific methods).

As mentioned in section 1.4 of the introduction, Kaltenbach and colleagues conducted a large-scale protein interaction study in an attempt to identify novel HTT fragment-interacting proteins and identified an isoform of the mammalian Mef2, Mef2D, as a physical interactant of the first 450aa (amino acids) of wild-type (WT) and mHTT (Kaltenbach et al., 2007). Therefore, the first experiment aimed to replicate this finding. To do this, primers were designed to cut the Mef2D protein into a 1-350aa fragment and 134-514aa fragment. The first 350 amino acids (aa) of Mef2D (Mef2D 1-350) physically interacts with wild-type (23 CAG repeats) and mHTT (51 CAG repeats) (Figure 3.21A/B). Y2H assays also showed that the Mef2D 134-514 aa fragment does not physically interact with wild-type and mHTT (Figure 3.21A/B).

The next experiment was to test whether the human Mef2C protein could physically interact with WT and mHTT. Primers were designed to cut the Mef2C protein into a 1-350aa fragment, 134-455aa fragment and a 1-134aa fragment. Y2H analysis showed that Mef2C 1-350aa physically interacts with WT and mHTT 1-450aa (Figure 3.22Bi/Ci). Mef2C 134-455aa does not physically interact with the WT or mHTT 1-450aa fragment (Figure 3.22Bii/Cii). Interestingly, there was no physical interaction between WT or mHTT with the Mef2C 1-134aa fragment (Figure 3.22Biii/Ciii). To conclude, the Mef2C 1-350aa fragment of the protein physically interacts with the wild-type and mutant HTT protein.

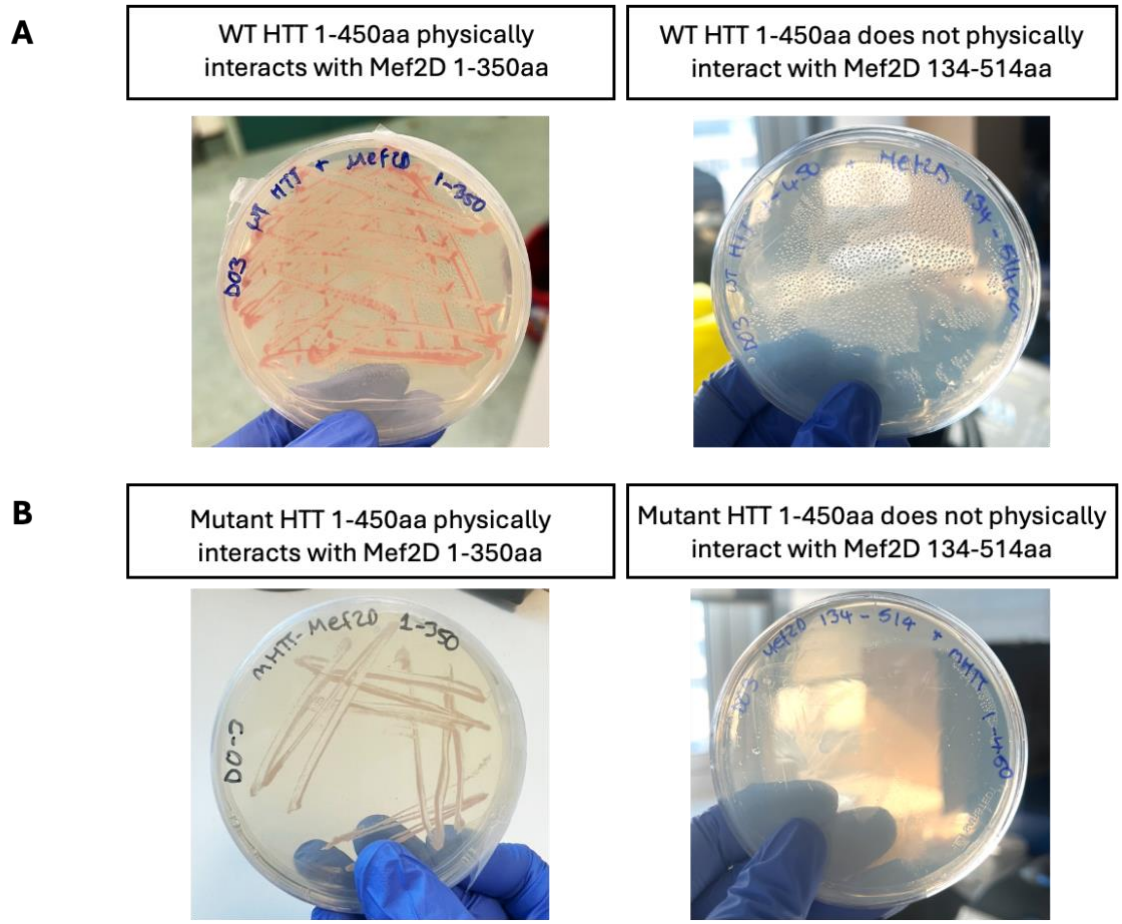

Figure 3.21. Mef2D 1-350aa physically interacts with HTT.

The Yeast-2-Hybrid assay was used to confirm reports from Kaltenbach et al., 2007, that the Mef2D 1-350aa fragment physically interacts with wild-type (WT) (A) and mutant HTT (B) as seen by growth of cells. Mef2D 134-514aa fragment does not physically interact with wild-type (A) or mutant HTT (B) as seen by a lack of growth.

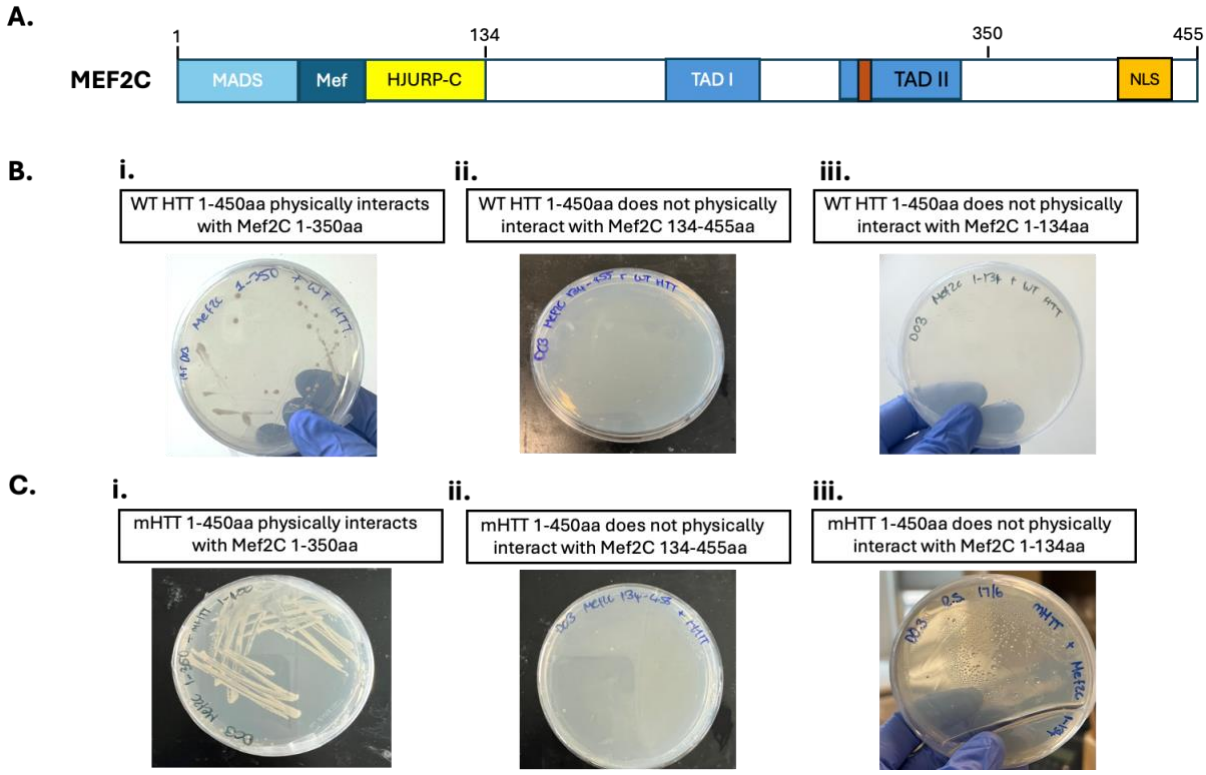

Figure 3.22. Mef2C 1-350aa physically interacts with WT and mHTT.
A). Schematic of Mef2C protein, including the highly conserved domains. Numbers indicate the amino-acid length at each point. MADS: MADS box domain, MEF: Mef2 DNA-binding domain, HJURP-C: holliday junction recognition protein, TAD I: transcriptional activation domain 1, TAD II: transcriptional activation domain 2, NLS: Nuclear localisation signal. Beta domain indicated by the organise box. B) The Yeast-2-Hybrid assay was used to test physical interactions between Mef2C protein fragments with WT (B) and mHTT (C) protein. Cell growth indicates a positive physical interaction. No growth indicates no interaction.

3.4 Discussion

The single *Mef2* and mammalian *Mef2* transcription factors have been widely implicated in brain development and function (Ali, 2022; Ana C. Barbosa et al., 2008a; Crittenden et al., 2018). In the context of HD, *Drosophila* have been used to study mHTT-induced degeneration and identify new genetic modifiers of the disease. A chromosomal deficiency including the *Mef2* gene, in a *Drosophila* model of HD, had been shown to suppress a mHTT-induced phenotype (Kaltenbach et al., 2007). However, it had not been shown whether sole *Mef2*

downregulation was responsible for this suppression; a gap that has been addressed in this chapter. The first experiments in this chapter looked to determine the extent of whole-eye degeneration and pan-neuronal loss of rhabdomeres in a mHTT-induced model prior to investigating further implications of *Mef2* manipulation.

3.4.1 The *Drosophila* eye as a model of mHTT-induced degeneration

In 1998, Jackson and colleagues were the first to describe a *Drosophila* model with an expanded polyQ region in the human HTT protein that was expressed under the control of the eye-specific promoter, GMR (Jackson et al., 1998). They showed that the presence of mHTT led to PR cell degeneration and the presence of nuclear inclusions. A couple of years later, Kazemi-Esfarjani and Benzer used these *Drosophila* models to identify genetic modifiers that could suppress this mHTT-induced degenerative phenotype (Kazemi-Esfarjani & Benzer, 2000). Researchers crossed ~7,000 potential modifiers and assessed the progeny for suppression or enhancement of the whole-eye mHTT-degenerative phenotype. One of the identified genes was *Drosophila* HDJ1, an ortholog of the human HSP40 (heat shock protein 40), a molecular chaperone which has since been implicated in Alzheimer's Disease, Parkinson's Disease, HD, and can suppress mHTT-induced neurotoxicity by directly interacting with exon 1 of the HTT protein (Kazemi-Esfarjani & Benzer, 2000; Wankhede et al., 2022). Since then, the *Drosophila* eye has become a known model system for studying neurodegenerative disease, in particular, as a way to determine whether candidate modifiers or molecular pathways might contribute to disease progression (Nitta & Sugie, 2022).

Before investigating whether genetic modifiers might be implicated in neurodegeneration progression, it is important to establish a baseline in these models. Whilst GMR-Gal4 and Elav^{c155}Gal4 are standard drivers for driving mHTT in the whole-eye and neurons, respectively, the specific mHTT line, presence of the full-length protein or truncated mHTT protein, CAG repeat length, and temperature sensitivity can cause variability in reports (Table 1.1). In this chapter, the UAS constructs used contained the N-terminal human HTT exon 1 with 93 or 120 CAG repeats, and were generated by Larry Marsh (FBrf0236625, Flybase.org). Consistent with the literature and the human condition, a longer CAG repeat length led to a more degenerative whole-eye phenotype (Figure 3.1) (Jackson et al., 1998; Lee et al., 2012). Additionally, pan-

neuronal expression of mHTT with 93 CAG repeats, showed a steady decline in rhabdomere number, which would allow further investigations with respect to exacerbating or suppressing disease phenotypes.

3.4.2 Expression of mHTT in the *Drosophila* photoreceptors does not affect structural rhabdomere formation

As mentioned briefly in this chapter, a common observation, consistent with the literature, is that flies with pan-neuronal expression of mHTT have fewer rhabdomeres on the day of eclosion compared with wild-type flies (Figure 3.3-4). This led to question whether the rhabdomeres in mHTT-expressing flies were made and had already started to degenerate, whether they were ever made in the first place. Confocal imaging of rhabdomeres at two- and one-day prior to eclosion, showed that the rhabdomeres were made, and indicated that mHTT-induced degeneration during development of the eye led to rhabdomere death prior to eclosion. I wanted to investigate how time-specific expression of mHTT would influence rhabdomere loss. As far as I am aware, there are no known studies that have used the temperature-sensitive GAL80^{ts} system in *Drosophila* to investigate time-specific effects of pan-neuronal mHTT expression. Results from this experiment showed that pre-exposure of mHTT in the neurons of the *Drosophila* during eye development, led to significant rhabdomere loss, far more than in *Drosophila* where mHTT was expressed later in pupal development or in the young adult fly (Figure 3.6/3.7). This suggests that whilst the neurons were able to develop structurally, they are vulnerable to the toxic effects of the mHTT protein, and subsequently degenerate in the young adult fly.

2.4.3 Pre-exposure of mHTT in the *Drosophila* photoreceptors leads to more extensive rhabdomere loss

In this chapter, I have shown that when mHTT is expressed in the adult fly eye, the neurons and surrounding cells have developed normally, and over a 15-day period, there is very little degeneration of rhabdomeres. By contrast, expression of mHTT during eye development leads to rhabdomere loss on the day of eclosion and further rhabdomere loss over this 15-day period. This may indicate that allowing fly neurons of the eye to develop normally makes them more resilient to the effects of mHTT and able to withstand the toxic pressures of aggregates

for longer. Additionally, one might also expect there to be fewer mHTT protein aggregates due to late onset expression. Early, pre-exposure of mHTT to these neurons might mean that they are not developing normally, which may mean that neurons are highly vulnerable and degenerate early. Using the GMR-Gal4 whole-eye driver, studies have shown that the presence of mHTT leads the aggregate accumulation in axons of the *Drosophila* eye-brain complex, and in the growth cones of adult photoreceptors (Krench & Littleton, 2013). Interestingly, these aggregates appear to relocate from the cytoplasm in larval developing PRs, to the nucleus of these PRs as the flies age (Huelsmeier et al., 2021; Jackson et al., 1998). Further investigations have shown that pan-neuronal mutations in proteins involved in synaptic transmission, such as Snap can suppress mHTT-induced degeneration of PRs, indicating that increased neurotransmitter release in HD models may be a mechanism for neuronal degeneration (Romero et al., 2008). Together, these studies indicate that the presence of mHTT may overwhelm the cells' ability to function normally, leading to accumulation of the toxic protein in the nucleus and eventually, programmed cell death in the neurons. My observations contribute to the existing debate in the HD research field, that HD is a neurodevelopmental disorder, with a neurodegenerative component (Molero et al., 2016; Schultz et al., 2023; van der Plas et al., 2020).

3.4.4 Downregulation of *Mef2* suppresses mHTT-induced degeneration

Once the degenerative phenotype in the whole-eye and neurons of flies expressing mHTT had been established, these models could be used to investigate whether downregulation of just *Mef2* was responsible for suppression of mHTT-induced degeneration in a whole-eye and pan-neuronal model of HD. I indeed found that downregulation of *Mef2* in a mHTT-induced *Drosophila* model could suppress mHTT-induced degeneration.

Mef2 as a loss-of-function suppressor of mHTT-degeneration is an interesting concept. In many situations, *Mef2* factors have been thought to be involved in neuronal survival. For example, both inhibition of *Mef2* in cultured cortical neurons, and knockout of mammalian Mef2 transcription factors, have been shown to cause neuronal apoptosis (Akhtar et al., 2012; Lyons et al., 1995). Additionally, previous work in the host laboratory has shown that striatal-specific loss of *Mef2C* increases apoptosis in the P3 mouse striatum (Ali, H et al., in

preparation). Other studies have shown that conditional knockout of *Mef2D* in the mouse retina causes PR cell degeneration and vision loss (Andzelm et al., 2015). However, there are some studies have shown that loss of *Mef2* transcription factors can have protective effects. For example, *Mef2A* gene silencing has been shown to improve survival of retinal ganglion cells (Andzelm et al., 2015). Additionally, *Mef2* was found to be reduced in the muscles of two models of polyQ disease - SBMA and HD (R6/2). In the SMBA model, muscle-fibre size was rescued by restoring *Mef2* gene expression (Nath et al., 2020). Interestingly, one study reported that onset of *Mef2* expression correlates with inhibition of neuronal differentiation, and subsequent neuron maturation (Lyons et al., 1995). Combining the literature, it may be that loss of *Mef2* expression and associated mRNA/protein slows neuronal maturation, a key factor in neurodegenerative disease. Slowing neuronal maturation may delay disease onset by slowing aging of the neurons in these animals. Therefore, whilst there is a body of evidence that indicates *Mef2* factors have neuroprotective properties, there are also context-specific exceptions that show *Mef2* loss in neurological diseases can contribute to suppression of disease progression, and slowing of neural maturation may lead to delayed disease onset.

3.4.5 Downregulation of *Mef2* shows variable degree of rhabdomere suppression and longevity

Another consideration of downregulation of *Mef2* studies in this chapter is that using three different RNAi lines of *Mef2* showed slight differences with respect to their ability to suppress mHTT-induced degeneration for prolonged periods of time, and to prolong fly survival. For example, *Mef2* RNAi knockdown using BL38247 significantly suppressed mHTT-induced rhabdomere loss between 0- and 10-days post-eclosion, however, was unable to prolong fly survival. By contrast, using the 15550 line, mHTT-induced rhabdomere loss was not suppressed until 7-days post eclosion, however, flies lived significantly longer compared with flies expressing mHTT, only (Figure 3.9-10). Understanding how RNAi lines knock down gene expression is an important concept when considering (i) how reliable these lines are, and (ii) how these results might be translated into a more complex mammalian model, such as the mouse. Table 3.1 outlines the properties of each RNAi line.

Table 3.1. Table outlining the differences between Mef2RNAi lines, VDRC15550, BL38247 and 1429R1.

Information collated from Flybase and the UP-TORR database (flyrnai.org).

UAS line	Type	Vector	Sequence length (bp)	On-Targets	Off-targets	Target Type	Target Region
BL 38247 (HMS0169)	TriP Short Hairpin (sh) RNA	Valium20	21	Mef2 gene, all isoforms	0	mRNA	5'UTR
VDRC 15550	VDRC GD long hairpin (lh) RNA		300	Mef2 gene, all isoforms	1 (Rab18)	mRNA	Coding Sequence
1429R1	NIG	pUAST-R57	500	Mef2 gene, all isoforms	1 (Rab18)	mRNA	Coding Sequence

The VDRC 15550 stock was generated as part of a project to create a genome-wide transgenic RNAi library for conditional inactivation (Dietzl et al., 2007). UAS-driven inverted repeat (UAS-IR) transgenes were generated using short gene fragments and randomly inserted into the *Drosophila* genome via germline transformation using a hyperactive P-element transposase (Dietzl et al., 2007). This library produces long hairpin double-stranded RNAs (lhRNA). This contrasts with the RNAi libraries in the Valium20 vector, used to make BL38247, which is distinct in generating short hairpin RNAs (shRNAs) (Bartoletti et al., 2017). The 1429R1 line was made as part of the National Institute of Genetics (NIG) RNAi-mutant fly bank which, when induced using the Gal4/UAS system, produces double stranded RNA in vivo 'inducible RNAi' (https://shigen.nig.ac.jp). Through this method, expression of the RNAi line leads to tissue-specific gene silencing, similar to that of the VDRC RNAi library.

LhRNAs are not integrated into the host genome and are degraded to make small interfering RNAs (siRNA). This permits rapid processing and effective initiation of targeted RNA interference and subsequent gene knockdown (Ge et al., 2010; Lambeth & Smith, 2013). As a lhRNA, 15550 is likely to process and effectively target the endogenous *Mef2* more rapidly than a shRNA, such as BL38247. shRNAs spontaneously form hairpin structures in the nucleus

with a loop of 4-11 nucleotides before being recognised by the innate cellular RNAi machinery, exported from the nucleus and processed by Dicer. These shRNAs provide efficient and long-lasting gene silencing which may be more suitable for therapeutics (Ge et al., 2010; Lambeth & Smith, 2013). BL38247 may knock down endogenous *Mef2* more slowly than 15550, but is able to silence the gene more effectively, and more long-term. Based on the make-up of the 1429R1 RNAi, it is likely to act similarly to 15550.

Another way to determine the strength of *Mef2* RNAi knockdown is to investigate this using a muscle assay, as *Mef2* is required for the formation of adult muscle (Soler et al., 2012). In the lab, a muscle assay was conducted to explore this. Both BL38247 and 15550 showed significant loss of dorso-longitudinal muscles compared with a wild-type control (Figure 3.23). Soler and colleagues (2012) showed that 1429R1 leads to less muscle loss (Soler et al., 2012). Soler and colleagues also showed that there is an allelic-series of *Mef2* RNAi and mutant lines that lead to varying *Mef2* loss-of-function in the dorso-lateral muscles This may also be an important concept to consider in future eye experiments when exploring *Mef2* downregulation in mHTT-induced degeneration.

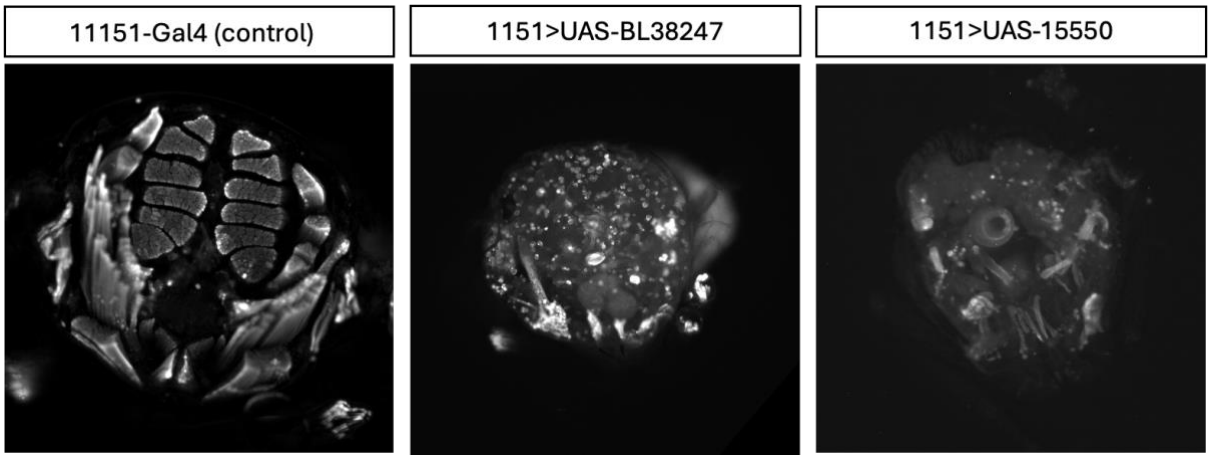

Figure 3.23 Mef2 knockdown inhibits adult muscle formation.
Downregulation of *Mef2* using BL38247 and 15550 leads to loss of all dorso-lateral muscles in the fly thorax, compared with the wild-type thorax.

3.4.6 Mef2 is expressed in the adult eye-brain complex

This chapter aimed to investigate *Mef2* expression in the adult and developing eye-brain complex. I found that *Mef2* is expressed in the developing larval brain, and in the pupal brain, but does not appear to be expressed in the PRs. Previous studies of *Mef2* expression in the brain have focused on the mushroom body. In 1996, Schulz and colleagues observed that *Mef2* is expressed in embryonic and larval Kenyon cells; the neurons that make up the adult mushroom body. This is the brain region in *Drosophila* known to function in learning and memory (Schulz et al., 1996). These neurons extend single neurites into the mushroom body calyx, pedunculus, and lobes (Figure 3.24) (Crittenden et al., 2018). It has also been reported that the olfactory antennal lobe and the visual optic lobes are directly connected to the mushroom body calyx (Yagi et al., 2016). Therefore, genes associated with the neurons of the mushroom body might indirectly affect neurons associated with the eye through these connections.

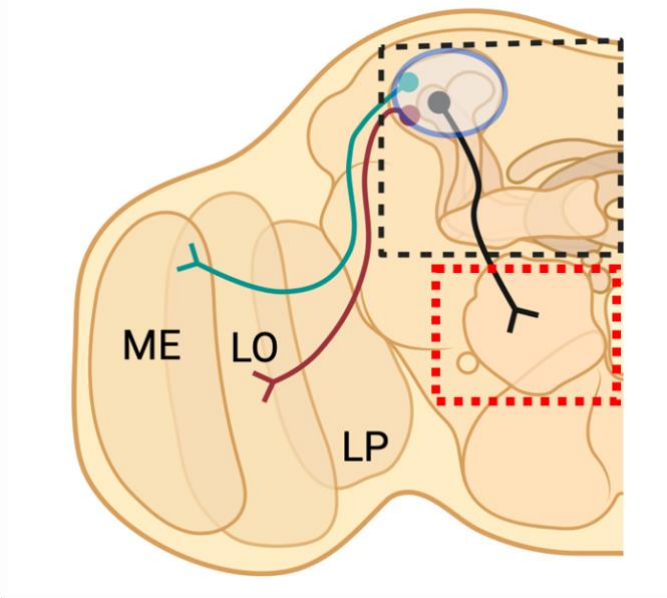

Figure 3.24. Schematic of the optic lobe – mushroom body neural networks.
Schematic diagram to show the neural connections that occur between the optic lobe and mushroom body (black dashed box), and the antennal lobe (red dashed box) and mushroom body. Visual projection neurons (green) project from the medulla, forming synapses with Kenyon cells in the mushroom body. Lobular projection neurons (red) also form synapses with Kenyon cells of the mushroom body. Antennal projection neurons (black) send signals from the antennal lobe glomerulus to the mushroom body. ME: Medulla, LO: Lobula, LP: Lobular Plate, black dashed line: mushroom body, red dashed line: antennal lobe glomerulus. Blue circle: Mushroom body calyx. This schematic was made using biorender.

Using the large-scale single-nucleus transcriptomic atlas of the adult *Drosophila* (https://scope.aertslab.org), there is evidence to show that, in addition to neurons of the brain, *Mef2* is expressed in all PR cells of the eye as well as cells of the optic and antennal lobes (Li et al., 2022). The RNA Seq dataset obtained from Scope showed that *Mef2* is expressed in the inner PR, namely R1-R6, and the outer PR, namely R7 and R8 (Figure 3.25). However, it is unclear at which timepoint this dataset came from. This conflicts the results that I have shown, where *Mef2* expression was not seen in the PRs using the Mef2GFP line. Definitively establishing when and where Mef2 is expressed in the adult eye will provide a better understanding as to the processes that could be impacted by knockdown of *Mef2* and hint toward mechanisms of effects on mHTT-induced degeneration.

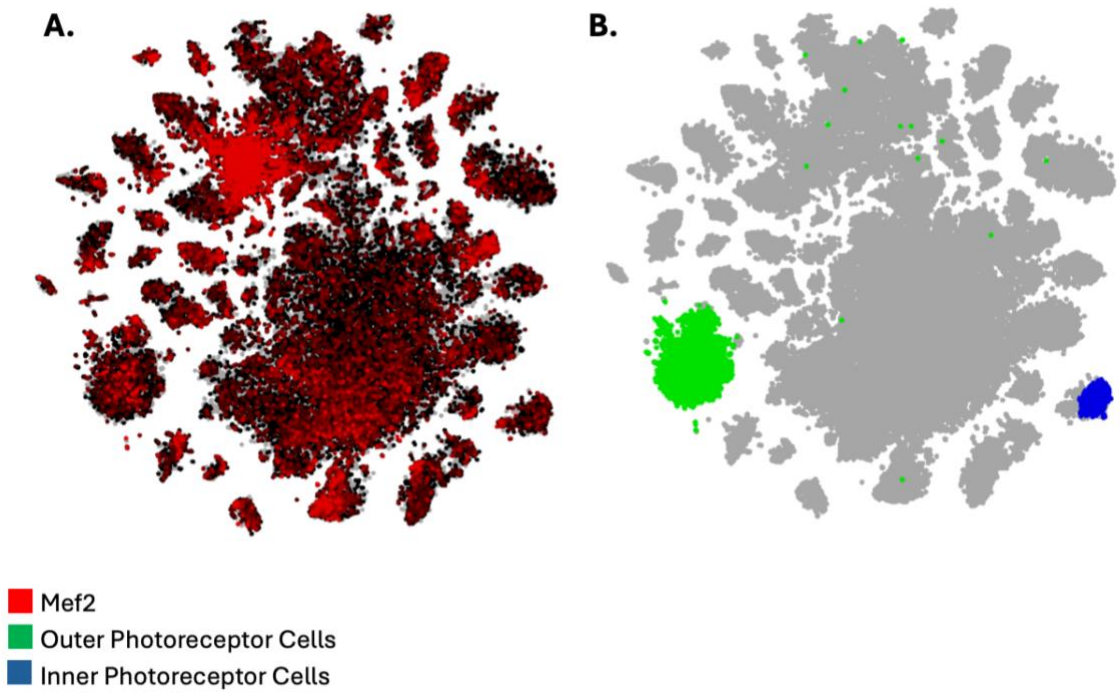

Figure 3.25. Mef2 expression in the adult head.
A) *Mef2* expression in the adult brain, and B) location of Inner and Outer photoreceptor cells of the adult eye showing positive *Mef2* expression in these regions. Grey cells represent all other cells of the adult head. Information from Scope (https://scope.aertslab.org).

3.4.6 *Drosophila* Mef2 is expressed in the developing brain, but not the photoreceptors

In this chapter the Mef2GFP line was used to determine the expression of endogenous Mef2 protein in the developing eye-brain complex. I showed that Mef2 protein is expressed in the eye-brain complex, from the L3 larval brain, through pupation, into adulthood. In the context of *Drosophila*, *Mef2* is particularly known for its role in the mushroom body of the brain and has been shown to be required for maintaining robust circadian behaviour (Blanchard et al., 2010; Crittenden et al., 2018), both processes of which have indirect communication with the *Drosophila* eye. In this chapter, I have shown that Mef2 is expressed in the L3 larval brain, but not the antennal-eye disc. During pupal development, Mef2 continues to be expressed in a population of cells in the central brain and appears in nuclei of neurons in the medulla (Figure 5). Interestingly, the Mef2-GFP line used in this project did not appear to show Mef2 expression in the mushroom body. However this was also previously reported by Blanchard and colleagues (2010) who stated that Mef2Gal4 driving UAS-LacZ expression did not detect Mef2 in mushroom body, attributing this to a more distal *Mef2* enhancer being responsible of expression in this brain region (Blanchard et al., 2010). Even more interestingly, using the Mef2-GFP line, I was unable to detect Mef2 in the PRs, which three papers have reported previously (Blanchard et al., 2010; Crittenden et al., 2018; Hall et al., 2017). Both Blanchard et al., (2010) and Crittenden et al. (2018) reported seeing Mef2 protein expression in the PR however, neither produced images to show this, and did not discuss the statement further. Hall and colleagues (2017) identified *Mef2* as an up-regulated gene in the aging PR transcriptome, which may indicate its' presence in the aging adult fly (Hall et al., 2017). Unlike other reports that use antibodies to detect *Mef2* expression, the Mef2-GFP fly line used in this project includes a GFP tag on the C-terminal end of the endogenous Mef2 protein which allows visualisation of endogenous protein in the live *Drosophila* system. Therefore, we can be sure that the expression is not impacted by autofluorescence and additional artifacts from imaging. As alluded to in the previous section, it may be that *Mef2* expression in the medulla of the optic lobe, has an indirect impact on the PRs and subsequent degeneration in the mHTT model.

3.4.7 *Mef2* may restore mHTT-affected synapses

Previous research has reported that pan-neuronal expression of mHTT in a *Drosophila* model of HD, abolishes synaptic transmission in response to light, and that PR depolarisation is

reduced (Rosas-Arellano et al., 2018). mHTT expression in these flies also leads to increased cell death in the central brain and optic lobes, as well as reduced axonal connectivity (Rosas-Arellano et al., 2018). The lamina of the optic lobe receives input from the outer PRs, R1-6, and serve as the main input to the motion vision circuitry (Kind et al., 2021). The medulla receives inputs from the inner PRs, R7-8, and the five Lamina Monopolar Cells (LMC) of the lamina (Courgeon & Desplan, 2019). These inner PRs form synaptic contacts with downstream neurons in the medulla, which in turn, influences behaviours such as phototaxis and navigation (Currier et al., 2023). These optic lobe regions are essential components for the visual processing system and disruption to these regions can lead to PR degeneration (Kind et al., 2021; Zheng et al., 2006). One such way that this may occur is through synaptic disruption. Studies have shown that information from outer PRs are transmitted via histaminergic synapses to two classes of interneuron within the lamina; LMCs and amacrine cells (AC) (Figure 3.24). (Zheng et al., 2006). Subsequently, PR axons receive feedback from the AC interneurons, providing direct communication to PR terminals (Figure 3.26). Studies have also shown that silencing lamina neurons affects basic visual behaviour and motion circuits (Tuthill et al., 2013). This may suggest that prolonged disruption of synaptic connections and subsequent abnormal signalling may lead to PR degeneration over time. Taking these observations together, it may be that reducing *Mef2* in my experiments, is able to slow down these processes, keeping synapses in-tact, and normalising PR depolarisation, which in turn, will keep PRs healthy.

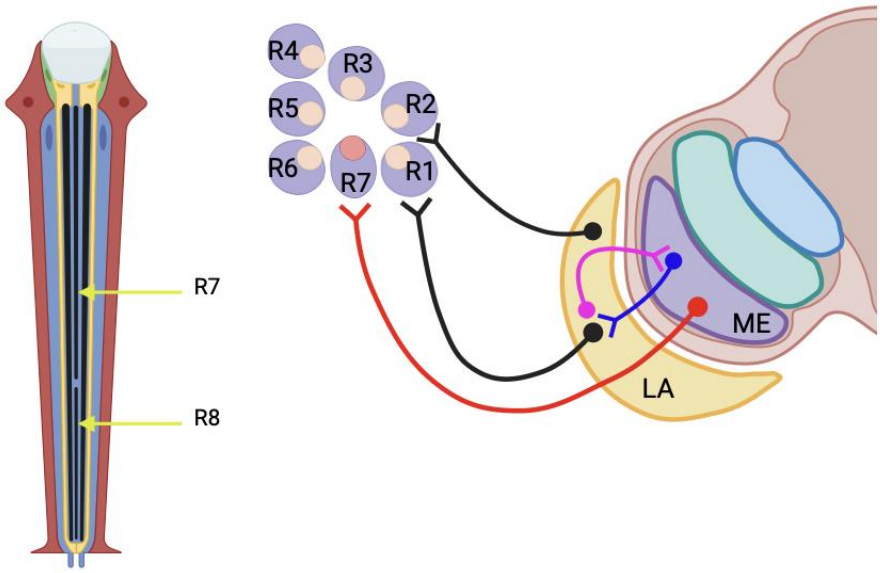

Figure 3.26. Schematic diagram of the Drosophila eye and photoreceptor connections to the optic lobe of the brain.

Schematic diagram of the rhabdomeres R1-R8, showing that outer photoreceptors, R1-R6, project photoreceptor axons to the lamina (black), and synapse with either laminar monopolar cells (blue) that synapse in the medulla, or amacrine cells (pink) that provide feedback to the photoreceptors. Inner photoreceptors R7 and R8 project photoreceptor axons (red) directly to the medulla. LA: Lamina, ME: Medulla. This schematic was made using biorender. Based on (Sahin & Çelik, 2013; Zheng et al., 2006).

When considering synapse vulnerability in the mammal, both *Mef2* and HTT are involved in the striatal neuronal function and survival (M. Lisek et al., 2023; Schulte & Littleton, 2011). Another protein involved in this process, is BDNF (West & Greenberg, 2011). BDNF has significant roles in differentiation, maturation and survival of neurons, and plays an active role in neurogenesis (Bathina & Das, 2015). It is also an important factor in HD, as it aids in survival of striatal neurons, and is known to be decreased in HD patients (Gauthier et al., 2004). One paper reported that downregulation of *Mef2D* in rat cortical neurons increased activity-dependent expression of BDNF (Avarlaid et al., 2024). It is important to note that Avarlaid and colleagues also showed that silencing of *Mef2D* reduced the activity-dependent induction of BDNF in rat hippocampal neurons (Avarlaid et al., 2024). The *Drosophila* ortholog of BDNF is a highly conserved Neurotophin (DNT1) (Lim et al., 2015). If this were reduced in the HD fly model, it might be restored by knocking down *Mef2*. However, it appears that *Mef2* can have brain-region specific effects, that would need to be addressed in both mouse and *Drosophila* models of HD. In future experiments, immunostaining of the *Drosophila* eye-brain complex,

should include DNT1, *Mef2*, and mHTT, to investigate their relative expression and to pave the way for studies of potential functional interactions.

3.4.8 Mef2C physically interacts with wild-type and mHTT

The Y2H assays conducted in this chapter confirmed that Mef2C 1-350aa physically interacts with WT and mHTT (1-450aa). Whilst the physical interaction between *Drosophila* Mef2 and mHTT was not investigated, due to the conserved nature of the MADS and Mef2 domains in the protein, it is likely that Mef2 and mHTT will physically interact. Notably, it would be valuable to test for physical interactions between the *Drosophila* Mef2 protein and HTT to confirm this. Using the Mef2GFP line, *Mef2* expression was not observed in the PRs, and therefore, it is unlikely that a physical interaction in the PRs is responsible for the suppression of rhabdomere loss. However, it might be that Mef2 and mHTT physically interact in Mef2-positive cells of the medulla, impacting the surrounding cells. For example, and as mentioned above, PR axons can receive feedback from AC interneurons, that synapse with LMCs in the medulla (Figure 3.23) (Tuthill et al., 2013). If Mef2 were present in the AC interneurons, and physically interacted with mHTT, it may be disruptive to cells, leading to PR degeneration. This would mean that downregulating Mef2 would reduce this happening. Further experiments should include defining the Mef2-positive cells that are in the medulla.

Interestingly, further Y2H assays in this chapter indicated that there is no physical interaction between the shorted Mef2C fragment (1-134aa) with either wild-type or mHTT. As well as the Mef2 and MADS domains, an additional 30aa region is conserved across the Mef2A, Mef2C and Mef2D mammalian proteins, the HJURP-C domain (Chaudhary et al., 2021; Wenwu Wu et al., 2011). This domain has been implicated in the assembly of centromere-specific nucleosomes and might suggest a role in PPIs or binding of DNA (Zasadzińska et al., 2013). Interestingly, reports have shown that the transcriptional activation domains of the C-terminus, TAD I and TAD II, complement the HJURP-C domain and are required for the activation of multiple transcriptional processes (Chaudhary et al., 2021). Therefore, it might mean that the presence of TAD I and/or TAD II are required with HJURP-C to bind. Next steps in this process could be to generate a plasmid containing the HJURP-C and TAD I/TAD II domains (for example, 86-174aa) and test for physical interactions with wild-type and mHTT.

3.4.9 Limitations and next steps

This chapter has provided insight into the role of *Mef2* in progression of mHTT-induced degeneration and lays the foundation for further experimentation in the future.

3.4.9.1 Expanding on the GAL80tsGal4/UAS system

Using the GAL80^{ts}Gal4/UAS system was a valuable method for investigating the potential neurodevelopmental contribution of mHTT expression in later degeneration. One limiting factor of the GAL80^{ts} system was the inability to investigate the effect of lifespan on pre-exposure to mHTT, and the presence of *Mef2* in this system, as 30°C is a temperature that flies tend not to survive well in. A recent publication described a collection of drug stabilising GAL80 lines as an alternative way to control gene expression (Kogenaru et al., 2024). Using a destabilising domain, fused to the GAL80 protein, gene expression can be controlled by the presence or absence of Trimethoprim (TMP) in normal food. In this method, the presence of TMP induces binding of the destabilising domain to the GAL80 protein, inhibiting Gal4 expression. In the absence of TMP, the destabilising domain unbinds, inducing Gal4 inducing expression of the transgene by UAS (Kogenaru et al., 2024). Methods such as this would provide an effective way to achieve conditional control of mHTT gene expression and provide an opportunity to investigate lifespan and motor function assays, without additional confounding variables.

3.4.9.2 Understanding how much Mef2 is downregulated using Mef2RNAi lines

As mentioned in section 3.4.4, downregulating *Mef2* using different RNAi lines had subtle but different effects on mHTT-induced degeneration. It would be valuable to understand the degree of *Mef2* downregulation using these RNAi lines. This could be achieved using the Mef2GFP line. By pan-neuronally downregulating *Mef2* in the Mef2GFP flies (Elav; Mef2GFP>UAS-Mef2RNAi), the progeny could be taken, eye-brain complexes stained for Mef2 using anti-GFP, and confocal images taken to quantify the levels of Mef2. Additionally, protein could be extracted from the flies and Western Blot conducted.

3.5 Conclusion

In this chapter, I have shown that *Drosophila* can be used to model mHTT-induced degeneration and investigate the effects of genetic modifiers on this process. I have also used the *Drosophila* model of mHTT-induced degeneration to investigate how the pre-exposure of neurons to mHTT can lead to neuronal vulnerability and significant development of rhabdomeres in the adult fly eye. Additionally, I have shown that *Mef2* downregulation can suppress a mHTT-induced degenerative phenotype in a whole-eye and pan-neuronal model of HD and that downregulation *Mef2* can also prolong fly survival.

Further experiments are required to investigate the full extent of mHTT pre-exposure in the developing and adult eye, which may include the use of the drug inducible GAL80. Additionally, immunostaining for mHTT, alongside markers of PR development and maintenance such as Rhodopsin, might provide additional insight into mHTT roles in degeneration, and the role of *Mef2* in suppressing degeneration.

Chapter 4: Striatal knockout of *Mef2C* in a mouse model of HD reduces the presence of mHTT

4.1 Introduction

The *Drosophila* work performed in chapter 3 has shown that downregulation of the single *Drosophila Mef2* gene is able to suppress disease progression in a whole-eye and pan-neuronal HD model (Figure 3.8/3.9). However, there is a lack of investigation of this phenomenon in a mammalian system. Global knockout of the mammalian *Mef2C* gene is embryonic lethal due to the severe cardiac complications during development, and therefore, investigations of *Mef2C* impacting the brain must be investigated by brain-specific knockout (Lin et al., 1997).

In the late 1990's, Eric Olson's laboratory in Texas reported that *Mef2* gene expression appears to follow gradients of neuronal maturation, with distinct, but overlapping patterns of expression in the regions of the frontal cortex, thalamus, hippocampus, and hindbrain (Lyons et al., 1995). In situ hybridisation of mouse embryonic tissue, with RNA probes for each Mef gene transcript detected *Mef2C* expression in the intermediate zone of the preoptic area of the telencephalon from 11.5 days post conception (dpc) (Lyons et al., 1995). The preoptic area of the telencephalon is reported to be one of the first regions of the embryonic brain in which neurons begin to differentiate. Mef2C mRNA expression is detected from 13.5 dpc in cells of the intermediate zone of the frontal cortex, regions of which contain differentiated neurons (Lyons et al., 1995). Due to the onset of *Mef2* gene expression and the initiation of neuronal differentiation in the associated brain regions, it was proposed that *Mef2* factors play a critical role in these processes. In the early 2000s, laboratories continued to study the role of *Mef2* isoforms in the developing brain, reporting roles in synapse formation and activity, neuronal cell fate, differentiation and apoptosis (A. C. Barbosa et al., 2008; Flavell et al., 2006; Leifer et al., 1993). In 2008, Olson's lab engineered a conditional knockout model to knockout *Mef2C* in neural stem/progenitor cells using the nestin-cre promoter (Hao Li et al., 2008). Only 60% of these n-Cre^{+}/Mef2C$^{loxp/\Delta 2}$-null mutant mice survived to adulthood, and in those that survived, researchers reported reduced brain size, reduced cortical thickness, and lower body

weight (H. Li et al., 2008)Behaviourally, these mice demonstrated abnormal anxiety-like behaviours and impaired cognitive function, as evidenced by behavioural changes in the elevated plus maze and the novel object recognition task (H. Li et al., 2008). Together, this research provided further evidence of *Mef2C*s role in neuronal differentiation.

A large body of research has successfully characterised the expression profile of *Mef2C* and its potential functional role in the cortex, hippocampus, and cerebellum (Kamath & Chen, 2019; Leifer et al., 1994b; Leifer et al., 1993; M. Lisek et al., 2023; Lyons et al., 1995). However, until recently, its role in the developing and adult mouse striatum has been largely unexplored. A microarray analysis performed in the host laboratory, identified *Mef2C* as a major up-regulated gene in embryonic striatal development (Precious et al., 2016) and as a result, a previous PhD student, Dr Heba Ali, produced a *Mef2C* gene expression profile in the mouse LGE, developing striatum, and adult striatum, and reported that mRNA expression levels varied across ages (Ali, 2022). mRNA levels of Mef2C were minimal at E12 but became evident at E14, and further increased by E16. There was a significant peak of Mef2C mRNA expression in the P0 striatum that gradually reduced, with minimal expression observed in the adult striatum (P21). Protein expression followed a similar pattern, although delayed, compared with that of mRNA in the early developing striatum, with detectable levels at E16. In the early postnatal striatum, Mef2C was found to be expressed more medially, with the most prominent expression found in the ventral-lateral aspect of the striatum, with minimal expression levels seen in the rostro-caudal regions. As with mRNA levels, protein expression was almost undetectable by P14 and into adulthood (Ali, 2022). Taken together, research in the wild-type striatum clearly implicates *Mef2C* in striatal development.

Using the Gsx2-driven Cre LoxP (Kessaris et al., 2006; Qin et al., 2016) to conditionally knockout *Mef2C* in the striatum, work in the host laboratory also confirmed significantly reduced striatal volume, MSN and total neuron cell count in a *Mef2C* striatal-knockout mouse (Ali, 2022), implicating *Mef2C* in MSN development. Other research has demonstrated that *Mef2C* co-localises with Ctip2, a transcription factor central to striatal development and MSN differentiation (Arlotta et al., 2008). Furthermore, *Mef2C* was shown to associate more prominently with the matrix compartment of the striatum which makes up roughly 80% of the total mammalian striatum (Morigaki & Goto, 2017).

Dr Ali's work is of particular interest to this project since MSNs are the neuronal subtype most vulnerable in HD (Ehrlich, 2012). Research has shown that MSNs in the striatum of mouse models of HD express lower levels of key markers of MSN identity compared with healthy MSNs (Matsushima et al., 2023). Additionally, imbalances in the activity of these neurons may be indicative of disease progression, associated with mHTT-related neurotoxicity and with motor and behavioural dysfunction (Morigaki & Goto, 2017). Further research using transcriptomic analysis in grade 1 human HD striata, and early stage R6/2 and zQ175 brains showed that striosome and matrix MSNs are differentially susceptible to degeneration through disease progression, with severe degeneration first in striosome MSNs that express D2Rs, followed by striosome MSNs expressing D1Rs, before degeneration of D2R-expressing matrix MSNs (Matsushima et al., 2023).

Since previous research in the laboratory has shown that *Mef2*C plays a role in development of striatal MSNs, and that subtypes of MSNs are more susceptible than others, it would be interesting to manipulate *Mef2C* in this brain region and determine whether this can manipulate neuronal phenotypes and subsequent disease progression. This work will also provide a step forward from the results outlined in chapter 3 that showed that downregulation of *Mef2* in a *Drosophila* model of HD is capable of significantly suppressing disease progression. Work in chapter 3 also identified a physical interaction between wild-type and mHTT with the N-terminal Mef2C protein fragment, which may indicate a potential mechanistic pathway of *Mef2* and mammalian *Mef2C* in HD disease progression. Therefore, it is important to know whether this phenomenon is translatable to the mammalian brain.

In this chapter, the R6/1 mouse model has been used to model the HD phenotype. The R6/1 mouse is a well-established transgenic line, with behavioural deficits such as hyperactivity and impulsive-like behaviour being reported from as young as 4-weeks of age (Bolivar et al., 2004; Rodríguez-Urgellés et al., 2022). By 16 weeks of age, additional motor and cognitive deficits have been reported using the balance beam and rotarod assays and automated activity boxes (Bolivar et al., 2004; Brooks, Janghra, et al., 2012; Brooks, Jones, et al., 2012). These behavioural phenotypes have been associated with the presence of neuronal inclusions and HTT aggregates in the striatum, decreased FoxP1 protein – which will be explained in more

detail in chapter 5 - and mRNA in the striatum, increased Iba1 in the hippocampus, and reduced Ctip2 and Darpp32+ MSNs (Brooks, Jones, et al., 2012; Louis Sam Titus et al., 2017; Naver, Stub, Moller, et al., 2003). For a detailed discussion of HD mouse models, please refer to section 1.3.2.3 of the introduction.

The aim of this chapter is to investigate whether striatal knockout of *Mef2C* in a mammalian model of HD can rescue phenotypic deficits observed in the HD mouse, and whether there are any changes to HD-associated pathology. To do this, I will generate a HD mouse model with striatal knockout of *Mef2C* and characterise the behavioural changes in these mice, before performing histological analysis. It is hypothesised that knockdown of *Mef2C* in the HD striatum will result in reduced HTT pathology, and increase MSN cell number, which may be implicated behaviourally by improvement on cognitive and behavioural tasks.

4.2 Methods

4.2.1 Experimental design

The four experimental groups used in this study were wild-type, $Cre^{+}Mef2C^{fl/fl}$, R6/1, and $R6/1Cre^{+}Mef2C^{fl/fl}$. To obtain mice in all experimental groups, $Cre^{-}Mef2C^{fl/fl}R6/1^{+}$ males were crossed with $Cre^{+}Mef2C^{fl/fl}R6/1^{-}$ females to avoid the presence of *Mef2C* deletion in the germline at testes level (Ali, 2022) (see section 4.2.2 for full breeding strategy). Table 4.1 outlines the full genotype of mice in each experimental group. 53 mice were tested on a battery of behavioural tasks at 6-, 8-, 12- and 16-weeks. The behavioural tasks included vertical pole, inverted grip strength, rotarod, balance beam, and open field (Ethovision). Following behavioural experiments at 16 weeks, mice were culled by transcardial perfusion. The brain tissue was harvested and IHC analyses of total neurons (NeuN), MSNs (DARPP-32), and mHTT inclusions (MW8) were conducted.

4.2.2 Generation of the R6/1Gsx2-Cre^{+}Mef2C$^{fl/fl}$ mouse line

The *Mef2C* striatal-knockout mouse line was generated by a previous PhD student in the host laboratory (Ali, 2022). In brief, *Mef2C* knockout is driven by the Gsx2 promoter, formally Gsh2, which is expressed along the anterior-posterior axis of the CNS, and is critical for establishing identity of the LGE (Deacon et al., 1994; Qin et al., 2016). To generate a new mouse line by which R6/1 HD mice also have striatal knockout of *Mef2C*, Gsx2-Cre^{-} Mef2C$^{fl/fl}$ females were crossed with males positive for the R6/1 transgene (Figure 4.1 F0). The resulting litter contained mice heterozygous for the *Mef2C* floxed allele, Mef2C$^{fl/+}$, that were either positive or negative for the R6/1 transgene. A Gsx2-Cre^{-} Mef2C$^{fl/+}$ male that was positive for the R6/1 transgene, was crossed to a Gsx2-Cre^{+} Mef2C$^{fl/fl}$ female (Figure 4.1 F1) to generate litters with varying combinations of Gsx2-Cre presence, Mef2C$^{fl/fl}$, Mef2C$^{fl/+}$ alleles, positive or negative for the R6/1 transgene (Table 4.1 F1). To maintain the colony, Gsx2-Cre^{-} Mef2C$^{fl/fl}$ R6/1 or Gsx2-Cre^{-} Mef2C$^{fl/+}$ R6/1 male mice were crossed with Gsx2-Cre^{+} Mef2C$^{fl/fl}$ or Gsx2-Cre^{+} Mef2C$^{fl/+}$ female mice, negative for the R6/1 transgene.

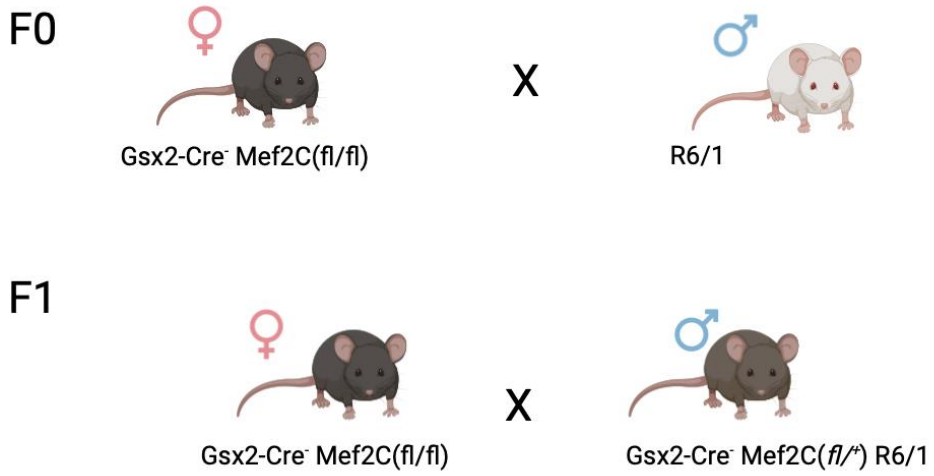

Figure 4.1. Breeding scheme to generate R6/1 Cre^{+}Mef2C $^{fl/fl}$ mouse line.
Gsx2-Cre^{-}Mef2C$^{fl/fl}$ females were crossed with males, positive for the R6/1 transgene (Figure 1 F0) to generate litters that were heterozygous for the *Mef2C* floxed allele (*Mef2C*$^{fl/+}$), that were either positive or negative for R6/1. A Gsx2-Cre^{-} Mef2C$^{fl/+}$ male, positive for the R6/1 transgene was crossed to a Gsx2-Cre^{+} Mef2C$^{fl/fl}$ female to generate a combination of genotypes that would be used for the experiment (Table 1).

Table 4.1 Experimental groups

fl/+ = heterozygous for Mef2C LoxP sites. fl/fl = homozygous for Mef2C LoxP sites.

Experimental Group	Presence of Gsx2-Cre	Presence of R6/1 transgene	Presence of Mef2C LoxP sites	N in group
Wild type	-	-	fl/fl or fl/+	20
$Cre^{+}Mef2C^{fl/fl}$	+	-	fl/fl	9
R6/1	-	+	fl/fl or fl/+	11
$R6/1Cre^{+}Mef2C^{fl/fl}$	+	+	fl/fl	13

4.2.3 Behavioural analysis

In the following experiment, there were four experimental groups: wild-type, $Cre^{+}Mef2C^{fl/fl}$, R6/1, and $Cre^{+}Mef2C^{fl/fl}$R6/1. All mice in the experiment were littermates, and behavioural testing of all genotypes were conducted at the same time. Mice were run on the behavioural apparatus at 6-, 8-, 12- and 16-weeks. Data from the 16-week timepoint are presented here for analysis since the phenotype in the R6/1 mice at earlier timepoints was subtle, making it challenging to assess the impact of knocking down *Mef2C.* The first question addressed in this chapter is whether the R6/1 colony produce the expected behavioural phenotype, and show significant deficits compared with the wild-type mice. Following, behavioural data was analysed to determine whether striatal knockout of *Mef2C* in the R6/1 influenced behaviour of the mice. It should be noted that the R6/1 data presented in sections 4.3 through 4.4 are the same. For weight data, repeated measures statistical analysis was used, with sex and weight as factors. For data obtained from all other behavioural tests, univariate ANOVA was used, with Genotype as a factor and Weight as a co-variate. For these analyses, both male and female data were pooled. Correcting for multiple comparisons was conducted using Bonferroni. Significance was reported is $p<0.05$.

4.2.4 Histological analysis

Following completion of behavioural experiments at 16-weeks-of-age, mice were culled, transcardially perfused and the whole brain stored until ready for histology. Brain tissue was cut coronally in 30μm sections, and antigen retrieval performed prior to histological staining.

Anti-NeuN was used to stain neuronal nuclei to determine the total number of neurons in the striatum. Using this stain, it was also possible to outline and measure the area of all striatal sections per sample, to determine brain volume. DARPP-32 was used as a marker for MSNs and MW8 used to observe the presence of mHTT inclusions. Images were taken using a light microscope, and ImageJ used to evaluate density of staining, total cell counts, and presence of mHTT inclusions. See section 2.3.5 of the methods for a full explanation of image analysis. As with behavioural tests, the R6/1 data presented next to wild-type and R6/1Cre^{+}Mef2C$^{fl/fl}$ data in section 4.4 is the same. Independent t-tests were used to determine differences between 16-week-old wild-type and R6/1 mouse brains, prior to investigating differences between R6/1 mouse brains, and R6/1 brains with striatal knockout of *Mef2C*. Bonferroni was used to correct for multiple comparisons and statistical significance was reached if $p<0.05$.

4.3 Behavioural Results

4.3.1 R6/1 mice have reduced body weight compared with wildtype littermates.

Mice were weighed at the end of each experimental week, and the data revealed that the R6/1 mice had significantly reduced body weight compared with wild-type controls (Effect of Genotype: $F_{1,90} = 6.299$, $p=0.019$) (Figure 4.2). Further analysis showed that there was no effect of Sex (Genotype*Sex: $F_{1,90} = 0.463$, $p=0.502$) (Figure 4.2). As there was no significant interaction between Genotype and Sex, post-hoc analysis was not run.

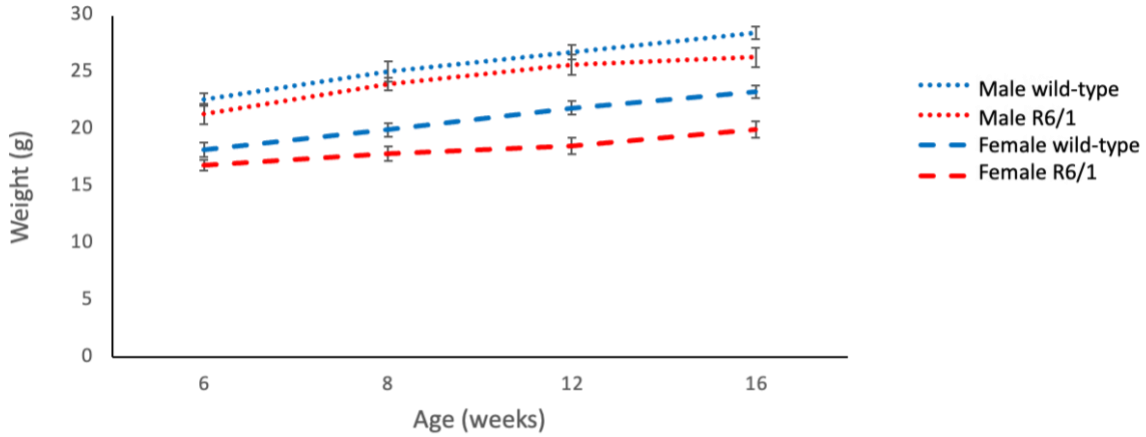

Figure 4.2. R6/1 mice show reduced weight compared with wild-type littermates.
A line graph representing the average weight data at each experimental timepoint for the R6/1 (red) and wild-type (blue) mice. Data points represent the average weight for each timepoint for the genotype, split by sex. Dotted lines represent male data, and dashed lines represent female data. R6/1

mice had reduced body weight compared with wild-type controls (Effect of Genotype: $F_{1,90}$ = 6.299, p=0.019). There was no effect of Sex (Genotype*Sex: $F_{1,90}$ = 0.463, p=0.502). Error bars = SEM.

4.3.2 R6/1 mice take significantly more time to descend the vertical pole compared with wild type littermates.

The vertical pole is used to assess motor coordination and spatial orientation in mice and is a proven evaluator of movement in conjunction with striatal abnormalities (Matsuura et al., 1997). The time taken for mice to descend the vertical pole was measured. At 16 weeks, R6/1 mice were slower to descend the vertical pole, compared with wild-type littermates (wild-type: 5.4s +/- 0.46 (mean +/- SEM); R6/1: 11.1s +/- 0.95; Effect of Genotype: $F_{1,28}$ = 36.613, p<0.001) (Figure 4.3).

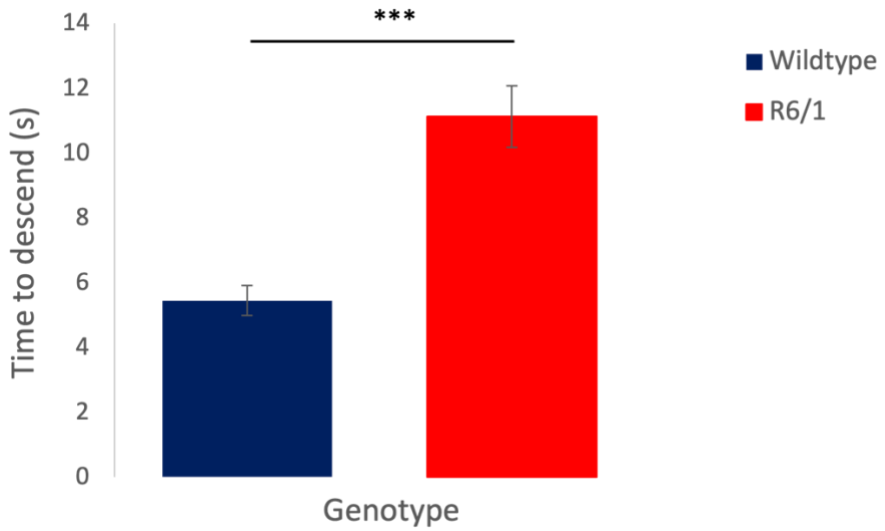

Figure 4.3. R6/1 mice are significantly slower to descend a vertical pole compared with wild-type littermates.
Graph to show that at 16-weeks, R6/1 mice take significantly longer to descend the vertical pole compared with wild-type littermates (wild-type 5.4s +/- 0.46, R6/1 11.1s +/- 0.95, Effect of Genotype: $F_{1,28}$ = 36.613, p<0.001). ***p<0.001.

4.3.3 R6/1 mice do not show significant deficits in the inverted grip strength compared with wild type mice.

A test of inverted grip strength indicates strength of the mice, and any potential abnormalities in the ability to hold on to a given object (Deacon, 2013). The time the mouse spent grasping the grid without falling, in a 60 second period, was recorded as the latency to fall. There was

no significant difference in the latency to fall in a 60-second period between R6/1 and wild-type littermates, at 16 weeks of age (wild-type: 48s +/- 4.7, R6/1: 52s +/- 3.8, Effect of Genotype: $F_{1,20}$ = 0.026, p=0.874) (Figure 4.4).

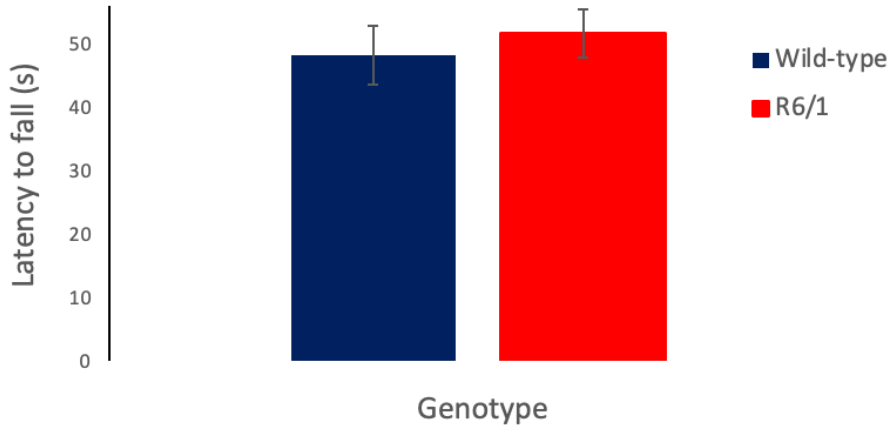

Figure 4.4. R6/1 mice do not show any deficits in the inverted grip strength test compared with wild type mice.
A graph to show that at 16 week of age, R6/1 mice do not show any genotype differences in the latency for mice to fall from the metal grid (wild-type: 48s +/- 4.7, R6/1: 52s +/- 3.8, $F_{1,20}$ = 0.026, p=0.874).

4.3.4 R6/1 mice fall much sooner, and fall more times per trial on the rotarod, compared with wild-type mice.

The rotarod can also reveal deficits in motor coordination and balance and is often used when testing models of degeneration (Hamm et al., 1994; Wagner et al., 2008). The accelerating rotarod tests the ability to stay on a rod of gradually increasing speed, whilst the fixed rotarod tests the ability of mice to stay on a rod at a constant speed of, for example, 12rpm. At 16 weeks of age, R6/1 mice fell from the accelerating rotarod faster compared with wild-type mice (wild-type: 159s +/- 10.8, R6/1 79s +/0 10.5, Effect of Genotype: $F_{1,28}$ = 36.292, p<0.001) (Figure 4.5A). In addition, R6/1 mice fell faster from the fixed rotarod, compared with wild-type littermates (wild-type: 57s +/- 1.4, R6/1: 22s +/- 4.1, Effect of Genotype: $F_{1,28}$ = 59.797, p<0.001) (Figure 4.5Bi). On the fixed rotarod, an additional measure of total falls, was calculated. At 16 weeks, R6/1 mice fell on average, more times across the three trials from the fixed rotarod compared with wild-type littermates (wild-type: 1 +/- 0.4, R6/1: 12 +/- 1.6, Effect of Genotype: $F_{1,29}$ = 50.503, p<0.001).

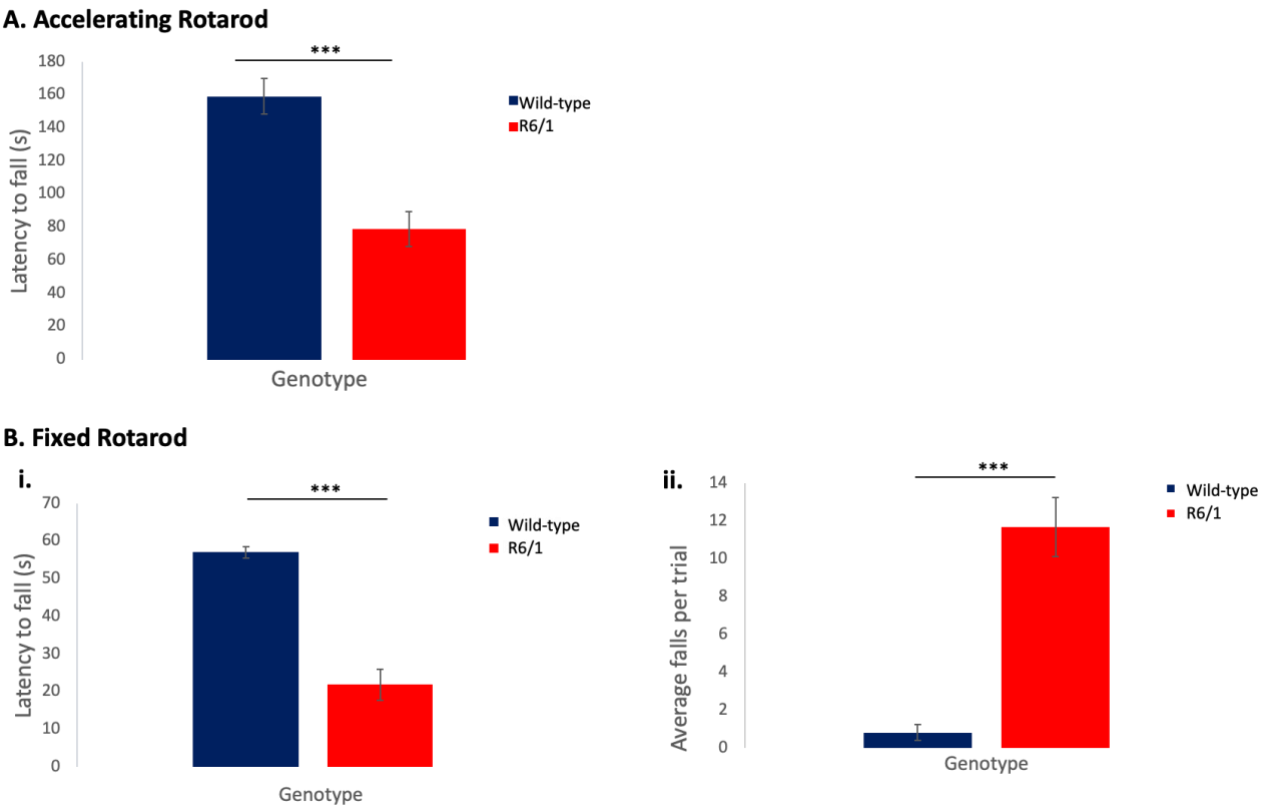

Figure 4.5. R6/1 mice show deficits in accelerating and fixed rotarod.
A). Graph to show that at 16-weeks of age, R6/1 mice fall from the accelerating rotarod much sooner than wild-type littermates wild-type: 159s +/- 10.8, R6/1 79s +/0 10.5, Effect of Genotype: $F_{1,28}$ = 36.292, p<0.001). Bi). At 16-weeks, R6/1 mice fall from the fixed rotarod much sooner than wild-type littermates (wild-type: 57s +/- 1.4, R6/1: 22s +/- 4.1, Effect of Genotype: $F_{1,28}$ = 59.797, p<0.001). Bii). Similarly, at 16-weeks, R6/1 mice fell from the fixed rotarod, on average, more times per trial, compared with wild-type mice (wild-type: 1 +/- 0.4, R6/1: 12 +/- 1.6, Effect of Genotype: $F_{1,28}$ = 50.503, p<0.001). ***p<0.001.

4.3.5 R6/1 mice take longer to turn and traverse the beam, and travel less up the beam, compared with wild-type littermates.

The balance beam tests mice fine motor coordination and balance (Luong et al., 2011). The time taken for the mice to turn 180° and face the beam and the time taken to traverse the beam were recorded. An average of three test trials were taken and reported here. At 16 weeks, R6/1 mice took longer to turn 180° and face the beam compared with wild-type littermates (wild-type: 6.7s +/- 3.9, R6/1: 35.1s +/- 7.6. Effect of Genotype: $F_{1,28}$ = 14.052, p<0.001) (Figure 4.6A). The R6/1 mice also took longer to traverse the beam compared with wild-type littermates (wild-type: 46.6s +/- 10.0, R6/1: 107.6s +/- 9.7. Effect of Genotype: $F_{1,28}$ = 14.257, p<0.001) (Figure 4.6B). However, upon visualisation of the experiment, it was noticed that whilst some mice don't reach the top of the beam in the allotted 2 minutes, they

do travel some distance. Therefore, the average distance travelled up the beam across the three trials was calculated. R6/1 mice travel significantly less up the beam compared with the wild-type littermates (wild-type 90cm +/- 5, R6/1 12cm +/- 8, $F_{1,28}$ = 49.544, p<0.001) (Figure 4.6C).

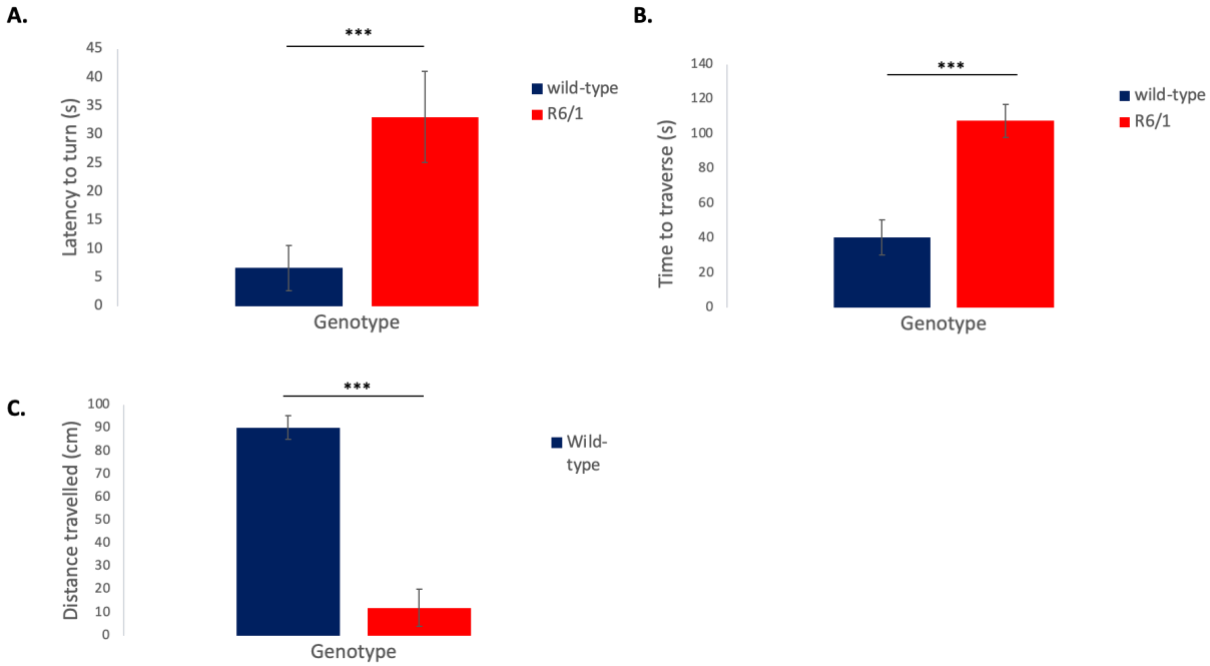

Figure 4.6. R6/1 mice take significantly longer to turn, longer to traverse the balance beam and do not travel as far up the beam, compared with wild type.

A). Graph to show that at 16 weeks, R6/1 mice take longer to turn 180° and face the beam, compared with wild-type littermates (wild-type: 6.7s +/- 3.9, R6/1: 35.1s +/- 7.6. Effect of Genotype: $F_{1,28}$ = 14.052, p<0.001). B). Additionally, 16-week-old R6/1 mice take significantly longer to traverse the balance beam, compared with wild-type littermates (wild-type: 46.6s +/- 10.0, R6/1: 107.6s +/- 9.7. Effect of Genotype: $F_{1,28}$ = 14.247 p<0.001). C) R6/1 mice travel significantly less up the balance beam compared with wild-type littermates (wild-type 90cm +/- 5, R6/1 12cm +/- 8, $F_{1,28}$ = 49.544, p<0.001).

4.3.6 R6/1 mice move more slowly, moved a lesser distance, and reared less frequently, compared with wild-type littermates.

The open field activity boxes were used to assess locomotor activity in an open arena. The Ethovision software recorded several exploratory parameters over a 5-minute period and data was automatically collected for subsequent analysis. Parameters analysed include total distance moved (cm), mean velocity (cm/s), total duration of movement (s), and frequency of rearing. The 16-week-old R6/1 mice moved less in the 5-minute period, moved more slowly,

moved a lesser distance, and reared less frequently, compared with wild-type littermates (Total distance moved: wild-type 3736cm +/- 309, R6/1 1481cm +/- 330, Effect of Genotype: $F_{1,28}$ = 19.967, p<0.001. Mean velocity: wild-type 16.1cm/s +/- 2.2, R6/1 5.5cm/s +/- 1.2, Effect of Genotype: $F_{1,28}$ =9.751, p<0.004. Total duration of movement: wild-type 260s +/- 6.5, R6/1 171s +/- 16.8, Effect of Genotype: $F_{1,28}$ = 26.462, p<0.001. Frequency of rearing: wild-type 57 +/- 5, R6/1 24 +/- 4, Effect of Genotype: F_1 = 19.223, p<0.001) (Figure 4.7).

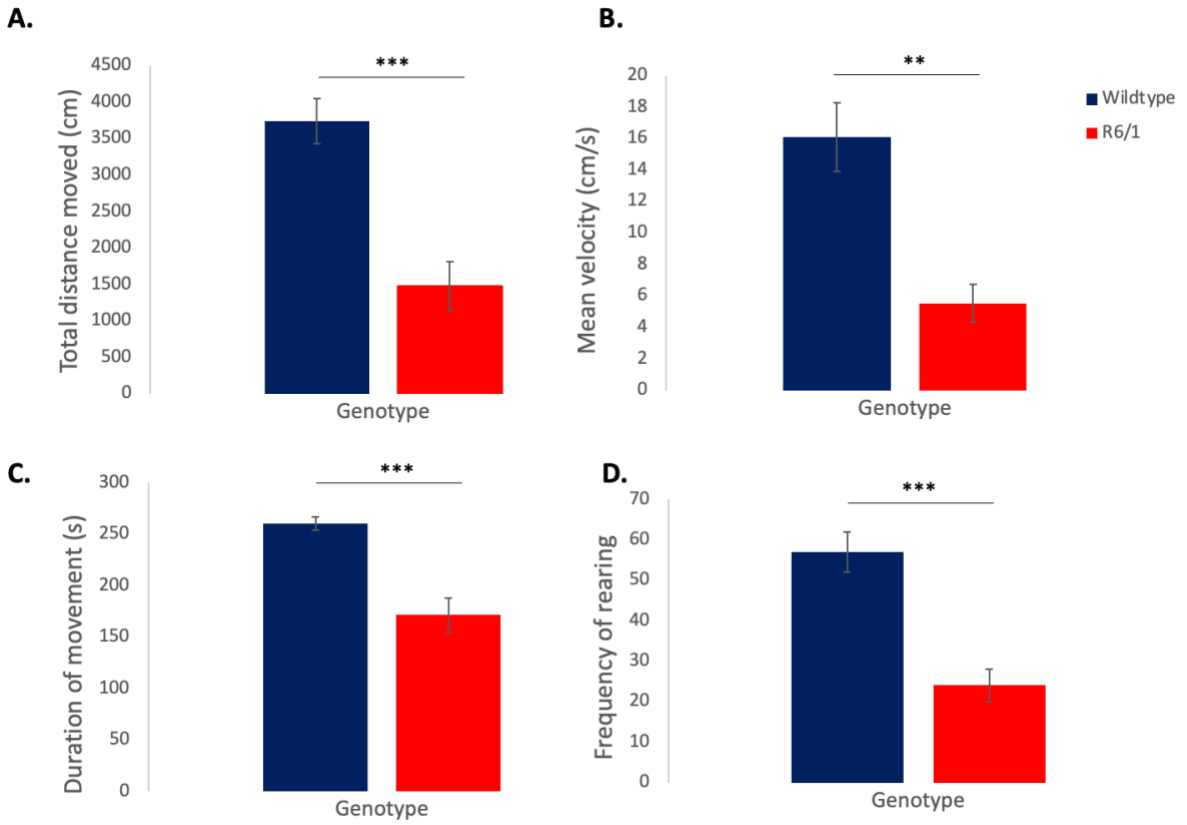

Figure 4.7. R6/1 mice move more slowly, moved a lesser distance, and reared less frequently, compared with wild-type littermates.

Graphical representation of open field parameters in the 16-week-old R6/1 mouse compared with wild-type littermates. The 16-week-old R6/1 mice moved less in the 5-minute period (A), moved more slowly, (B) moved a lesser distance (C), and reared less frequently, (D) compared with wild-type littermates (Total distance moved: wild-type 3736cm +/- 309, R6/1 1481cm +/- 330, Effect of Genotype: $F_{1,28}$ = 19.967, p<0.001. Mean velocity: wild-type 16.1cm/s +/- 2.2, R6/1 5.5cm/s +/- 1.2, Effect of Genotype: $F_{1,28}$ =9.751, p<0.004. Total duration of movement: wild-type 260s +/- 6.5, R6/1 171s +/- 16.8, Effect of Genotype: $F_{1,28}$ = 26.462, p<0.001. Frequency of rearing: wild-type 57 +/- 5, R6/1 24 +/- 4, Effect of Genotype: $F_{1,28}$ = 19.223, p<0.001). **p<0.01, ***p<0.001.

The previous section has shown that the R6/1 colony used in this experiment have the expected behavioural phenotype compared with that which has been reported in the

literature (Naver, Stub, Moller, et al., 2003). The next question to address was whether striatal knockout of Mef2C influenced any of these behavioural phenotypes. As mentioned above, behavioural testing of all genotypes was run together, and the R6/1 data presented in section 4.2 is the same as the data presented in section 4.1. Weight was analysed using a repeated measures analysis with Genotype and Sex as factors. Behavioural data was analysed using a univariate ANOVA, with Sex and Genotype as factors. Significance was achieved if $p<0.05$ and correcting for multiple comparisons was conducted using Bonferroni.

4.3.7 Striatal knockout of *Mef2C* in R6/1 mice does not influence body weight

The weight of mice at 6-, 8-, 12- and 16-weeks of age were recorded. There was no overall effect of genotype in the weights of R6/1 mice and R6/1 mice with striatal knockout of *Mef2C* across the timepoints recorded (Effect of Genotype: $F_{1,80} = 0.663$, $p=0.436$) (Figure 4.8). Since there were no effects, further post-hoc analyses were not run.

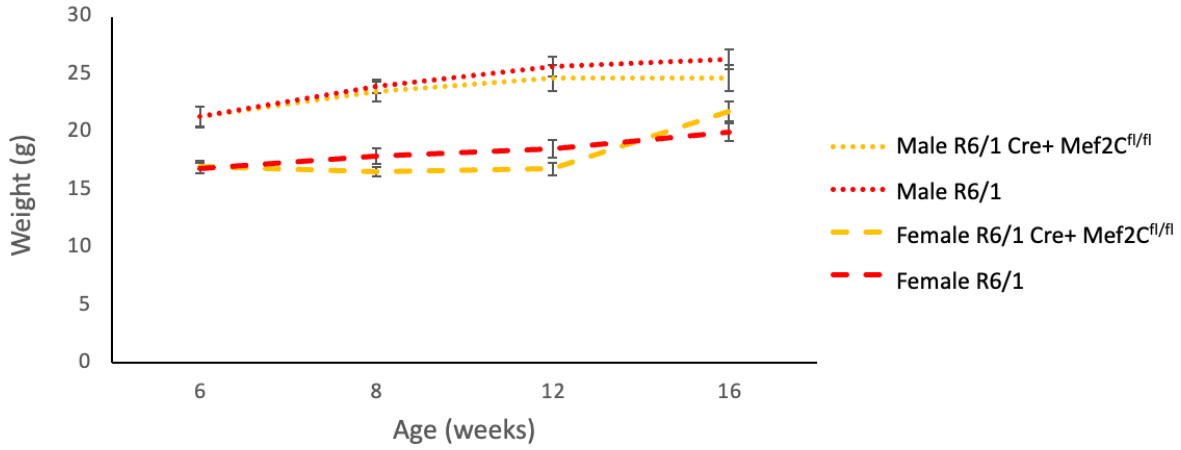

Figure 4.8. Striatal knockout of Mef2C in the R6/1 mouse does not influence body weight.
Line graph to represent the change of weight across time, of R6/1 mouse (red) and R6/1 mouse with striatal knockout of *Mef2C* (orange). Data points represent the average weight for each timepoint for the genotype, split by sex. Data points represent the average weight for each timepoint for the genotype, split by sex. Dotted lines represent male data, and dashed lines represent female data. There was no overall difference in weight between R6/1 mice and R6/1 mice with striatal knockout of the same sex (Effect of Genotype: $F_{1,80} = 0.663$, $p=0.436$). R6/1 data presented here is the same as data presented in Figure 4.2

4.3.8 There is no difference on vertical pole performance in R6/1 mice with striatal knockout of *Mef2C* compared with R6/1

The time taken to descend a vertical pole was measured at 16-weeks of age. At 16-weeks, there was no difference in time taken to descend the pole between the R6/1 mice with striatal knockout of *Mef2C* and the R6/1 mice (R6/1: 11.1s +/- 0.9, R6/1 Cre+ Mef2C$^{fl/fl}$: 12.5s +/- 2, Effect of Genotype: $F_{1,20}$ = 0.813, p=0.378) (Figure 4.9).

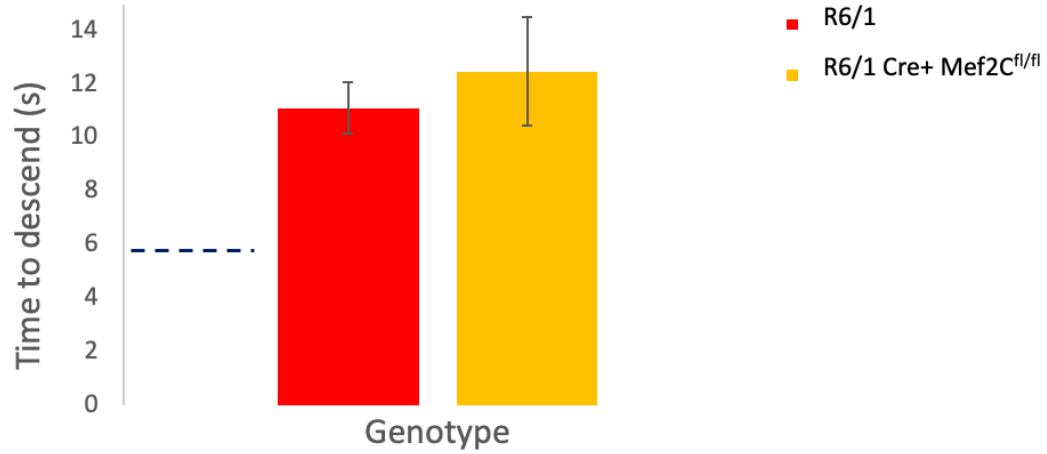

Figure 4.9. Striatal knockout of Mef2C in an R6/1 model does not influence ability to perform vertical pole.
Graphical representation of time taken to descend a vertical pole. At 16-weeks, there was no difference between genotypes: R6/1: 11.1s +/- 0.9, R6/1 Cre+ Mef2C$^{fl/fl}$: 12.5s +/- 2, Effect of Genotype: $F_{1,20}$ = 0.813, p=0.378). Dotted line indicates the average wild-type data. R6/1 data presented here is the same as data presented in Figure 4.3.

4.3.9 R6/1 mice with striatal knockout of *Mef2C* fall faster in the inverted grip strength test, compared with the R6/1 mice, alone.

Mice were put on a metal grid, which was inverted, and the latency to fall from the grid was recorded. At 16 weeks, R6/1 mice with striatal knockout of *Mef2C* held on to the grid for less time than the R6/1 mice (R6/1: 51.6s +/- 3.8, R6/1 Cre+Mef2C$^{fl/fl}$: 32.9s +/- 7.0, Effect of Genotype: $F_{1,20}$ = 6.881, p=0.016) (Figure 4.10).

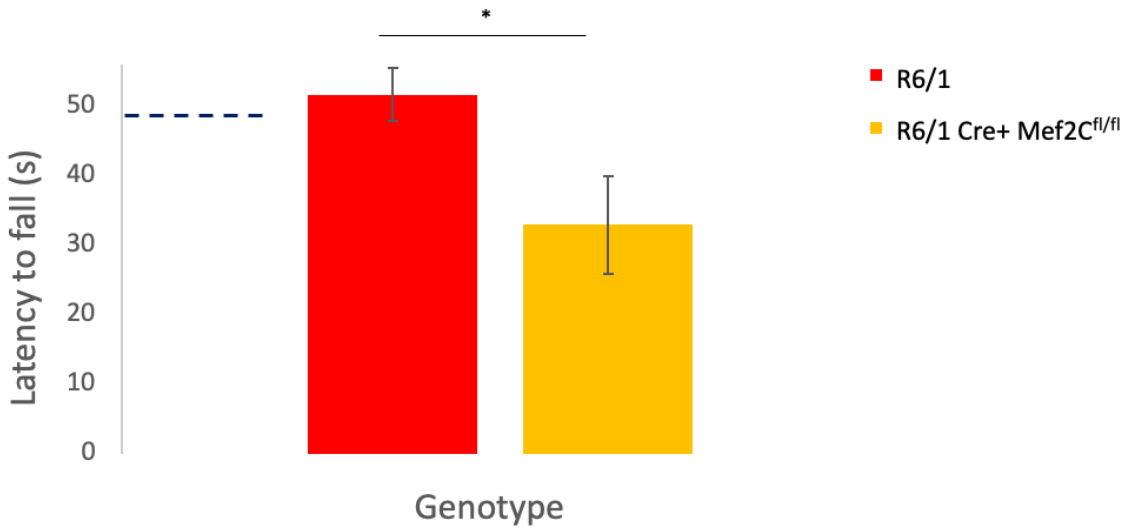

Figure 4.10. Striatal knockout of Mef2C significantly reduces ability for mice to hold on to a metal grid.

Graphical representation of data to show that the 16-week-old R6/1 mice with striatal knockout of *Mef2C*, fall faster in the inverted grip strength test, compared with R6/1 mice, alone (R6/1: 51.6s +/- 3.8, R6/1 Cre+Mef2C$^{fl/fl}$: 32.9s +/- 7.0, Effect of Genotype: $F_{1,20}$ = 6.881, p=0.016). Dotted line indicates the average wild-type data. R6/1 data presented here is the same as data presented in Figure 4.4.

4.3.10 Striatal knockout of *Mef2C* in R6/1 mice does not influence latency to fall from the rotarod or number of falls per trial.

R6/1 mice are unable to stay on an accelerating or fixed speed rotarod compared with wild-type littermates and fall significantly more from the fixed rotarod (Figure 4.5A-C). Striatal knockout of *Mef2C* in the R6/1 model did not influence the latency to fall from the accelerating or fixed rotarod (Accelerating Rotarod: R6/1 79s +/- 10.5, R6/1 Cre+Mef2C$^{fl/fl}$ 69s +/- 10.0, Effect of Genotype: $F_{1,20}$ = 0.730, p=0.403). Fixed Rotarod: R6/1 21.9s +/- 4.1, R6/1 Cre+Mef2C$^{fl/fl}$ 30.5s +/- 4.9, Effect of Genotype: $F_{1,20}$ = 1.371, p=0.255) (Figure 4.11 A, B). Regarding average total falls per trial on the fixed rotarod, 16-week R6/1 mice with striatal knockout of *Mef2C* fall a similar number of times to R6/1 mice (R6/1 12 +/- 2, R6/1 Cre+Mef2C$^{fl/fl}$ 14 +/- 2, Effect of Genotype: $F_{1,20}$ = 0.051, p=0.823) (Figure 4.11C).

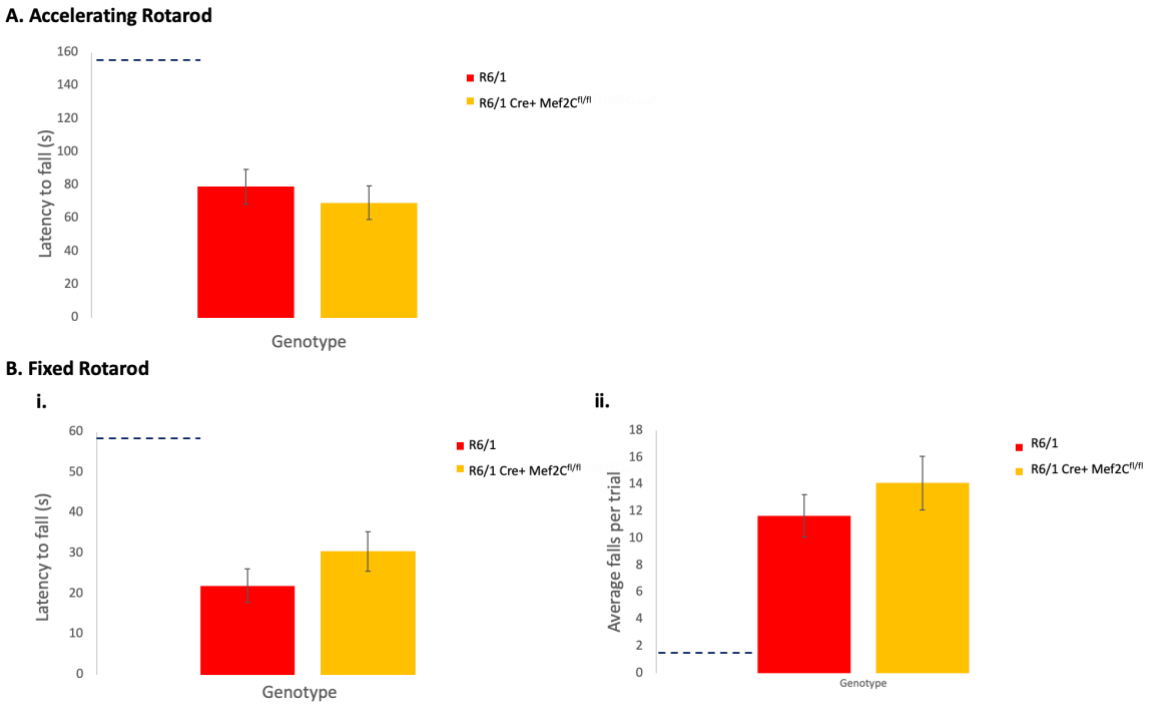

Figure 4.11. Striatal knockout of Mef2C in R6/1 mice does not significantly influence rotarod parameters.

Graphical representation of 16-week-old rotarod data to show that striatal knockout of *Mef2C in the R6/1 mice does not lead to changes in latency to fall from an (A) accelerating rotarod (R6/1 79s +/- 10.5, R6/1 Cre+Mef2C$^{fl/fl}$ 69s +/- 10.0, Effect of Genotype: $F_{1,20} = 0.730$, p=0.403), (B) latency to fall from a fixed rotarod (R6/1 21.9s +/- 4.1, R6/1 Cre+Mef2C$^{fl/fl}$ 30.5s +/- 4.9, Effect of Genotype: $F_{1,20} = 1.371$, p=0.255), or (C) average falls per fixed rotarod trial (R6/1 12 +/- 2, R6/1 Cre*+Mef2C$^{fl/fl}$ 14 +/- 2, Effect of Genotype, $F_{1,20}$ = 0.051, p=0.823). Dotted line indicates the average wild-type data. R6/1 data presented here is the same as data presented in Figure 4.5.

4.3.11 R6/1 mice with striatal knockout of *Mef2C* travel further on the balance beam compared with R6/1 mice.

16-week-old R6/1 with striatal knockout of *Mef2C* do not turn 180° faster on the beam prior to traversing it (R6/1 35s +/- 7.6, R6/1 Cre+Mef2C$^{fl/fl}$ 19.2s +/- 4.9, Effect of Genotype: $F_{1,20}$ =0.673, p=0.422) (Figure 4.12A). There was no difference between the two genotypes regarding time to traverse the balance beam (R6/1 107.6s +/- 9.7, R6/1 Cre+Mef2C$^{fl/fl}$ 85.2s +/- 12.8, Effect of Genotype: $F_{1,20}$ = 1.209, p=0.285) (Figure 4.12B). However, when running the beam, it was noticed, that whilst most of these mice did not reach the top, the R6/1 mice with striatal knockout of *Mef2C* were getting further toward the end point. Therefore, videos were analysed and the distance travelled up the beam was recorded. At 16-weeks of age, R6/1 mice with striatal knockout of *Mef2C* travelled considerably further up the beam compared

with R6/1 only littermates (R6/1 12cm +/- 8, R6/1 Cre+Mef2C$^{fl/fl}$ 73cm +/- 10, Effect of Genotype: $F_{1,20}$ = 22.592, p<0.001) (Figure 4.12C).

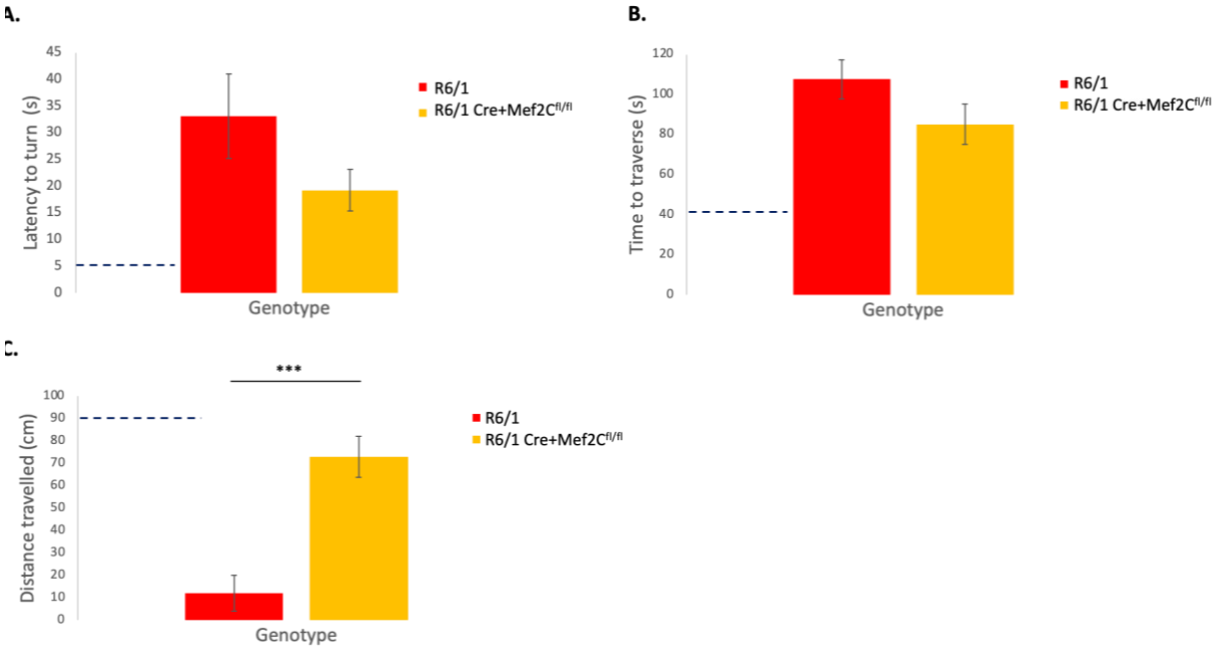

Figure 4.12. R6/1 mice with striatal knockout of *Mef2*C travel further up the beam compared with R6/1 mice.

Graphical representation of 16-week-old R6/1 and R6/1 Cre^{+}Mef2C$^{fl/fl}$ balance beam parameters. A) R6/1 mice with striatal knockout of *Mef2C* do not turn faster on the balance beam, compared with R6/1 mice (R6/1 35s +/- 7.6, R6/1 Cre^{+}Mef2C$^{fl/fl}$ 19.2s +/- 4.9, Effect of Genotype: $F_{1,20}$ =0.673, p=0.422). B) There is no difference between genotypes when comparing time taken to traverse the beam (R6/1 107.6s +/- 9.7, R6/1 Cre^{+}Mef2C$^{fl/fl}$ 85.2s +/- 12.8, Effect of Genotype: $F_{1,20}$ = 1.209, p=0.285). C) R6.1 mice with striatal knockout of Mef2C travel further up the balance beam compared with R6/1 littermates (R6/1 12cm +/- 8, R6/1 Cre^{+}*Mef2C*$^{fl/fl}$ 73cm +/- 10, Effect of Genotype: $F_{1,20}$ = 22.592, p<0.001). ***p<0.001. Dotted line indicates the average wild-type data. R6/1 data presented here is the same as data presented in Figure 4.6.

4.3.12 Striatal knockout of *Mef2C* in R6/1 mice does not impact total distance moved, duration of movement, mean velocity or rearing in the open field.

Mice were placed in the open field arena for 5 minutes and Ethovision software used to report total distance moved, mean velocity of movement, total duration of movement, and frequency of rearing. The 16-week-old R6/1 mice with striatal knockout of *Mef2C* did not show any behavioural differences when in the open field area, and there were no changes in total distance moved (R6/1 1481cm +/- 330, R6/1 Cre^{+}Mef2C$^{fl/fl}$ 1595cm +/- 303, Effect of

Genotype: $F_{1,20}$ = 0.006, p=0.940), mean velocity (R6/1 5.5cm/s +/0 1.2, R6/1 Cre+Mef2C$^{fl/fl}$ 4.3cm/s +/- 0.9, Effect of Genotype: $F_{1,20}$ =1.251, p=0.277), total duration of movement (R6/1 171s +/- 16.8, R6/1 Cre+Mef2C$^{fl/fl}$ 173s +/- 18.1, Effect of Genotype: $F_{1,20}$ = 0.013,, p=0.911), or frequency of rearing (R6/1 24 +/- 4, R6/1 Cre+Mef2C$^{fl/fl}$ 27 +/- 7, Effect of Genotype: $F_{1,20}$ = 0.033, p=0.857) when compared with R6/1 mice, alone (Figure 4.13).

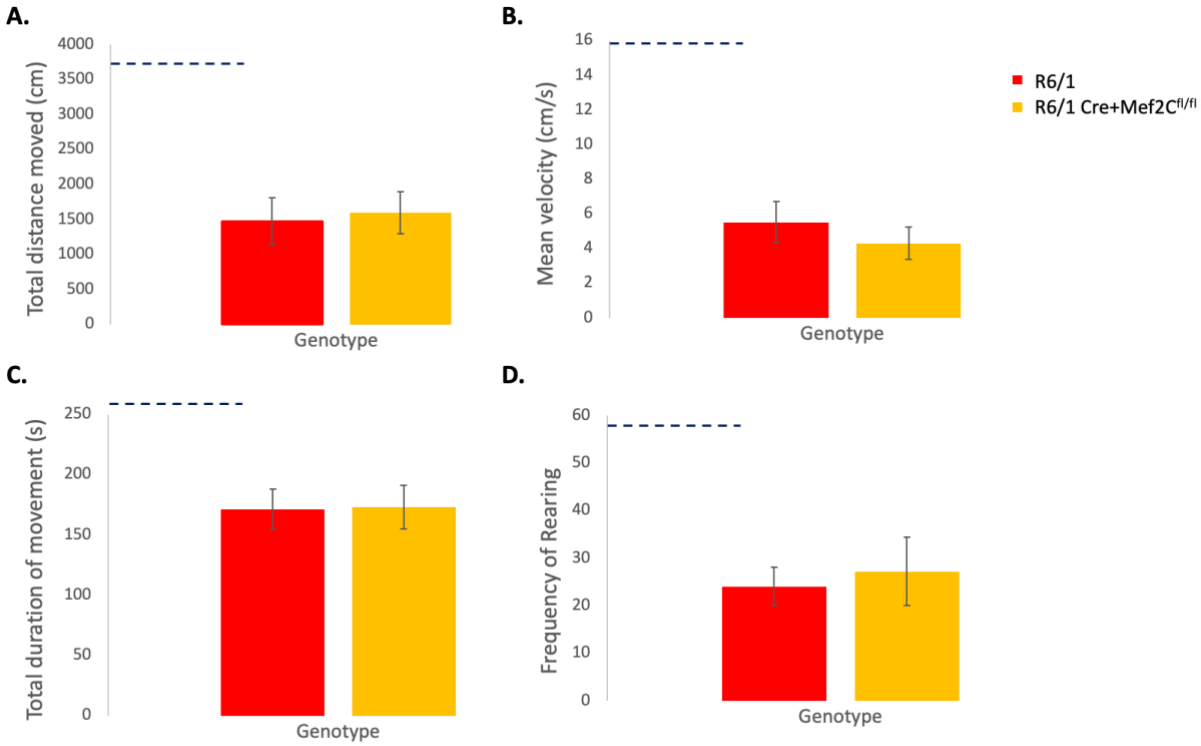

Figure 4.13. R6/1 mice with striatal knockout of Mef2C show no changes in distance moved, velocity, duration of movement or rearing in open-field arena.

Graphical representation of 16-week-old open field data, comparing R6/1 mice and R6/1 mice with striatal knockout of *Mef2C*. R6/1 with striatal knockout of Mef2C show no changes in total distance moved (R6/1 1481cm +/- 330, R6/1 Cre^{+}Mef2C$^{fl/fl}$ 1595cm +/- 303, Effect of Genotype: $F_{1,20}$ = 0.006, p=0.940) (A), mean velocity (R6/1 5.5cm/s +/0 1.2, R6/1 Cre^{+}Mef2C$^{fl/fl}$ 4.3cm/s +/- 0.9, Effect of Genotype: $F_{1,20}$ = 1.251, p=0.277) (B), total duration of movement (R6/1 171s +/- 16.8, R6/1 Cre^{+}Mef2C$^{fl/fl}$ 173s +/- 18.1, Effect of Genotype: $F_{1,20}$ = 0.013,, p=0.911) (C), or frequency of rearing (R6/1 24 +/- 4, R6/1 Cre^{+}Mef2C$^{fl/fl}$ 27 +/- 7, Effect of Genotype: $F_{1,20}$ = 0.033, p=0.857) (D) when compared with R6/1 mice, alone (Figure 4.13). Dotted line indicates the average wild-type data. R6/1 data presented here is the same as data presented in Figure 4.7.

4.4 Histological analysis

4.4.1 R6/1 mice have significantly reduced striatal volume and total NeuN+ nuclei compared with wild-type littermates.

The total volume of the striatum was calculated in the 16-week-old wild-type and R6/1 brain tissue to determine differences between these two genotypes. At 16 weeks, the R6/1 striatum is significantly smaller than wild-type littermates (wild-type: 3.8 mm^3 +/- 0.06, R6/1: 3.1 mm^3 +/- 0.1, t_{28}= 5.757, $p<0.001$) (Figure 4.14B). The number of NeuN-positive cells were also calculated per mm^3, and analysis showed that there is no difference in the number of NeuN-positive cells per mm^3 in the R6/1 striatum compared with the wild-type striatum (wild-type 16,444 cells/mm^3 +/- 516, R6/1 18,538 cells/mm^3 +/- 1,370, Effect of Genotype: t_{29} = -1.429, p=0.087) (figure 4.14A/C). Neither was there a difference between the total number of NeuN-positive cells in the whole striatum of the wild-type and R6/1 brain (wild-type: 64,996 cells +/- 2,625, R6/1: 58,583 cells +/= 4984, t_{29}= 1.25, p=0.111) (Figure 4.14D).

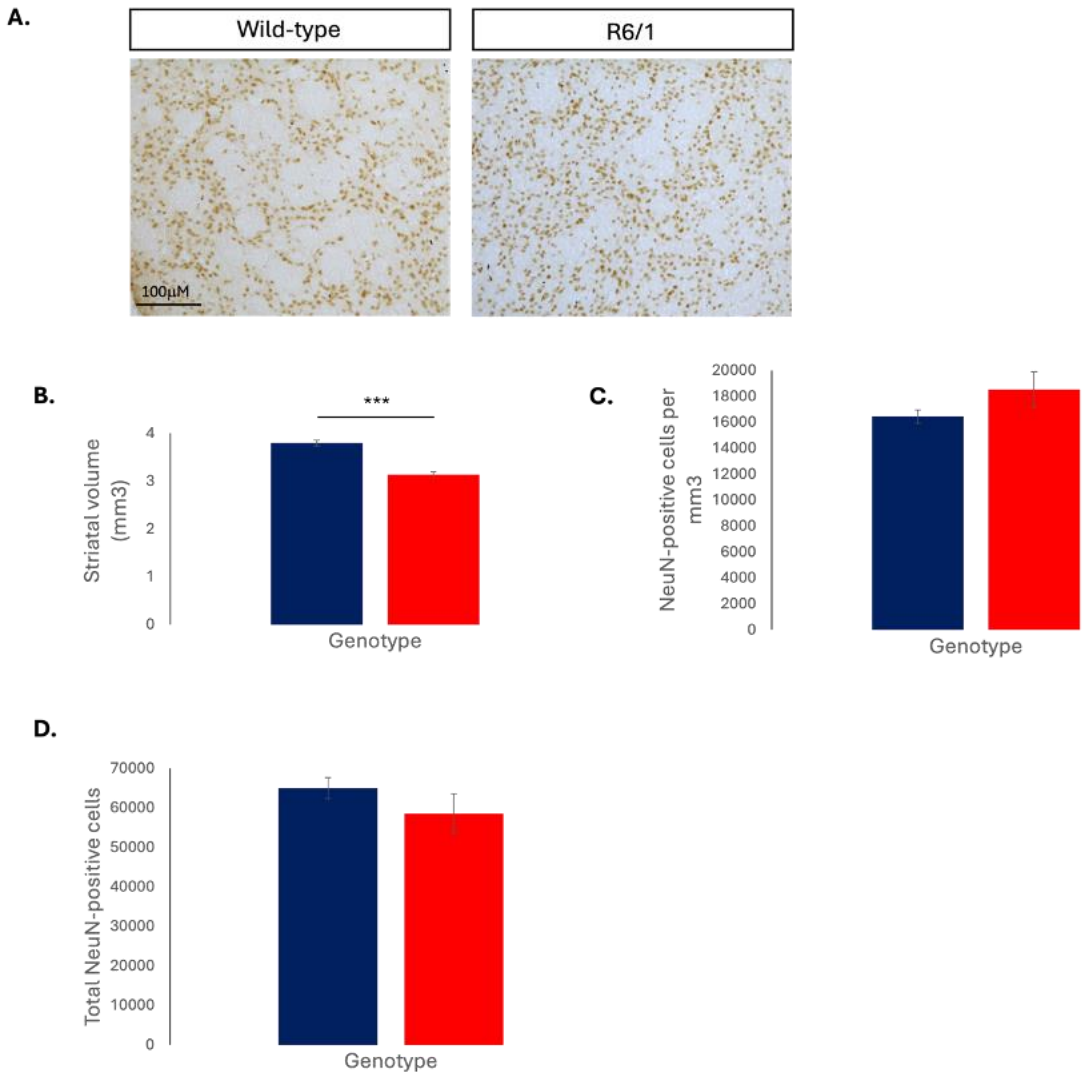

Figure 4.14. R6/1 mice have a smaller striatum and fewer NeuN+ cells compared with the wild-type striatum.

A) Representative images of wild-type and R6/1 striatum showing NeuN-positive cells under light microscopy, at 10x magnification. B) Graphical representation of the 16-week striatal volume in the R6/1 mouse, compared with wild-type littermates. The R6/1 striatum is significantly smaller than the wild-type striatum at this timepoint (wild-type: 3.8 mm^3 +/- 0.1, R6/1: 3.1mm^3 +/- 0.1, t_{28}= 5.757, p<0.001). B) At 16 weeks, there is no difference in the number of NeuN+ cells per mm^3 (wild-type 16,444 cells/mm^3 +/- 516, R6/1 18,538 cells/mm^3 +/- 1,370, Effect of Genotype: t_{29} = -1.429, p=0.087). D) There was no difference in the total NeuN count per striatum in the wild-type versus R6/1 brain (wild-type: 64,996 cells +/- 2,625, R6/1: 58,583 cells +/= 4984, t_{29}= 1.25, p=0.111). ***p<0.001. Scale bar = 100µm.

4.4.2 The R6/1 striatum has significantly fewer DARPP32-positive cells than wild-type littermates.

DARPP32 is known as a gold standard marker of striatal MSNs and is a common marker used to investigate changes in model of HD since MSNs are the vulnerable neuronal subtype in this disease (Ehrlich, 2012). There was no difference between the number DARPP32+ cells per mm^3in the 16-week-old R6/1 striatum, compared with the wild-type striatum (wild-type 16,996 cells per mm^3 +/- 520, R6/1 15,704 cells per mm^3 +/- 718, Effect of Genotype: t_{25} = 1.481, p=0.076) (Figure 4.15A/B). When calculating the number of DARPP32+ cells in the whole striatum there were significantly fewer DARPP32+ cells in the R6/1 striatum compared with the wild-type striatum (wild-type 64,842 cells +/- 1,571, R6/1 48,505 cells +/-1,528, Effect of Genotype: t_{26} =6.795, p<0.001) (Figure 4.15C).

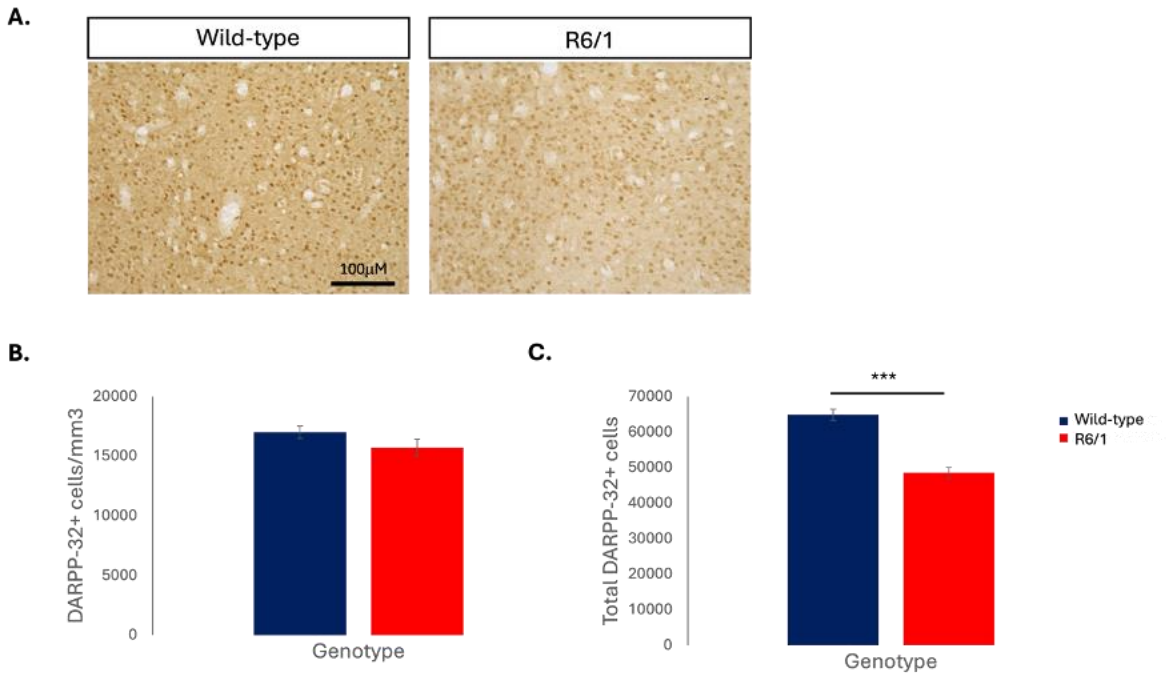

Figure 4.15. The R6/1 striatum has fewer DARPP32+ cells compared with the wild-type striatum.
A) Images of DARPP32-positive staining in the 16-week-old wild-type and R6/1 striatum. Images taken at 10x magnification. B) Graphical representation of the number of DARPP32-positive cells, calculated per mm^3. Whilst there is a trend toward fewer cells in the R6/1 striatum, there is no difference between genotypes (wild-type 16,996 cells per mm^3 +/- 520, R6/1 15,704 cells per mm^3 +/- 718, Effect of Genotype: t_{25} = 1.481, p=0.076). C) Graphical representation of the total number of DARPP32+ cells in the whole striatum. R6/1 striatum has significantly fewer DARPP32+ cells compared with the whole wild-type striatum (wild-type 64,842 cells +/- 1,571, R6/1 48,505 cells +/-1,528, Effect of Genotype: t_{26} =6.795, p<0.001). Scale bar = 100µm. ***p<0.001.

4.4.3 Striatal knockdown of *Mef2C* in the R6/1 mouse does not impact striatal volume or total cell count.

Histological analysis in section 4.4.1 and 4.4.2, showed that the 16-week-old R6/1 striatum was considerably smaller and had fewer DARPP32-positive MSNs, compared with the wild-type striatum. The next question to address was whether striatal knockdown of *Mef2C* in the R6/1 striatum impacts striatal volume or the presence of cells within the striatum. As with the behavioural experiments, the R6/1 data presented here is the same data reported in section 4.4.1 and 4.4.2. Statistical analysis was conducted using independent t-tests.

Striatal knockdown of *Mef2C* in the R6/1 mouse did not significantly impact the total striatal volume compared with the R6/1 mouse striatum (R6/1 3.1 mm^3 +/- 0.1, R6/1 $Cre^{+}Mef2C^{fl/fl}$: 3.2 mm^3 +/- 0.5, t_{21}= 0.632, p=0.261) (Figure 4.16A). There was also no difference in the number of NeuN+ cells per mm^3 (R6/1 18,538 cells per mm^3 +/- 1,370 , R6/1 $Cre^{+}Mef2C^{fl/fl}$ 18,440 cells per mm^3+/- 990, Effect of Genotype: t_{21} = -0.054, p=0.479) (Figure 4.16B) or in the whole-striatum (R6/1 58,583 cells +/- 4,984, R6/1 $Cre^{+}Mef2C^{fl/fl}$ 60,955 cells +/- 3,677, Effect of Genotype: t_{19} = 0.360, p=0.362) (Figure 4.16C) between the two genotypes.

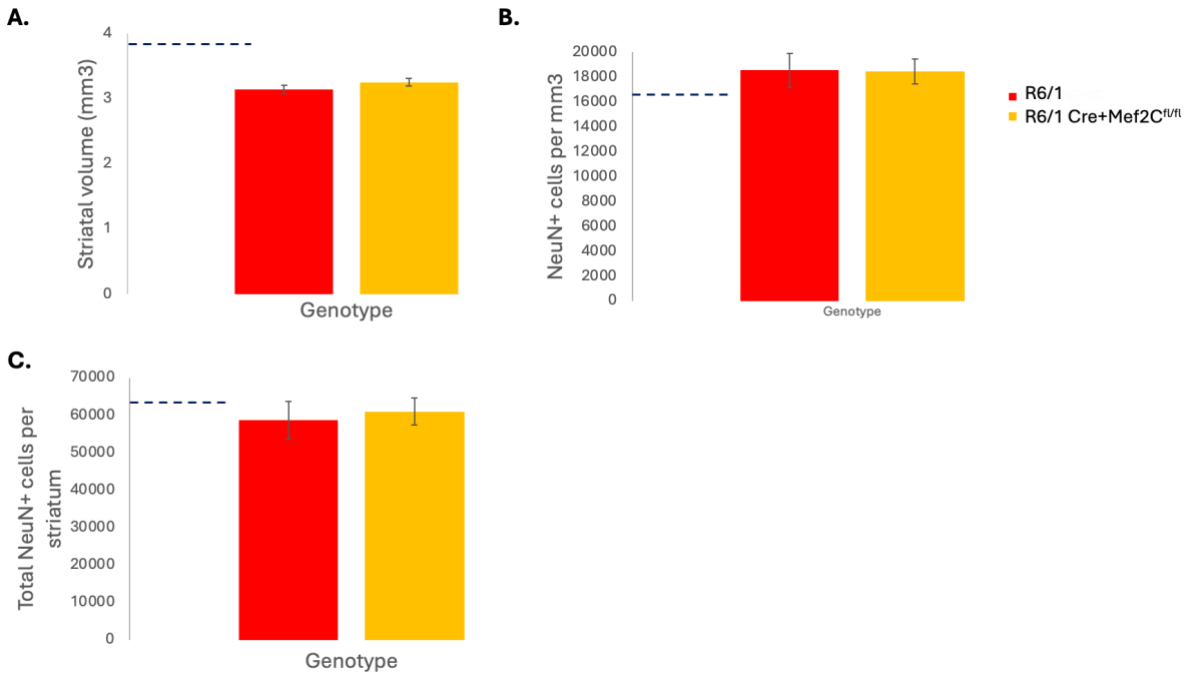

Figure 4.16. Striatal knockout of Mef2C does not impact R6/1 striatal volume or cell count.
A) Graphical representation of striatal volume (A), NeuN cell count per mm^2 (B) and total NeuN cell count (C) in the 16-week-old of R6/1 striatum, and R6/1 striatum with striatal knockdown of Mef2C. A) There is no difference between the striatal volume of R6/1 mice and the R6/1 mice with striatal

knockdown of Mef2C (R6/1 3.1 mm^3 +/- 0.1, R6/1 $Cre^{+}Mef2C^{fl/fl}$: 3.2 mm^3 +/- 0.5, t_{21}= 0.632, p=0.261). B). The NeuN cell count per mm^3 is not different between the R6/1 striatum and the R6/1 striatum with striatal knockdown of Mef2C (R6/1 18,538 cells per mm^3 +/- 1,370, R6/1 $Cre^{+}Mef2C^{fl/fl}$ 18,440 cells per mm^3+/- 990, Effect of Genotype: t_{21} = -0.054, p=0.479). C) Neither is there a difference in the total NeuN cell count (R6/1 58,583 cells +/- 4,984, R6/1 $Cre^{+}Mef2C^{fl/fl}$ 60,955 cells +/- 3,677, Effect of Genotype: t_{19} = 0.360, p=0.362). Dotted line indicates the average wild-type data. R6/1 data presented here is the same as data presented in Figure 4.14.

4.4.4 Striatal knockout of *Mef2C* in the R6/1 mouse does not influence the presence of DARPP32+ MSNs

Striatal knockdown of *Mef2C* in the R6/1 striatum at 16 weeks does not influence the number of DARPP32+ cells per mm^3 (R6/1 15,704 cells per mm^3 +/- 718 , R6/1 R6/1 $Cre^{+}Mef2C^{fl/fl}$ 15,537 cells per mm^3 +/- 1,220, Effect of Genotype: t_{17} = -0.122, p=0.452) (Figure 4.17A) or in the total striatum (R6/1 48,505 cells +/- 1529, R6/1 $Cre^{+}Mef2C^{fl/fl}$ 48,813 +/-4,171, Effect of Genotype: $t_{10.131}$ = 0.069, p=0.473) (Figure 4.17B), compared with the 16-week R6/1 striatum.

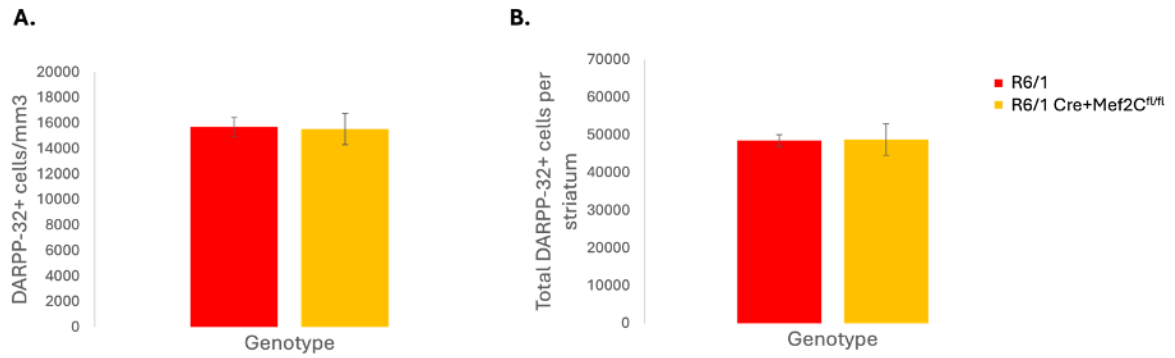

Figure 4.17. Striatal knockout of Me2C in the R6/1 striatum does not influence presence of MSNs.
A) Graphical representation of the number of DARPP32+ cells per mm^3in the 16-week-old R6/1 striatum with striatal knockdown of *Mef2C*, compared with the R6/1 striatum, alone (R6/1 15,704 cells per mm^3 +/- 718, R6/1 R6/1 $Cre^{+}Mef2C^{fl/fl}$ 15,537 cells per mm^3 +/- 1,220, Effect of Genotype: t_{17} = -0.122, p=0.452). B) The total number of DARPP32+ cells in the striatum does not differ between the two genotypes (R6/1 58,583 cells +/- 4,984, R6/1 $Cre^{+}Mef2C^{fl/fl}$ 60,955 cells +/- 3,677, Effect of Genotype: t_{19} = 0.360, p=0.362). Dotted line indicates the average wild-type data. R6/1 data presented here is the same as data presented in Figure 4.15.

4.4.5 Striatal knockout of *Mef2C* significantly reduces presence of mHTT inclusions in R6/1 mouse

The presence of mHTT inclusions is a pathological hallmark of HD and is present throughout the brain in the R6/1 mouse using the MW8 antibody (Bayram-Weston et al., 2016). Using the MW8 antibody to detect the presence of mHTT inclusions, 3x 20x magnification images were taken to represent the lateral, medial and ventral portions of the striatum to determine an average number of mHTT inclusions per mm^3 (Figure 4.18). mHTT inclusions were present throughout the striatum of the 16-week-old R6/1 striatum (Figure 4.18Ai-Aiii). mHTT inclusions were also present throughout the striatum of the 16-week-old R6/1 striatum with striatal knockdown of *Mef2C* (Figure 4.18Bi-iii). The number of mHTT inclusions across all 9 images were used to calculate an average number of mHTT inclusions per mm^3, and an independent t-test used to determine any difference between the presence of mHTT inclusions in the brains of these two genotypes. There were significantly fewer mHTT inclusions per mm^3 in the R6/1 striatum with striatal knockdown of *Mef2C*, compared with the R6/1 striatum (R6/1 34,821 cells per mm^3 +/- 1,045, R6/1 $Cre^{+}Mef2C^{fl/fl}$ 27,208 cells per mm^3 +/- 2,672, Effect of Genotypes: $t_{21} = -2.741$, p=0.006) (Figure 4.19A).

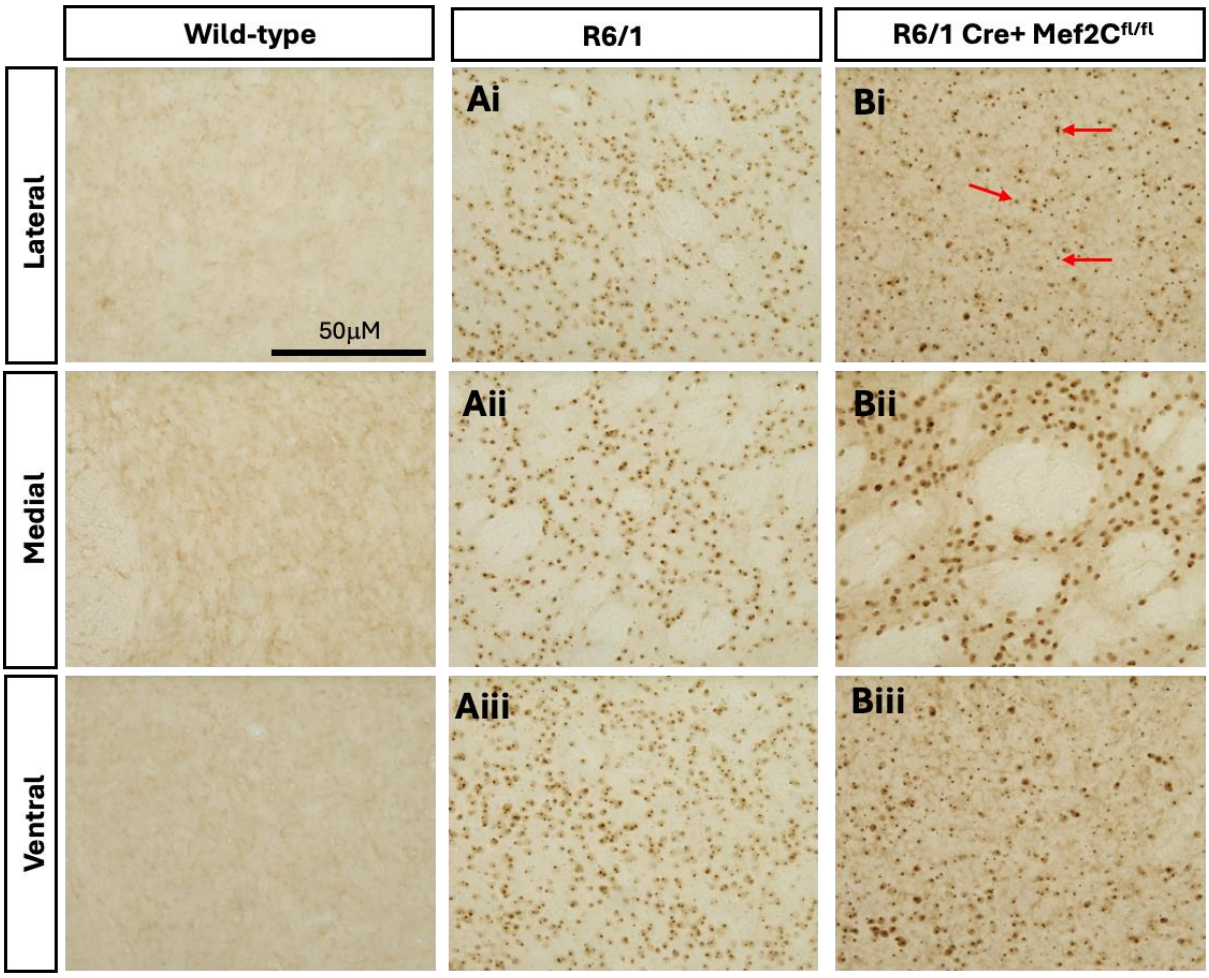

Figure 4.18. Striatal knockout of Mef2C in an R6/1 model significantly reduces presence of mHTT inclusions.

Figure to show the presence of mHTT inclusions via anti-MW8 immunohistochemistry in the lateral, medial and ventral striatum. mHTT inclusions are not present in the wild-type striatum but are present throughout the 16-week R6/1 striatum (Ai-Aiii) and R6/1 striatum with striatal knockout of *Mef2C* (Bi-Biii). Red arrows indicate mHTT inclusions. Scale bar = 50μm.

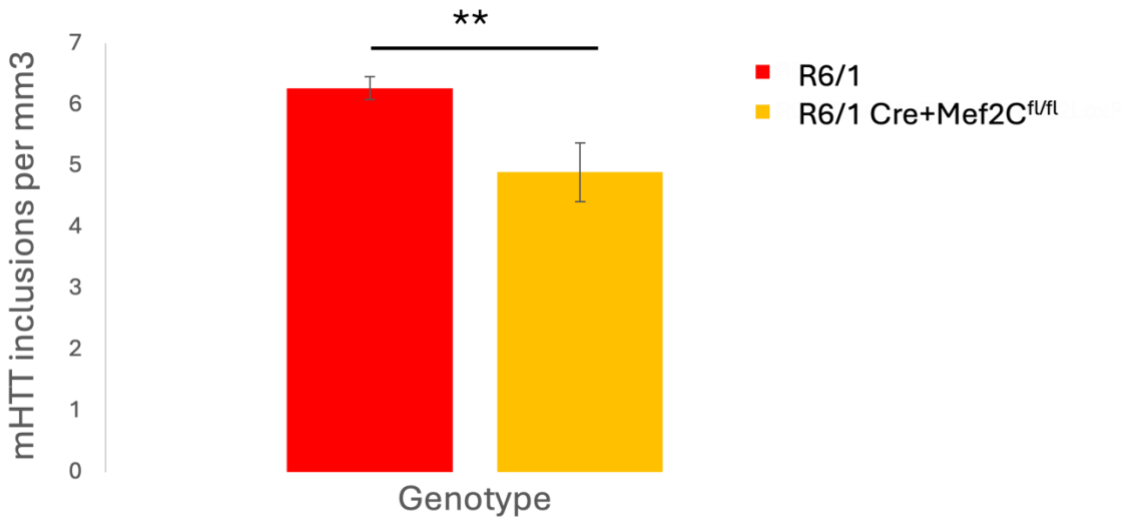

Figure 4.19. Striatal knockout of Mef2C in an R6/1 model leads to fewer mHTT inclusions.
Graphical representation of the number of mHTT inclusions per mm^3 in the R6/1 striatum, compared with the R6/1 striatum with striatal knockout of *Mef2C*. There are fewer mHTT inclusions in the R6/1 striatum with *Mef2C* knockout, compared with the R6/1 striatum, alone (R6/1 6.3 cells per mm^3+/- 0.1, R6/1 $Cre^{+}Mef2C^{fl/fl}$ 4.9 cells per mm^3 +/- 0.5, Effect of Genotypes: t_{21} = 2.741, p=0.006). **p<0.01.

Since there were significantly fewer mHTT inclusions per mm^3 in the R6/1 striatum with knockdown of *Mef2C*, and the data collected was representative of the medial, lateral, and ventral regions, further analysis was done to determine whether the mHTT inclusions were present in a specific region and if the loss was specific to a particular region. Multivariate analysis with correction of multiple comparisons with Bonferroni, showed that the medial region of R6/1 striatum with striatal knockout of *Mef2C* had significantly fewer mHTT inclusions compared with the medial region of the R6/1 striatum (R6/1 5.6 inclusions per mm^3 +/- 0.2, R6/1 $Cre^{+}Mef2C^{fl/fl}$ 4.4 inclusions per mm^3 +/- 0.5, Effect of Genotype: $F_{1,22}$ = 5.266, p=0.032) (Figure 4.20). Whilst there was a trend toward fewer mHTT inclusions in the lateral and ventral regions of the striatum, these did not reach significance (Lateral striatum: R6/1 6.5 inclusions per mm^3 +/- 0.2, R6/1 $Cre^{+}Mef2C^{fl/fl}$ 5.6 inclusions per mm^3 +/- 0.4, Effect of Genotype: $F_{1,22}$ = 2.944, p=0.100. Ventral striatum: R6/1 6.5 inclusions per mm^3 +/- 0.2, R6/1 $Cre^{+}Mef2C^{fl/fl}$ 6.1 inclusions per mm^3 +/- 0.1, Effect of Genotype: $F_{1,22}$ = 1.797, p=0.194) (Figure 4.20).

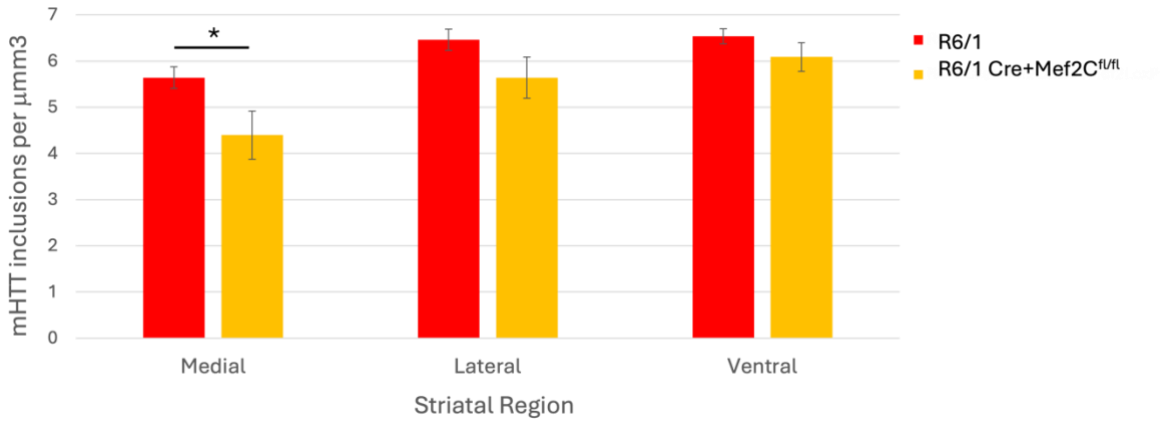

Figure 4.20 There are fewer mHTT inclusions in the medial striatum of an R6/1 mouse with striatal knockout of Mef2C.

Graphical representation of the average number of mHTT inclusions (as stained for with MW8) per mm^2 in the medial, lateral, and ventral striatum. There is significantly reduced mHTT in the medial striatum of R6/1 brains with striatal knockout of *Mef2C*, which is not seen in the lateral or ventral region (Medial striatum: R6/1 5.6 inclusions per mm^3 +/- 0.2, R6/1 $Cre^{+}Mef2C^{fl/fl}$ 4.4 inclusions per mm^3 +/- 0.5, Effect of Genotype: $F_{1,22}$ = 5.266, p=0.032. Lateral striatum: R6/1 6.5 inclusions per mm^3 +/- 0.2, R6/1 $Cre^{+}Mef2C^{fl/fl}$ 5.6 inclusions per mm^3 +/- 0.4, Effect of Genotype: $F_{1,22}$ = 2.944, p=0.100. Ventral striatum: R6/1 6.5 inclusions per mm^3 +/- 0.2, R6/1 $Cre^{+}Mef2C^{fl/fl}$ 6.1 inclusions per mm^3 +/- 0.3, Effect of Genotype: $F_{1,22}$ = 1.797, p=0.194). *p<0.05

4.5 Discussion

The experiments in this chapter aimed to investigate whether striatal knockout of *Mef2C* in a mouse model of HD could influence phenotypic deficits and pathology of the HD mouse, as an extension of work in chapter 3 which showed that *Mef2* downregulation in a mHTT-induced *Drosophila* model could suppress degeneration. In this chapter, I have generated a new mouse model in which *Mef2C* was knocked down in the striatum of an R6/1 mouse model of HD. To summarise the findings in this chapter, I found that R6/1 mice with striatal knockout of *Mef2C* had significantly fewer striatal mHTT inclusions compared with the R6/1 striatum, but no differences in striatal volume, numbers of neurons or numbers of MSNs. These mice performed less well on the inverted grip strength test compared to R6/1 mice; but they travelled further on the balance beam, compared with R6/1 mice and all other behavioural outcomes were not significantly different to R6/1 alone.

4.5.1 R6/1 mice show the anticipated phenotype compared with literature reports

The first section of this chapter aimed to address whether the R6/1 colony produce the expected behavioural phenotype and pathology as reported in the literature. Behaviourally, the R6/1 colony used in this experiment were significantly lighter than the wild-type littermates which has been previously reported from 14 weeks of age, and as late as 24 weeks (Bolivar et al., 2004; García-Lara, 2018; Naver, Stub, Moller, et al., 2003; Rattray et al., 2013). Some studies have reported sex differences, however this does not appear to be a commonly reported observation (Brooks, Janghra, et al., 2012). 16-weeks of age was the timepoint reported for all behavioural tasks tested during this study. At 16-weeks, R6/1 mice took longer to descend a vertical pole, showed general reduced locomotor activity from open field data, and showed deficits on balance beam and rotarod, compared with wild-type littermates. R6/1 mice did not show any deficits on the inverted grip strength test compared with wild-type littermates at 16-weeks. Previous experiments have reported deficits on balance beam and rotarod from as young as 8-weeks and 12-weeks, respectively, with reports of hypoactivity from as young as 6 weeks (Bolivar et al., 2004; Brooks, Janghra, et al., 2012). These reports suggest that behaviourally, the R6/1 colony used in this experiment show the anticipated phenotype when compared to the literature.

From analysis of the brains at 16-weeks, the R6/1 colony used in the experiment showed reduced whole-striatal volume compared with the striatum of wild-type littermates. The R6/1 striatum also had fewer NeuN and DARPP-32-positive cells per mm^3. A longitudinal MRI study showed that whole-volume of the R6/1 brain was reduced from 9-weeks of age, with significant striatal volume decrease at 17 weeks (Rattray et al., 2013). Neuronal numbers and DARPP-32-positive cells have been reportedly reduced from 19-weeks and 16-weeks, respectively, however other studies have reported no changes to NeuN-positive staining by 30-weeks (Naver, Stub, Moller, et al., 2003; Rattray et al., 2013). The R6/1 mouse striatum also showed presence of mHTT inclusions which is consistent with previous studies that have reported the presence of mHTT inclusions in the striatum from 8-weeks of age (Gatto et al., 2021; Naver, Stub, Moller, et al., 2003). Overall, the histological results seen in the R6/1 colony used for this experiment appear to be consistent with previous reports. Subtle changes in

results may be due to somatic CAG expansion which has been reported in the R6/1 model (Møllersen et al., 2010; Vatsavayai et al., 2007).

4.5.2 Striatal knockout of *Mef2C* in HD mice leads to fewer striatal mHTT inclusions

In the R6/1 mice with striatal knockout of *Mef2C*, there were significantly fewer striatal mHTT inclusions compared with the R6/1 striatum (Figure 4.18-20). This is important because mHTT aggregates/inclusions are a pathological hallmark of HD and are associated with death of MSNs (Arrasate et al., 2004). mHTT aggregates form from the cleavage of mHTT, which releases N-terminal fragments containing the expanded polyQ region (Aktar et al., 2019; Landles et al., 2010). The formation of these inclusions involves the complex interplay between mHTT and other small molecules such as ubiquitin and chaperones (Jimenez-Sanchez et al., 2017). Although aggregates are strongly associated with disease progression, whether they are directly toxic to the cells or are protective, is not yet resolved. For example, studies of post-mortem HD brains revealed that mHTT is more prevalent in the cortex than in the striatum, despite striatal neuronal loss being much more significant (Arrasate & Finkbeiner, 2012; Gutekunst et al., 1999), which may be due to the rapid loss of MSNs prior to aggregate formation, or reflect that aggregates are protective. By contrast, inhibition of mHTT aggregation and the formation of inclusions via C2-8, a synthetic drug-like small molecule inhibitor of polyQ aggregation, was shown to suppress mHTT-induced degeneration in a *Drosophila* model of HD, as well as improving motor performance and neuronal atrophy in the R6/2 model (Chopra et al., 2007; Wang et al., 2013). Overall, it is likely that reducing the levels of mHTT is beneficial to the brain, and as a result, striatal knockout of *Mef2C* in the R6/1 model is protective.

Reports have shown that in the post-natal brain, *Mef2C* is expressed more medially than laterally (Ali, 2022). Additionally, striatal *Mef2C* knockout using the same $Cre^{+}Mef2C^{fl/fl}$ mouse colony used in this experiment, showed a significant decrease in *Mef2C* immunoreactivity in the dorso-medial striatum compared with the dorso-lateral striatum (Ali, 2022). Therefore, I wanted to ask whether there were region-specific differences with regard to the loss of mHTT inclusions in the R6/1$Cre^{+}Mef2C^{fl/fl}$ striatum. Interestingly, there were significantly fewer mHTT inclusions in the medial compartment of the R6/1$Cre^{+}Mef2C^{fl/fl}$ striatum, while this

didn't reach significance in the lateral and ventral regions (Figure 4.20). One explanation for why mHTT inclusions are reduced in the medial region of the striatum would be that *Mef2C* is more highly expressed in the medial striatum and could be more highly impacted by its' knockdown.

4.5.3 Striatal knockout of *Mef2C* in HD may influence motor function

Given the reduced striatal inclusions in R6/1Cre^{+}Mef2C$^{fl/fl}$ compared with the R6/1, it is interesting to understand whether there were any functional correlates on behavioural testing. 16-week-old R6/1Cre^{+}Mef2C$^{fl/fl}$ mice travelled further up the balance beam compared with R6/1 mice, indicating an improvement in motor coordination and control. There were no apparent differences between the two genotypes on vertical pole and rotarod performance. Neither were there any differences in the parameters measured in open field testing. However, at 16-weeks, R6/1Cre^{+}Mef2C$^{fl/fl}$ mice spent less time holding onto an inverted metal grip compared with R6/1 mice.

4.5.3.1 R6/1 mice with Striatal knockout of Mef2C perform better on the balance beam compared with R6/1 mice

The 16-week-old R6/1Cre^{+}Mef2C$^{fl/fl}$ mice travelled further up the balance beam compared with R6/1 mice (Figure 4.12). Whilst not significant, Cre^{+}Mef2C$^{fl/fl}$ mice did appear to perform slightly less well on the balance beam compared with wild-type mice, indicating that there is positive interaction from *Mef2C* knockout in the presence of mHTT (Appendix 1C). The balance beam task is likely to target motor learning, cognitive processing and balance control with regard to functions of the striatum (Patel et al., 2019; Sipp et al., 2013). Dysfunction in specific areas of the striatum might be one such route for *Mef2C* knockout improving these outcomes. The striatum is defined by the topographic distribution of monoaminergic and glutamatergic projections to the dorsomedial, dorsolateral, and ventral regions (Stanley et al., 2021). The ventral striatum, known as the limbic domain, is involved in reward processing and motivational behaviour (Valjent & Gangarossa, 2021). The dorsolateral striatum is known as the sensorimotor domain and is involved in habit formation, whilst the dorsomedial striatum is known as the associative domain, and is involved in driving goal-directed behaviour (Brimblecombe & Cragg, 2017; Sturm et al., 2016; Valjent & Gangarossa, 2021).

Of particular interest is the function of the dorsomedial striatum since the significant reduction of mHTT aggregates was localised to this region (Figure 4.20). The dorsomedial striatum receives excitatory outputs from the prefrontal cortices in dominant early learning and associative phases, contributing to behavioural flexibility (Devan et al., 2011; Turner et al., 2022). Additionally, this region is a site of conjunction for neurons arriving from the limbic system, implicating the dorsomedial striatum in some aspects of cognitive processing (Devan et al., 2011). Therefore, the presence of mHTT and loss of neurons in the dorsomedial striatum would lead to deficits in cognitive processing, motor learning and behavioural flexibility, which may be seen by deficits in a task like the balance beam. Since *Mef2C* was shown to be more highly expressed in the medial striatum of post-natal mice (Ali, 2022), changes to *Mef2C* expression may play a role in these processes. Strikingly, a microarray analysis conducted in the host laboratory showed that *Mef2C* is highly up-regulated in the 4-month R6/1 striatum, but not in the 2- or 6-month striatum (Brooks et al., unpublished). This might suggest an imbalance in *Mef2C* expression throughout progression of the disease that leads to dysfunctional transcription of *Mef2C*-associated genes, and subsequent vulnerability of cells to mHTT aggregation and death. Striatal knockout of *Mef2C* might reduce any potential imbalance of the gene, protecting the neurons from further transcriptional dysregulation. In turn, this might lead to reduced mHTT inclusions and a less-diseased brain that could lead to improved cognitive processing and motor control, improving the mice' ability to travel the balance beam (Figure 4.12). To confirm these findings, further research could include testing R6/1Cre^{+}Mef2C$^{fl/fl}$ mice on more complex behavioural tasks such as the T- or Y- maze. It would also be interesting to look at whole neurons and their projections to see whether axons and dendrites are affected by striatal *Mef2C* knockout, and how these might play a role in the regulation of striatal pathways.

4.5.3.2 R6/1 mice with Striatal knockout of Mef2C perform worse on the inverted grip strength test compared with R6/1 mice

At 16-weeks, R6/1 mice with striatal knockout of *Mef2C* spent less time holding onto an inverted metal grip compared with R6/1 mice (Figure 4.10). There was no difference between wild-type mice and Cre^{+}Mef2C$^{fl/fl}$ mice on this apparatus (see Appendix 1B), potentially

suggesting a genetic interaction occurring due to the loss of *Mef2C* in the R6/1 model. *Mef2C* is thought to be required for the development of matrix MSNs rather that striosome MSNs (Ali, 2022). The matrix compartment of the striatum receives preferential inputs from the primary motor and sensory cortices, whilst the striosome compartment comprise a higher percentage of neurons with axonal projections to structures of the limbic system and amygdala (Miyamoto et al., 2018; Prager & Plotkin, 2019). Due to the importance of *Mef2C* in the development of matrix neurons, loss of striatal *Mef2C* may contribute to altered GABA signalling and subsequent reduction of GABA neurotransmitter release. However, this would need to be tested to determine whether this related to any motor impairment. Interestingly, histological analysis of the 16-week brains in this experiment, did not show any changes in the presence of DARPP32- and NeuN-positive neurons. *Mef2C* loss may impact GABA receptor signalling, as opposed to physical loss of neurons. A previous study of conditional knockout of *Mef2C* in forebrain excitatory neurons was linked with increased inhibitory synaptic transmission (Harrington et al., 2016). Further studies could explore the presence of known striatal neurotransmitters such as GABA and dopamine, to investigate whether striatal knockout of *Mef2C* influences the presence of neurotransmitters in the striatum, which may implicate downstream pathways (Jamwal & Kumar, 2019).

Since R6/1Cre^{+}Mef2C$^{fl/fl}$ mice show deficits on the inverted grip strength test, this may suggest an additional component that leads to the improvement on the balance beam, such as motivation or anxiety-driven behaviour. Elevated levels of striatal dopamine due to reduced dopamine transporter expression, has been attributed to higher motivation for food rewards (Cagniard et al., 2006; Palmiter, 2008). Additionally, dysregulation of GATA genes that are expressed highly in dopaminergic cells has been implicated in early development of a large selection of neurons including GABAergic midbrain and serotonergic hindbrain neurons, as well as increased anxiety-like behaviour (Chen et al., 2022; Lentjes et al., 2016; Tikker et al., 2020). More specifically, previous reports have shown that in the absence of GATA-2, serotonergic neurons fail to differentiate, and that inactivation of co-factors of GATA-2 lead to abnormal development of serotonergic neurons and increased anxiety-like behavioural in the elevated plus maze, and novel object recognition task (Tikker et al., 2020). *Mef2C* may be involved in pathways associated with GATA-2 via serotonergic or dopaminergic neurons, influencing the downstream pathways that lead to motivational and anxiety-driven

behaviours. To do this, further studies could involve additional behavioural tasks such as the elevated plus maze and novel object recognition to determine any changes in R6/1 mice with striatal knockout of *Mef2C*, compared with R6/1 mice.

4.6 Conclusion

In this chapter, I have generated an R6/1 mouse model of HD with striatal knockout of *Mef2C* to investigate how *Mef2C* might impact disease progression in the R6/1 HD mouse model. The brains of 16-week-old R6/1Cre^{+}Mef2C$^{fl/fl}$ mice have significantly fewer striatal mHTT inclusions compared with the R6/1 brain. There was little evidence to suggest that knockdown of *Mef2C* in the R6/1 HD mouse model has significant effects on behavioural changes, however, the R6/1Cre^{+}Mef2C$^{fl/fl}$ mice could travel further up a balance beam which may indicate a potential consequence of behavioural changes and the reduction of mHTT inclusions. Results indicate that there is a genetic interaction that occurs with striatal *Mef2C knockout* in the R6/1 model of HD, however, further experiments are required to unveil the full extent of differences.

Chapter 5: N-terminal *FoxP1* can suppress mHTT-induced degeneration in *Drosophila* model of HD.

5.1 Introduction

Through a microarray study of genes expressed in the developing striatum, the host laboratory previously identified that *FoxP1* was the most highly up-regulated gene between E12 and E16 (Precious et al., 2016). Furthermore, *FoxP1* was identified as being required to produce DARPP-32-expressing neurons from the developing striatum, cultured in vitro (Precious et al., 2016). In 2006, Desplats and colleagues were the first to report downregulation of *FoxP1* mRNA in the 6-month R6/1 striatum (Desplats et al., 2006). Since then, further studies have shown reduced FoxP1 mRNA and protein levels in the striatum and cortex of knock-in and transgenic models of HD, as well as those of the human HD cortex and caudate, further linking *FoxP1* to dysregulation in HD disease pathogenesis (Araujo et al., 2017; Hodges et al., 2008; Louis Sam Titus et al., 2017). Table 1.4 of the Introduction outlines the publications to date that have reported *FoxP1* changes in HD disease models. Many of these publications refer to timepoints where FoxP1 is significantly reduced, however, they do not reference the fact that FoxP1 protein levels in the HD brain appear to be comparable to the wild-type brain prior to this decrease. For example, Louis Sam Titus and colleagues reported a reduction in FoxP1 protein in the R6/2 striatum and cortex at 6 weeks, however there was no change at 2 weeks (Louis Sam Titus et al., 2017). This pattern of FoxP1 loss may indicate a role for *FoxP1* in disease pathogenesis and should be explored further.

Since FoxP1 is found to be reduced in mouse models of HD and in the human HD brain, the question was asked as to whether restoring FoxP1 expression levels in HD a therapeutic avenue could be to suppress symptom onset. Louis Sam Titus and colleagues showed that elevating FoxP1 levels by ectopic expression in mouse cortical neurons in culture, was able to protect these neurons from 2-Hydroxy-Docosahexaenoic Acid (HCA)-induced death and mHTT-induced neurotoxicity (Louis Sam Titus et al., 2017). Furthermore, Louis Sam Titus and colleagues also showed that over-expressing *FoxP1* was able to suppress a degenerative eye phenotype in a specific *Drosophila* model with mHTT-expressed in the eye (ApplGal4; GMR-

HttQ120 > UAS-FoxP1). Flies over-expressing FoxP1 also performed significantly better in the phototaxis behavioural assay, compared to mHTT-expressing flies (GMR-HttQ120), indicating a functional improvement. Using co-immunoprecipitation, Tang et al., (2012) reported a physical PPI between mHTT and FoxP1 in cortical homogenates from 6-month-old R6/1 mice (Tang et al., 2012). However, using these techniques, it isn't possible to determine where within the protein, this interaction occurs. Neither was it reported whether wild-type HTT physically interacts with FoxP1, indicating whether this is expected.

The current research suggests that F*oxP1* plays an important role in MSN development and maturation. As mentioned above, FoxP1 mRNA and protein levels are reportedly reduced in several HD mouse models, however there isn't much previous data about *FoxP1* expression levels in the younger HD mice, where behavioural deficits are not so prominent. In the first part of this chapter, I wanted to establish whether these changes could be observed in the striatum of a 'transgenic' R6/1 HD mouse, whose phenotype is very progressive, and the knock-in HdhQ150 mouse model whose phenotype is much slower. Secondly, I wanted to extend the time-course to better characterise when FoxP1 protein is reduced in these HD models. Characterising this pattern of expression will provide insight into whether these changes have occurred over embryonic development, or whether they are associated with core disease pathogenesis. Additionally, it will be beneficial to determine whether these changes are comparable across different HD mouse models.

In the second section of this chapter, I aim to explore the effects of over-expressing *FoxP1* in a whole-eye and pan-neuronal *Drosophila* model of mHTT-induced degeneration. Louis Sam Titus and colleagues (2017) showed that elevating full-length *FoxP1* using a weak pan-neuronal driver, in a whole-eye *Drosophila* model of HD can suppress mHTT-induced degeneration (as shown by suppressed rhabdomere loss)(Louis Sam Titus et al., 2017). However, this has not been explored in mHTT-expressing neurons. Furthermore, whilst there is an indication of a physical interaction between mHTT and FoxP1, there is no evidence as to where this physical interaction may occur. Understanding this may indicate a potential mechanism for restoring HD-associated impairments by *FoxP1* over-expression.

5.2 Methods

5.2.1 Experimental design

In the first experiment of this chapter, the presence of FoxP1-positive nuclei, and FoxP1 protein expression was quantified in the 1-, 3-, 4- and 6-month R6/1 striatum and 10-, 18-, and 24-month HdhQ150 striatum, compared with the wild-type striatum. These timepoints were taken due to the availability of brain tissue in the lab, in addition to providing a range of timepoints that capture pre- and post-manifest ages of these models. R6/1 and HdhQ150 brain tissue was taken from existing archives of HD time-course studies from the host laboratory to address the principles of the 3Rs (https://NC3RS.org.uk). Wild-type tissue was also taken from age-matched littermates of the HD mice, within existing archives. Tissue was stained with anti-FoxP1 to identify FoxP1 nuclei. Stereological counting in the Visiopharm software was used to count the number of FoxP1-positive nuclei, and 10x magnification images were taken for processing in ImageJ and calculation of protein expression per FoxP1-positive nuclei via O.D. See section 2.3.5 for full methods.

Following this, the Gal4/UAS system was used to investigate the effects of over-expressing FoxP1 in a whole-eye and pan-neuronal *Drosophila* model of HD. The whole-eye driver, GMR-Gal4 was used to investigate any effects to whole-eye degeneration (GMR>UAS-hFoxP1; UAS-hHTTex1.Q93), and the pan-neuronal driver Elav^{C155}-Gal4 used to investigate the effects of mHTT-induced loss of rhabdomeres (Elav>UAS-hFoxP1; UAS-hHTTex1.Q93). The Gal80^{ts}Gal4/UAS system was then used to determine whether *FoxP1* over-expression in these mHTT models at different timepoints during eye development, could influence mHTT-induced degeneration (See section 2.1.4-7). In addition to this work, using the GMR-hHTTex1.Q120 fly line could provide a way of independently expressing mHTT and *FoxP1*, to investigate whether over-expressing *FoxP1* in the neurons, could influence mHTT-induced degeneration in all cells of the eye (Appl; GMR-hHTTex1.Q93>UAS-FoxP1).

Finally, Y2H assays were used to investigate the domains of FoxP1 protein that are required for the physical interaction between wild-type HTT and mHTT.

5.2.2 Statistical analysis

The work involving histological staining in mouse tissue were analysed using multivariate analysis. For all fly work, a multivariate analysis was used to determine any statistically significant changes in rhabdomere counts under different conditions. Bonferroni was used to test for multiple comparisons. For all analyses, statistical significance was reported when $p<0.05$.

5.3 Results

5.3.1 FoxP1 protein expression and FoxP1-positive nuclei are significantly reduced in the 3-months R6/1 HD striatum.

The first experiment aimed to investigate changes in FoxP1 protein expression and the presence of FoxP1-positive nuclei, across the time course of HD progression in the mouse. To do this, brain tissue from R6/1 transgenic mice and their wild-type littermates were taken at 1-, 3-, 4- and 6-months of age. Tissue was stained for FoxP1 and O.D values were determined for striatal FoxP1-positive nuclei, where a higher O.D value was indicative of higher protein expression (Figure 5.1). ANOVA results show that there is a significant difference in the O.D values of FoxP1-positive nuclei between the R6/1 and wild-type striata at the different ages assessed (Figure 5.1A/B; Effect of Genotype*Time $F_{1,43} = 21.277$, $p<0.001$). Post-hoc analysis showed that at 1-month, FoxP1 protein expression levels were comparable between R6/1 and wild-type ($p=0.618$) but at 3-months, there was a small but significant decrease in the FoxP1 protein expression per nuclei, in the R6/1 striatum, compared with the wild-type striatum (R6/1 71 +/- 9.9, wild-type 98 +/- 7.9, $p=0.015$). By 4-months, there was a further significant decrease in protein expression in the R6/1 striatum, compared to wild-type (wild-type 58 +/- 7, R6/1 28 +/- 1.5, $p>0.001$), and FoxP1 protein expression was still decreased in the R6/1 striatum compared with wild-type at 6-months (wild-type 91 +/- 4.5, R6/1 69 +/- 5.2, $p<0.004$) (Figure 5.1Ai). O.D is also presented as a percentage of wild-type protein levels to account for differences in the tissue, since tissue samples from each time point came from different tissue archives (Figure 5.1Aii).

Using stereological sampling, the total number of FoxP1-positive cells per mm^3 was calculated in the R6/1 and wild-type striatum at 4 months. Due to time constraints, the 4-month timepoint was chosen since there was a significant difference in the protein expression per nuclei at this age. There were fewer FoxP1-positive cells in the 4-month R6/1 striatum compared with the wild-type striatum (wild-type 4911 cells +/- 429, R6/1 2984 cells +/- 818, Effect of Genotype: t_{19} =2.59, P=0.018) (Figure 5.1B). To conclude, FoxP1 protein expression is significantly reduced in the R6/1 striatum from 4-months, and at 4-months, there are significantly fewer FoxP1-positive cells compared with the wild-type striatum.

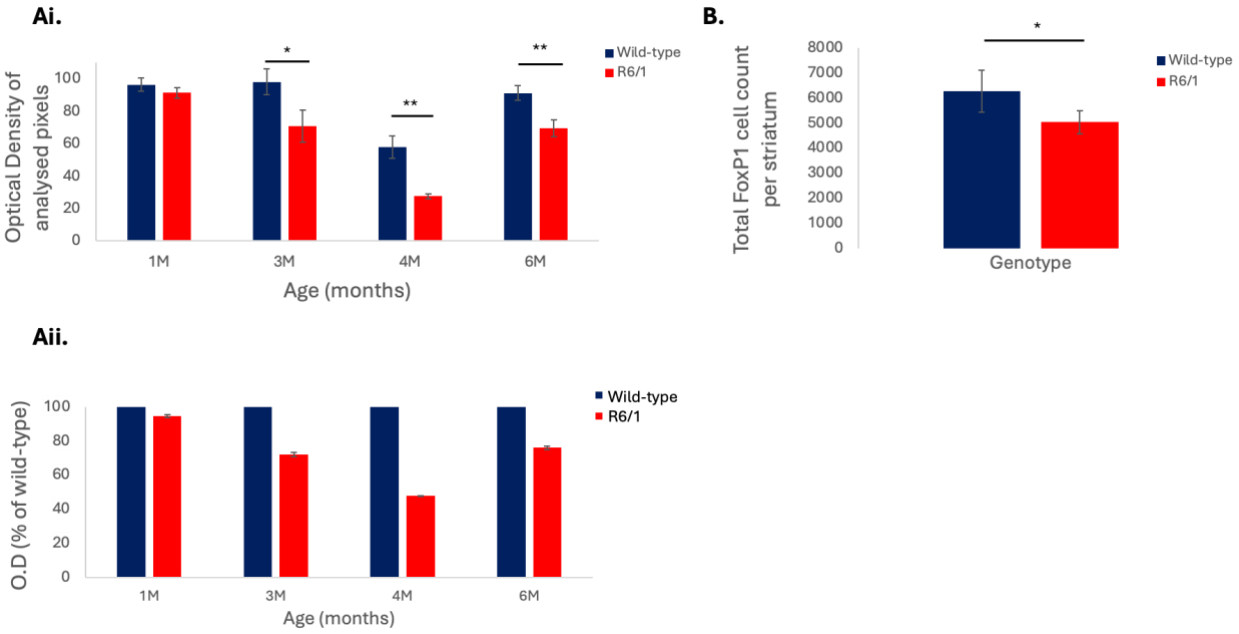

Figure 5.1. FoxP1 protein expression and FoxP1-positive cell number are significantly reduced in the R6/1 4-month striatum.

A). Graph to show the changes in striatal FoxP1 protein expression across the lifespan of the R6/1 mouse, compared with wildtype (Effect of Genotype $F_{1,43}$ = 21.277, p<0.001) (Ai). Optical density (O.D) of the analysed pixels was also measured as a percentage of wild-type protein levels to account for differences in the tissue, since tissue at each timepoint was an independent sample (Aii). B) Graph to show the total number of FoxP1-positive cell nuclei per striatum, in the 4-month R6/1 and wild-type brain (wild-type 4911 cells +/- 429, R6/1 2984 cells +/- 818, Effect of Genotype: t_{19} =2.59, p=0.018). *p<0.05, **p<0.01.

5.3.2 FoxP1 Protein expression and FoxP1-positive nuclei are significantly reduced in the 10-month HdhQ150 HD striatum.

In the next experiment, the number of FoxP1-positive nuclei and FoxP1 protein expression was quantified in the HdhQ150 knock-in mouse line compared with wild-type littermates. To do this, brain tissue was taken from the 10-, 18- and 24-month HdhQ150 mice and wild-type littermates, and stained with anti-FoxP1. 10x magnification images were taken to determine O.D of analysed pixels and stereological sampled used to calculate the total number of FoxP1-positive nuclei. ANOVA analysis showed that there was a significant difference in the O.D values of FoxP1-positive nuclei between the HdhQ150 and wild-type striata at the different ages assessed (Effect of Genotype*Time $F_{1,51}$ = 18.923, p<0.001). Post hoc analysis revealed that at 10 months, there was a reduction in the FoxP1 protein expression per nuclei, in the HdhQ150 mouse striatum compared with the wild-type striatum (HdhQ150 OD: 88 +/- 16, wild-type OD: 122 +/- 15, p=0.026). By 18 months, FoxP1 protein expression per nuclei in the R6/1 striatum was further reduced compared with the wild-type striatal nuclei (p=0.016) which was further reduced by 24 months (p=0.005) (Figure 5.2A). O.D is also presented as a percentage of wild-type protein levels to account for differences in the tissues from independent samples (Figure 5.2Aii). Using stereological sampling, the total number of FoxP1-positive cell nuclei was calculated at 24 months (Figure 5.2B). Due to time constraints, the 24-month timepoint was chosen due to the large reduction in FoxP1 protein expression in the HdhQ150 mouse striatum compared with the wild-type striatum. There were significantly fewer FoxP1-positive nuclei in the 24-month HdhQ150 striatum, compared with wildtype (t_{16} =3.00, p=0.009) (Figure 5.2B). To conclude, FoxP1 protein expression is reduced in the HdhQ150 striatum compared with wild-type striatum from 18-months, and the total number FoxP1-positive nuclei is significantly fewer in the 24-month striatum.

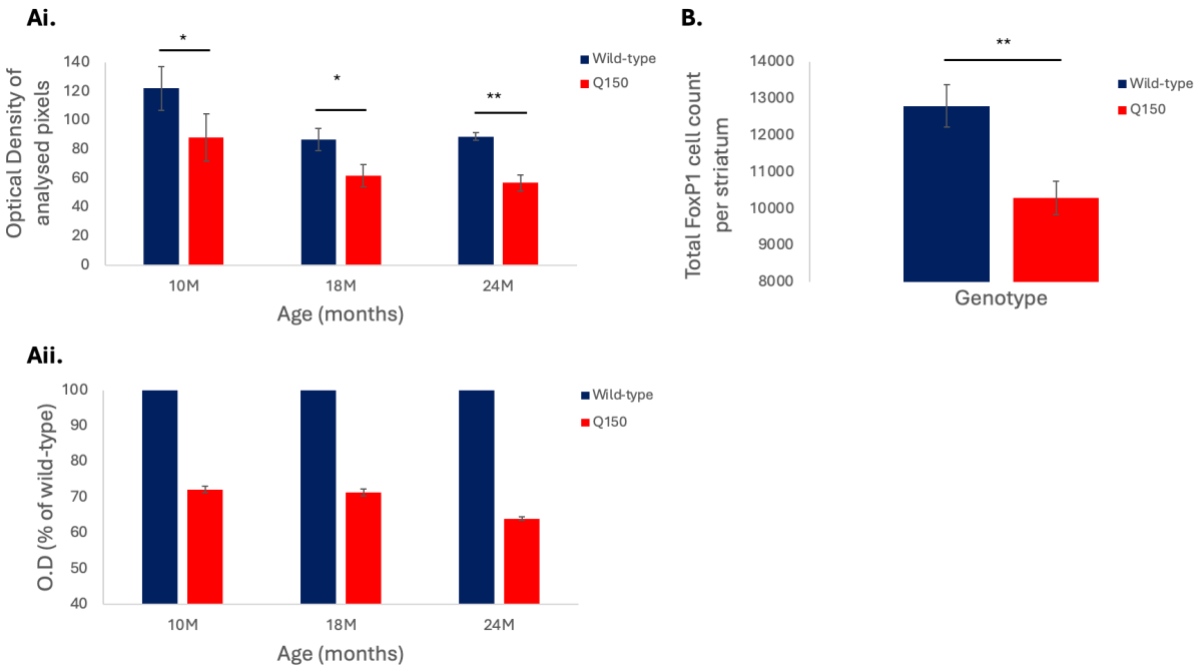

Figure 5.2. FoxP1 protein expression and total FoxP1-positive cell number are significantly reduced in the HdhQ150 18- and 24-month striatum.

A). FoxP1 protein expression measured across lifespan shows that there is a significant difference in protein expression (as presented by O.D) between the HdhQ150 mouse striatum and wild-type striatum (Effect of Genotype $F_{1,51}$ = 18.923, p<0.001). (Ai). Optical density (O.D) is presented as a percentage of wild-type protein levels to account for differences in the tissue, since tissue at each timepoint was an independent sample (Aii). B) At 24-months, there is a significantly reduced total FoxP1+ cell count, compared to wild-type (t_{16} = 3.00, p=0.009).

5.3.3 Over-expression of the human *FoxP1* N-terminal fragment suppresses mHTT-induced whole eye degeneration.

The previous two sections confirmed previous findings that, in mouse models of HD, the number of FoxP1-positive nuclei and the expression of FoxP1 protein expression per cell, is significantly reduced. As a first step towards understanding whether loss of *FoxP1* impacts HD pathology, I asked whether restoring *FoxP1* levels might suppress a mHTT-induced degenerative phenotype. Louis Sam Titus and colleagues (2017) have provided evidence that over-expression of *FoxP1* in a *Drosophila* whole-eye model of mHTT can suppress degeneration, as measured by loss of rhabdomeres (Louis Sam Titus et al., 2017). Therefore, I wanted to address this hypothesis in *Drosophila* models of HD used in this project. In this experiment, the UAS-FoxP1 construct from Bloomington was used, which expresses just the N-terminal fragment of human *FoxP1* (referred to as *hFoxP1*). To do this, a *Drosophila* model

of mHTT-induced degeneration was used to test whether over-expression of *hFoxP1* could suppress a whole-eye degenerative phenotype. Using the Gal4/UAS system, female flies expressing the whole-eye driver GMR-Gal4, were crossed with male flies expressing mHTT with 93 CAG repeats (Q93) and *hFoxP1*. The resulting progeny expressed both constructs, resulting in Q93 and *hFoxP1* being driven in the whole-eye of the fly (GMR>UAS-hFoxP1; hHTTex1.Q93). As mentioned in section 3.3.1, by 15 days post-eclosion, flies expressing Q93 show a degenerative phenotype compared with the wild-type eye (see section 3.1.1-2 for initial establishment of this model) (Figure 5.3A/B). Therefore, confocal images were taken of the whole-eye expressing Q93 and *hFoxP1*, at this timepoint. Whole-eye over-expression of *hFoxP1* in Q93-expressing flies suppresses the whole-eye degeneration seen in Q93 flies, alone (Figure 5.3C). To conclude, whole-eye over-expression of *hFoxP1* can suppress a mHTT-induced whole-eye degenerative phenotype.

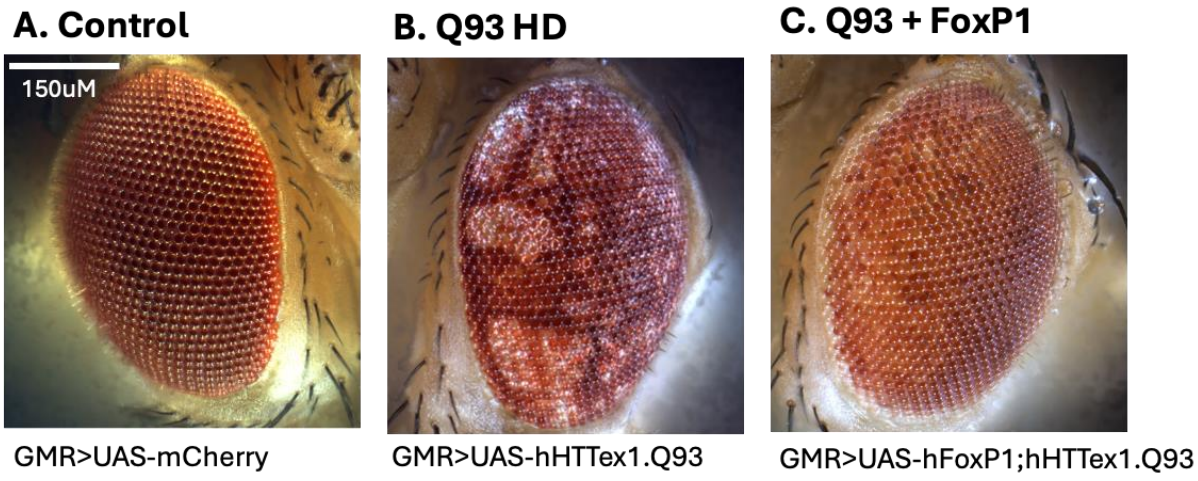

Figure 5.3. N-terminal human FoxP1 (hFoxP1) suppresses mHTT-induced whole-eye degeneration.
Representative confocal microscopy images of the whole eye showing (A) a control eye, (B) rough-eye phenotype in a *Drosophila* model of HD, and (C) suppression of mHTT-induced whole-eye degeneration by over-expression of *hFoxP1*.

5.3.4 Pan-neuronal over-expression of human N-terminal *FoxP1* shows small effect on mHTT-induced loss of rhabdomeres

The next section aimed to investigate whether pan-neuronal over-expression of *hFoxP1* could suppress mHTT-induced degeneration of rhabdomeres. To do this, the pan-neuronal driver, ELAV^{C155}-Gal4 was used. Rhabdomeres were counted from 2 days prior to eclosion, to 12 days

post-eclosion. Prior to counting, images were taken under a light microscope at 15 days post-eclosion, and flies expressing Q93 and *hFoxP1* have visibly more rhabdomeres compared to the flies expressing Q93 (Figure 5.4A). Multivariate analysis showed that pan-neuronal over-expression of *hFoxP1* significantly suppressed the mHTT-induced degenerative phenotype, as quantified by pseudopupil analysis (Genotype*Time: $F_{6,193}$ = 28.047, p<0.001) (Figure 5.4B). Post-hoc analysis revealed that there was no difference between the two genotypes upon eclosion (p=0.427), but by 5 days post-eclosion, Q93-expressing flies with over-expression of *hFoxP1* had more rhabdomeres compared to the flies only expressing Q93 (Elav>UAS-hHTTex1.Q93 4.29 rhabdomeres +/- 0.1, Elav>UAS-hFoxP1; hHTTex1.Q93 4.51 rhabdomeres +/- 0.1, p<0.001). This continued to 12 days post-eclosion which was the last timepoint analysed in this experiment (Elav>UAS-hHTex1.Q93 4.2 rhabdomeres +/- 0.1, Elav>UAS-hFoxP1; hHTTex1.Q93 4.7 rhabdomeres +/- 0.05, p<0.001) (Figure 5.4B). An additional line was generated to control for the addition of a second UAS construct in the flies expressing Q93 and *hFoxP1*. This line had UAS-mCherry on the 2nd chromosome (Elav>UAS-mCherry; UAS-hHTTex1.Q93). Multivariate analysis using this line showed that there was a significant effect between flies expressing Q93 and *hFoxP1* and those expressing Q93 and mCherry (Genotype*Day: $F_{5,96}$ = 0.415, p=0.004). Post-hoc analysis revealed that on the day prior to eclosion, flies expressing *hFoxP1* and Q93 had fewer rhabdomeres compared with flies expressing Q93 and mCherry (p<0.001), and at 7 days post-eclosion, flies expressing *hFoxP1* and Q93 had more rhabdomeres compared with flies expressing Q93 and mCherry (p=0.044). However, there were no other differences. Due to time constraints, the numbers counted at days -1, 5, 7, 10, and 12 are small in the Elav>UAS-mCherry; hHTTex1.Q93 group (day -1 (n=5), day 5 (n=2), day 7 (n= 4), day 10 (n=4), day 12 (n=3)), however, these results suggest that the presence of a second UAS construct may be responsible for the effect seen when UAS-hFoxP1 is over-expressed in the Q93 fly model. To fully determine the effect of *hFoxP1* over-expression in the Q93 line, further analysis is required. To conclude, pan-neuronal over-expression of *hFoxP1* in a mHTT-induced degenerative model may suppress mHTT-induced loss of rhabdomeres.

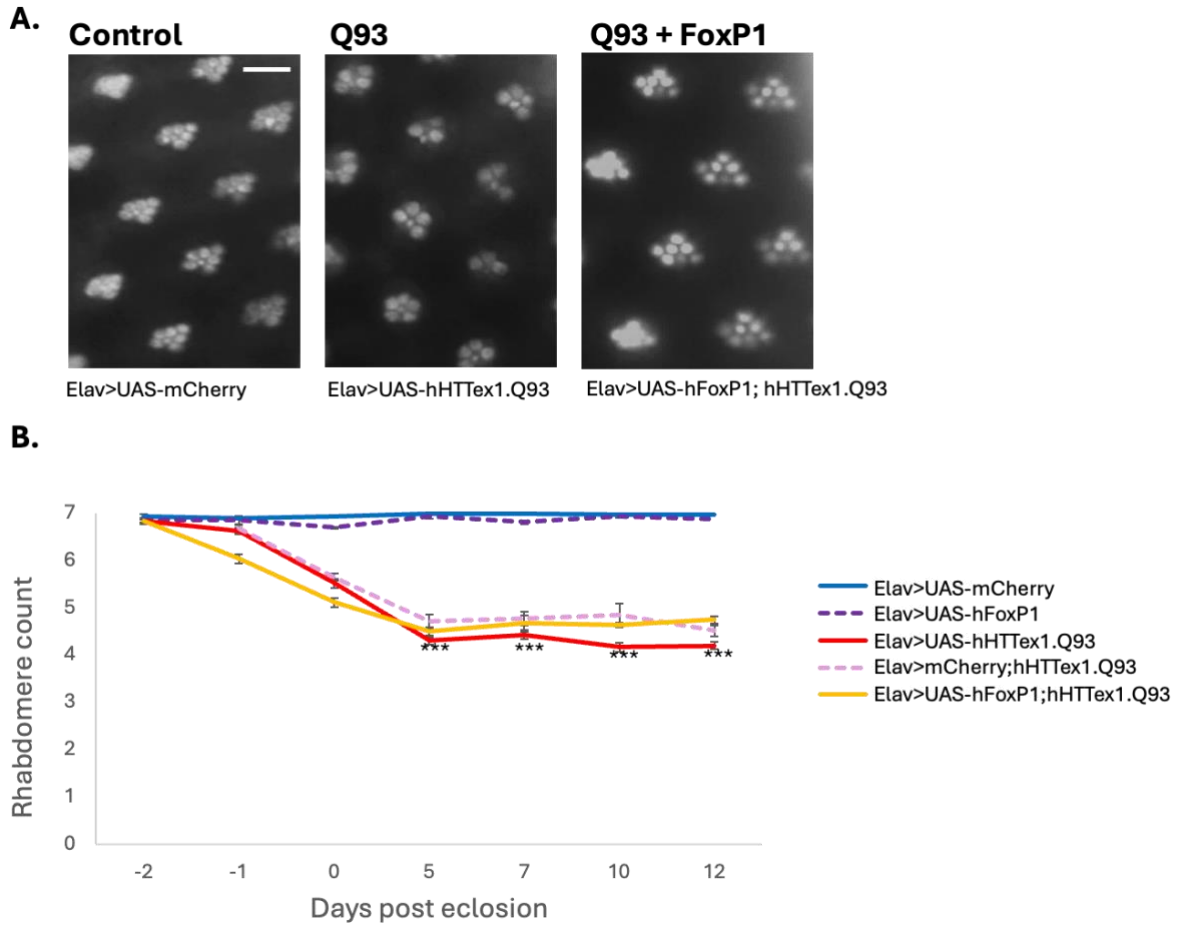

Figure 5.4. Pan-neuronal over-expression of hFoxP1 has a small effect on mHTT-induced loss of rhabdomeres.
A). Representative light microscopy images showing rhabdomeres in a control fly eye, and that pan-neuronal over-expression of *hFoxP1* in a *Drosophila* model of HD can suppress rhabdomere loss. B) Graphical representation of average rhabdomere counts from 2 days prior to eclosion, to 12 days post-eclosion. Each datapoint represents an average rhabdomere count of each condition with SEM plotted as error bars. Scale bar = 10μm.

5.3.5 Pan-neuronal over-expression of human N-terminal *FoxP1* in a mHTT-induced model can prolong survival

The next experiment aimed to investigate whether pan-neuronal over-expression of *hFoxP1* in a *Drosophila* model of mHTT could prolong survival. To do this, male flies carrying Elav^{c155}Gal4 were crossed with females carrying UAS-mCherry; hHTTex1.Q93, and females carrying UAS-hFoxP1; hHTTx1.Q93, at 21°C. Flies driving pan-neuronal expression of mCherry (Elav>UAS-mCherry) were used as controls. Upon eclosion, flies were placed in fresh food vials at 25°C and placed in new food vials every two days. At this point, the number of surviving flies was recorded. Pan-neuronal over-expression of *hFoxP1* in Q93-expressing flies

significantly increases fly survival, compared with Q93-expressing flies, alone (Log rank test: t_{414} = 5.366, p<0.001). To conclude, pan-neuronal over-expression of *hFoxP1* in a mHTT-induced model of HD can prolong survival, compared to mHTT expression, alone.

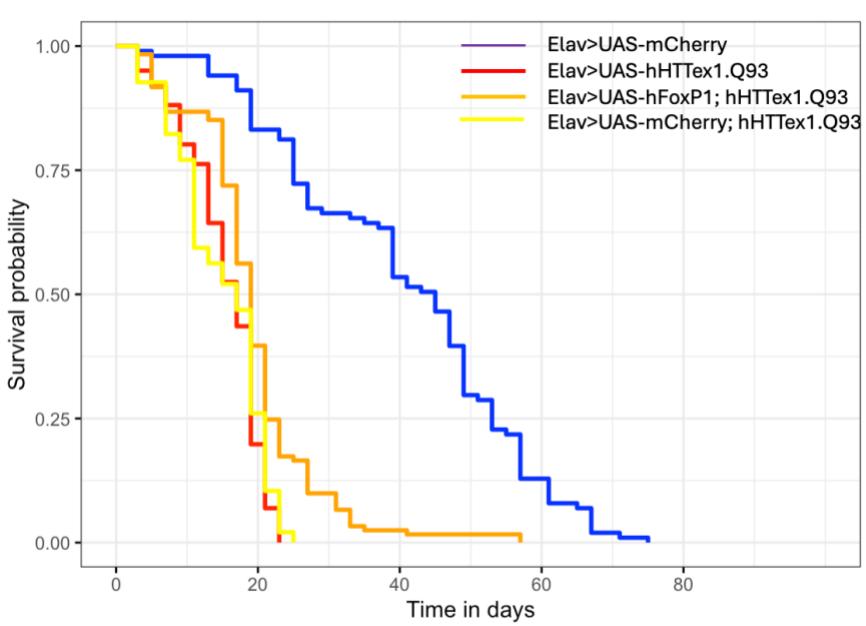

Figure 5.5. Panneuronal overexpression of hFoxP1 significantly increases lifespan in a Drosophila model of HD.
A Kaplan-Meier plot showing survival probability of *Drosophila* expressing mHTT in the neurons, with and without, pan-neuronal over-expression of *hFoxP1*. Pan-neuronal over-expression of *hFoxP1* in the mHTT-induced model significantly increased the survival probability in these flies (Log rank test: t_{414} = 5.366, p<0.001).

5.3.6 Pan-neuronal over-expression of *hFoxP1* rescues a whole-eye mHTT model

The next experiment looked to investigate whether expressing *hFoxP1* in the neurons of a *Drosophila* eye model of mHTT could rescue the whole-eye degenerative phenotype, which was the assay used by Louis Sam Titus and colleagues (Louis Sam Titus et al., 2017). To do this, the GMR-hHTTex1.Q120 line was used which expresses mHTT with 120 CAG repeats, in the whole eye, only. Appl-Gal4 was then used to over-express *hFoxP1* to replicate the findings of Louis Sam Titus and colleagues (Appl; GMR-hHTTex1.Q120>UAS-hFoxP1) (Louis Sam Titus et al., 2017). At 7 days post-eclosion, flies were taken, heads cryosectioned and samples stained with phalloidin for visualising the rhabdomeres. Univariate analysis was used to compare the extent of rhabdomere loss in the GMR-hHTTex1.Q120 fly line compared with wild-type flies, and the extent of rescue when hFoxP1 was over-expressed in the GMR-hHTTex1.Q120 line.

There was a significant difference between the three genotypes ($F_{2,15}$ = 8.978, p<0.001). Post-hoc analysis revealed that there were significantly fewer rhabdomeres in the fly eyes expressing mHTT with 120 CAG repeats compared with the wild-type fly eye (wild-type: 6.9 rhabdomeres +/- 0.001, GMR-hHTTex1.Q120: 4.41 +/- 0.3, p<0.001). This equates to a 37% reduction in the number of rhabdomeres (Figure 5.6B). Pan-neuronal over-expression of *hFoxP1* in a whole-eye model of mHTT has significantly more rhabdomeres at 7 days post-eclosion compared to flies expressing only mHTT (GMR-hHTTex1.Q120 4.4 rhabdomeres +/- 0.28, Appl;GMR-hHTTex1.Q120>UAS-hFoxP1 5.6 rhabdomeres +/- 0.13, p<0.001). This equates to a 21% reduction in rhabdomeres compared with the wild-type fly eye, indicating a suppression in the extent of mHTT-induced degeneration of rhabdomeres (Figure 5.6A/B). To conclude, this experiment has shown that over-expressing *hFoxP1* in the neurons can suppress a mHTT-induced degenerative phenotype where mHTT is expressed in all cells of the eye.

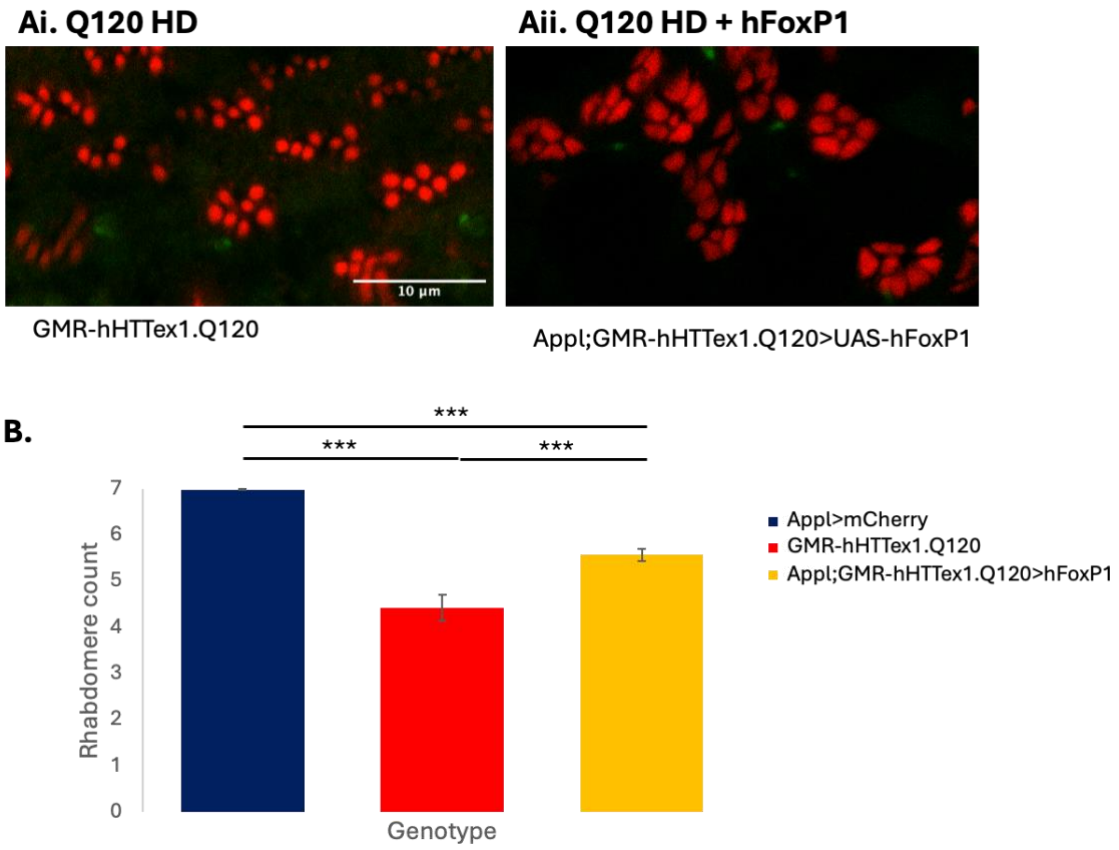

Figure 5.6 Pan-neuronal over-expression of hFoxP1 in a whole-eye model of mHTT can suppress rhabdomere degeneration.

A) Representative confocal microscopy images with phalloidin staining to show whole-eye mHTT-induced degeneration using GMR-hHTTex1.Q120 (Ai) and pan-neuronal over-expression of *hFoxP1* in this model, using Appl-Gal4 at 7 days post-eclosion (Aii). B) Representative bar graph of rhabdomere

counts of flies expressing mHTT with 120 CAG repeats in the whole-eye, with and without pan-neuronal over-expression of *hFoxP1*, and compared with the wild-type fly. Scale bar in (A) = 10μm.

5.3.7 Over-expression of *hFoxP1* in fully developed photoreceptors can significantly suppress mHTT-induced degeneration.

As described in section 3.3.5, pre-exposure of neurons to mHTT during eye development results in increased loss of rhabdomeres compared with the neurons exposed to mHTT following completion of eye development (Figure 3.6-3.7). Therefore, the next experiment aimed to determine whether over-expressing *hFoxP1* in the developed photoreceptor neurons could influence mHTT-induced degeneration. To do this, the GAL80^{ts}Gal4/UAS system was used to induce *hFoxP1* over-expression and mHTT with 93 CAG repeats (Q93) on the day prior to eclosion (D-1) (Elav; Gal80ts>UAS-hFoxP1; hHTTex1.Q93). In this experiment, over-expression of *hFoxP1* in Q93-expressing flies led to reduced rhabdomere loss compared with flies expressing only Q93 (Effect of Genotype*Time: $F_{6,246} = 4.166$, $p<0.001$) (Figure 5.7). Upon eclosion, Q93-expressing flies with *hFoxP1* over-expression had more rhabdomeres compared with Q93-expressing flies, alone (Elav; Gal80ts>UAS-hFoxP1; UAS-hHTTex1.Q93 6.7 +/- 0.1, Elav; Gal80ts>UAS-hHTTex1.Q93 6.5 rhabdomeres +/- 0.1, p=0.016). This difference was maintained throughout the experimental time course of 12 days (p=0.04) except at day 7, where the difference did not reach significance (p=0.189) (Figure 5.7). To conclude, pan-neuronal over-expression of *hFoxP1* in the developed PR can suppress the mHTT-induced loss of rhabdomeres.

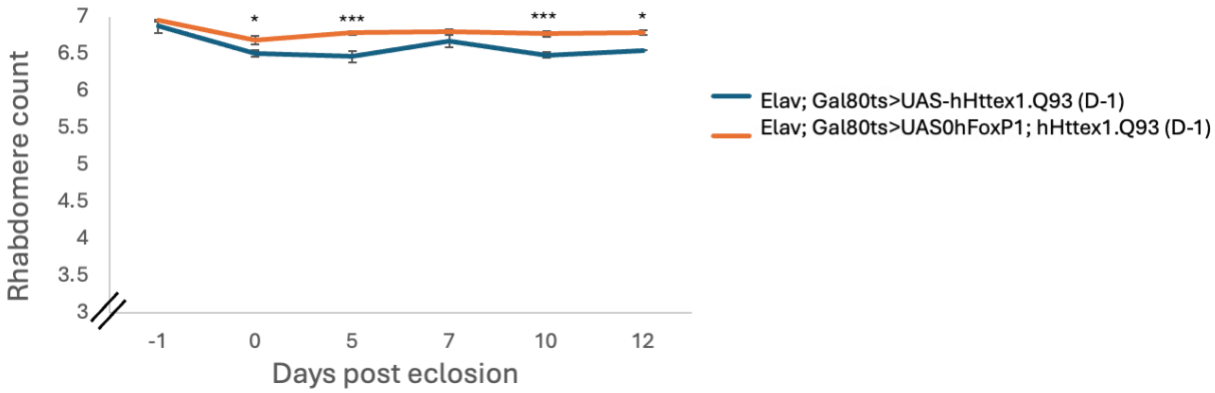

Figure 5.7. mHTT-induced degeneration in developed photoreceptors is suppressed by over-expression of hFoxP1.
Graphical representation of rhabdomere counts from 1 day prior to eclosion, to 12 days post eclosion. Each data point represents an average count for that condition with SEM plotted as error bars. Pan-

neuronal over-expression of *hFoxP1* with mHTT in the fully developed photoreceptors, can significantly suppress mHTT-induced degeneration in the adult fly (Effect of Genotype: $F_{6,246}$ = 4.166, p<0.001). *p<0.05, *p<0.001

5.3.8 Over-expression of full-length human *FoxP1* (FoxP1-FL) in a *Drosophila* model of HD is lethal mid-pupation

The results above demonstrate that over-expression of N-terminal *hFoxP1* can suppress mHTT-induced degeneration. In accord with these findings, Louis Sam Titus and colleagues (2017) showed that full-length *FoxP1* was able to rescue a mHTT-induced degenerative phenotype, when pan-neuronally expressed, using Appl-Gal4 (Louis Sam Titus et al., 2017). They also showed that *FoxP1* lacking the Leucine Zipper and Forkhead domains of the C-terminal region, was unable to protect against mHTT-induced toxicity in mammalian cortical cells in culture. Therefore, it is interesting that the N-terminal fragment of *FoxP1* (which lacks the leucine zipper and forkhead domains, Figure 5.8) used in this thesis, can suppress a mHTT-induced degenerative phenotype. The next experiment was to investigate whether full-length human *FoxP1* (FoxP1-FL), including these important C-terminal fragments (Figure 5.5) could further suppress mHTT induced degenerative phenotype. To do this, I generated a UAS-FoxP1-FL construct which was sent to BestGene (https://thebestgene.com) for microinjection into flies.

5.3.8.1 Whole-eye overexpression of FoxP1-FL in a mHTT model using GMR-Gal4, is lethal

The first question to ask was whether over-expressing FoxP1-FL in a whole-eye model of mHTT with 93 CAG repeats, could rescue a whole-eye degenerative phenotype. To do this, the GMR-Gal4 driver was used (GMR>UAS-FoxP1-FL; UAS-hHTTex1.Q93). Whole-eye over-expression of *FoxP1-FL* in Q93-expressing flies was lethal midway through pupation precluding an assessment of any possible effect on the eye phenotype. To ensure that this was not down to over-expression of *FoxP1-FL* alone, GMR-Gal4 was used to drive expression of *FoxP1-FL*, only (GMR>FoxP1-FL). Whole-eye over-expression of *FoxP1-FL* alone did not produce any observable eye phenotype (Figure 5.9A). To conclude, whole-eye over-expression of *FoxP1-FL* in a mHTT model is lethal.

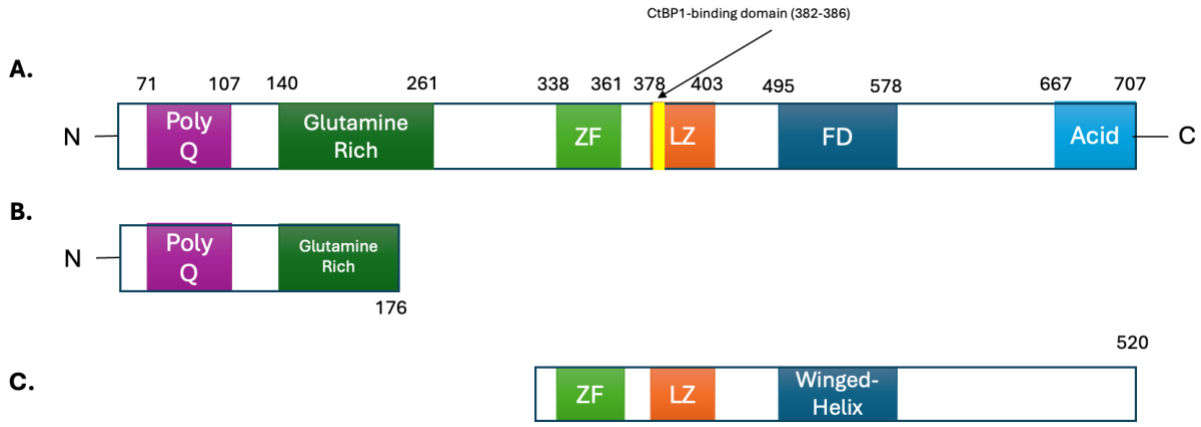

Figure 5.8. Schematic to show the differences between the full-length FoxP1 fragment and N-terminal fragment present in the UAS-hFoxP1 fly line.
A) Schematic to show the canonical full-length FoxP1 protein, and the important functional domains. B). The N-terminal fragment present in the UAS-hFoxP1 fly line. C) A schematic diagram of the *Drosophila* FoxP protein. PolyQ = polyglutamine, ZF = zinc finger domain, LZ, leucine zipper domain, FD = forkhead domain. Edited by work from (Johnson et al., 2018; B. Wang et al., 2003).

5.3.8.2 Pan-neuronal over-expression of FoxP1-FL in a mHTT model using ELAV^{C155}-Gal4, is lethal

The previous sub-section showed that whole-eye over-expression of *FoxP1-FL* in a mHTT model was lethal. Therefore, the next question to address was whether this could be due to neuronal expression, or expression in other cells of the eye. To do this, the pan-neuronal driver ELAV^{C155}-Gal4 was used. Pan-neuronal over-expression of *FoxP1-FL* in Q93-expressing flies was lethal midway through pupation, disabling the opportunity to assess any possible effect on the number of rhabdomeres. Pan-neuronal over-expression of *FoxP1-FL* alone, did not produce a rhabdomere phenotype (Figure 5.9B). To conclude, pan- neuronal over-expression of *FoxP1-FL* in a mHTT model is lethal.

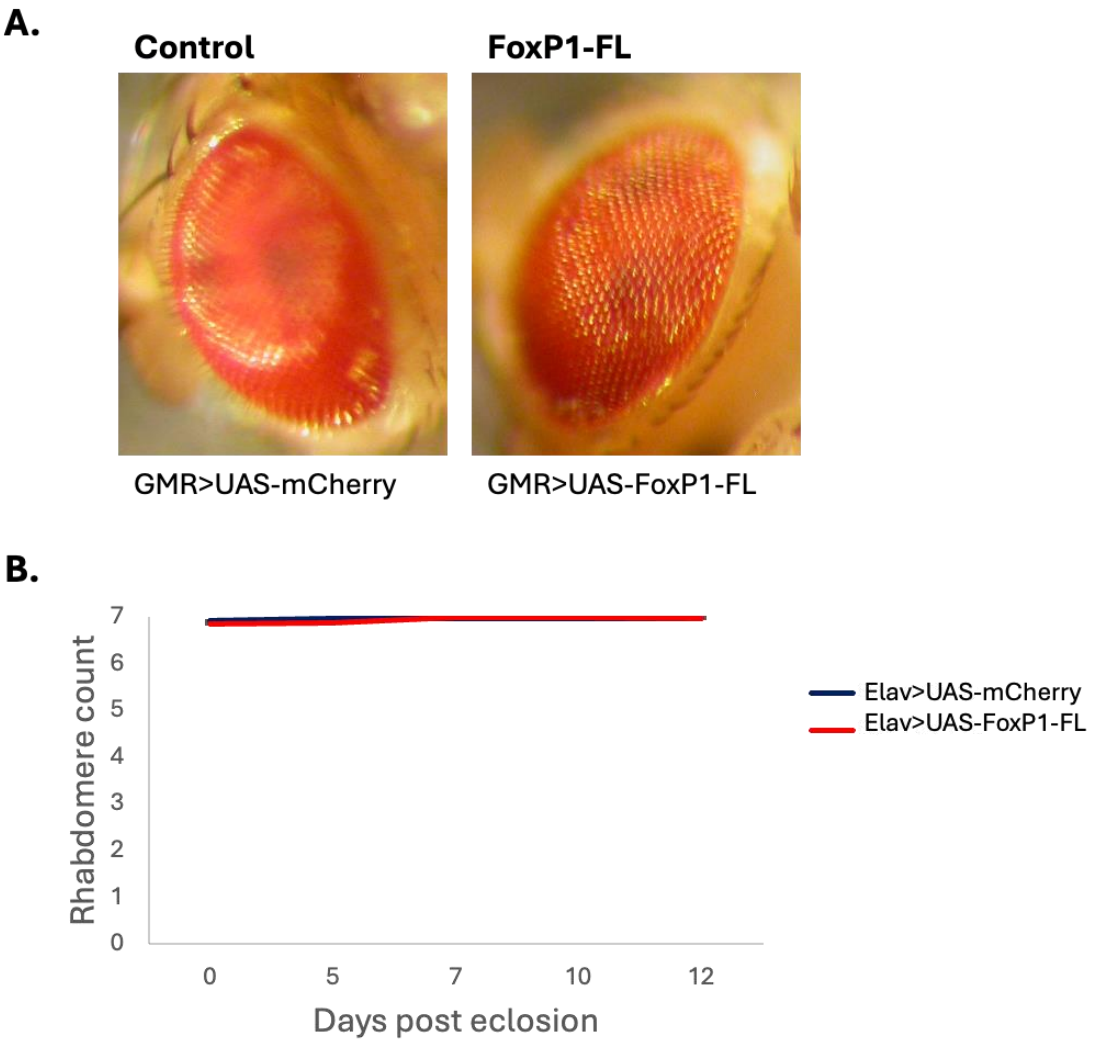

Figure 5.9 Full length FoxP1 (FoxP1-FL) expression in the whole-eye and neurons does not produce any degeneration.

A) Representative images of the fly with whole-eye expression of *FoxP1-FL* (GMR>UAS-FoxP1-FL) which is not different to control flies (GMR>UAs-mCherry). B) Representative rhabdomere counts from flies expressing *FoxP1-FL* (Elav>UAS-FoxP1-FL) in the neurons, versus control (Elav>UAS-mCherry). Rhabdomere counts taken from eclosion, to 12 days post-eclosion.

5.3.8.3 Pan-neuronal over-expression of FoxP1-FL using Appl-Gal4 in a mHTT-induced Drosophila model is lethal.

The next experiment looked to determine whether using a different, weaker pan-neuronal driver would lead to flies eclosing, making it possible to count rhabdomeres (Louis Sam Titus et al., 2017). To do this, the pan-neuronal driver Appl-Gal4 was used to drive expression of mHTT with 93 CAG repeats (Q93) with or without the presence of *FoxP1-FL*. In the Q93-expressing flies, there was no degeneration of rhabdomeres by 12 days post-eclosion (Figure

5.10), and was comparable to that of wild-type rhabdomere counts (Appl>UAS-hHTTex1.Q93 6.98 rhabdomeres +/- 0.001, Appl>UAS-mCherry 6.98 rhabdomeres +/- 0.01, Genotype*Time: $F_{2,20}$ = 1.577, p=0.231). By contrast, pan-neuronal overexpressing of *FoxP1-FL* in the Q93-expressing flies was lethal. To conclude, using a weaker pan-neuronal driver, Appl-Gal4, to induce Q93 leads to no mHTT-induced degeneration, and over-expressing *FoxP1-FL* in the mHTT-induced *Drosophila* model, is lethal.

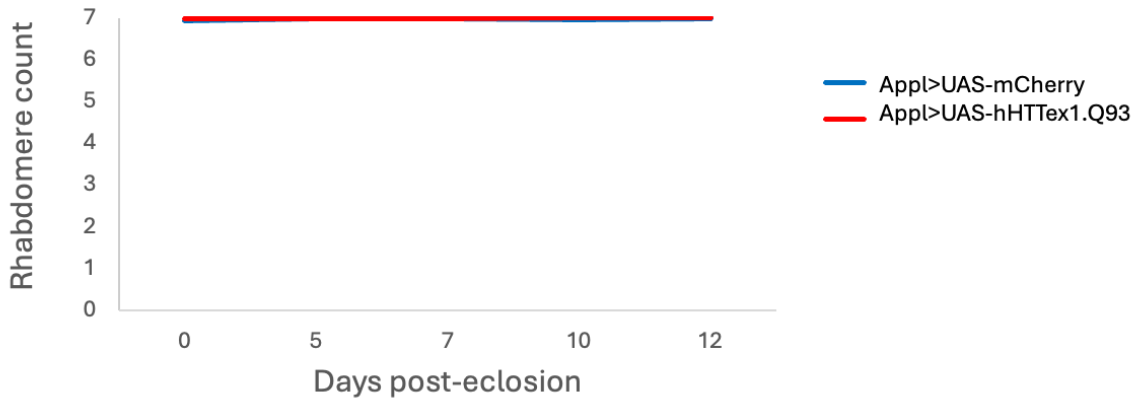

Figure 5.10 Pan-neuronal expression of mHTT with Appl-Gal4 does not induce rhabdomere degeneration.
Graphical representation of rhabdomere counts from flies expressing Q93 in the neurons, using Appl-Gal4, compared to control flies. Counts taken from eclosion, to 12 days post-eclosion. There was no difference in rhabdomere counts between flies expressing Q93 and control flies, (Genotype*Time: $F_{2,20}$ = 1.577, p=0.231).

5.3.9 Rhabdomere-specific expression of *FoxP1-FL* may have an effect on mHTT-induced degeneration.

In the previous experiments, it was shown that pan-neuronal over-expression of *FoxP1-FL* in a mHTT-induced model of degeneration, was lethal. Therefore, the next experiment aimed to investigate whether over-expressing *FoxP1* specifically in the rhabdomeres, would lead to eclosion of flies, and if so, if this had an impact on mHTT-induced rhabdomere degeneration. To do this, the Rh1-Gal4 driver was used. Rh1-Gal4 drives transgene expression the outer PR, R1-R6, and does not drive expression in the larval eye imaginal disc (Escobedo et al., 2021). Using the Rh1-Gal4 driver, these flies did eclose and rhabdomeres were taken from the day of eclosion, to 12 days post-eclosion. Multivariate analysis showed that there was a significant

difference between flies expressing Q93 with *FoxP1-FL*, and those expressing Q93, alone (Genotype*Time: $F_{4,45}$ = 0.347, p=0.001). Post-hoc analysis revealed that that there was no difference in the number of rhabdomeres upon eclosion, (Rh1>UAS-FoxP1-FL; hHTTex1.Q93 6.4 rhabdomeres +/- 0.2, Rh1>UAS-hHTTex1.Q93 6.5 rhabdomeres +/- 0.2, p=0.472) or at 5 days post-eclosion (Rh1<UAS-FoxP1-FL; hHTTex1.Q93, 6.5 rhabdomeres +/- 0.08, Rh1>UAS-hHTTex1.Q93 6.7 rhabdomeres +/- 0.05, p=0.141). Interestingly, at 7 days post-eclosion flies expressing Q93 and *FoxP1-FL* have fewer rhabdomeres than those expressing Q93 (Rh1<UAS-FoxP1-FL; hHTTex1.Q93, 6.4 rhabdomeres +/- 0.07, Rh1>UAS-hHTTex1.Q93, 6.7 rhabdomeres +/- 0.09, p=0.03), but at 10 days post-eclosion, flies expressing Q93 and *FoxP1-FL* had more rhabdomeres than those expressing Q93 (Rh1<UAS-FoxP1-FL; hHTTex1.Q93 6.8 rhabdomeres +/- 0.07, Rh1>UAS-hHTTex1.Q93 6.2 rhabdomeres +/- 0.02, p=0.003). At 12 days post-eclosion, there was no significant difference between the two genotypes, however there was a trend toward flies expressing Q93 and *FoxP1-FL* having more rhabdomeres than Q93-expressing flies (p=0.077). To conclude, whilst there were statistically significant effects at various timepoints between the two genotypes which may indicate an interaction, it is not possible to conclude any specific effects that PR-specific over-expression of *hFoxP1* has on Q93-expressing flies.

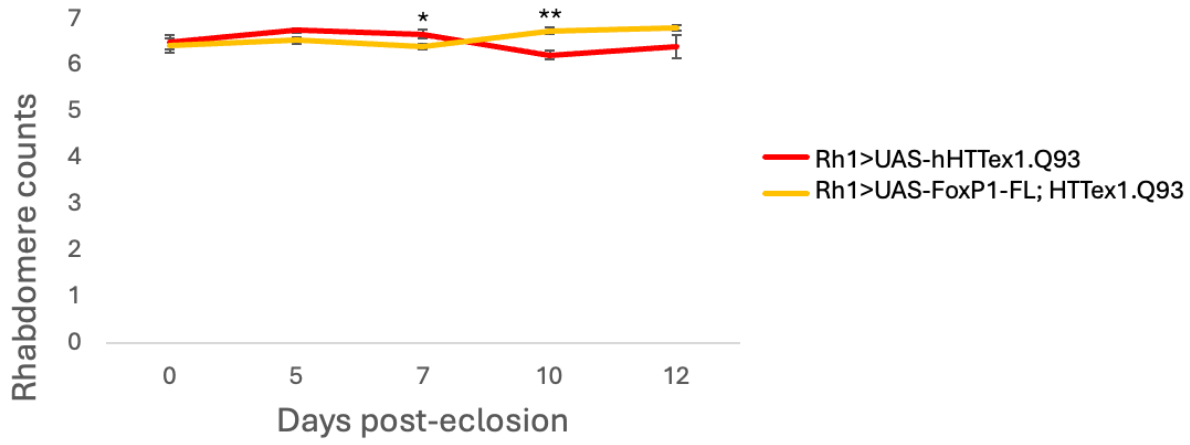

Figure 5.11 PR-specific expression of full-length FoxP1 may influence mHTT-induced rhabdomere degeneration.

Graph to show representative rhabdomere number from photoreceptor-specific expression of Q93 in the presence and absence of *FoxP1-FL*. Rhabdomere counts taken between eclosion and 12-days post eclosion and error bars indicate SEM. *p<0.05, **p<0.01.

5.3.10 Pan-neuronal over-expression of *Drosophila FoxP* has no effect on mHTT-induced degeneration

The next experiment aimed to investigate whether over-expressing *Drosophila FoxP* would influence mHTT-induced loss of rhabdomeres. The *Drosophila* FoxP protein does not include the same N-terminal region present in the mammalian protein but does include the conserved C-terminal region (Figure 5.8C) (Castells-Nobau et al., 2019). Based on the previous experiment using *FoxP*1-FL, it might be that *Drosophila FoxP* over-expression in a mHTT model, is also lethal. In this experiment the pan-neuronal driver, $ELAV^{C155}$-Gal4, was used to over-express *Drosophila FoxP* in Q93-expressing flies. First, using the UAS *Drosophila FoxP* construct on the 2nd chromosome, the pan-neuronal expression was found to be lethal. Therefore, this UAS-FoxP construct was not used to over-express *FoxP* in Q93-expressing flies. Instead, the UAS-FoxP construct on the 3rd chromosome was used, which showed no degenerative phenotype when expressed in the neurons (Figure 5.11). This could then be crossed with flies expressing a mHTT construct with Q93 CAG repeats, on the 2nd chromosome (UAS-Q93-II; FoxP). Rhabdomere counts were taken from the day of eclosion, to 7 days post-eclosion due to the small sample size (n=2 per timepoint). There was no difference between the flies expressing Q93-II and *Drosophila FoxP* compared to those expressing Q93-II, alone (Genotype*Time = $F_{2,30}$ = 0.023, p=0.978) (Figure 5.11). To conclude, pan-neuronal over-expression of *Drosophila FoxP* has no effect on mHTT-induced loss of rhabdomeres, in contrast to the results using human *FoxP1*.

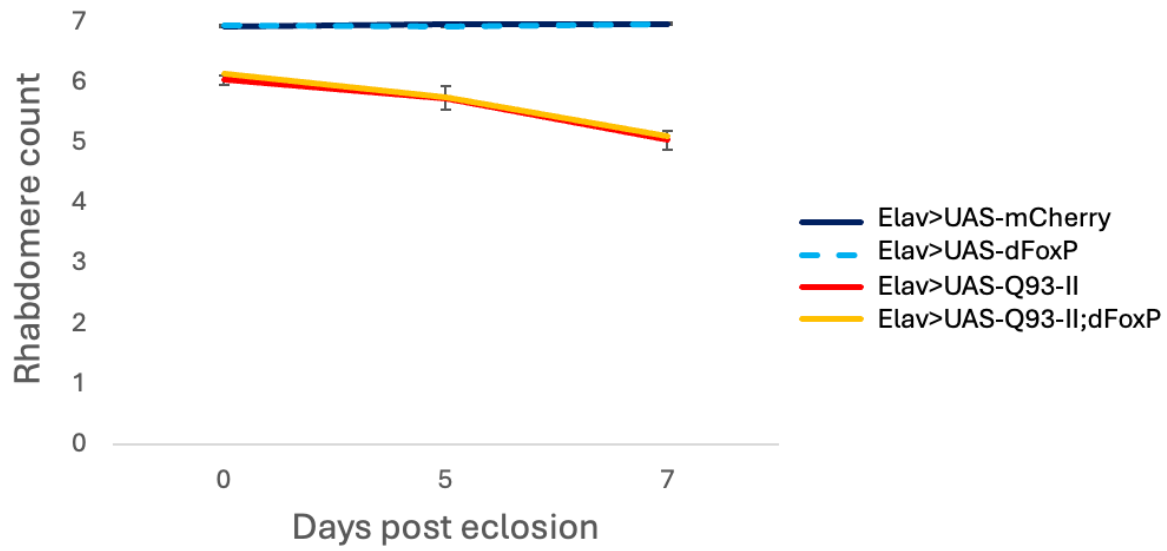

Figure 5.11 Pan-neuronal over-expression of Drosophila FoxP has no effect on mHTT-induced loss of rhabdomeres.
Graphical representation of rhabdomere counts from flies expressing mHTT with 93 CAG repeats (Q93-II) and over-expression of *Drosophila* FoxP. Rhabdomere counts taken from the day of eclosion, to 7 days post-eclosion. Error bars = SEM.

5.3.11 C-terminal FoxP1 physically interacts with WT and mHTT.

The results presented above show that *FoxP1* is capable of suppressing mHTT-induced degeneration. However, the effects of the full-length protein and the N-terminal fragment, only show contrasting results. Tang and colleagues (2015) used co-immunoprecipitation to show that there is a physical interaction between mHTT and FoxP1. Therefore, as an additional step to understanding what might cause these genetic interactions, the next question to ask was which domains of the protein this physical interaction might require. To do this, primers were designed to fragment the FoxP1-FL protein, and cloned into bait (pP6) protein plasmids, with wild-type and mHTT fragments in prey (pB27) plasmids. These plasmids were then grown in yeast cells and plated on 90mm petri dishes to test for physical interactions in the yeast-2-hybrid assay. Growth on these plates indicated a physical interaction, with lack of growth indicating, no interaction (see section 2.2 for detailed methodology).

When testing for a physical interaction between the first 300aa of FoxP1 (FoxP1 1-300aa) with wild-type or mHTT, there was no growth observed after 72 hours incubation at 30°C, indicating

that there is not a physical interaction between these proteins (Figure 5.12B). However, in contrast, there was a physical interaction between FoxP1 301-580aa fragment and both wild-type and mHTT (Figure 5.12C). The C-terminal 301-580aa fragment physically interacts with both wild-type and mHTT. To determine specifically, which part of the C-terminal fragment is involved in the physical interaction, primers were designed to fragment the C-terminus into the following fragments: 301-463aa, to include the leucine zipper and zinc finger domains; and 464-580aa, to include the forkhead domain (Figure 12A). There was a clear physical interaction between FoxP1 301-463aa fragment and wild-type HTT, but not with the FoxP1 463-580aa fragment and wild-type HTT (Figure 5.13 B/C). However, the interaction with mHTT was different. There was just a weak physical interaction between the FoxP1 463-580aa fragment and mHTT, but not wild-type HTT (Figure 5.13B). To conclude, FoxP1 and HTT do physically interact, but there is a difference in the interaction sites of FoxP1 with wild-type and mHTT.

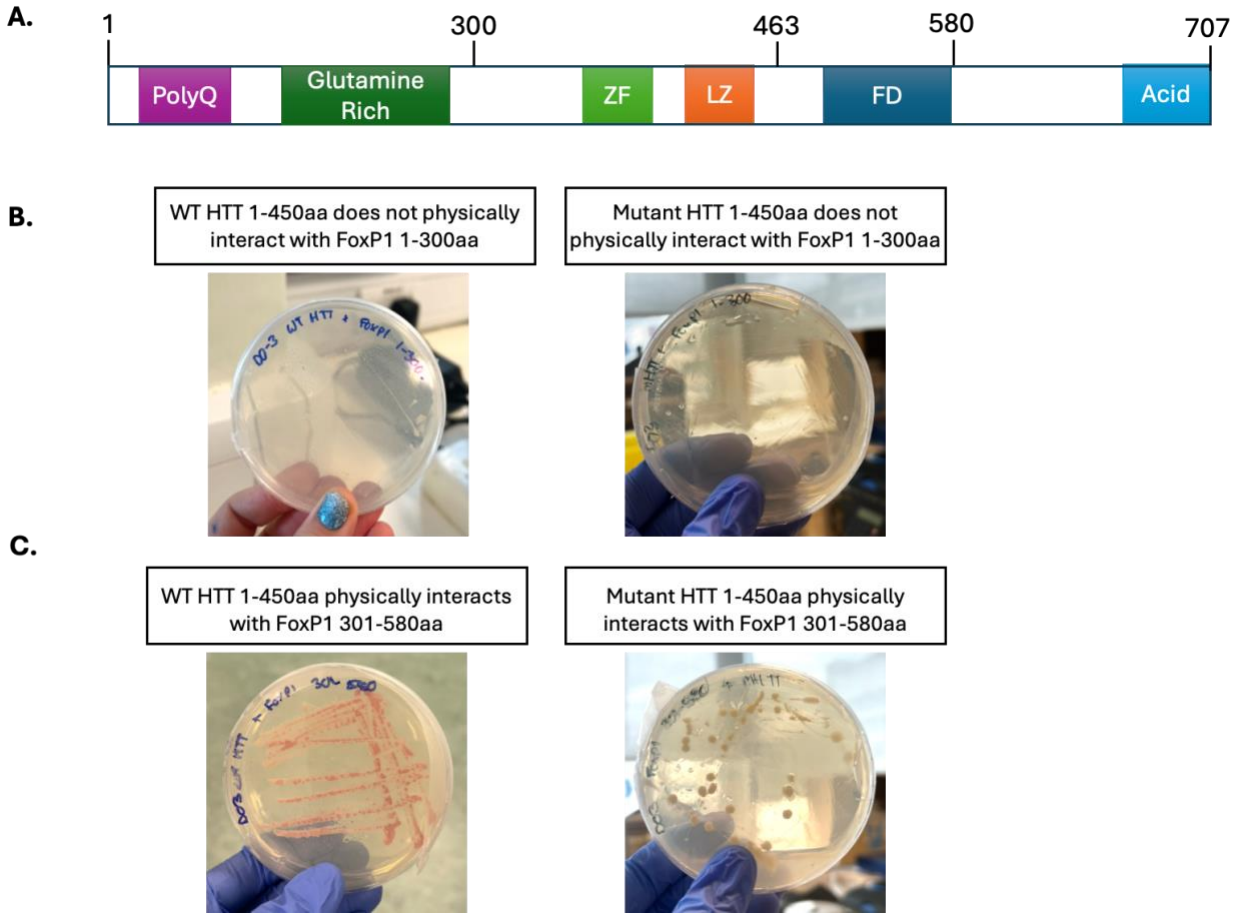

Figure 5.12 FoxP1 physically interacts with Wild-type (WT) and mHTT.

A) Schematic diagram to show the important functional domains present in the FoxP1 protein, and indication of amino acid length (represented by small numbers above the schematic). B) Results from yeast-2-hybrid assay to show that there is no physical interaction (as shown by the lack of growth) between FoxP1 1-300aa fragment with wild-type and mHTT. C) There was a physical interaction between FoxP1 301-580aa and wild-type and mHTT, as presented by growth on the plates.

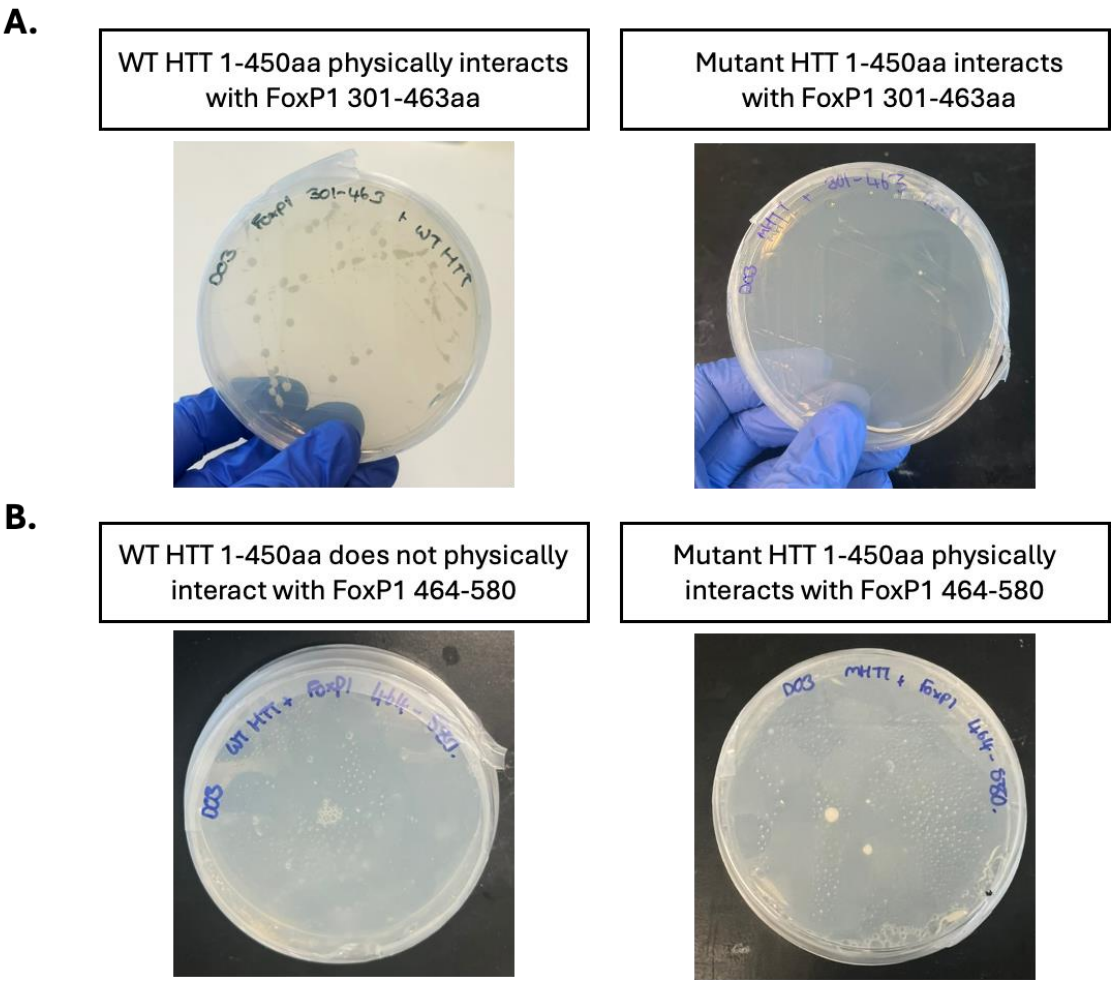

Figure 5.13. FoxP1 464-580aa physically interacts with mutant, but not wild-type (WT) HTT.
Yeast-2-hybrid results from testing physical interactions between the FoxP1 301-463aa and FoxP1 463-580aa fragments, with wild-type and mHTT 1-4500aa. A) There is a physical interaction between the FoxP1 301-463aa fragment and wild-type HTT, which is not replicated in the mHTT protein. B) There is no physical interaction between wild-type HTT and FoxP1 464-580aa, however, there is a physical interaction between this FoxP1 fragment and mHTT.

5.4 Discussion

Over the past 20 years, mammalian *FoxP1* has been widely implicated in the developing striatum, and also in several biological processes, such as the regulation and survival of neurons and maintenance of synaptic currents (Bacon et al., 2015; Desplats et al., 2006; Louis Sam Titus et al., 2017; Precious et al., 2016). Additionally, studies using disease models have implicated the mammalian *FoxP1* gene in several neurological disorders such as ASD and HD (Chien et al., 2013; Li et al., 2019; Louis Sam Titus et al., 2017). In the context of *Drosophila*, the single *FoxP* gene has been found to co-localise with dopaminergic, GABAergic, and

cholinergic neurons of the brain and its expression has been implicated in locomotion, operant learning and memory, and decision making (Castells-Nobau et al., 2019; DasGupta et al., 2014; Mendoza et al., 2014). Previous research has shown that FoxP1 is reduced in the HD brain and that *FoxP1* elevation can protect neurons from mHTT-toxicity in cell culture. Studies have also used *Drosophila* models to show that over-expressing *FoxP1* in a whole-eye model of mHTT can suppress a degenerative phenotype (Hodges et al., 2006; Louis Sam Titus et al., 2017). However, studies have not reported in detail, the change in the *FoxP1* expression profile over-time, and investigated the mechanisms by which FoxP1 might suppress a degenerative phenotype. In this chapter, experiments using mouse brain tissue from HD models, have shown that the FoxP1 protein expression and FoxP1-positive cell number is not affected during early pre-manifest stages, but is significantly reduced during progression of the disease. Specifically, in the R6/1 mouse, it was shown that FoxP1 protein expression and the number of FoxP1-positive nuclei were not affected at 1-month but were significantly reduced compared with the wild-type striatum, from 3-months of age. Additionally, this chapter has used a *Drosophila* model of mHTT-induced degeneration to further investigate the effects of over-expressing *FoxP1* in the whole-eye and neurons in those expressing mHTT. Results have shown that *FoxP1* over-expression can suppress a mHTT-induced degenerative model. Furthermore, it was shown that FoxP1 can physically interact with both wild-type and mHTT and may indicate a mechanism for disease suppression and progression.

5.4.1 FoxP1 protein expression is reduced in striatum of HD mice from manifest stages

The first question addressed in this chapter was how the expression profile of FoxP1 protein and the number of FoxP1-positive cells might change over the time-course of progression in two mouse models of HD. In the transgenic R6/1 model of HD, FoxP1 protein expression per cell and the number of FoxP1-positive cells in the striatum were comparable to that of the wild-type striatum at pre-manifest stages (1-month) but was significantly reduced in the striatum of manifest mice (from 3-months). In the knock-in HdhQ150 mouse model of HD, FoxP1 protein expression per cell was reduced in the striatum from 10-months which correlates with first reports of behavioural and cognitive deficits (Farshim & Bates, 2018). It has been postulated that the presence of mHTT inclusions is responsible for the downregulation of FoxP1, potentially via mHTT-mediated precipitation of FoxP1 (Pogoda et

al., 2021; Tang et al., 2012). One interpretation of this may be that the FoxP1 protein is able to function normally and is not affected by mHTT during striatal development. The absence of mHTT aggregates at this early timepoint might be a reason for that. However, during later life, mHTT aggregates are present in large numbers of cells, and may interact with *FoxP1*, reducing the levels seen in the HD mouse brains at manifest stages. One piece of evidence to support this is an experiment that looked at the co-localisation of mHTT and FoxP1, and showed that >98% of FoxP1-positive neurons in the striatum of 6-month R6/1 mice also contained large HTT aggregates (Tang et al., 2012). This questioned whether mHTT aggregation appears earlier in other brain regions of the HD mouse striatum which could be used to further understand the relationship between mHTT and FoxP1. One publication reported a significantly higher presence of mHTT aggregates in the CA1 region of the hippocampus compared to the CA2 and CA3 regions, and levels overall, were higher in the hippocampus than the striatum, of the 3-month R6/1 brain (Cabanas et al., 2020). To further this experiment, it would be interesting to look at additional brain regions in these mice, such as the hippocampus, for the presence of mHTT inclusions.

Research has shown that conditional knockout of FoxP1 in striatal MSNs, reduces PPP1R1B (also known as DARPP-32) (Anderson et al., 2020), a 'gold standard' marker of striatal MSNs. Previous reports have shown DARPP-32 to be significantly reduced in the 16-week-old R6/1 striatum, with no difference at 9 weeks of age (Naver, Stub, Møller, et al., 2003). This correlates well with the results of this chapter that show significantly reduced FoxP1 protein expression at 3-months (Figure 5.1). Naver and colleagues did not stain for FoxP1, and it is currently unknown as to whether reduced FoxP1 expression is responsible for the loss of DARPP-32 expression, or vice versa. An immunofluorescent stain, co-labelling and quantification of DARPP32 and FoxP1, in HD brain tissue would be an effective way to determine a relationship between these two proteins, and a time-course analysis would indicate how these proteins might be responsible for loss of the other, and subsequent loss of MSNs.

Another protein that may interact with *FoxP1* and play a role in the mechanism for *FoxP1* loss and disease progression, is NR2F1. NR2F1 (also known as COUP-TF1) is a transcriptional regulator of embryonic and postnatal neural cells, and a Bioluminescence resonance energy transfer (BRET) assay showed that NR2F1 may physically interact with *FoxP1* via an NRF2

binding motif F/YSXXLXXL/Y. Additionally, Nr2F1 has been shown to co-localise with FoxP2-positive cells in the mouse cerebral cortex (Estruch et al., 2018). The protein structure of NR2F1 includes a zinc finger DNA-binding domain, and a putative ligand-binding domain, necessary for binding of cofactors (Tocco et al., 2021). Additionally, whilst this protein has not been directly implicated in HD, NR2F1 has been found to bind with other transcription factors, such as Sp1, which is reportedly up-regulated in transgenic mouse models of HD, and may contribute to disease pathology (Qiu et al., 2006; Tocco et al., 2021). *Drosophila* has a highly conserved ortholog of NR2F1 (Nr2f) that has already been used in the study of neurodegenerative diseases (Guo et al., 2021). Investigating how Nr2f may be involved in mHTT-induced degeneration and the function of *FoxP1*, may further aid in understanding how *FoxP1* is associated with mechanisms of degeneration. A starting point for this could include over-expressing and downregulating Nrf2 in a whole-eye and pan-neuronal *Drosophila* model of HD.

5.4.2 Over-expression of FoxP1 in *Drosophila* can suppress a mHTT-induced degenerative phenotype

As mentioned in the Introduction and indicated by immunostaining of the HD mouse brain which has shown reduced FoxP1 protein levels, restoring FoxP1 protein levels to near wild type in the HD brain, may suppress a neurodegenerative phenotype. Previously, it had been shown that pan-neuronal over-expression of full-length F*oxP1* could suppress rhabdomere loss in a whole-eye *Drosophila* model of HD (Louis Sam Titus et al., 2017). In this publication, the pan-neuronal driver, Appl-Gal4, was used; a driver that expresses transgenes in the larval nervous system, and thus may not drive transgene expression directly in the eye. Additionally, in this experiment, mHTT was present in the whole-eye which consists of PR neurons, non-neuronal cone cells, pigment cells, and glia (Cagan, 2009). Therefore, over-expressing *FoxP1* in this way, may not be specific to mHTT-induced neurons. Over-expression of *FoxP1* in a pan-neuronal model of mHTT-induced degeneration, and in the developing and adult *Drosophila* CNS had not been established; a gap that has been addressed in this chapter. To achieve this, the pan-neuronal driver Elav^{c155}Gal4 was used to drive expression of mHTT with 93 CAG repeats together with the N-terminal fragment of human *FoxP1* (Elav>UAS-hFoxP1; hHTTex1.Q93). Pan-neuronal over-expression of *hFoxP1* was able to suppress rhabdomere loss in a mHTT-induced model of HD, and significantly prolonged survival of these flies (Figure 5.3-

5.4). This is interesting because the UAS-hFoxP1 construct used in these experiments does not include the functional domains thought to be required for normal *FoxP1* transcriptional activity and function (Louis Sam Titus et al., 2017). There are multiple reports that have shown that other proteins with polyQ stretches can interact with the expanded CAG repeat of mHTT, and may be sequestered into HTT aggregates (Wanker et al., 2019). The N-terminal region of the FoxP1 protein does include a polyQ domain which stretches 37-40 residues, so may be a common protein-protein interacting motif (B. Wang et al., 2003) (Figure 5.8A). One paper reported that FoxP1 protein lacking the polyQ region is a stronger repressor than those expressing the full polyQ region, and suggested that a combination of alternative splicing and subunit-subunit interactions may be important depending on the individual needs of a cell (B. Wang et al., 2003). Based on the aberrant effects of mHTT, the over-expression of N-terminal FoxP1 may be beneficial in suppressing some of the abnormal interactions that occur due to mHTT presence. However, Y2H assays conducted in this chapter indicate that the N-terminal fragment of *FoxP1* does not physically interact with mHTT (see Figure 5.10). It could be, that the N-terminal *hFoxP1* genetically interacts with mHTT via a different mechanism, that in turn, can suppress the degenerative phenotype. Further experiments could include immunostaining of neurons in the *Drosophila* eye and brain, to determine where the protein localises and whether there is any relationship between *FoxP1* and mHTT presence in cells.

5.4.3 C-terminal FoxP1 interacts abnormally with mHTT

The Y2H assays conducted in this chapter indicate that FoxP1 interacts with HTT in the C-terminal region, and that there is an additional physical interaction between mHTT and the 464-580aa fragment of FoxP1 that doesn't occur with the wild-type HTT protein (Figure 5.11). There is a lot of information in the literature that the FOXP family of transcription factors are involved PPIs (Estruch et al., 2018; Li et al., 2004). The FOXP family of proteins is characterised by the presence of a zinc finger domain, leucine zipper motif, and forkhead domain, all within the C-terminus (see Figure 5.5). These regions have been implicated in transcriptional repression, and as sites of hetero- and homo-dimerisation (Li et al., 2004; Shirasaki et al., 2012; W. Shu et al., 2001; B. Wang et al., 2003). Research has reported that mutations or deletions of the leucine zipper and forkhead domains severely diminished transcriptional

repression and can produce confirmational changes of the protein, leading to reduced numbers of protein-protein contacts (Han et al., 2019; Johnson et al., 2018; Louis Sam Titus et al., 2017). Additionally, in a review of de novo mutation in FOX genes, ~80% of missense mutations were in the forkhead domain, and correlated with intellectual delay and severe language delay (Han et al., 2019).

It has also been well documented that HTT with an expanded CAG repeat can interact abnormally with proteins that ordinarily bind to wild-type HTT (Liu et al., 2023) and FoxP1 may be one of them. For example, HTT interacts with the transcription factor Sp1, which regulates the expression of genes involved in cell growth and differentiation, apoptosis, and immune responses (Liu et al., 2023; Vizcaíno et al., 2015). Experiments have shown that Sp1 binding to mHTT leads to reduced transcriptional activity of Sp1, and dysregulation TAFII130 (Dunah et al., 2002). There are examples where proteins binds more strongly to the mHTT protein compared with wild-type HTT protein, which may indicate a pathway for FoxP1 protein loss (Berger & Moller, 2002). For example, peroxisome-activated receptor delta (PPAR-δ) has been found to bind more strongly to mHTT compared to the wild-type HTT protein (Wanker et al., 2019). PPAR-δ regulates the production of mitochondrial energy in skeletal muscle and brain, as well as regulating lipid metabolism (Berger & Moller, 2002). This additional binding has been thought to contribute to mitochondrial dysfunction in mouse models of HD and activation of PPAR-δ can restore this dysfunction, protecting MSNs from mHTT-induced neurotoxicity (Dickey et al., 2016). The additional interaction between mHTT and FoxP1 may be responsible for degradation of the FoxP1 protein and subsequent loss of MSNs. To further investigate this, PPI assays could be used to investigate the strength of FoxP1 and mHTT interaction with HTT proteins that have varying CAG repeat lengths.

5.4.4 Pan-neuronal expression of full-length FoxP1 in a mHTT-induced model is lethal.

The experiments conducted in this chapter show that pan-neuronal over-expression of *FoxP1-FL* in a mHTT-induced model, using Elav^{c155}Gal4 and Appl-Gal4, is lethal. The presence of the C-terminal region in the FoxP1-FL protein and the identified abnormal physical interaction with mHTT in the 464-580aa region, may indicate a potential pathway for further neuronal death and subsequent lethality in these flies. However, it should be noted that pan-neuronal

drivers express the transgenes in all neurons of the fly body, and *FoxP1-FL* interactions with mHTT throughout the CNS may be responsible for this death. This may also indicate why the results in this chapter contradict those seen in the Louis Sam Titus paper, that show pan-neuronal over-expression of full-length *FoxP1* to be beneficial in a whole-eye mHTT model (Louis Sam Titus et al., 2017). Additionally, over-expression of *FoxP1-FL* in mHTT-induced eye cells using the Rh1-Gal4 driver, did not lead to lethality and indicated a potential genetic interaction. This provides further evidence that over-expression of *FoxP1-FL* in other neurons of the fly might be responsible for early death. To over-come this, further experiments could include the use of the Gal80^{ts}Gal4/UAS system, whereby, flies could be kept at permissive temperatures during larval development, with mHTT and *FoxP1-FL* transgenes being expressed during pupation.

Turning attention to mouse models, there is one publication that has over-expressed FoxP1 in a mouse model of HD (Tang et al., 2012). As mentioned briefly in the introduction to this chapter, Tang and colleagues bi-laterally expressed human FoxP1 via lentiviral administration to the striatum of 3-month-old YAC128 transgenic mice. This lentiviral administration led to an increase in endogenous FoxP1 as well as reduced levels of the astrocyte marker, GFAP, and increased levels of the potassium voltage-gated channel marker, KCNIP2 (Tang et al., 2012). These are promising results since increased GFAP levels have been associated with disease severity and clinical staging of the human disease (You et al., 2021) and potassium channel dysfunction has been shown to exacerbate MSN vulnerability (Zhang et al., 2018). Unfortunately, this paper did not explore changes to the presence of any HD-associated phenotype in these mice, a major avenue that should be explored in the future. Additionally, exploring this avenue in the presence of N-terminal FoxP1 only, versus full-length FoxP1 would be a valuable contribution.

5.5 Conclusion

In this chapter, I have shown that FoxP1 protein expression and the number of FoxP1-positive nuclei are reduced in a transgenic and knock-in model of HD, consistent with previously reported literature. I have also added to knowledge by investigating the time-course of FoxP1 expression and shown that FoxP1 levels are comparable in the early mouse and decrease in

the HD mouse brain at symptomatic timepoints which may indicate a potential mechanism for FoxP1 loss in the presence of mHTT inclusions. Using a *Drosophila* model of HD, I showed that over-expressing the N-terminal fragment of human FoxP1 in a whole-eye and pan-neuronal model of HD can suppress a mHTT-induced degenerative phenotype, however, over-expressing the full-length FoxP1 fragment in these experiments proved lethal. Furthermore, whilst the N-terminal human FoxP1 fragment was shown to genetically interact with mHTT, there was no physical interaction between this fragment and wild-type or mHTT. However, I identified an additional physical interaction between the FoxP1 464-580aa fragment and mHTT which was not observed with wild-type HTT. Combined with the results shown from experiments in *Drosophila*, this may indicate that the N-terminal FoxP1 fragment genetically interacts via a different mechanism which in turn, is beneficial to the system, and can suppress mHTT-induced degeneration. By contrast, the additional interaction between the FoxP1 464-580aa fragment and mHTT may induce an aberrant molecular pathway that implicates full-length FoxP1 in death during pupal stages, when expressed in mHTT neurons. Further investigations should focus on untangling these differences and may aid in unpicking associated mechanisms for mHTT-induced degeneration.

Chapter 6: General Discussion

6.1 Summary

To date, there is no disease-modifying therapy available for the treatment of HD. A thorough understanding of how gene changes influence the complex molecular pathways that are dysregulated in HD progression and pathology may facilitate the development of more effective therapeutics. The focus of the research in this dissertation was to explore the potential effects that *Mef2* and *FoxP* have on the pathological processes associated with HD. To do this, *Drosophila* and mouse models of HD were used to explore the outcomes of manipulating these genes in mHTT-induced models of degeneration, in an attempt to unpick potential mechanisms for suppressing disease progression.

6.2 Importance of using different model systems to investigate disease progression.

Using different animal models during the experiments of this thesis has been integral to understanding the effects of gene expression changes in the development and progression of mHTT-induced degeneration. The *Drosophila* provided a simple biological system that allows for easy genetic manipulation as a way of beginning to explore how potential genetic modifiers can influence mHTT-induced degeneration. In this thesis, I used the *Drosophila* eye to explore how FoxP1 and *Mef2* might be implicated in this process. The *Drosophila* eye comprise neurons and glia as well as a pigmentation and compact structure that can be visually disrupted upon mHTT expression (Nitta & Sugie, 2022). Particularly, the *Drosophila* rhabdomeres that can be visualised by light microscopy, provide a means for quantitative analysis of the effects of mHTT and other genes on neuronal structure (Nitta & Sugie, 2022). In chapters 3 and 5, I utilised this model system to explore whether manipulating the single *Drosophila Mef2* gene and the human *FoxP1* gene could influence mHTT-induced degeneration. In chapter 3, I showed that downregulation of the single *Drosophila Mef2* gene can suppress a mHTT-induced whole-eye and pan-neuronal degenerative phenotype, and that this could be replicated with different models of mHTT and *Mef2* knockdown (Figure 3.8-9). It

was also shown that *Mef2* downregulation in these models could prolong fly survival (Figure 3.10). By contrast, in chapter 5, I showed that over-expression of the human N-terminal FoxP1 fragment could suppress a whole-eye mHTT-induced degenerative phenotype and prolong fly survival (Figure 5.3-5). In this way, I was able to focus on the specific effects that these two genes play in the mHTT degenerative process and how manipulating these genes may modulate progression of mHTT-induced degeneration. However, a limitation of these *Drosophila* models are the physiological and biological differences compared with humans. As a result, mouse models provide an opportunity to expand on the knowledge gained from *Drosophila* models and start to dissect how these genes might play a role in the complex pathways of HD disease progression. In chapter 4, I generated a new HD mouse line with striatal knockout of *Mef2C*. I showed that striatal knockout of *Mef2C* in an R6/1 HD mouse model could influence motor deficits, and that striatal knockout of *Mef2C* in the R6/1 HD brain led to reduced striatal mHTT inclusions. In summary, I have shown that one can utilise the unique tools of different in vivo models to investigate different aspects of mHTT-induced degeneration, which will aid in understanding how different genes might play a role in disease progression.

6.3 The neurodevelopmental impact of mHTT in disease progression

An additional component of HD disease progression that was investigated in this dissertation was the potential interplay between development and degeneration. In chapters 3 and 5, a common observation across the *Drosophila* eye assays was that the number of rhabdomeres was already reduced at the time of eclosion. Two questions came out of these observations: 1), in the context of *Drosophila* eye models of HD, do the normal number of PRs develop, and 2), how important are the developmental changes known to take place in HD patients, important for subsequent disease pathogenesis?

In chapter 3, I showed that the expressing mHTT during fly development, led to rhabdomeres that appeared structurally developed during pupation, but were vulnerable to degeneration in the adult fly (Figure 3.4). When restricting expression of mHTT to the adult fly, the extent of rhabdomere degeneration was very small compared with rhabdomere degeneration seen when mHTT expression was induced during development of the eye (Figure 3.6/3.7). This

indicated that pre-exposure of neurons to mHTT during development may lead to more vulnerable neurons, and that there are events in development that have implications in further progression of mHTT-induced degeneration. In the field of neurodegenerative diseases, the neurodevelopmental hypothesis stipulates that the disease-causing gene can affect developmental brain circuitry, which is initially compensated for in early life, and leads to no overt symptoms. However, the initial vulnerability of these cells then leads to toxic degeneration and cell death in adulthood (van der Plas et al., 2020). This may be happening in the *Drosophila* model of mHTT. A recent study recorded a loss of cortical excitatory synaptic transmission in the first postnatal week (P1-P6) of $Hdh^{Q111/Q7}$ mice, which correlated with downregulation of the AMPA receptor subunit GluA1 regulated in the P2, P5, and P8 HD mouse, compared to wild-type littermates (Braz et al., 2022; Ratié & Humbert, 2024). These alterations were transient, and self-corrected by P21. Behaviourally, these pups were less able to establish huddling behaviour, and delayed righting reflex, a test of sensorimotor development. What is striking is that by 6-months of age, these mice showed additional behavioural impairments in the Y-maze task, open field, horizontal ladder, and gap crossing (Braz et al., 2022). Interestingly, neonatal treatment with CX516, a drug that increases the responsiveness of AMPA receptors, restored sensorimotor function in the pups and prevented HD mice from developing behavioural deficits (Braz et al., 2022). The results of this thesis showed that when PRs were exposed to mHTT in the pan-neuronal model (Elav>UAS-hHTTex1.Q93), the rhabdomeres looked structurally normally in the two days prior to eclosion, comparable to those in the wild-type *Drosophila*, despite there being a reduction in the number of rhabdomeres on the day of eclosion (Figure 3.4). However, based on Braz and colleagues (2022) report on postnatal loss of synaptic transmission, which was self-corrected, the PRs that have been exposed to mHTT may look structurally normal but may not be functioning normally. This thesis did not explore any expression changes for the genes that are important for the development of the photoreceptors. Further research could include expressing mHTT in the *Drosophila* PRs and exploring whether there are any changes to the expression profile of genes involved in the initiation and progression of eye development. This might include Rhodopsin, Hedgehog and EGFR signalling (Katz & Minke, 2009; Pappu et al., 2003).

Another experiment that has investigated the expression of mHTT during development is one that generated a BACHD mouse colony with restricted expression of mHTT during neural development using a tamoxifen-inducible cre recombinase ($Q97^{cre}$) (Molero et al., 2016). In this experiment, Molero and colleagues (2016) treated the offspring of these BACHD mice with tamoxifen at post-natal day 21 to stop further mHTT expression into adulthood, generating a model where mHTT was only expressed during development. Behaviourally, these mice produced HD-like progressive motor deficits and studies in the 9-month brain, and the striatal volume and the number of striatal NeuN-positive cells were reduced, which was comparable with the reductions seen in the Q97 model. This indicates that the presence of mHTT during neural development is sufficient to produce vulnerability of striatal cells to degeneration and cell death (Molero et al., 2016). The mHTT-induced degeneration observed in my *Drosophila* experiments may also indicate that exposure to mHTT during eye development is sufficient to produce a mHTT-induced degenerative phenotype in the adult fly. In further studies, the $Gal80^{ts}$Gal4/UAS system could be used to induce mHTT expression during eye development and halting mHTT expressing when the flies eclose, to see whether the rhabdomeres continue to degenerate in the adult fly.

The results obtained in my *Drosophila* experiments have contributed to evidence showing that mHTT exposure during development does play a role in the onset of degeneration later in life. Further investigations may be able to unravel the interplay between early pathogenic abnormalities and compensatory mechanisms.

6.4 *FoxP1* and *Mef2C* transcriptional activation and repression

Both *Mef2C* and *FoxP1* are transcription factors that have both been implicated in neuronal differentiation and maturation, have been shown to be involved in striatal development, and have been linked to various neurodevelopmental disorders such as ASD intellectual ability and schizophrenia (Ali, 2022; Kamath & Chen, 2019; Hao Li et al., 2008; Mitchell et al., 2018; Precious et al., 2016). Showing that both of these genes can be manipulated to suppress mHTT-induced degeneration questions whether it is just a co-incidence that both genes are involved in similar neurodevelopmental processes, and that both are implicated in HD

pathogenesis, or whether the pathways that these transcription factors are a part of is a general route to suppressing mHTT-induced degeneration.

One of the interesting differences between these two proteins, is that *FoxP1* is known as a transcriptional repressor, whilst *Mef2C* is predominantly an activator, albeit with the ability to act as a repressor (Ahmed et al., 2024; Di Giorgio et al., 2017). Interestingly, reports have shown that *Mef2* can be converted from an activator to a repressor after binding to class IIa HDACs (Histone deacetylases), the interplay of which has been linked to the aggressiveness of leiomyosarcomas (Di Giorgio et al., 2017). This is an example of how *Mef2C*-regulated gene expression might be modified in response to certain cellular and developmental cues and might be a potential avenue for understanding how *Mef2* downregulation suppresses mHTT-induced degeneration in the *Drosophila*.

Interestingly, *Mef2C* hypofunction in the brain has been associated with reduced excitability and inhibitory synaptic transmission in the mouse pre-frontal cortex (Cho et al., 2024). By contrast, *FoxP1* regulates the development and maturation of excitatory glutamatergic inputs onto MSNs (Khandelwal et al., 2024). In the mammalian brain, this may indicate that *FoxP1* targets genes and subsequent excitatory pathways, that upon FoxP1 reduction in the HD brain would lead to reduced activation of downstream gene transcription. By contrast, *Mef2C* may be activating inhibitory pathways in the mammalian brain that are already affected by reduced excitatory input, and thus, downregulating *Mef2C* in this pathway, could be beneficial. Further investigations could include using markers for different neuronal sub-sets to co-label with *Mef2C* and *FoxP1* in the mouse brain, to determine where these genes are expressed and hence, which downstream pathways might be implicated. This would provide additional insight into the interplay between complex pathways in the brain and how they are dysregulated in the diseased brain.

6.5 A potential mechanism through direct PPIs

As alluded to above, an important aspect of these experiments is understanding how *Mef2C* and *FoxP1* mechanistically affect mHTT-induced degeneration. In this thesis, I have shown that both *FoxP1* and *Mef2* can impact mHTT-induced degeneration in a *Drosophila* model of mHTT,

and in the case of *Mef2C,* impacts a mouse model of HD. However, it is currently unknown as to what lies behind these genetic interactions. One possible route to consider is through direct PPIs. PPIs are required for a multitude of biological processes, with over 350,000 interactions thought to occur in the human cell (Wong et al., 2017). Since its development in the late 1980s, Y2H has been one of the most widely used genetic systems for testing and identifying novel PPIs (Brückner et al., 2009; Fields & Song, 1989). The Y2H method is a cost-effective, versatile and scalable genetic approach that directly detects interacting proteins using living yeast cells, and has been used in various high-throughput genome-wide studies as well as protein studies for specific diseases, such as HD (Brückner et al., 2009; Formstecher et al., 2005; Kaltenbach et al., 2007; Mehla et al., 2017). In this thesis, I showed that both FoxP1 and Mef2C physically interact with both wild-type and mHTT (Figure 3.19; Figure 5.12-13). Additionally, I showed that there is a physical interaction between the FoxP1 464-580aa fragment and mHTT that does not occur between FoxP1 464-580aa and wild-type HTT (Figure 5.13). Using a full-length FoxP1 protein and an N-terminal FoxP1 fragment, I showed that the presence of these fragments appears to genetically interact with mHTT in the *Drosophila* model of mHTT-induced degeneration, and the presence of this additional physical interaction may provide insight into a mechanism for this. More in-depth analysis of how *FoxP1-FL* and *hFoxP1* expression in a *Drosophila* model affect neurons, might contribute to further understanding as to the role *FoxP1* plays in progression and pathology in HD.

6.6 Concluding remarks

The work of this thesis has contributed novel findings that downregulating the sole *Drosophila Mef2* gene can suppress mHTT-induced degeneration, and added additional knowledge as to *FoxP1* over-expression suppressing mHTT-induced degeneration, both in *Drosophila* models of HD. Further studies will enhance our understanding as to the mechanisms associated with this phenotypic suppression. Furthermore, the use of *Drosophila* models of HD has been instrumental in investigating potential pathways for how *Mef2C* knockout and *FoxP1* over-expression can protect neurons from mHTT-induced degeneration. Additionally, I have successfully translated the work from *Drosophila* models into a more complex mammalian system by generating a new mouse line to investigate striatal *Mef2C* knockout in the R6/1 HD mouse. Specifically, knocking down *Mef2C* in the R6/1 brain led to reduced mHTT inclusions,

which is a significant step toward understanding *Mef2C*'s role in HD pathogenesis. This has shown that combining model systems in research is fundamental for understanding disease development and progression. Finally, using the *Drosophila* eye as an in vivo test tube for modelling mHTT-induced degeneration has further indicated a neurodevelopmental aspect for progression of HD, which may be significant in the development of future therapeutics.

Appendix

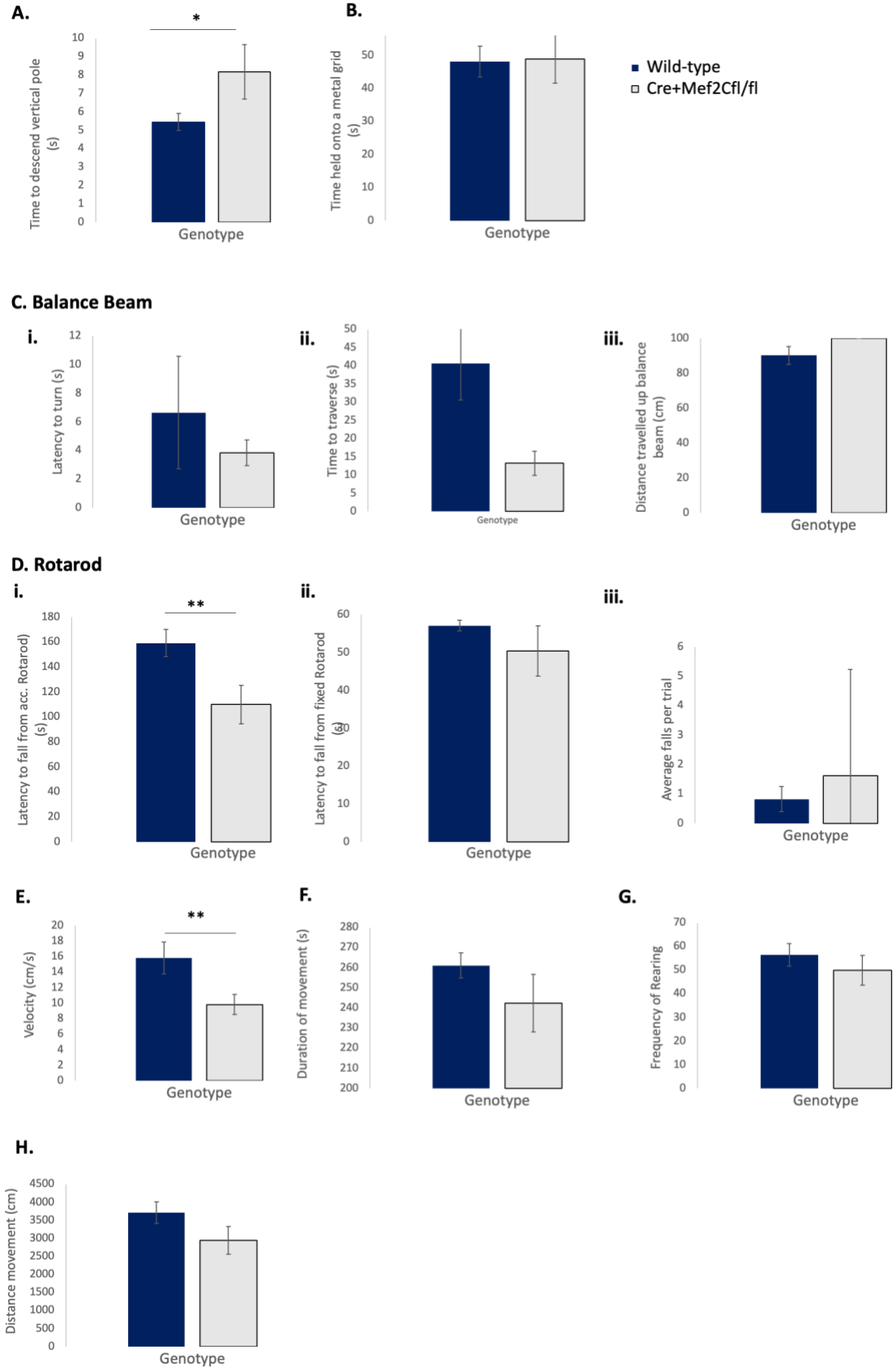

Appendix 1. Behavioural analysis of Gsx2Cre^{+}Mef2C mice compared with wild-type mice.

Graphical representation to show the differences in behavioural parameters between wild-type mice, and those with striatal knockout of *Mef2C* (Gsx2Cre^{+}Mef2C). A) Gsx2Cre^{+}Mef2C mice take longer to descend the vertical pole compared with wild-type mice (Effect of Genotype: $F_{1,23}$ = 7.321, p=0.013). There was no difference between Gsx2Cre^{+}Mef2C mice and wild-type on the B) inverted grip strength test (Effect of Genotype: $F_{1,24}$ = 0.012, p=0.915) or the C) balance beam (Latency to turn, Effect of Genotype: $F_{1,24}$ = 2.043, p=0.166; Time to traverse, Effect of Genotype: $F_{1,24}$ = 3.238, p=0.085; Distance travelled, Effect of Genotype: $F_{1,24}$ = 1.484, p=0.235). Di) Gsx2Cre^{+}Mef2C mice fall from the accelerating rotarod more quickly that wild-type mice (Effect of Genotype: $F_{1,24}$ = 7.996, p=0.009), but do not show any differences on ii) latency to fall from the fixed rotarod (Effect of Genotype: $F_{1,24}$ = 1.474, p=0.237) or iii) falls per trial (Effect of Genotype: $F_{1,24}$ = 2.421, p=0.147). E) Gsx2Cre^{+}Mef2C mice travel more slowly in an open arena compared to wild-type mice (Effect of Genotype: $F_{1,24}$ = 3.122, p=0.009), but did not show any differences in F) duration of movement (Effect of Genotype: $F_{1,24}$ = 2.021, p=0.168), G) frequency of rearing (Effect of Genotype: $F_{1,24}$ = 0.516, p=0.480), or H) distance travelled (Effect of Genotype: $F_{1,24}$ = 2.025, p=0.168).

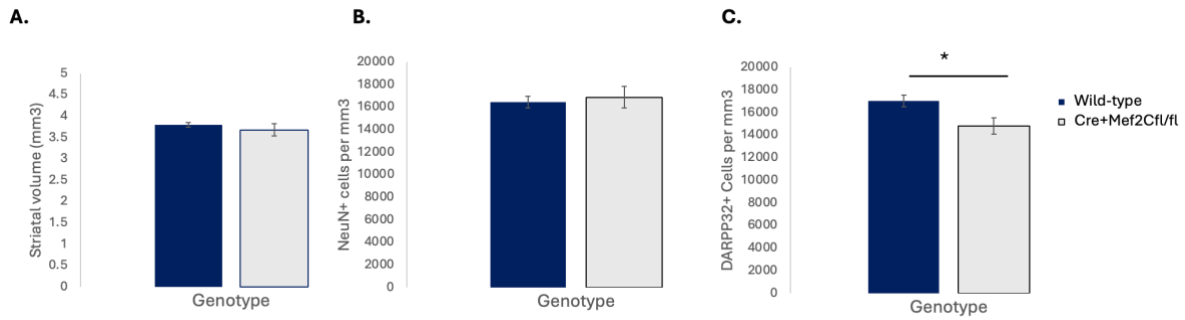

Appendix 2. Striatal volume, NeuN and MSN counts in Gsx2Cre^{+}Mef2C mice compared with wild-type mice

Graphical representation of A) striatal volume, and the number of B) NeuN-positive and C) DARPP-32-positive cells per mm^3 in the striatum of Gsx2Cre^{+}Mef2C mice and wild-type littermates. There were no differences in striatal volume and NeuN counts per mm^3 (Striatal volume, t_{24} = 0.634, p=0.266. NeuN, t_{21} = -0.255, p=0.412), however there were fewer DARPP-32-positive cells in the Gsx2Cre^{+}Mef2C mice compared with wild-type mice (t_{19} = 2.335, p=0.015).

References

Adachi, M., Lin, P. Y., Pranav, H., & Monteggia, L. M. (2016). Postnatal Loss of Mef2c Results in Dissociation of Effects on Synapse Number and Learning and Memory. *Biol Psychiatry*, *80*(2), 140-148. https://doi.org/10.1016/j.biopsych.2015.09.018

Aggleton, J. P., Albasser, M. M., Aggleton, D. J., Poirier, G. L., & Pearce, J. M. (2010). Lesions of the rat perirhinal cortex spare the acquisition of a complex configural visual discrimination yet impair object recognition. *Behav Neurosci*, *124*(1), 55-68. https://doi.org/10.1037/a0018320

Agrawal, N., Pallos, J., Slepko, N., Apostol, B. L., Bodai, L., Chang, L.-W., Chiang, A.-S., Thompson, L. M., & Marsh, J. L. (2005). Identification of combinatorial drug regimens for treatment of Huntington's disease using Drosophila. *Proceedings of the National Academy of Sciences*, *102*(10), 3777-3781. https://doi.org/doi:10.1073/pnas.0500055102

Ahmed, N. I., Khandelwal, N., Anderson, A. G., Oh, E., Vollmer, R. M., Kulkarni, A., Gibson, J. R., & Konopka, G. (2024). Compensation between FOXP transcription factors maintains proper striatal function. *Cell Rep*, *43*(5), 114257. https://doi.org/10.1016/j.celrep.2024.114257

Akhtar, M. W., Kim, M.-S., Adachi, M., Morris, M. J., Qi, X., Richardson, J. A., Bassel-Duby, R., Olson, E. N., Kavalali, E. T., & Monteggia, L. M. (2012). In Vivo Analysis of MEF2 Transcription Factors in Synapse Regulation and Neuronal Survival. *PLOS ONE*, *7*(4), e34863. https://doi.org/10.1371/journal.pone.0034863

Akimov, S. S., Jiang, M., Kedaigle, A. J., Arbez, N., Marque, L. O., Eddings, C. R., Ranum, P. T., Whelan, E., Tang, A., Wang, R., DeVine, L. R., Talbot, C. C., Cole, R. N., Ratovitski, T., Davidson, B. L., Fraenkel, E., & Ross, C. A. (2021). Immortalized striatal precursor neurons from Huntington's disease patient-derived iPS cells as a platform for target identification and screening for experimental therapeutics. *Hum Mol Genet*, *30*(24), 2469-2487. https://doi.org/10.1093/hmg/ddab200

Aktar, F., Burudpakdee, C., Polanco, M., Pei, S., Swayne, T. C., Lipke, P. N., & Emtage, L. (2019). The huntingtin inclusion is a dynamic phase-separated compartment. *Life Science Alliance*, *2*(5), e201900489. https://doi.org/10.26508/lsa.201900489

Ali, H. (2022). *Mef2c Transcription Factor is Required for the Development of Medium Spiny Neurons of the Mouse Striatum*. Cardiff University. https://books.google.co.uk/books?id=lX2izwEACAAJ

Amartumur, S., Nguyen, H., Huynh, T., Kim, T. S., Woo, R.-S., Oh, E., Kim, K. K., Lee, L. P., & Heo, C. (2024). Neuropathogenesis-on-chips for neurodegenerative diseases. *Nature Communications*, *15*(1), 2219. https://doi.org/10.1038/s41467-024-46554-8

Anderson, A. G., Kulkarni, A., Harper, M., & Konopka, G. (2020). Single-Cell Analysis of Foxp1-Driven Mechanisms Essential for Striatal Development. *Cell Reports*, *30*(9), 3051-3066.e3057. https://doi.org/https://doi.org/10.1016/j.celrep.2020.02.030

Andzelm, M. M., Cherry, T. J., Harmin, D. A., Boeke, A. C., Lee, C., Hemberg, M., Pawlyk, B., Malik, A. N., Flavell, S. W., Sandberg, M. A., Raviola, E., & Greenberg, M. E. (2015). MEF2D drives photoreceptor development through a genome-wide competition for

tissue-specific enhancers. *Neuron*, *86*(1), 247-263. https://doi.org/10.1016/j.neuron.2015.02.038

Angeles-López, Q. D., García-Lara, L., Aguirre-Pineda, N., Castañeda-Arellano, R., Elizondo-Azuela, G., Pérez-Severiano, F., & Segovia, J. (2021). The absence of the aryl hydrocarbon receptor in the R6/1 transgenic mouse model of Huntington's disease improves the neurological phenotype. *Behavioural Brain Research*, *408*, 113230. https://doi.org/https://doi.org/10.1016/j.bbr.2021.113230

Araujo, D. J., Toriumi, K., Escamilla, C. O., Kulkarni, A., Anderson, A. G., Harper, M., Usui, N., Ellegood, J., Lerch, J. P., Birnbaum, S. G., Tucker, H. O., Powell, C. M., & Konopka, G. (2017). Foxp1 in Forebrain Pyramidal Neurons Controls Gene Expression Required for Spatial Learning and Synaptic Plasticity. *J Neurosci*, *37*(45), 10917-10931. https://doi.org/10.1523/jneurosci.1005-17.2017

Ardan, T., Baxa, M., Levinská, B., Sedláčková, M., Nguyen, T. D., Klíma, J., Juhás, Š., Juhásová, J., Šmatlíková, P., Vochozková, P., Motlík, J., & Ellederová, Z. (2019). Transgenic minipig model of Huntington's disease exhibiting gradually progressing neurodegeneration. *Dis Model Mech*, *13*(2). https://doi.org/10.1242/dmm.041319

Arlotta, P., Molyneaux, B. J., Jabaudon, D., Yoshida, Y., & Macklis, J. D. (2008). Ctip2 controls the differentiation of medium spiny neurons and the establishment of the cellular architecture of the striatum. *J Neurosci*, *28*(3), 622-632. https://doi.org/10.1523/jneurosci.2986-07.2008

Arrasate, M., & Finkbeiner, S. (2012). Protein aggregates in Huntington's disease. *Exp Neurol*, *238*(1), 1-11. https://doi.org/10.1016/j.expneurol.2011.12.013

Arrasate, M., Mitra, S., Schweitzer, E. S., Segal, M. R., & Finkbeiner, S. (2004). Inclusion body formation reduces levels of mutant huntingtin and the risk of neuronal death. *Nature*, *431*(7010), 805-810. https://doi.org/10.1038/nature02998

Assali, A., Harrington, A. J., & Cowan, C. W. (2019). Emerging roles for MEF2 in brain development and mental disorders. *Curr Opin Neurobiol*, *59*, 49-58. https://doi.org/10.1016/j.conb.2019.04.008

Avarlaid, A., Falkenberg, K., Lehe, K., Mudò, G., Belluardo, N., Di Liberto, V., Frinchi, M., Tuvikene, J., & Timmusk, T. (2024). An upstream enhancer and MEF2 transcription factors fine-tune the regulation of the Bdnf gene in cortical and hippocampal neurons. *J Biol Chem*, *300*(6), 107411. https://doi.org/10.1016/j.jbc.2024.107411

Babcock, D. T., & Ganetzky, B. (2015). Transcellular spreading of huntingtin aggregates in the Drosophila brain. *Proc Natl Acad Sci U S A*, *112*(39), E5427-5433. https://doi.org/10.1073/pnas.1516217112

Bacon, C., Schneider, M., Le Magueresse, C., Froehlich, H., Sticht, C., Gluch, C., Monyer, H., & Rappold, G. A. (2015). Brain-specific Foxp1 deletion impairs neuronal development and causes autistic-like behaviour. *Mol Psychiatry*, *20*(5), 632-639. https://doi.org/10.1038/mp.2014.116

Bai, M., Ye, D., Guo, X., Xi, J., Liu, N., Wu, Y., Jia, W., Wang, G., Chen, W., Li, G., Jiapaer, Z., & Kang, J. (2020). Critical regulation of a NDIME/MEF2C axis in embryonic stem cell neural differentiation and autism. *EMBO reports*, *21*(11), e50283. https://doi.org/https://doi.org/10.15252/embr.202050283

Bamford, I. J., & Bamford, N. S. (2019). The Striatum's Role in Executing Rational and Irrational Economic Behaviors. *Neuroscientist*, *25*(5), 475-490. https://doi.org/10.1177/1073858418824256

Baonza, A., & Freeman, M. (2002). Control of Drosophila eye specification by Wingless signalling. *Development*, *129*(23), 5313-5322. https://doi.org/10.1242/dev.00096

Barbaro, B. A., Lukacsovich, T., Agrawal, N., Burke, J., Bornemann, D. J., Purcell, J. M., Worthge, S. A., Caricasole, A., Weiss, A., Song, W., Morozova, O. A., Colby, D. W., & Marsh, J. L. (2015). Comparative study of naturally occurring huntingtin fragments in Drosophila points to exon 1 as the most pathogenic species in Huntington's disease. *Hum Mol Genet*, *24*(4), 913-925. https://doi.org/10.1093/hmg/ddu504

Barbosa, A. C., Kim, M.-S., Ertunc, M., Adachi, M., Nelson, E. D., McAnally, J., Richardson, J. A., Kavalali, E. T., Monteggia, L. M., Bassel-Duby, R., & Olson, E. N. (2008a). MEF2C, a transcription factor that facilitates learning and memory by negative regulation of synapse numbers and function. *Proceedings of the National Academy of Sciences of the United States of America*, *105*(27), 9391-9396.

Barrans, S. L., Fenton, J. A. L., Banham, A., Owen, R. G., & Jack, A. S. (2004). Strong expression of FOXP1 identifies a distinct subset of diffuse large B-cell lymphoma (DLBCL) patients with poor outcome. *Blood*, *104*(9), 2933-2935. https://doi.org/10.1182/blood-2004-03-1209

Barré-Sinoussi, F., & Montagutelli, X. (2015). Animal Models are Essential to Biological Research: Issues and Perspectives. *Future Science OA*, *1*(4), FSO63. https://doi.org/10.4155/fso.15.63

Barry, J., Akopian, G., Cepeda, C., & Levine, M. S. (2018). Striatal Direct and Indirect Pathway Output Structures Are Differentially Altered in Mouse Models of Huntington's Disease. *J Neurosci*, *38*(20), 4678-4694. https://doi.org/10.1523/jneurosci.0434-18.2018

Bartoletti, R., Capozzoli, B., Moore, J., Moran, J., Shrawder, B., & Vivekanand, P. (2017). Short hairpin RNA is more effective than long hairpin RNA in eliciting pointed loss-of-function phenotypes in Drosophila. *Genesis*, *55*(7), e23036. https://doi.org/https://doi.org/10.1002/dvg.23036

Barwell, T., Geld, S., & Seroude, L. (2023). Comparison of GAL80ts and Tet-off GAL80 transgenes. *MicroPubl Biol*, *2023*. https://doi.org/10.17912/micropub.biology.000770

Bathina, S., & Das, U. N. (2015). Brain-derived neurotrophic factor and its clinical implications. *Arch Med Sci*, *11*(6), 1164-1178. https://doi.org/10.5114/aoms.2015.56342

Bayram-Weston, Z., Jones, L., Dunnett, S. B., & Brooks, S. P. (2016). Comparison of mHTT Antibodies in Huntington's Disease Mouse Models Reveal Specific Binding Profiles and Steady-State Ubiquitin Levels with Disease Development. *PLOS ONE*, *11*(5), e0155834. https://doi.org/10.1371/journal.pone.0155834

Bayram-Weston, Z., Torres, E. M., Jones, L., Dunnett, S. B., & Brooks, S. P. (2012). Light and electron microscopic characterization of the evolution of cellular pathology in the Hdh(CAG)150 Huntington's disease knock-in mouse. *Brain Research Bulletin*, *88*(2), 189-198. https://doi.org/https://doi.org/10.1016/j.brainresbull.2011.03.014

Behrens, P. F., Franz, P., Woodman, B., Lindenberg, K. S., & Landwehrmeyer, G. B. (2002). Impaired glutamate transport and glutamate-glutamine cycling: downstream effects of the Huntington mutation. *Brain*, *125*(Pt 8), 1908-1922. https://doi.org/10.1093/brain/awf180

Berger, J., & Moller, D. E. (2002). The mechanisms of action of PPARs. *Annu Rev Med*, *53*, 409-435. https://doi.org/10.1146/annurev.med.53.082901.104018

Bhattacharyya, K. B. (2016). The story of George Huntington and his disease. *Ann Indian Acad Neurol*, *19*(1), 25-28. https://doi.org/10.4103/0972-2327.175425

Bilen, J., & Bonini, N. M. (2005). Drosophila as a model for human neurodegenerative disease. *Annu Rev Genet*, *39*, 153-171. https://doi.org/10.1146/annurev.genet.39.110304.095804

Black, B. L., & Cripps, R. M. (2010). Chapter 9.5 - Myocyte Enhancer Factor 2 Transcription Factors in Heart Development and Disease. In N. Rosenthal & R. P. Harvey (Eds.), *Heart Development and Regeneration* (pp. 673-699). Academic Press. https://doi.org/https://doi.org/10.1016/B978-0-12-381332-9.00030-X

Black, B. L., & Olson, E. N. (1998). Transcriptional control of muscle development by myocyte enhancer factor-2 (MEF2) proteins. *Annual review of cell and developmental biology*, *14*, 167-196. https://doi.org/10.1146/annurev.cellbio.14.1.167

Blanchard, F. J., Collins, B., Cyran, S. A., Hancock, D. H., Taylor, M. V., & Blau, J. (2010). The transcription factor Mef2 is required for normal circadian behavior in Drosophila. *J Neurosci*, *30*(17), 5855-5865. https://doi.org/10.1523/jneurosci.2688-09.2010

Blumenstock, S., & Dudanova, I. (2020). Cortical and Striatal Circuits in Huntington's Disease. *Front Neurosci*, *14*, 82. https://doi.org/10.3389/fnins.2020.00082

Bolivar, V. J., Manley, K., & Messer, A. (2004). Early exploratory behavior abnormalities in R6/1 Huntington's disease transgenic mice. *Brain Research*, *1005*(1), 29-35. https://doi.org/https://doi.org/10.1016/j.brainres.2004.01.021

Bolus, H., Crocker, K., Boekhoff-Falk, G., & Chtarbanova, S. (2020). Modeling Neurodegenerative Disorders in Drosophila melanogaster. *Int J Mol Sci*, *21*(9). https://doi.org/10.3390/ijms21093055

Bonini, N. M., Leiserson, W. M., & Benzer, S. (1993). The eyes absent gene: Genetic control of cell survival and differentiation in the developing Drosophila eye. *Cell*, *72*(3), 379-395. https://doi.org/https://doi.org/10.1016/0092-8674(93)90115-7

Borghi, S., Molinari, S., Razzini, G., Parise, F., Battini, R., & Ferrari, S. (2001). The nuclear localization domain of the MEF2 family of transcription factors shows member-specific features and mediates the nuclear import of histone deacetylase 4. *J Cell Sci*, *114*(Pt 24), 4477-4483. https://doi.org/10.1242/jcs.114.24.4477

Bostock, M. P., Prasad, A. R., Chaouni, R., Yuen, A. C., Sousa-Nunes, R., Amoyel, M., & Fernandes, V. M. (2020). An immobilization technique for long-term time-lapse imaging of explanted Drosophila tissues. *bioRxiv*, 2020.2008.2004.234864. https://doi.org/10.1101/2020.08.04.234864

Braid, L. R., & Verheyen, E. M. (2008). Drosophila Nemo Promotes Eye Specification Directed by the Retinal Determination Gene Network. *Genetics*, *180*(1), 283-299. https://doi.org/10.1534/genetics.108.092155

Braz, B. Y., Wennagel, D., Ratié, L., de Souza, D. A. R., Deloulme, J. C., Barbier, E. L., Buisson, A., Lanté, F., & Humbert, S. (2022). Treating early postnatal circuit defect delays Huntington's disease onset and pathology in mice. *Science*, *377*(6613), eabq5011. https://doi.org/doi:10.1126/science.abq5011

Brimblecombe, K. R., & Cragg, S. J. (2017). The Striosome and Matrix Compartments of the Striatum: A Path through the Labyrinth from Neurochemistry toward Function. *ACS Chemical Neuroscience*, *8*(2), 235-242. https://doi.org/10.1021/acschemneuro.6b00333

Brooks, S. P., Janghra, N., Workman, V. L., Bayram-Weston, Z., Jones, L., & Dunnett, S. B. (2012). Longitudinal analysis of the behavioural phenotype in R6/1 (C57BL/6J) Huntington's disease transgenic mice. *Brain Research Bulletin*, *88*(2), 94-103. https://doi.org/https://doi.org/10.1016/j.brainresbull.2011.01.010

Brooks, S. P., Jones, L., & Dunnett, S. B. (2012). Comparative analysis of pathology and behavioural phenotypes in mouse models of Huntington's disease. *Brain Research Bulletin*, *88*(2), 81-93. https://doi.org/https://doi.org/10.1016/j.brainresbull.2011.10.002

Brown, P. J., Ashe, S. L., Leich, E., Burek, C., Barrans, S., Fenton, J. A., Jack, A. S., Pulford, K., Rosenwald, A., & Banham, A. H. (2008). Potentially oncogenic B-cell activation-induced smaller isoforms of FOXP1 are highly expressed in the activated B cell-like subtype of DLBCL. *Blood*, *111*(5), 2816-2824. https://doi.org/10.1182/blood-2007-09-115113

Brückner, A., Polge, C., Lentze, N., Auerbach, D., & Schlattner, U. (2009). Yeast two-hybrid, a powerful tool for systems biology. *Int J Mol Sci*, *10*(6), 2763-2788. https://doi.org/10.3390/ijms10062763

Bryda, E. C. (2013). The Mighty Mouse: the impact of rodents on advances in biomedical research. *Mo Med*, *110*(3), 207-211.

Bunting, E., Donaldson, J., Olive, J., Kordasiewicz, H., Bennett, F., Cumming, S. A., Monckton, D. G., Flower, M., & Tabrizi, S. J. (2022). I01 Msh3-targeting antisense oligonucleotides halt CAG repeat expansions in Huntington's disease IPSC-derived neurons. In: BMJ Publishing Group Ltd.

Cabanas, M., Piquemal, M., Pistono, C., Arnaud, S., Rakesh, D., Poinama, E., Guillou, J. L., Garret, M., & Cho, Y. H. (2020). Correlations Between Mutant Huntingtin Aggregates and Behavioral Changes in R6/1 Mice. *J Huntingtons Dis*, *9*(1), 33-45. https://doi.org/10.3233/jhd-190352

Cagan, R. (2009). Principles of Drosophila eye differentiation. *Curr Top Dev Biol*, *89*, 115-135. https://doi.org/10.1016/s0070-2153(09)89005-4

Cagan, R. L., & Ready, D. F. (1989). The emergence of order in the Drosophila pupal retina. *Dev Biol*, *136*(2), 346-362. https://doi.org/10.1016/0012-1606(89)90261-3

Cagniard, B., Balsam, P. D., Brunner, D., & Zhuang, X. (2006). Mice with Chronically Elevated Dopamine Exhibit Enhanced Motivation, but not Learning, for a Food Reward. *Neuropsychopharmacology*, *31*(7), 1362-1370. https://doi.org/10.1038/sj.npp.1300966

Canals, J. M., Checa, N., Marco, S., Åkerud, P., Michels, A., Pérez-Navarro, E., Tolosa, E., Arenas, E., & Alberch, J. (2001). Expression of Brain-Derived Neurotrophic Factor in Cortical Neurons Is Regulated by Striatal Target Area. *The Journal of Neuroscience*, *21*(1), 117-124. https://doi.org/10.1523/jneurosci.21-01-00117.2001

Carmichael, R. E., Wilkinson, K. A., Craig, T. J., Ashby, M. C., & Henley, J. M. (2018). MEF2A regulates mGluR-dependent AMPA receptor trafficking independently of Arc/Arg3.1. *Scientific Reports*, *8*(1), 5263. https://doi.org/10.1038/s41598-018-23440-0

Caron, N. S., Southwell, A. L., Brouwers, C. C., Cengio, L. D., Xie, Y., Black, H. F., Anderson, L. M., Ko, S., Zhu, X., van Deventer, S. J., Evers, M. M., Konstantinova, P., & Hayden, M. R. (2020). Potent and sustained huntingtin lowering via AAV5 encoding miRNA preserves striatal volume and cognitive function in a humanized mouse model of Huntington disease. *Nucleic Acids Res*, *48*(1), 36-54. https://doi.org/10.1093/nar/gkz976

Casella, C., Kelly, B., Murillo Bartolome, A., Mills-Smith, B., Parker, G. D., Von Ruhland, C., Syed, Y. A., Dion, V., Rosser, A. E., Metzler-Baddeley, C., Jones, D. K., & Lelos, M. J. (2023). Differences in white matter detected by ex vivo 9.4T MRI are associated with axonal changes in the R6/1 model of Huntington's Disease. *bioRxiv*, 2023.2010.2002.560424. https://doi.org/10.1101/2023.10.02.560424

Castells-Nobau, A., Eidhof, I., Fenckova, M., Brenman-Suttner, D. B., Scheffer-de Gooyert, J. M., Christine, S., Schellevis, R. L., van der Laan, K., Quentin, C., van Ninhuijs, L., Hofmann, F., Ejsmont, R., Fisher, S. E., Kramer, J. M., Sigrist, S. J., Simon, A. F., & Schenck, A. (2019). Conserved regulation of neurodevelopmental processes and behavior by FoxP in Drosophila. *PLOS ONE*, *14*(2), e0211652. https://doi.org/10.1371/journal.pone.0211652

Chanut, F., & Heberlein, U. (1997). Role of decapentaplegic in initiation and progression of the morphogenetic furrow in the developing Drosophila retina. *Development*, *124*(2), 559-567. https://doi.org/10.1242/dev.124.2.559

Chaudhary, R., Agarwal, V., Kaushik, A. S., & Rehman, M. (2021). Involvement of myocyte enhancer factor 2c in the pathogenesis of autism spectrum disorder. *Heliyon*, *7*(4), e06854. https://doi.org/10.1016/j.heliyon.2021.e06854

Chauhan, P., Wadhwa, K., & Singh, G. (2022). Caenorhabditis elegans as a model system to evaluate neuroprotective potential of nano formulations [Review]. *Frontiers in Nanotechnology*, *4*. https://doi.org/10.3389/fnano.2022.1018754

Chen, P., Wu, Y., Zhuang, J., Liu, X., Luo, Q., Wang, Q., Jiang, Z., He, A., Chen, S., Chen, X., Qiu, J., Li, Y., Yang, Y., Yu, K., & Zhuang, J. (2022). Gata3 Silencing Is Involved in Neuronal Differentiation and Its Abnormal Expression Impedes Neural Activity in Adult Retinal Neurocytes. *International Journal of Molecular Sciences*, *23*(5), 2495. https://www.mdpi.com/1422-0067/23/5/2495

Chen, X., Gao, B., Ponnusamy, M., Lin, Z., & Liu, J. (2017). MEF2 signaling and human diseases. *Oncotarget*, *8*(67). https://www.oncotarget.com/article/22899/text/

Cheng, Y., Zhang, S., & Shang, H. (2024). Latest advances on new promising molecular-based therapeutic approaches for Huntington's disease. *J Transl Int Med*, *12*(2), 134-147. https://doi.org/10.2478/jtim-2023-0142

Chien, W. H., Gau, S. S., Chen, C. H., Tsai, W. C., Wu, Y. Y., Chen, P. H., Shang, C. Y., & Chen, C. H. (2013). Increased gene expression of FOXP1 in patients with autism spectrum disorders. *Mol Autism*, *4*(1), 23. https://doi.org/10.1186/2040-2392-4-23

Cho, J. Y., Rumschlag, J. A., Tsvetkov, E., Proper, D. S., Lang, H., Berto, S., Assali, A., & Cowan, C. W. (2024). MEF2C Hypofunction in GABAergic Cells Alters Sociability and Prefrontal Cortex Inhibitory Synaptic Transmission in a Sex-Dependent Manner. *Biological Psychiatry Global Open Science*, *4*(2), 100289. https://doi.org/https://doi.org/10.1016/j.bpsgos.2024.100289

Chopra, V., Fox, J. H., Lieberman, G., Dorsey, K., Matson, W., Waldmeier, P., Housman, D. E., Kazantsev, A., Young, A. B., & Hersch, S. (2007). A small-molecule therapeutic lead for Huntington's disease: preclinical pharmacology and efficacy of C2-8 in the R6/2 transgenic mouse. *Proc Natl Acad Sci U S A*, *104*(42), 16685-16689. https://doi.org/10.1073/pnas.0707842104

Clifford, J. J., Drago, J., Natoli, A. L., Wong, J. Y. F., Kinsella, A., Waddington, J. L., & Vaddadi, K. S. (2002). Essential fatty acids given from conception prevent topographies of motor deficit in a transgenic model of Huntington's disease. *Neuroscience*, *109*(1), 81-88. https://doi.org/https://doi.org/10.1016/S0306-4522(01)00409-2

Cole, C. J., Mercaldo, V., Restivo, L., Yiu, A. P., Sekeres, M. J., Han, J. H., Vetere, G., Pekar, T., Ross, P. J., Neve, R. L., Frankland, P. W., & Josselyn, S. A. (2012). MEF2 negatively regulates learning-induced structural plasticity and memory formation. *Nat Neurosci*, *15*(9), 1255-1264. https://doi.org/10.1038/nn.3189

Cordeiro, L. M., Soares, M. V., da Silva, A. F., Machado, M. L., Bicca Obetine Baptista, F., da Silveira, T. L., Arantes, L. P., & Soares, F. A. A. (2022). Neuroprotective effects of rutin on ASH neurons in Caenorhabditis elegans model of Huntington's disease. *Nutritional Neuroscience*, *25*(11), 2288-2301. https://doi.org/10.1080/1028415X.2021.1956254

Cornwell, J. D., & McDermott, J. C. (2023). MEF2 in cardiac hypertrophy in response to hypertension. *Trends in Cardiovascular Medicine*, *33*(4), 204-212. https://doi.org/https://doi.org/10.1016/j.tcm.2022.01.002

Courgeon, M., & Desplan, C. (2019). Coordination of neural patterning in the Drosophila visual system. *Curr Opin Neurobiol*, *56*, 153-159. https://doi.org/10.1016/j.conb.2019.01.024

Cowin, R. M., Bui, N., Graham, D., Green, J. R., Grueninger, S., Yuva-Paylor, L. A., Syed, A. U., Weiss, A., & Paylor, R. (2011). Onset and progression of behavioral and molecular phenotypes in a novel congenic R6/2 line exhibiting intergenerational CAG repeat stability. *PLOS ONE*, *6*(12), e28409. https://doi.org/10.1371/journal.pone.0028409

Crittenden, J. R., Skoulakis, E. M. C., Goldstein, E. S., & Davis, R. L. (2018). Drosophila mef2 is essential for normal mushroom body and wing development. *Biol Open*, *7*(9). https://doi.org/10.1242/bio.035618

Currier, T. A., Pang, M. M., & Clandinin, T. R. (2023). Visual processing in the fly, from photoreceptors to behavior. *Genetics*, *224*(2). https://doi.org/10.1093/genetics/iyad064

Cutler, T., Sarkar, A., Moran, M., Steffensmeier, A., Puli, O. R., Mancini, G., Tare, M., Gogia, N., & Singh, A. (2015). Drosophila Eye Model to Study Neuroprotective Role of CREB Binding Protein (CBP) in Alzheimer's Disease. *PLOS ONE*, *10*(9), e0137691. https://doi.org/10.1371/journal.pone.0137691

DasGupta, S., Ferreira, C. H., & Miesenböck, G. (2014). FoxP influences the speed and accuracy of a perceptual decision in Drosophila. *Science*, *344*(6186), 901-904. https://doi.org/doi:10.1126/science.1252114

Datson, N. A., González-Barriga, A., Kourkouta, E., Weij, R., van de Giessen, J., Mulders, S., Kontkanen, O., Heikkinen, T., Lehtimäki, K., & van Deutekom, J. C. (2017). The expanded CAG repeat in the huntingtin gene as target for therapeutic RNA modulation throughout the HD mouse brain. *PLOS ONE*, *12*(2), e0171127. https://doi.org/10.1371/journal.pone.0171127

Deacon, R. M. (2013). Measuring the strength of mice. *J Vis Exp*(76). https://doi.org/10.3791/2610

Deacon, T. W., Pakzaban, P., & Isacson, O. (1994). The lateral ganglionic eminence is the origin of cells committed to striatal phenotypes: neural transplantation and developmental evidence. *Brain Res*, *668*(1-2), 211-219. https://doi.org/10.1016/0006-8993(94)90526-6

Desplats, P. A., Kass, K. E., Gilmartin, T., Stanwood, G. D., Woodward, E. L., Head, S. R., Sutcliffe, J. G., & Thomas, E. A. (2006). Selective deficits in the expression of striatal-enriched mRNAs in Huntington's disease [https://doi.org/10.1111/j.1471-4159.2005.03588.x]. *Journal of Neurochemistry*, *96*(3), 743-757. https://doi.org/https://doi.org/10.1111/j.1471-4159.2005.03588.x

Devan, B. D., Hong, N. S., & McDonald, R. J. (2011). Parallel associative processing in the dorsal striatum: Segregation of stimulus–response and cognitive control subregions. *Neurobiology of Learning and Memory*, *96*(2), 95-120. https://doi.org/https://doi.org/10.1016/j.nlm.2011.06.002

Dhapola, R., Kumari, S., Sharma, P., & HariKrishnaReddy, D. (2023). Insight into the emerging and common experimental in-vivo models of Alzheimer's disease. *Laboratory Animal Research*, *39*(1), 33. https://doi.org/10.1186/s42826-023-00184-1

Di Giorgio, E., Franforte, E., Cefalù, S., Rossi, S., Dei Tos, A. P., Brenca, M., Polano, M., Maestro, R., Paluvai, H., Picco, R., & Brancolini, C. (2017). The co-existence of transcriptional activator and transcriptional repressor MEF2 complexes influences tumor aggressiveness. *PLOS Genetics*, *13*(4), e1006752. https://doi.org/10.1371/journal.pgen.1006752

Dickey, A. S., Pineda, V. V., Tsunemi, T., Liu, P. P., Miranda, H. C., Gilmore-Hall, S. K., Lomas, N., Sampat, K. R., Buttgereit, A., Torres, M. J., Flores, A. L., Arreola, M., Arbez, N., Akimov, S. S., Gaasterland, T., Lazarowski, E. R., Ross, C. A., Yeo, G. W., Sopher, B. L., . . . La Spada, A. R. (2016). PPAR-δ is repressed in Huntington's disease, is required for normal neuronal function and can be targeted therapeutically. *Nat Med*, *22*(1), 37-45. https://doi.org/10.1038/nm.4003

Dietzl, G., Chen, D., Schnorrer, F., Su, K. C., Barinova, Y., Fellner, M., Gasser, B., Kinsey, K., Oppel, S., Scheiblauer, S., Couto, A., Marra, V., Keleman, K., & Dickson, B. J. (2007). A genome-wide transgenic RNAi library for conditional gene inactivation in Drosophila. *Nature*, *448*(7150), 151-156. https://doi.org/10.1038/nature05954

Dunah, A. W., Jeong, H., Griffin, A., Kim, Y.-M., Standaert, D. G., Hersch, S. M., Mouradian, M. M., Young, A. B., Tanese, N., & Krainc, D. (2002). Sp1 and TAFII130 Transcriptional Activity Disrupted in Early Huntington's Disease. *Science*, *296*(5576), 2238-2243. https://doi.org/doi:10.1126/science.1072613

Ehrlich, M. E. (2012). Huntington's disease and the striatal medium spiny neuron: cell-autonomous and non-cell-autonomous mechanisms of disease. *Neurotherapeutics*, *9*(2), 270-284. https://doi.org/10.1007/s13311-012-0112-2

Escobedo, S. E., Shah, A., Easton, A. N., Hall, H., & Weake, V. M. (2021). Characterizing a gene expression toolkit for eye- and photoreceptor-specific expression in Drosophila. *Fly (Austin)*, *15*(1), 73-88. https://doi.org/10.1080/19336934.2021.1915683

Estevez-Fraga, C., Tabrizi, S. J., & Wild, E. J. (2024). Huntington's Disease Clinical Trials Corner: March 2024. *J Huntingtons Dis*, *13*(1), 1-14. https://doi.org/10.3233/jhd-240017

Estrella, N. L., Desjardins, C. A., Nocco, S. E., Clark, A. L., Maksimenko, Y., & Naya, F. J. (2015). MEF2 transcription factors regulate distinct gene programs in mammalian skeletal muscle differentiation. *J Biol Chem*, *290*(2), 1256-1268. https://doi.org/10.1074/jbc.M114.589838

Estruch, S. B., Graham, S. A., Quevedo, M., Vino, A., Dekkers, D. H. W., Deriziotis, P., Sollis, E., Demmers, J., Poot, R. A., & Fisher, S. E. (2018). Proteomic analysis of FOXP proteins reveals interactions between cortical transcription factors associated with neurodevelopmental disorders. *Human Molecular Genetics*, *27*(7), 1212-1227. https://doi.org/10.1093/hmg/ddy035

Evers, M. M., Miniarikova, J., Juhas, S., Vallès, A., Bohuslavova, B., Juhasova, J., Skalnikova, H. K., Vodicka, P., Valekova, I., Brouwers, C., Blits, B., Lubelski, J., Kovarova, H., Ellederova, Z., van Deventer, S. J., Petry, H., Motlik, J., & Konstantinova, P. (2018). AAV5-miHTT Gene Therapy Demonstrates Broad Distribution and Strong Human Mutant Huntingtin Lowering in a Huntington's Disease Minipig Model. *Mol Ther*, *26*(9), 2163-2177. https://doi.org/10.1016/j.ymthe.2018.06.021

Faber, P. W., Alter, J. R., MacDonald, M. E., & Hart, A. C. (1999). Polyglutamine-mediated dysfunction and apoptotic death of a Caenorhabditis elegans sensory neuron. *Proc Natl Acad Sci U S A*, *96*(1), 179-184. https://doi.org/10.1073/pnas.96.1.179

Farshim, P. P., & Bates, G. P. (2018). Mouse Models of Huntington's Disease. In S. V. Precious, A. E. Rosser, & S. B. Dunnett (Eds.), *Huntington's Disease* (pp. 97-120). Springer New York. https://doi.org/10.1007/978-1-4939-7825-0_6

Feng, X., Ippolito, G. C., Tian, L., Wiehagen, K., Oh, S., Sambandam, A., Willen, J., Bunte, R. M., Maika, S. D., Harriss, J. V., Caton, A. J., Bhandoola, A., Tucker, P. W., & Hu, H. (2010). Foxp1 is an essential transcriptional regulator for the generation of quiescent naive T cells during thymocyte development. *Blood*, *115*(3), 510-518. https://doi.org/10.1182/blood-2009-07-232694

Ferland, R. J., Cherry, T. J., Preware, P. O., Morrisey, E. E., & Walsh, C. A. (2003). Characterization of Foxp2 and Foxp1 mRNA and protein in the developing and mature brain. *Journal of Comparative Neurology*, *460*(2), 266-279. https://doi.org/https://doi.org/10.1002/cne.10654

Fernández-Moreno, M. A., Farr, C. L., Kaguni, L. S., & Garesse, R. (2007). Drosophila melanogaster as a model system to study mitochondrial biology. *Methods Mol Biol*, *372*, 33-49. https://doi.org/10.1007/978-1-59745-365-3_3

Ferrer, I., Goutan, E., Marín, C., Rey, M. J., & Ribalta, T. (2000). Brain-derived neurotrophic factor in Huntington disease. *Brain Res*, *866*(1-2), 257-261. https://doi.org/10.1016/s0006-8993(00)02237-x

Fields, S., & Song, O. (1989). A novel genetic system to detect protein-protein interactions. *Nature*, *340*(6230), 245-246. https://doi.org/10.1038/340245a0

Filomena, M. C., & Bang, M.-L. (2018). In the heart of the MEF2 transcription network: novel downstream effectors as potential targets for the treatment of cardiovascular disease. *Cardiovascular Research*, *114*(11), 1425-1427. https://doi.org/10.1093/cvr/cvy123

Flavell, S. W., Cowan, C. W., Kim, T.-K., Greer, P. L., Lin, Y., Paradis, S., Griffith, E. C., Hu, L. S., Chen, C., & Greenberg, M. E. (2006). Activity-Dependent Regulation of MEF2 Transcription Factors Suppresses Excitatory Synapse Number. *Science*, *311*(5763), 1008-1012. https://doi.org/doi:10.1126/science.1122511

Fleming, S. M., & Chesselet, M.-F. (2005). CHAPTER B6 - Phenotypical Characterization of Genetic Mouse Models of Parkinson Disease. In M. LeDoux (Ed.), *Animal Models of Movement Disorders* (pp. 183-192). Academic Press. https://doi.org/https://doi.org/10.1016/B978-012088382-0/50015-3

Fogarty, M., Richardson, W. D., & Kessaris, N. (2005). A subset of oligodendrocytes generated from radial glia in the dorsal spinal cord. *Development*, *132*(8), 1951-1959. https://doi.org/10.1242/dev.01777

Formstecher, E., Aresta, S., Collura, V., Hamburger, A., Meil, A., Trehin, A., Reverdy, C., Betin, V., Maire, S., Brun, C., Jacq, B., Arpin, M., Bellaiche, Y., Bellusci, S., Benaroch, P., Bornens, M., Chanet, R., Chavrier, P., Delattre, O., . . . Daviet, L. (2005). Protein interaction mapping: a Drosophila case study. *Genome Res*, *15*(3), 376-384. https://doi.org/10.1101/gr.2659105

Gabut, M., Samavarchi-Tehrani, P., Wang, X., Slobodeniuc, V., O'Hanlon, D., Sung, H.-K., Alvarez, M., Talukder, S., Pan, Q., Mazzoni, Esteban O., Nedelec, S., Wichterle, H., Woltjen, K., Hughes, Timothy R., Zandstra, P. W., Nagy, A., Wrana, Jeffrey L., & Blencowe, Benjamin J. (2011). An Alternative Splicing Switch Regulates Embryonic

Stem Cell Pluripotency and Reprogramming. *Cell*, *147*(1), 132-146. https://doi.org/https://doi.org/10.1016/j.cell.2011.08.023

García-Lara, L., Morales-Martínez A, Angeles-López QD, Pedraza-Espitia H, Pérez-Neri I, Rodríguez-Balderas CA, Pérez-Severiano F. (2018). Establishment and maintenance of an R6/1 transgenic mouse colony and validation of its progressive neurological phenotype to study Huntington's disease. *Vet Mex*, *5*(1), 1-12.

Gatto, R. G., Weissmann, C., Amin, M., Angeles-López, Q. D., García-Lara, L., Castellanos, L. C. S., Deyoung, D., Segovia, J., Mareci, T. H., Uchitel, O. D., & Magin, R. L. (2021). Evaluation of early microstructural changes in the R6/1 mouse model of Huntington's disease by ultra-high field diffusion MR imaging. *Neurobiology of Aging*, *102*, 32-49. https://doi.org/https://doi.org/10.1016/j.neurobiolaging.2021.02.006

Gauthier, L. R., Charrin, B. C., Borrell-Pagès, M., Dompierre, J. P., Rangone, H., Cordelières, F. P., De Mey, J., MacDonald, M. E., Leßmann, V., Humbert, S., & Saudou, F. (2004). Huntingtin Controls Neurotrophic Support and Survival of Neurons by Enhancing BDNF Vesicular Transport along Microtubules. *Cell*, *118*(1), 127-138. https://doi.org/https://doi.org/10.1016/j.cell.2004.06.018

Ge, Q., Ilves, H., Dallas, A., Kumar, P., Shorenstein, J., Kazakov, S. A., & Johnston, B. H. (2010). Minimal-length short hairpin RNAs: the relationship of structure and RNAi activity. *Rna*, *16*(1), 106-117. https://doi.org/10.1261/rna.1894510

Ghosh, R., Wood-Kaczmar, A., Dobson, L., Smith, E. J., Sirinathsinghji, E. C., Kriston-Vizi, J., Hargreaves, I. P., Heaton, R., Herrmann, F., Abramov, A. Y., Lam, A. J., Heales, S. J., Ketteler, R., Bates, G. P., Andre, R., & Tabrizi, S. J. (2020). Expression of mutant exon 1 huntingtin fragments in human neural stem cells and neurons causes inclusion formation and mitochondrial dysfunction. *Faseb j*, *34*(6), 8139-8154. https://doi.org/10.1096/fj.201902277RR

Gossett, L. A., Kelvin, D. J., Sternberg, E. A., & Olson, E. N. (1989). A new myocyte-specific enhancer-binding factor that recognizes a conserved element associated with multiple muscle-specific genes. *Mol Cell Biol*, *9*(11), 5022-5033. https://doi.org/10.1128/mcb.9.11.5022-5033.1989

Gourfinkel-An, I., Parain, K., Hartmann, A., Mangiarini, L., Brice, A., Bates, G., & Hirsch, E. C. (2003). Changes in GAD67 mRNA expression evidenced by in situ hybridization in the brain of R6/2 transgenic mice. *J Neurochem*, *86*(6), 1369-1378. https://doi.org/10.1046/j.1471-4159.2003.01916.x

Gray, M., Shirasaki, D. I., Cepeda, C., André, V. M., Wilburn, B., Lu, X. H., Tao, J., Yamazaki, I., Li, S. H., Sun, Y. E., Li, X. J., Levine, M. S., & Yang, X. W. (2008). Full-length human mutant huntingtin with a stable polyglutamine repeat can elicit progressive and selective neuropathogenesis in BACHD mice. *J Neurosci*, *28*(24), 6182-6195. https://doi.org/10.1523/jneurosci.0857-08.2008

Guo, Q., Wang, B., Wang, X., Smith, W. W., Zhu, Y., & Liu, Z. (2021). Activation of Nrf2 in Astrocytes Suppressed PD-Like Phenotypes via Antioxidant and Autophagy Pathways in Rat and Drosophila Models. *Cells*, *10*(8). https://doi.org/10.3390/cells10081850

Gusella, J. F., MacDonald, M. E., & Lee, J.-M. (2014). Genetic modifiers of Huntington's disease. *Movement Disorders*, *29*(11), 1359-1365. https://doi.org/https://doi.org/10.1002/mds.26001

Gutekunst, C. A., Li, S. H., Yi, H., Mulroy, J. S., Kuemmerle, S., Jones, R., Rye, D., Ferrante, R. J., Hersch, S. M., & Li, X. J. (1999). Nuclear and neuropil aggregates in Huntington's

disease: relationship to neuropathology. *J Neurosci*, *19*(7), 2522-2534. https://doi.org/10.1523/jneurosci.19-07-02522.1999

Ha, N. M., Tran, S. H., Shim, Y.-H., & Kang, K. (2022). Caenorhabditis elegans as a powerful tool in natural product bioactivity research. *Applied Biological Chemistry*, *65*(1), 18. https://doi.org/10.1186/s13765-022-00685-y

Hafer, N., & Schedl, P. (2006). Dissection of larval CNS in Drosophila melanogaster. *J Vis Exp*(1), 85. https://doi.org/10.3791/85

Hakim, N. H. A., Kounishi, T., Alam, A. H. M. K., Tsukahara, T., & Suzuki, H. (2010). Alternative splicing of Mef2c promoted by Fox-1 during neural differentiation in P19 cells. *Genes to Cells*, *15*(3), 255-267. https://doi.org/https://doi.org/10.1111/j.1365-2443.2009.01378.x

Hall, H., Medina, P., Cooper, D. A., Escobedo, S. E., Rounds, J., Brennan, K. J., Vincent, C., Miura, P., Doerge, R., & Weake, V. M. (2017). Transcriptome profiling of aging Drosophila photoreceptors reveals gene expression trends that correlate with visual senescence. *BMC Genomics*, *18*(1), 894. https://doi.org/10.1186/s12864-017-4304-3

Hamm, R. J., Pike, B. R., O'Dell, D. M., Lyeth, B. G., & Jenkins, L. W. (1994). The rotarod test: an evaluation of its effectiveness in assessing motor deficits following traumatic brain injury. *J Neurotrauma*, *11*(2), 187-196. https://doi.org/10.1089/neu.1994.11.187

Han, L., Chen, M., Wang, Y., Wu, H., Quan, Y., Bai, T., Li, K., Duan, G., Gao, Y., Hu, Z., Xia, K., & Guo, H. (2019). Pathogenic missense mutation pattern of forkhead box genes in neurodevelopmental disorders. *Mol Genet Genomic Med*, *7*(7), e00789. https://doi.org/10.1002/mgg3.789

Hansson, O., Petersén, A., Leist, M., Nicotera, P., Castilho, R. F., & Brundin, P. (1999). Transgenic mice expressing a Huntington's disease mutation are resistant to quinolinic acid-induced striatal excitotoxicity. *Proc Natl Acad Sci U S A*, *96*(15), 8727-8732. https://doi.org/10.1073/pnas.96.15.8727

Harper, S. Q., Staber, P. D., He, X., Eliason, S. L., Martins, I. H., Mao, Q., Yang, L., Kotin, R. M., Paulson, H. L., & Davidson, B. L. (2005). RNA interference improves motor and neuropathological abnormalities in a Huntington's disease mouse model. *Proc Natl Acad Sci U S A*, *102*(16), 5820-5825. https://doi.org/10.1073/pnas.0501507102

Harrington, A. J., Raissi, A., Rajkovich, K., Berto, S., Kumar, J., Molinaro, G., Raduazzo, J., Guo, Y., Loerwald, K., Konopka, G., Huber, K. M., & Cowan, C. W. (2016). MEF2C regulates cortical inhibitory and excitatory synapses and behaviors relevant to neurodevelopmental disorders. *eLife*, *5*. https://doi.org/10.7554/eLife.20059

Hassan, A., Scott, H., & Hill, M. (2021). Regulation of microglial transcription factor MEF2C by Alzheimer's disease-relevant stimuli. *Alzheimer's & Dementia*, *17*(S3), e057448. https://doi.org/https://doi.org/10.1002/alz.057448

Heng, M. Y., Tallaksen-Greene, S. J., Detloff, P. J., & Albin, R. L. (2007). Longitudinal evaluation of the Hdh(CAG)150 knock-in murine model of Huntington's disease. *J Neurosci*, *27*(34), 8989-8998. https://doi.org/10.1523/jneurosci.1830-07.2007

Hickman, D., Johnson, J., Vemulapalli, T. H., Crisler, J. R., & Shepherd, R. (2016). Commonly Used Animal Models. *Principles of Animal Research for Graduate and Undergraduate Students*, 117 - 175.

Hodges, A., Hughes, G., Brooks, S., Elliston, L., Holmans, P., Dunnett, S. B., & Jones, L. (2008). Brain gene expression correlates with changes in behavior in the R6/1 mouse model of Huntington's disease [https://doi.org/10.1111/j.1601-183X.2007.00350.x]. *Genes,*

Brain and Behavior, *7*(3), 288-299. https://doi.org/https://doi.org/10.1111/j.1601-183X.2007.00350.x

Hodges, A., Strand, A. D., Aragaki, A. K., Kuhn, A., Sengstag, T., Hughes, G., Elliston, L. A., Hartog, C., Goldstein, D. R., Thu, D., Hollingsworth, Z. R., Collin, F., Synek, B., Holmans, P. A., Young, A. B., Wexler, N. S., Delorenzi, M., Kooperberg, C., Augood, S. J., . . . Luthi-Carter, R. (2006). Regional and cellular gene expression changes in human Huntington's disease brain. *Hum Mol Genet*, *15*(6), 965-977. https://doi.org/10.1093/hmg/ddl013

Hölter, S. M., Stromberg, M., Kovalenko, M., Garrett, L., Glasl, L., Lopez, E., Guide, J., Götz, A., Hans, W., Becker, L., Rathkolb, B., Rozman, J., Schrewed, A., Klingenspor, M., Klopstock, T., Schulz, H., Wolf, E., Wursta, W., Gillis, T., . . . Wheeler, V. C. (2013). A broad phenotypic screen identifies novel phenotypes driven by a single mutant allele in Huntington's disease CAG knock-in mice. *PLOS ONE*, *8*(11), e80923. https://doi.org/10.1371/journal.pone.0080923

Hsiung, F., & Moses, K. (2002). Retinal development in Drosophila: specifying the first neuron. *Human Molecular Genetics*, *11*(10), 1207-1214. https://doi.org/10.1093/hmg/11.10.1207

Hu, H., Wang, B., Borde, M., Nardone, J., Maika, S., Allred, L., Tucker, P. W., & Rao, A. (2006). Foxp1 is an essential transcriptional regulator of B cell development. *Nat Immunol*, *7*(8), 819-826. https://doi.org/10.1038/ni1358

Hubbert, S. (2023). *Mef2 in muscle: A CRISPR-based approach to investigate the regulation of a master transcription factor.* Cardiff University. https://orca.cardiff.ac.uk/id/eprint/171253/

Huelsmeier, J., Walker, E., Bakthavachalu, B., & Ramaswami, M. (2021). A C-terminal ataxin-2 disordered region promotes Huntingtin protein aggregation and neurodegeneration in Drosophila models of Huntington's disease. *G3 Genes|Genomes|Genetics*, *11*(12). https://doi.org/10.1093/g3journal/jkab355

Infantino, V., Convertini, P., Menga, A., & Iacobazzi, V. (2013). MEF2C exon α: Role in gene activation and differentiation. *Gene*, *531*(2), 355-362. https://doi.org/https://doi.org/10.1016/j.gene.2013.08.044

Jackson, G. R., Salecker, I., Dong, X., Yao, X., Arnheim, N., Faber, P. W., MacDonald, M. E., & Zipursky, S. L. (1998). Polyglutamine-expanded human huntingtin transgenes induce degeneration of Drosophila photoreceptor neurons. *Neuron*, *21*(3), 633-642. https://doi.org/10.1016/s0896-6273(00)80573-5

Jacobsen, J. C., Bawden, C. S., Rudiger, S. R., McLaughlan, C. J., Reid, S. J., Waldvogel, H. J., MacDonald, M. E., Gusella, J. F., Walker, S. K., Kelly, J. M., Webb, G. C., Faull, R. L., Rees, M. I., & Snell, R. G. (2010). An ovine transgenic Huntington's disease model. *Hum Mol Genet*, *19*(10), 1873-1882. https://doi.org/10.1093/hmg/ddq063

Jamwal, S., & Kumar, P. (2019). Insight Into the Emerging Role of Striatal Neurotransmitters in the Pathophysiology of Parkinson's Disease and Huntington's Disease: A Review. *Curr Neuropharmacol*, *17*(2), 165-175. https://doi.org/10.2174/1570159x16666180302115032

Janson, C. G., Chen, Y., Li, Y., & Leifer, D. (2001). Functional regulatory regions of human transcription factor MEF2C. *Molecular Brain Research*, *97*(1), 70-82. https://doi.org/https://doi.org/10.1016/S0169-328X(01)00187-5

Jennings, B. H. (2011). Drosophila – a versatile model in biology & medicine. *Materials Today*, *14*(5), 190-195. https://doi.org/https://doi.org/10.1016/S1369-7021(11)70113-4

Jimenez-Sanchez, M., Licitra, F., Underwood, B. R., & Rubinsztein, D. C. (2017). Huntington's Disease: Mechanisms of Pathogenesis and Therapeutic Strategies. *Cold Spring Harb Perspect Med*, *7*(7). https://doi.org/10.1101/cshperspect.a024240

Johnson, E. B., & Gregory, S. (2019). Chapter 6 - Huntington's disease: Brain imaging in Huntington's disease. In J. T. Becker & A. D. Cohen (Eds.), *Progress in Molecular Biology and Translational Science* (Vol. 165, pp. 321-369). Academic Press. https://doi.org/https://doi.org/10.1016/bs.pmbts.2019.04.004

Johnson, T. B., Mechels, K., Anderson, R. H., Cain, J. T., Sturdevant, D. A., Braddock, S., Pinz, H., Wilson, M. A., Landsverk, M., Roux, K. J., & Weimer, J. M. (2018). Characterization of a recurrent missense mutation in the forkhead DNA-binding domain of FOXP1. *Scientific Reports*, *8*(1), 16161. https://doi.org/10.1038/s41598-018-34437-0

Jurcau, A. (2022). Molecular Pathophysiological Mechanisms in Huntington's Disease. *Biomedicines*, *10*(6). https://doi.org/10.3390/biomedicines10061432

Kacher, R., Lejeune, F. X., Noël, S., Cazeneuve, C., Brice, A., Humbert, S., & Durr, A. (2021). Propensity for somatic expansion increases over the course of life in Huntington disease. *eLife*, *10*. https://doi.org/10.7554/eLife.64674

Kaltenbach, L. S., Romero, E., Becklin, R. R., Chettier, R., Bell, R., Phansalkar, A., Strand, A., Torcassi, C., Savage, J., Hurlburt, A., Cha, G.-H., Ukani, L., Chepanoske, C. L., Zhen, Y., Sahasrabudhe, S., Olson, J., Kurschner, C., Ellerby, L. M., Peltier, J. M., . . . Hughes, R. E. (2007). Huntingtin Interacting Proteins Are Genetic Modifiers of Neurodegeneration. *PLOS Genetics*, *3*(5), e82. https://doi.org/10.1371/journal.pgen.0030082

Kamath, S. P., & Chen, A. I. (2019). Myocyte Enhancer Factor 2c Regulates Dendritic Complexity and Connectivity of Cerebellar Purkinje Cells. *Mol Neurobiol*, *56*(6), 4102-4119. https://doi.org/10.1007/s12035-018-1363-7

Katz, B., & Minke, B. (2009). Drosophila photoreceptors and signaling mechanisms. *Front Cell Neurosci*, *3*, 2. https://doi.org/10.3389/neuro.03.002.2009

Kazantsev, A., Walker, H. A., Slepko, N., Bear, J. E., Preisinger, E., Steffan, J. S., Zhu, Y. Z., Gertler, F. B., Housman, D. E., Marsh, J. L., & Thompson, L. M. (2002). A bivalent Huntingtin binding peptide suppresses polyglutamine aggregation and pathogenesis in Drosophila. *Nat Genet*, *30*(4), 367-376. https://doi.org/10.1038/ng864

Kazemi-Esfarjani, P., & Benzer, S. (2000). Genetic suppression of polyglutamine toxicity in Drosophila. *Science*, *287*(5459), 1837-1840. https://doi.org/10.1126/science.287.5459.1837

Kelemen, O., Convertini, P., Zhang, Z., Wen, Y., Shen, M., Falaleeva, M., & Stamm, S. (2013). Function of alternative splicing. *Gene*, *514*(1), 1-30. https://doi.org/https://doi.org/10.1016/j.gene.2012.07.083

Kessaris, N., Fogarty, M., Iannarelli, P., Grist, M., Wegner, M., & Richardson, W. D. (2006). Competing waves of oligodendrocytes in the forebrain and postnatal elimination of an embryonic lineage. *Nat Neurosci*, *9*(2), 173-179. https://doi.org/10.1038/nn1620

Khandelwal, N., Kulkarni, A., Ahmed, N. I., Harper, M., Konopka, G., & Gibson, J. R. (2024). FOXP1 regulates the development of excitatory synaptic inputs onto striatal neurons and induces phenotypic reversal with reinstatement. *Sci Adv*, *10*(18), eadm7039. https://doi.org/10.1126/sciadv.adm7039

Kim, J.-H., Hwang, J., Jung, J. H., Lee, H.-J., Lee, D. Y., & Kim, S.-H. (2019). Molecular networks of FOXP family: dual biologic functions, interplay with other molecules and clinical implications in cancer progression. *Molecular Cancer*, *18*(1), 180. https://doi.org/10.1186/s12943-019-1110-3

Kind, E., Longden, K. D., Nern, A., Zhao, A., Sancer, G., Flynn, M. A., Laughland, C. W., Gezahegn, B., Ludwig, H. D., Thomson, A. G., Obrusnik, T., Alarcón, P. G., Dionne, H., Bock, D. D., Rubin, G. M., Reiser, M. B., & Wernet, M. F. (2021). Synaptic targets of photoreceptors specialized to detect color and skylight polarization in Drosophila. *eLife*, *10*. https://doi.org/10.7554/eLife.71858

Klapstein, G. J., Fisher, R. S., Zanjani, H., Cepeda, C., Jokel, E. S., Chesselet, M. F., & Levine, M. S. (2001). Electrophysiological and morphological changes in striatal spiny neurons in R6/2 Huntington's disease transgenic mice. *J Neurophysiol*, *86*(6), 2667-2677. https://doi.org/10.1152/jn.2001.86.6.2667

Koch, E. T., Cheng, J., Ramandi, D., Sepers, M. D., Hsu, A., Fong, T., Murphy, T. H., Yttri, E., & Raymond, L. A. (2024). Deep behavioural phenotyping of the Q175 Huntington disease mouse model: effects of age, sex, and weight. *BMC Biology*, *22*(1), 121. https://doi.org/10.1186/s12915-024-01919-9

Kogenaru, V., Isalan, M., & Kogenaru, M. (2024). A drug stabilizable GAL80ds for conditional control of gene expression via GAL4-UAS and CRISPR-Cas9 systems in Drosophila. *Scientific Reports*, *14*(1), 5893. https://doi.org/10.1038/s41598-024-56343-4

Kordasiewicz, H. B., Stanek, L. M., Wancewicz, E. V., Mazur, C., McAlonis, M. M., Pytel, K. A., Artates, J. W., Weiss, A., Cheng, S. H., Shihabuddin, L. S., Hung, G., Bennett, C. F., & Cleveland, D. W. (2012). Sustained therapeutic reversal of Huntington's disease by transient repression of huntingtin synthesis. *Neuron*, *74*(6), 1031-1044. https://doi.org/10.1016/j.neuron.2012.05.009

Kovalenko, M., Milnerwood, A., Giordano, J., St Claire, J., Guide, J. R., Stromberg, M., Gillis, T., Sapp, E., DiFiglia, M., MacDonald, M. E., Carroll, J. B., Lee, J. M., Tappan, S., Raymond, L., & Wheeler, V. C. (2018). HttQ111/+ Huntington's Disease Knock-in Mice Exhibit Brain Region-Specific Morphological Changes and Synaptic Dysfunction. *J Huntingtons Dis*, *7*(1), 17-33. https://doi.org/10.3233/jhd-170282

Krench, M., & Littleton, J. T. (2013). Modeling Huntington disease in Drosophila: Insights into axonal transport defects and modifiers of toxicity. *Fly (Austin)*, *7*(4), 229-236. https://doi.org/10.4161/fly.26279

Kuhn, A., Goldstein, D. R., Hodges, A., Strand, A. D., Sengstag, T., Kooperberg, C., Becanovic, K., Pouladi, M. A., Sathasivam, K., Cha, J.-H. J., Hannan, A. J., Hayden, M. R., Leavitt, B. R., Dunnett, S. B., Ferrante, R. J., Albin, R., Shelbourne, P., Delorenzi, M., Augood, S. J., . . . Luthi-Carter, R. (2007). Mutant huntingtin's effects on striatal gene expression in mice recapitulate changes observed in human Huntington's disease brain and do not differ with mutant huntingtin length or wild-type huntingtin dosage. *Human Molecular Genetics*, *16*(15), 1845-1861. https://doi.org/10.1093/hmg/ddm133

Kumar, J. P., & Moses, K. (2001). EGF receptor and Notch signaling act upstream of Eyeless/Pax6 to control eye specification. *Cell*, *104*(5), 687-697. https://doi.org/10.1016/s0092-8674(01)00265-3

Lambert, J. C., Ibrahim-Verbaas, C. A., Harold, D., Naj, A. C., Sims, R., Bellenguez, C., DeStafano, A. L., Bis, J. C., Beecham, G. W., Grenier-Boley, B., Russo, G., Thorton-Wells, T. A., Jones, N., Smith, A. V., Chouraki, V., Thomas, C., Ikram, M. A., Zelenika, D., Vardarajan, B. N., . . . Amouyel, P. (2013). Meta-analysis of 74,046 individuals identifies 11 new susceptibility loci for Alzheimer's disease. *Nat Genet*, *45*(12), 1452-1458. https://doi.org/10.1038/ng.2802

Lambeth, L. S., & Smith, C. A. (2013). Short Hairpin RNA-Mediated Gene Silencing. In D. J. Taxman (Ed.), *siRNA Design: Methods and Protocols* (pp. 205-232). Humana Press. https://doi.org/10.1007/978-1-62703-119-6_12

Landles, C., Sathasivam, K., Weiss, A., Woodman, B., Moffitt, H., Finkbeiner, S., Sun, B., Gafni, J., Ellerby, L. M., Trottier, Y., Richards, W. G., Osmand, A., Paganetti, P., & Bates, G. P. (2010). Proteolysis of mutant huntingtin produces an exon 1 fragment that accumulates as an aggregated protein in neuronal nuclei in Huntington disease. *J Biol Chem*, *285*(12), 8808-8823. https://doi.org/10.1074/jbc.M109.075028

Langfelder, P., Cantle, J. P., Chatzopoulou, D., Wang, N., Gao, F., Al-Ramahi, I., Lu, X. H., Ramos, E. M., El-Zein, K., Zhao, Y., Deverasetty, S., Tebbe, A., Schaab, C., Lavery, D. J., Howland, D., Kwak, S., Botas, J., Aaronson, J. S., Rosinski, J., . . . Yang, X. W. (2016). Integrated genomics and proteomics define huntingtin CAG length-dependent networks in mice. *Nat Neurosci*, *19*(4), 623-633. https://doi.org/10.1038/nn.4256

Lawton, K. J., Wassmer, T. L., & Deitcher, D. L. (2014). Conserved role of Drosophila melanogaster FoxP in motor coordination and courtship song. *Behavioural Brain Research*, *268*, 213-221. https://doi.org/https://doi.org/10.1016/j.bbr.2014.04.009

Le Cann, K., Foerster, A., Rösseler, C., Erickson, A., Hautvast, P., Giesselmann, S., Pensold, D., Kurth, I., Rothermel, M., Mattis, V. B., Zimmer-Bensch, G., von Hörsten, S., Denecke, B., Clarner, T., Meents, J., & Lampert, A. (2021). The difficulty to model Huntington's disease in vitro using striatal medium spiny neurons differentiated from human induced pluripotent stem cells. *Sci Rep*, *11*(1), 6934. https://doi.org/10.1038/s41598-021-85656-x

Le Meur, N., Holder-Espinasse, M., Jaillard, S., Goldenberg, A., Joriot, S., Amati-Bonneau, P., Guichet, A., Barth, M., Charollais, A., Journel, H., Auvin, S., Boucher, C., Kerckaert, J. P., David, V., Manouvrier-Hanu, S., Saugier-Veber, P., Frébourg, T., Dubourg, C., Andrieux, J., & Bonneau, D. (2010). MEF2C haploinsufficiency caused by either microdeletion of the 5q14.3 region or mutation is responsible for severe mental retardation with stereotypic movements, epilepsy and/or cerebral malformations. *J Med Genet*, *47*(1), 22-29. https://doi.org/10.1136/jmg.2009.069732

Lee, A. L., Ung, H. M., Sands, L. P., & Kikis, E. A. (2017). A new Caenorhabditis elegans model of human huntingtin 513 aggregation and toxicity in body wall muscles. *PLOS ONE*, *12*(3), e0173644. https://doi.org/10.1371/journal.pone.0173644

Lee, J.-M., Ramos, E. M., Lee, J.-H., Gillis, T., Mysore, J. S., Hayden, M. R., Warby, S. C., Morrison, P., Nance, M., Ross, C. A., Margolis, R. L., Squitieri, F., Orobello, S., Di Donato, S., Gomez-Tortosa, E., Ayuso, C., Suchowersky, O., Trent, R. J. A., McCusker, E., . . . Zauber, E. (2012). CAG repeat expansion in Huntington disease determines age at onset in a fully dominant fashion. *Neurology*, *78*(10), 690-695. https://doi.org/doi:10.1212/WNL.0b013e318249f683

Leifer, D., Golden, J., & Kowall, N. W. (1994a). Myocyte-specific enhancer binding factor 2C expression in human brain development. *Neuroscience*, *63*(4), 1067-1079. https://doi.org/10.1016/0306-4522(94)90573-8

Leifer, D., Krainc, D., Yu, Y. T., McDermott, J., Breitbart, R. E., Heng, J., Neve, R. L., Kosofsky, B., Nadal-Ginard, B., & Lipton, S. A. (1993). MEF2C, a MADS/MEF2-family transcription factor expressed in a laminar distribution in cerebral cortex. *Proc Natl Acad Sci U S A*, *90*(4), 1546-1550. https://doi.org/10.1073/pnas.90.4.1546

Lelos, M. J., Roberton, V. H., Vinh, N. N., Harrison, C., Eriksen, P., Torres, E. M., Clinch, S. P., Rosser, A. E., & Dunnett, S. B. (2016). Direct Comparison of Rat- and Human-Derived

Ganglionic Eminence Tissue Grafts on Motor Function. *Cell Transplant*, *25*(4), 665-675. https://doi.org/10.3727/096368915x690297

Lentjes, M. H., Niessen, H. E., Akiyama, Y., de Bruïne, A. P., Melotte, V., & van Engeland, M. (2016). The emerging role of GATA transcription factors in development and disease. *Expert Rev Mol Med*, *18*, e3. https://doi.org/10.1017/erm.2016.2

Lewis, E. A., & Smith, G. A. (2016). Using Drosophila models of Huntington's disease as a translatable tool. *Journal of Neuroscience Methods*, *265*, 89-98. https://doi.org/https://doi.org/10.1016/j.jneumeth.2015.07.026

Li, H., Janssens, J., De Waegeneer, M., Kolluru, S. S., Davie, K., Gardeux, V., Saelens, W., David, F. P. A., Brbić, M., Spanier, K., Leskovec, J., McLaughlin, C. N., Xie, Q., Jones, R. C., Brueckner, K., Shim, J., Tattikota, S. G., Schnorrer, F., Rust, K., . . . Zinzen, R. P. (2022). Fly Cell Atlas: A single-nucleus transcriptomic atlas of the adult fruit fly. *Science*, *375*(6584), eabk2432. https://doi.org/10.1126/science.abk2432

Li, H., Radford, J. C., Ragusa, M. J., Shea, K. L., McKercher, S. R., Zaremba, J. D., Soussou, W., Nie, Z., Kang, Y. J., Nakanishi, N., Okamoto, S., Roberts, A. J., Schwarz, J. J., & Lipton, S. A. (2008). Transcription factor MEF2C influences neural stem/progenitor cell differentiation and maturation in vivo. *Proc Natl Acad Sci U S A*, *105*(27), 9397-9402. https://doi.org/10.1073/pnas.0802876105

Li, J. Y., Popovic, N., & Brundin, P. (2005). The use of the R6 transgenic mouse models of Huntington's disease in attempts to develop novel therapeutic strategies. *NeuroRx*, *2*(3), 447-464. https://doi.org/10.1602/neurorx.2.3.447

Li, S., Wang, H., & Groth, C. (2014). Drosophila neuroblasts as a new model for the study of stem cell self-renewal and tumor formation. *Bioscience reports*, *34*. https://doi.org/10.1042/BSR20140008

Li, S., Weidenfeld, J., & Morrisey, E. E. (2004). Transcriptional and DNA binding activity of the Foxp1/2/4 family is modulated by heterotypic and homotypic protein interactions. *Mol Cell Biol*, *24*(2), 809-822. https://doi.org/10.1128/mcb.24.2.809-822.2004

Li, W.-K., Zhang, S.-Q., Peng, W.-L., Shi, Y.-H., Yuan, B., Yuan, Y.-T., Xue, Z.-Y., Wang, J.-C., Han, W.-J., Chen, Z.-F., Shan, S.-F., Xue, B.-Q., Chen, J.-L., Zhang, C., Zhu, S.-J., Tai, Y.-L., Cheng, T.-L., & Qiu, Z.-L. (2024). Whole-brain in vivo base editing reverses behavioral changes in Mef2c-mutant mice. *Nature Neuroscience*, *27*(1), 116-128. https://doi.org/10.1038/s41593-023-01499-x

Li, W. Z., Li, S. L., Zheng, H. Y., Zhang, S. P., & Xue, L. (2012). A broad expression profile of the GMR-GAL4 driver in Drosophila melanogaster. *Genet Mol Res*, *11*(3), 1997-2002. https://doi.org/10.4238/2012.August.6.4

Li, X., Han, X., Tu, X., Zhu, D., Feng, Y., Jiang, T., Yang, Y., Qu, J., & Chen, J. G. (2019). An Autism-Related, Nonsense Foxp1 Mutant Induces Autophagy and Delays Radial Migration of the Cortical Neurons. *Cereb Cortex*, *29*(7), 3193-3208. https://doi.org/10.1093/cercor/bhy185

Li, X., Xiao, J., Fröhlich, H., Tu, X., Li, L., Xu, Y., Cao, H., Qu, J., Rappold, G. A., & Chen, J. G. (2015). Foxp1 regulates cortical radial migration and neuronal morphogenesis in developing cerebral cortex. *PLOS ONE*, *10*(5), e0127671. https://doi.org/10.1371/journal.pone.0127671

Li, Z., McKercher, S. R., Cui, J., Nie, Z., Soussou, W., Roberts, A. J., Sallmen, T., Lipton, J. H., Talantova, M., Okamoto, S., & Lipton, S. A. (2008). Myocyte enhancer factor 2C as a neurogenic and antiapoptotic transcription factor in murine embryonic stem cells. *J Neurosci*, *28*(26), 6557-6568. https://doi.org/10.1523/jneurosci.0134-08.2008

Lim, J. Y., Reighard, C. P., & Crowther, D. C. (2015). The pro-domains of neurotrophins, including BDNF, are linked to Alzheimer's disease through a toxic synergy with Aβ. *Hum Mol Genet*, *24*(14), 3929-3938. https://doi.org/10.1093/hmg/ddv130

Lin, Q., Schwarz, J., Bucana, C., & Olson, E. N. (1997). Control of mouse cardiac morphogenesis and myogenesis by transcription factor MEF2C. *Science*, *276*(5317), 1404-1407. https://doi.org/10.1126/science.276.5317.1404

Lin, Y. H., Maaroufi, H. O., Ibrahim, E., Kucerova, L., & Zurovec, M. (2019). Expression of Human Mutant Huntingtin Protein in Drosophila Hemocytes Impairs Immune Responses. *Front Immunol*, *10*, 2405. https://doi.org/10.3389/fimmu.2019.02405

Lisek, M., Przybyszewski, O., Zylinska, L., Guo, F., & Boczek, T. (2023). The Role of MEF2 Transcription Factor Family in Neuronal Survival and Degeneration. *International Journal of Molecular Sciences*, *24*(4), 3120. https://www.mdpi.com/1422-0067/24/4/3120

Lisek, M., Przybyszewski, O., Zylinska, L., Guo, F., & Boczek, T. (2023). The Role of MEF2 Transcription Factor Family in Neuronal Survival and Degeneration. *Int J Mol Sci*, *24*(4). https://doi.org/10.3390/ijms24043120

Liu, L., Tong, H., Sun, Y., Chen, X., Yang, T., Zhou, G., Li, X. J., & Li, S. (2023). Huntingtin Interacting Proteins and Pathological Implications. *Int J Mol Sci*, *24*(17). https://doi.org/10.3390/ijms241713060

Lobato, A. G., Ortiz-Vega, N., Zhu, Y., Neupane, D., Meier, K. K., & Zhai, R. G. (2024). Copper enhances aggregational toxicity of mutant huntingtin in a Drosophila model of Huntington's Disease. *Biochimica et Biophysica Acta (BBA) - Molecular Basis of Disease*, *1870*(1), 166928. https://doi.org/https://doi.org/10.1016/j.bbadis.2023.166928

Louis Sam Titus, A. S. C., Yusuff, T., Cassar, M., Thomas, E., Kretzschmar, D., & D'Mello, S. R. (2017). Reduced Expression of Foxp1 as a Contributing Factor in Huntington's Disease. *J Neurosci*, *37*(27), 6575-6587. https://doi.org/10.1523/jneurosci.3612-16.2017

Loupe, J. M., Pinto, R. M., Kim, K. H., Gillis, T., Mysore, J. S., Andrew, M. A., Kovalenko, M., Murtha, R., Seong, I., Gusella, J. F., Kwak, S., Howland, D., Lee, R., Lee, J. M., Wheeler, V. C., & MacDonald, M. E. (2020). Promotion of somatic CAG repeat expansion by Fan1 knock-out in Huntington's disease knock-in mice is blocked by Mlh1 knock-out. *Hum Mol Genet*, *29*(18), 3044-3053. https://doi.org/10.1093/hmg/ddaa196

Lozano, R., Gbekie, C., Siper, P. M., Srivastava, S., Saland, J. M., Sethuram, S., Tang, L., Drapeau, E., Frank, Y., Buxbaum, J. D., & Kolevzon, A. (2021). FOXP1 syndrome: a review of the literature and practice parameters for medical assessment and monitoring. *Journal of Neurodevelopmental Disorders*, *13*(1), 18. https://doi.org/10.1186/s11689-021-09358-1

Lozano, R., Gbekie, C., Siper, P. M., Srivastava, S., Saland, J. M., Sethuram, S., Tang, L., Drapeau, E., Frank, Y., Buxbaum, J. D., & Kolevzon, A. (2021). FOXP1 syndrome: a review of the literature and practice parameters for medical assessment and monitoring. *J Neurodev Disord*, *13*(1), 18. https://doi.org/10.1186/s11689-021-09358-1

Luong, T. N., Carlisle, H. J., Southwell, A., & Patterson, P. H. (2011). Assessment of motor balance and coordination in mice using the balance beam. *J Vis Exp*(49). https://doi.org/10.3791/2376

Luthi-Carter, R., Strand, A., Peters, N. L., Solano, S. M., Hollingsworth, Z. R., Menon, A. S., Frey, A. S., Spektor, B. S., Penney, E. B., Schilling, G., Ross, C. A., Borchelt, D. R., Tapscott, S. J., Young, A. B., Cha, J. H., & Olson, J. M. (2000). Decreased expression of striatal

signaling genes in a mouse model of Huntington's disease. *Hum Mol Genet*, *9*(9), 1259-1271. https://doi.org/10.1093/hmg/9.9.1259

Lyons, G. E., Micales, B. K., Schwarz, J., Martin, J. F., & Olson, E. N. (1995). Expression of mef2 genes in the mouse central nervous system suggests a role in neuronal maturation. *J Neurosci*, *15*(8), 5727-5738. https://doi.org/10.1523/jneurosci.15-08-05727.1995

Malaiya, S., Cortes-Gutierrez, M., Herb, B. R., Coffey, S. R., Legg, S. R. W., Cantle, J. P., Colantuoni, C., Carroll, J. B., & Ament, S. A. (2021). Single-Nucleus RNA-Seq Reveals Dysregulation of Striatal Cell Identity Due to Huntington's Disease Mutations. *The Journal of Neuroscience*, *41*(25), 5534-5552. https://doi.org/10.1523/jneurosci.2074-20.2021

Mangiarini, L., Sathasivam, K., Seller, M., Cozens, B., Harper, A., Hetherington, C., Lawton, M., Trottier, Y., Lehrach, H., Davies, S. W., & Bates, G. P. (1996). Exon 1 of the HD gene with an expanded CAG repeat is sufficient to cause a progressive neurological phenotype in transgenic mice. *Cell*, *87*(3), 493-506. https://doi.org/10.1016/s0092-8674(00)81369-0

Marsh, J. L., Pallos, J., & Thompson, L. M. (2003). Fly models of Huntington's disease. *Human Molecular Genetics*, *12*(suppl_2), R187-R193. https://doi.org/10.1093/hmg/ddg271

Marsh, J. L., & Thompson, L. M. (2004). Can flies help humans treat neurodegenerative diseases? *BioEssays*, *26*(5), 485-496. https://doi.org/https://doi.org/10.1002/bies.20029

Matsumoto, K., Toh-e, A., & Oshima, Y. (1978). Genetic control of galactokinase synthesis in Saccharomyces cerevisiae: evidence for constitutive expression of the positive regulatory gene gal4. *Journal of Bacteriology*, *134*(2), 446-457. https://doi.org/doi:10.1128/jb.134.2.446-457.1978

Matsushima, A., Pineda, S. S., Crittenden, J. R., Lee, H., Galani, K., Mantero, J., Tombaugh, G., Kellis, M., Heiman, M., & Graybiel, A. M. (2023). Transcriptional vulnerabilities of striatal neurons in human and rodent models of Huntington's disease. *Nature Communications*, *14*(1), 282. https://doi.org/10.1038/s41467-022-35752-x

Matsuura, K., Kabuto, H., Makino, H., & Ogawa, N. (1997). Pole test is a useful method for evaluating the mouse movement disorder caused by striatal dopamine depletion. *J Neurosci Methods*, *73*(1), 45-48. https://doi.org/10.1016/s0165-0270(96)02211-x

McColgan, P., & Tabrizi, S. J. (2018a). Huntington's disease: a clinical review. *European Journal of Neurology*, *25*(1), 24-34. https://doi.org/https://doi.org/10.1111/ene.13413

McColgan, P., Thobhani, A., Boak, L., Schobel, S. A., Nicotra, A., Palermo, G., Trundell, D., Zhou, J., Schlegel, V., Ducray, P. S., Hawellek, D. J., Dorn, J., Simillion, C., Lindemann, M., Wheelock, V., Durr, A., Anderson, K. E., Long, J. D., Wild, E. J., . . . Doody, R. (2023). Tominersen in Adults with Manifest Huntington's Disease. *New England Journal of Medicine*, *389*(23), 2203-2205. https://doi.org/doi:10.1056/NEJMc2300400

McDermott, J. C., Cardoso, M. C., Yu, Y. T., Andres, V., Leifer, D., Krainc, D., Lipton, S. A., & Nadal-Ginard, B. (1993). hMEF2C gene encodes skeletal muscle- and brain-specific transcription factors. *Mol Cell Biol*, *13*(4), 2564-2577. https://doi.org/10.1128/mcb.13.4.2564-2577.1993

Medina, A., Mahjoub, Y., Shaver, L., & Pringsheim, T. (2022). Prevalence and Incidence of Huntington's Disease: An Updated Systematic Review and Meta-Analysis. *Movement Disorders*, *37*(12), 2327-2335. https://doi.org/https://doi.org/10.1002/mds.29228

Mehla, J., Caufield, J. H., Sakhawalkar, N., & Uetz, P. (2017). A Comparison of Two-Hybrid Approaches for Detecting Protein-Protein Interactions. *Methods Enzymol*, *586*, 333-358. https://doi.org/10.1016/bs.mie.2016.10.020

Menalled, L. B. (2005). Knock-in mouse models of Huntington's disease. *NeuroRx*, *2*(3), 465-470. https://doi.org/10.1602/neurorx.2.3.465

Menalled, L. B., Kudwa, A. E., Miller, S., Fitzpatrick, J., Watson-Johnson, J., Keating, N., Ruiz, M., Mushlin, R., Alosio, W., McConnell, K., Connor, D., Murphy, C., Oakeshott, S., Kwan, M., Beltran, J., Ghavami, A., Brunner, D., Park, L. C., Ramboz, S., & Howland, D. (2012). Comprehensive behavioral and molecular characterization of a new knock-in mouse model of Huntington's disease: zQ175. *PLOS ONE*, *7*(12), e49838. https://doi.org/10.1371/journal.pone.0049838

Menalled, L. B., Sison, J. D., Dragatsis, I., Zeitlin, S., & Chesselet, M.-F. (2003). Time course of early motor and neuropathological anomalies in a knock-in mouse model of Huntington's disease with 140 CAG repeats. *Journal of Comparative Neurology*, *465*(1), 11-26. https://doi.org/https://doi.org/10.1002/cne.10776

Mendoza, E., Colomb, J., Rybak, J., Pflüger, H. J., Zars, T., Scharff, C., & Brembs, B. (2014). Drosophila FoxP mutants are deficient in operant self-learning. *PLOS ONE*, *9*(6), e100648. https://doi.org/10.1371/journal.pone.0100648

Mishra, A. K., & Sprecher, S. G. (2023). Eye Development in Drosophila: From Photoreceptor Specification to Terminal Differentiation. In B. Egger (Ed.), *Neurogenetics : Current Topics in Cellular and Developmental Neurobiology* (pp. 105-128). Springer International Publishing. https://doi.org/10.1007/978-3-031-07793-7_6

Mitchell, A. C., Javidfar, B., Pothula, V., Ibi, D., Shen, E. Y., Peter, C. J., Bicks, L. K., Fehr, T., Jiang, Y., Brennand, K. J., Neve, R. L., Gonzalez-Maeso, J., & Akbarian, S. (2018). MEF2C transcription factor is associated with the genetic and epigenetic risk architecture of schizophrenia and improves cognition in mice. *Mol Psychiatry*, *23*(1), 123-132. https://doi.org/10.1038/mp.2016.254

Miyamoto, Y., Katayama, S., Shigematsu, N., Nishi, A., & Fukuda, T. (2018). Striosome-based map of the mouse striatum that is conformable to both cortical afferent topography and uneven distributions of dopamine D1 and D2 receptor-expressing cells. *Brain Struct Funct*, *223*(9), 4275-4291. https://doi.org/10.1007/s00429-018-1749-3

Molero, A. E., Arteaga-Bracho, E. E., Chen, C. H., Gulinello, M., Winchester, M. L., Pichamoorthy, N., Gokhan, S., Khodakhah, K., & Mehler, M. F. (2016). Selective expression of mutant huntingtin during development recapitulates characteristic features of Huntington's disease. *Proc Natl Acad Sci U S A*, *113*(20), 5736-5741. https://doi.org/10.1073/pnas.1603871113

Molkentin, J. D., Li, L., & Olson, E. N. (1996). Phosphorylation of the MADS-Box transcription factor MEF2C enhances its DNA binding activity. *J Biol Chem*, *271*(29), 17199-17204. https://doi.org/10.1074/jbc.271.29.17199

Møllersen, L., Rowe, A. D., Larsen, E., Rognes, T., & Klungland, A. (2010). Continuous and periodic expansion of CAG repeats in Huntington's disease R6/1 mice. *PLoS Genet*, *6*(12), e1001242. https://doi.org/10.1371/journal.pgen.1001242

Monckton, D. G. (2021). The Contribution of Somatic Expansion of the CAG Repeat to Symptomatic Development in Huntington's Disease: A Historical Perspective. *J Huntingtons Dis*, *10*(1), 7-33. https://doi.org/10.3233/jhd-200429

Mondo, E., Moser, R., Gao, G., Mueller, C., Sena-Esteves, M., Sapp, E., Pfister, E., O'Connell, D., Takle, K., Erger, K. E., Liu, W., Conlon, T. J., DiFiglia, M., Gounis, M. J., & Aronin, N.

(2018). Selective Neuronal Uptake and Distribution of AAVrh8, AAV9, and AAVrh10 in Sheep After Intra-Striatal Administration. *J Huntingtons Dis*, *7*(4), 309-319. https://doi.org/10.3233/jhd-180302

Morigaki, R., & Goto, S. (2017). Striatal Vulnerability in Huntington's Disease: Neuroprotection Versus Neurotoxicity. *Brain Sci*, *7*(6). https://doi.org/10.3390/brainsci7060063

Morton, A. J. (2018). Large-Brained Animal Models of Huntington's Disease: Sheep. *Methods Mol Biol*, *1780*, 221-239. https://doi.org/10.1007/978-1-4939-7825-0_12

Mukherjee, P., Roy, S., Ghosh, D., & Nandi, S. K. (2022). Role of animal models in biomedical research: a review. *Laboratory Animal Research*, *38*(1), 18. https://doi.org/10.1186/s42826-022-00128-1

Nath, S. R., Lieberman, M. L., Yu, Z., Marchioretti, C., Jones, S. T., Danby, E. C. E., Van Pelt, K. M., Sorarù, G., Robins, D. M., Bates, G. P., Pennuto, M., & Lieberman, A. P. (2020). MEF2 impairment underlies skeletal muscle atrophy in polyglutamine disease. *Acta Neuropathol*, *140*(1), 63-80. https://doi.org/10.1007/s00401-020-02156-4

Naver, B., Stub, C., Moller, M., Fenger, K., Hansen, A. K., Hasholt, L., & Sorensen, S. A. (2003). Molecular and behavioral analysis of the R6/1 Huntington's disease transgenic mouse. *Neuroscience*, *122*(4), 1049-1057. https://doi.org/10.1016/j.neuroscience.2003.08.053

Neely, M. D., Robert, E. M., Baucum, A. J., Colbran, R. J., Muly, E. C., & Deutch, A. Y. (2009). Localization of myocyte enhancer factor 2 in the rodent forebrain: Regionally-specific cytoplasmic expression of MEF2A. *Brain Research*, *1274*, 55-65. https://doi.org/https://doi.org/10.1016/j.brainres.2009.03.067

Nguyen, H. P., Metzger, S., Holzmann, C., Koczan, D., Thiesen, H. J., von Hörsten, S., Riess, O., & Bonin, M. (2008). Age-dependent gene expression profile and protein expression in a transgenic rat model of Huntington's disease. *Proteomics Clin Appl*, *2*(12), 1638-1650. https://doi.org/10.1002/prca.200800018

Nitta, Y., & Sugie, A. (2022). Studies of neurodegenerative diseases using Drosophila and the development of novel approaches for their analysis. *Fly (Austin)*, *16*(1), 275-298. https://doi.org/10.1080/19336934.2022.2087484

Nittari, G., Roy, P., Martinelli, I., Bellitto, V., Tomassoni, D., Traini, E., Tayebati, S. K., & Amenta, F. (2023). Rodent Models of Huntington's Disease: An Overview. *Biomedicines*, *11*(12). https://doi.org/10.3390/biomedicines11123331

O'Rourke, J. G., Gareau, J. R., Ochaba, J., Song, W., Raskó, T., Reverter, D., Lee, J., Monteys, A. M., Pallos, J., Mee, L., Vashishtha, M., Apostol, B. L., Nicholson, T. P., Illes, K., Zhu, Y. Z., Dasso, M., Bates, G. P., Difiglia, M., Davidson, B., . . . Thompson, L. M. (2013). SUMO-2 and PIAS1 modulate insoluble mutant huntingtin protein accumulation. *Cell Rep*, *4*(2), 362-375. https://doi.org/10.1016/j.celrep.2013.06.034

Okamoto, S.-i., Krainc, D., Sherman, K., & Lipton, S. A. (2000). Antiapoptotic role of the p38 mitogen-activated protein kinase–myocyte enhancer factor 2 transcription factor pathway during neuronal differentiation. *Proceedings of the National Academy of Sciences*, *97*(13), 7561-7566. https://doi.org/doi:10.1073/pnas.130502697

Palmiter, R. D. (2008). Dopamine signaling in the dorsal striatum is essential for motivated behaviors: lessons from dopamine-deficient mice. *Ann N Y Acad Sci*, *1129*, 35-46. https://doi.org/10.1196/annals.1417.003

Pappu, K. S., Chen, R., Middlebrooks, B. W., Woo, C., Heberlein, U., & Mardon, G. (2003). Mechanism of hedgehog signaling during Drosophila eye development. *Development*, *130*(13), 3053-3062. https://doi.org/10.1242/dev.00534

Patel, P. J., Bhatt, T., DelDonno, S. R., Langenecker, S. A., & Dusane, S. (2019). Examining Neural Plasticity for Slip-Perturbation Training: An fMRI Study [Original Research]. *Frontiers in Neurology*, *9*. https://doi.org/10.3389/fneur.2018.01181

Peak, J., Chieng, B., Hart, G., & Balleine, B. W. (2020). Striatal direct and indirect pathway neurons differentially control the encoding and updating of goal-directed learning. *eLife*, *9*, e58544. https://doi.org/10.7554/eLife.58544

Perlman, R. L. (2016). Mouse models of human disease: An evolutionary perspective. *Evol Med Public Health*, *2016*(1), 170-176. https://doi.org/10.1093/emph/eow014

Pfister, E. L., DiNardo, N., Mondo, E., Borel, F., Conroy, F., Fraser, C., Gernoux, G., Han, X., Hu, D., Johnson, E., Kennington, L., Liu, P., Reid, S. J., Sapp, E., Vodicka, P., Kuchel, T., Morton, A. J., Howland, D., Moser, R., . . . Aronin, N. (2018). Artificial miRNAs Reduce Human Mutant Huntingtin Throughout the Striatum in a Transgenic Sheep Model of Huntington's Disease. *Hum Gene Ther*, *29*(6), 663-673. https://doi.org/10.1089/hum.2017.199

Pinto, R. M., Dragileva, E., Kirby, A., Lloret, A., Lopez, E., St Claire, J., Panigrahi, G. B., Hou, C., Holloway, K., Gillis, T., Guide, J. R., Cohen, P. E., Li, G. M., Pearson, C. E., Daly, M. J., & Wheeler, V. C. (2013). Mismatch repair genes Mlh1 and Mlh3 modify CAG instability in Huntington's disease mice: genome-wide and candidate approaches. *PLoS Genet*, *9*(10), e1003930. https://doi.org/10.1371/journal.pgen.1003930

Plank, A. C., Canneva, F., Raber, K. A., Urbach, Y. K., Dobner, J., Puchades, M., Bjaalie, J. G., Gillmann, C., Bäuerle, T., Riess, O., Nguyen, H. H. P., & von Hörsten, S. (2018). Early Alterations in Operant Performance and Prominent Huntingtin Aggregation in a Congenic F344 Rat Line of the Classical CAG(n51trunc) Model of Huntington Disease. *Front Neurosci*, *12*, 11. https://doi.org/10.3389/fnins.2018.00011

Plinta, K., Plewka, A., Pawlicki, K., Zmarzły, N., Wójcik-Pędziwiatr, M., Rudziński, M., Krzak-Kubica, A., Doręgowska-Stachera, M., & Rudzińska-Bar, M. (2021). The Utility of BDNF Detection in Assessing Severity of Huntington's Disease. *J Clin Med*, *10*(21). https://doi.org/10.3390/jcm10215181

Pogoda, A., Chmielewska, N., Maciejak, P., & Szyndler, J. (2021). Transcriptional Dysregulation in Huntington's Disease: The Role in Pathogenesis and Potency for Pharmacological Targeting. *Current Medicinal Chemistry*, *28*(14), 2783-2806. https://doi.org/https://doi.org/10.2174/0929867327666200705225821

Pon, J. R., & Marra, M. A. (2016). MEF2 transcription factors: developmental regulators and emerging cancer genes. *Oncotarget*, *7*(3), 2297-2312. https://doi.org/10.18632/oncotarget.6223

Potthoff, M. J., & Olson, E. N. (2007). MEF2: a central regulator of diverse developmental programs. *Development*, *134*(23), 4131-4140. https://doi.org/10.1242/dev.008367

Prager, E. M., & Plotkin, J. L. (2019). Compartmental function and modulation of the striatum. *J Neurosci Res*, *97*(12), 1503-1514. https://doi.org/10.1002/jnr.24522

Precious, S. V., Kelly, C. M., Reddington, A. E., Vinh, N. N., Stickland, R. C., Pekarik, V., Scherf, C., Jeyasingham, R., Glasbey, J., Holeiter, M., Jones, L., Taylor, M. V., & Rosser, A. E. (2016). FoxP1 marks medium spiny neurons from precursors to maturity and is required for their differentiation. *Exp Neurol*, *282*, 9-18. https://doi.org/10.1016/j.expneurol.2016.05.002

Pütz, S. M., Kram, J., Rauh, E., Kaiser, S., Toews, R., Lueningschroer-Wang, Y., Rieger, D., & Raabe, T. (2021). Loss of p21-activated kinase Mbt/PAK4 causes Parkinson-like

phenotypes in Drosophila. *Dis Model Mech*, *14*(6). https://doi.org/10.1242/dmm.047811

Qin, S., Madhavan, M., Waclaw, R. R., Nakafuku, M., & Campbell, K. (2016). Characterization of a new Gsx2-cre line in the developing mouse telencephalon. *Genesis*, *54*(10), 542-549. https://doi.org/10.1002/dvg.22980

Qiu, Z., Norflus, F., Singh, B., Swindell, M. K., Buzescu, R., Bejarano, M., Chopra, R., Zucker, B., Benn, C. L., DiRocco, D. P., Cha, J.-H. J., Ferrante, R. J., & Hersch, S. M. (2006). Sp1 Is Up-regulated in Cellular and Transgenic Models of Huntington Disease, and Its Reduction Is Neuroprotective*. *Journal of Biological Chemistry*, *281*(24), 16672-16680. https://doi.org/https://doi.org/10.1074/jbc.M511648200

Raamsdonk, J. M. V., Hayden, M. R., & Leavitt, B. R. (2005). Experimental models of Huntington's disease. *Drug Discovery Today: Disease Models*, *2*(4), 291-297. https://doi.org/https://doi.org/10.1016/j.ddmod.2005.11.010

Rai, S., & Tapadia, M. G. (2022). Hsc70-4 aggravates PolyQ-mediated neurodegeneration by modulating NF-κB mediated immune response in Drosophila [Original Research]. *Frontiers in Molecular Neuroscience*, *15*. https://doi.org/10.3389/fnmol.2022.857257

Ramaswamy, S., McBride, J. L., & Kordower, J. H. (2007). Animal Models of Huntington's Disease. *ILAR Journal*, *48*(4), 356-373. https://doi.org/10.1093/ilar.48.4.356

Rana, N., Kapil, L., Singh, C., & Singh, A. (2024). Modeling Huntington's disease: An insight on in-vitro and in-vivo models. *Behavioural Brain Research*, *459*, 114757. https://doi.org/https://doi.org/10.1016/j.bbr.2023.114757

Ratié, L., & Humbert, S. (2024). A developmental component to Huntington's disease. *Revue Neurologique*, *180*(5), 357-362. https://doi.org/https://doi.org/10.1016/j.neurol.2024.04.001

Rattray, I., Smith, E. J., Crum, W. R., Walker, T. A., Gale, R., Bates, G. P., & Modo, M. (2013). Correlations of behavioral deficits with brain pathology assessed through longitudinal MRI and histopathology in the R6/1 mouse model of Huntington's disease. *PLOS ONE*, *8*(12), e84726. https://doi.org/10.1371/journal.pone.0084726

Ren, J., Zhang, S., Wang, X., Deng, Y., Zhao, Y., Xiao, Y., Liu, J., Chu, L., & Qi, X. (2022). MEF2C ameliorates learning, memory, and molecular pathological changes in Alzheimer's disease in vivo and in vitro. *Acta Biochim Biophys Sin (Shanghai)*, *54*(1), 77-90. https://doi.org/10.3724/abbs.2021012

Rinaldi, C., & Wood, M. J. A. (2018). Antisense oligonucleotides: the next frontier for treatment of neurological disorders. *Nature Reviews Neurology*, *14*(1), 9-21. https://doi.org/10.1038/nrneurol.2017.148

Rodríguez-Urgellés, E., Rodríguez-Navarro, I., Ballasch, I., del Toro, D., del Castillo, I., Brito, V., Alberch, J., & Giralt, A. (2022). Postnatal Foxp2 regulates early psychiatric-like phenotypes and associated molecular alterations in the R6/1 transgenic mouse model of Huntington's disease. *Neurobiology of Disease*, *173*, 105854. https://doi.org/https://doi.org/10.1016/j.nbd.2022.105854

Romero, E., Cha, G. H., Verstreken, P., Ly, C. V., Hughes, R. E., Bellen, H. J., & Botas, J. (2008). Suppression of neurodegeneration and increased neurotransmission caused by expanded full-length huntingtin accumulating in the cytoplasm. *Neuron*, *57*(1), 27-40. https://doi.org/10.1016/j.neuron.2007.11.025

Rosas-Arellano, A., Estrada-Mondragón, A., Piña, R., Mantellero, C. A., & Castro, M. A. (2018). The Tiny Drosophila Melanogaster for the Biggest Answers in Huntington's Disease. *Int J Mol Sci*, *19*(8). https://doi.org/10.3390/ijms19082398

Roshan, M. H., Tambo, A., & Pace, N. P. (2016). Potential Role of Caffeine in the Treatment of Parkinson's Disease. *Open Neurol J*, *10*, 42-58. https://doi.org/10.2174/1874205x01610010042

Rossignol, J., Fink, K. D., Crane, A. T., Davis, K. K., Bombard, M. C., Clerc, S., Bavar, A. M., Lowrance, S. A., Song, C., Witte, S., Lescaudron, L., & Dunbar, G. L. (2015). Reductions in behavioral deficits and neuropathology in the R6/2 mouse model of Huntington's disease following transplantation of bone-marrow-derived mesenchymal stem cells is dependent on passage number. *Stem Cell Res Ther*, *6*(1), 9. https://doi.org/10.1186/scrt545

Roth, J. R., Moraes, R. C. M. d., Xu, B. P., Crawley, S. R., Khan, M. A., & Melkani, G. C. (2023). Rapamycin reduces neuronal mutant huntingtin aggregation and ameliorates locomotor performance in Drosophila [Original Research]. *Frontiers in Aging Neuroscience*, *15*. https://doi.org/10.3389/fnagi.2023.1223911

Roy, J. C. L., Vitalo, A., Andrew, M. A., Mota-Silva, E., Kovalenko, M., Burch, Z., Nhu, A. M., Cohen, P. E., Grabczyk, E., Wheeler, V. C., & Mouro Pinto, R. (2021). Somatic CAG expansion in Huntington's disease is dependent on the MLH3 endonuclease domain, which can be excluded via splice redirection. *Nucleic Acids Res*, *49*(7), 3907-3918. https://doi.org/10.1093/nar/gkab152

Rubin, G. M., Yandell, M. D., Wortman, J. R., Gabor Miklos, G. L., Nelson, C. R., Hariharan, I. K., Fortini, M. E., Li, P. W., Apweiler, R., Fleischmann, W., Cherry, J. M., Henikoff, S., Skupski, M. P., Misra, S., Ashburner, M., Birney, E., Boguski, M. S., Brody, T., Brokstein, P., . . . Lewis, S. (2000). Comparative genomics of the eukaryotes. *Science*, *287*(5461), 2204-2215. https://doi.org/10.1126/science.287.5461.2204

Rubinsztein, D. C., Leggo, J., Coles, R., Almqvist, E., Biancalana, V., Cassiman, J. J., Chotai, K., Connarty, M., Crauford, D., Curtis, A., Curtis, D., Davidson, M. J., Differ, A. M., Dode, C., Dodge, A., Frontali, M., Ranen, N. G., Stine, O. C., Sherr, M., . . . et al. (1996). Phenotypic characterization of individuals with 30-40 CAG repeats in the Huntington disease (HD) gene reveals HD cases with 36 repeats and apparently normal elderly individuals with 36-39 repeats. *Am J Hum Genet*, *59*(1), 16-22.

Ruocco, H. H., Lopes-Cendes, I., Li, L. M., Santos-Silva, M., & Cendes, F. (2006). Striatal and extrastriatal atrophy in Huntington's disease and its relationship with length of the CAG repeat. *Braz J Med Biol Res*, *39*(8), 1129-1136. https://doi.org/10.1590/s0100-879x2006000800016

Sahin, H., & Çelik, A. (2013). Drosophila Eye Development and Photoreceptor Specification. In. https://doi.org/10.1002/9780470015902.a0001147.pub2

Santos, M. E., Athanasiadis, A., Leitão, A. B., DuPasquier, L., & Sucena, É. (2011). Alternative Splicing and Gene Duplication in the Evolution of the FoxP Gene Subfamily. *Molecular Biology and Evolution*, *28*(1), 237-247. https://doi.org/10.1093/molbev/msq182

Sathasivam, K., Neueder, A., Gipson, T. A., Landles, C., Benjamin, A. C., Bondulich, M. K., Smith, D. L., Faull, R. L. M., Roos, R. A. C., Howland, D., Detloff, P. J., Housman, D. E., & Bates, G. P. (2013). Aberrant splicing of HTT generates the pathogenic exon 1 protein in Huntington disease. *Proceedings of the National Academy of Sciences*, *110*(6), 2366-2370. https://doi.org/doi:10.1073/pnas.1221891110

Schulte, J., & Littleton, J. T. (2011). The biological function of the Huntingtin protein and its relevance to Huntington's Disease pathology. *Curr Trends Neurol*, *5*, 65-78.

Schultz, J. L., Neema, M., & Nopoulos, P. C. (2023). Unravelling the role of huntingtin: from neurodevelopment to neurodegeneration. *Brain*, *146*(11), 4408-4410. https://doi.org/10.1093/brain/awad353

Schulz, R. A., Chromey, C., Lu, M. F., Zhao, B., & Olson, E. N. (1996). Expression of the D-MEF2 transcription in the Drosophila brain suggests a role in neuronal cell differentiation. *Oncogene*, *12*(8), 1827-1831.

Schweitzer, J. K., & Livingston, D. M. (1997). Destabilization of CAG Trinucleotide Repeat Tracts by Mismatch Repair Mutations in Yeast. *Human Molecular Genetics*, *6*(3), 349-355. https://doi.org/10.1093/hmg/6.3.349

Seibenhener, M. L., & Wooten, M. C. (2015). Use of the Open Field Maze to measure locomotor and anxiety-like behavior in mice. *J Vis Exp*(96), e52434. https://doi.org/10.3791/52434

Sekiyama, Y., Suzuki, H., & Tsukahara, T. (2012). Functional gene expression analysis of tissue-specific isoforms of Mef2c. *Cell Mol Neurobiol*, *32*(1), 129-139. https://doi.org/10.1007/s10571-011-9743-9

Seredenina, T., & Luthi-Carter, R. (2012). What have we learned from gene expression profiles in Huntington's disease? *Neurobiol Dis*, *45*(1), 83-98. https://doi.org/10.1016/j.nbd.2011.07.001

Shenoy, S. A., Zheng, S., Liu, W., Dai, Y., Liu, Y., Hou, Z., Mori, S., Tang, Y., Cheng, J., Duan, W., & Li, C. (2022). A novel and accurate full-length HTT mouse model for Huntington's disease. *eLife*, *11*. https://doi.org/10.7554/eLife.70217

Shiraishi, R., Tamura, T., Sone, M., & Okazawa, H. (2014). Systematic analysis of fly models with multiple drivers reveals different effects of ataxin-1 and huntingtin in neuron subtype-specific expression. *PLOS ONE*, *9*(12), e116567. https://doi.org/10.1371/journal.pone.0116567

Shirasaki, D. I., Greiner, E. R., Al-Ramahi, I., Gray, M., Boontheung, P., Geschwind, D. H., Botas, J., Coppola, G., Horvath, S., Loo, J. A., & Yang, X. W. (2012). Network organization of the huntingtin proteomic interactome in mammalian brain. *Neuron*, *75*(1), 41-57. https://doi.org/10.1016/j.neuron.2012.05.024

Shu, W., Yang, H., Zhang, L., Lu, M. M., & Morrisey, E. E. (2001). Characterization of a New Subfamily of Winged-helix/Forkhead (Fox) Genes That Are Expressed in the Lung and Act as Transcriptional Repressors*. *Journal of Biological Chemistry*, *276*(29), 27488-27497. https://doi.org/https://doi.org/10.1074/jbc.M100636200

Sinadinos, C., Burbidge-King, T., Soh, D., Thompson, L. M., Marsh, J. L., Wyttenbach, A., & Mudher, A. K. (2009). Live axonal transport disruption by mutant huntingtin fragments in Drosophila motor neuron axons. *Neurobiology of Disease*, *34*(2), 389-395. https://doi.org/https://doi.org/10.1016/j.nbd.2009.02.012

Sipp, A. R., Gwin, J. T., Makeig, S., & Ferris, D. P. (2013). Loss of balance during balance beam walking elicits a multifocal theta band electrocortical response. *J Neurophysiol*, *110*(9), 2050-2060. https://doi.org/10.1152/jn.00744.2012

Slanzi, A., Iannoto, G., Rossi, B., Zenaro, E., & Constantin, G. (2020). In vitro Models of Neurodegenerative Diseases [Review]. *Frontiers in Cell and Developmental Biology*, *8*. https://doi.org/10.3389/fcell.2020.00328

Slow, E. J., van Raamsdonk, J., Rogers, D., Coleman, S. H., Graham, R. K., Deng, Y., Oh, R., Bissada, N., Hossain, S. M., Yang, Y.-Z., Li, X.-J., Simpson, E. M., Gutekunst, C.-A., Leavitt, B. R., & Hayden, M. R. (2003). Selective striatal neuronal loss in a YAC128 mouse model

of Huntington disease. *Human Molecular Genetics*, *12*(13), 1555-1567. https://doi.org/10.1093/hmg/ddg169

Sogorb-Gonzalez, M., Landles, C., Caron, N. S., Stam, A., Osborne, G., Hayden, M. R., Howland, D., van Deventer, S., Bates, G. P., Vallès, A., & Evers, M. (2024). Exon 1-targeting miRNA reduces the pathogenic exon 1 HTT protein in Huntington disease models. *Brain*. https://doi.org/10.1093/brain/awae266

Soler, C., Han, J., & Taylor, M. V. (2012). The conserved transcription factor Mef2 has multiple roles in adult Drosophila musculature formation. *Development*, *139*(7), 1270-1275. https://doi.org/10.1242/dev.077875

Song, W., Smith, M. R., Syed, A., Lukacsovich, T., Barbaro, B. A., Purcell, J., Bornemann, D. J., Burke, J., & Marsh, J. L. (2013). Morphometric analysis of Huntington's disease neurodegeneration in Drosophila. *Methods Mol Biol*, *1017*, 41-57. https://doi.org/10.1007/978-1-62703-438-8_3

Sonnenfeld, M. J. (2009). GAL4/UAS Expression System. In M. D. Binder, N. Hirokawa, & U. Windhorst (Eds.), *Encyclopedia of Neuroscience* (pp. 1662-1666). Springer Berlin Heidelberg. https://doi.org/10.1007/978-3-540-29678-2_1904

Southwell, A. L., Skotte, N. H., Villanueva, E. B., Østergaard, M. E., Gu, X., Kordasiewicz, H. B., Kay, C., Cheung, D., Xie, Y., Waltl, S., Dal Cengio, L., Findlay-Black, H., Doty, C. N., Petoukhov, E., Iworima, D., Slama, R., Ooi, J., Pouladi, M. A., Yang, X. W., . . . Hayden, M. R. (2017). A novel humanized mouse model of Huntington disease for preclinical development of therapeutics targeting mutant huntingtin alleles. *Hum Mol Genet*, *26*(6), 1115-1132. https://doi.org/10.1093/hmg/ddx021

Speidell, A., Bin Abid, N., & Yano, H. (2023). Brain-Derived Neurotrophic Factor Dysregulation as an Essential Pathological Feature in Huntington's Disease: Mechanisms and Potential Therapeutics. *Biomedicines*, *11*(8), 2275. https://www.mdpi.com/2227-9059/11/8/2275

Spires, T. L., Grote, H. E., Varshney, N. K., Cordery, P. M., van Dellen, A., Blakemore, C., & Hannan, A. J. (2004). Environmental Enrichment Rescues Protein Deficits in a Mouse Model of Huntington's Disease, Indicating a Possible Disease Mechanism. *The Journal of Neuroscience*, *24*(9), 2270-2276. https://doi.org/10.1523/jneurosci.1658-03.2004

Stanley, A. T., Lippiello, P., Sulzer, D., & Miniaci, M. C. (2021). Roles for the Dorsal Striatum in Aversive Behavior [Mini Review]. *Frontiers in Cellular Neuroscience*, *15*. https://doi.org/10.3389/fncel.2021.634493

Steffan, J. S., Bodai, L., Pallos, J., Poelman, M., McCampbell, A., Apostol, B. L., Kazantsev, A., Schmidt, E., Zhu, Y. Z., Greenwald, M., Kurokawa, R., Housman, D. E., Jackson, G. R., Marsh, J. L., & Thompson, L. M. (2001). Histone deacetylase inhibitors arrest polyglutamine-dependent neurodegeneration in Drosophila. *Nature*, *413*(6857), 739-743. https://doi.org/10.1038/35099568

Stöberl, N., Donaldson, J., Binda, C. S., McAllister, B., Hall-Roberts, H., Jones, L., Massey, T. H., & Allen, N. D. (2023). Mutant huntingtin confers cell-autonomous phenotypes on Huntington's disease iPSC-derived microglia. *Scientific Reports*, *13*(1), 20477. https://doi.org/10.1038/s41598-023-46852-z

Sturm, V. E., Haase, C. M., & Levenson, R. W. (2016). Chapter 22 - Emotional Dysfunction in Psychopathology and Neuropathology: Neural and Genetic Pathways. In T. Lehner, B. L. Miller, & M. W. State (Eds.), *Genomics, Circuits, and Pathways in Clinical Neuropsychiatry* (pp. 345-364). Academic Press. https://doi.org/https://doi.org/10.1016/B978-0-12-800105-9.00022-6

Tabrizi, S. J., Estevez-Fraga, C., van Roon-Mom, W. M. C., Flower, M. D., Scahill, R. I., Wild, E. J., Muñoz-Sanjuan, I., Sampaio, C., Rosser, A. E., & Leavitt, B. R. (2022). Potential disease-modifying therapies for Huntington's disease: lessons learned and future opportunities. *Lancet Neurol*, *21*(7), 645-658. https://doi.org/10.1016/s1474-4422(22)00121-1

Takahashi, H., Takahashi, K., & Liu, F. C. (2009). FOXP genes, neural development, speech and language disorders. *Adv Exp Med Biol*, *665*, 117-129. https://doi.org/10.1007/978-1-4419-1599-3_9

Tamura, S., Morikawa, Y., Iwanishi, H., Hisaoka, T., & Senba, E. (2003). Expression pattern of the winged-helix/forkhead transcription factor Foxp1 in the developing central nervous system. *Gene Expr Patterns*, *3*(2), 193-197. https://doi.org/10.1016/s1567-133x(03)00003-6

Tamura, S., Morikawa, Y., Iwanishi, H., Hisaoka, T., & Senba, E. (2004a). Foxp1 gene expression in projection neurons of the mouse striatum. *Neuroscience*, *124*(2), 261-267. https://doi.org/https://doi.org/10.1016/j.neuroscience.2003.11.036

Tamura, S., Morikawa, Y., Iwanishi, H., Hisaoka, T., & Senba, E. (2004b). Foxp1 gene expression in projection neurons of the mouse striatum. *Neuroscience*, *124*(2), 261-267. https://doi.org/10.1016/j.neuroscience.2003.11.036

Tamura, T., Sone, M., Yamashita, M., Wanker, E. E., & Okazawa, H. (2009). Glial cell lineage expression of mutant ataxin-1 and huntingtin induces developmental and late-onset neuronal pathologies in Drosophila models. *PLOS ONE*, *4*(1), e4262. https://doi.org/10.1371/journal.pone.0004262

Tang, B., Becanovic, K., Desplats, P. A., Spencer, B., Hill, A. M., Connolly, C., Masliah, E., Leavitt, B. R., & Thomas, E. A. (2012). Forkhead box protein p1 is a transcriptional repressor of immune signaling in the CNS: implications for transcriptional dysregulation in Huntington disease. *Hum Mol Genet*, *21*(14), 3097-3111. https://doi.org/10.1093/hmg/dds132

Tang, B., Seredenina, T., Coppola, G., Kuhn, A., Geschwind, D. H., Luthi-Carter, R., & Thomas, E. A. (2011). Gene expression profiling of R6/2 transgenic mice with different CAG repeat lengths reveals genes associated with disease onset and progression in Huntington's disease. *Neurobiol Dis*, *42*(3), 459-467. https://doi.org/10.1016/j.nbd.2011.02.008

Taylor, M. V., & Hughes, S. M. (2017). Mef2 and the skeletal muscle differentiation program. *Seminars in Cell & Developmental Biology*, *72*, 33-44. https://doi.org/https://doi.org/10.1016/j.semcdb.2017.11.020

Tebbenkamp, A. T., Green, C., Xu, G., Denovan-Wright, E. M., Rising, A. C., Fromholt, S. E., Brown, H. H., Swing, D., Mandel, R. J., Tessarollo, L., & Borchelt, D. R. (2011). Transgenic mice expressing caspase-6-derived N-terminal fragments of mutant huntingtin develop neurologic abnormalities with predominant cytoplasmic inclusion pathology composed largely of a smaller proteolytic derivative. *Hum Mol Genet*, *20*(14), 2770-2782. https://doi.org/10.1093/hmg/ddr176

Tikker, L., Casarotto, P., Singh, P., Biojone, C., Piepponen, T. P., Estartús, N., Seelbach, A., Sridharan, R., Laukkanen, L., Castrén, E., & Partanen, J. (2020). Inactivation of the GATA Cofactor ZFPM1 Results in Abnormal Development of Dorsal Raphe Serotonergic Neuron Subtypes and Increased Anxiety-Like Behavior. *J Neurosci*, *40*(45), 8669-8682. https://doi.org/10.1523/jneurosci.2252-19.2020

Tocco, C., Bertacchi, M., & Studer, M. (2021). Structural and Functional Aspects of the Neurodevelopmental Gene NR2F1: From Animal Models to Human Pathology [Review]. *Frontiers in Molecular Neuroscience*, *14*. https://doi.org/10.3389/fnmol.2021.767965

Tolwinski, N. S. (2017). Introduction: Drosophila-A Model System for Developmental Biology. *J Dev Biol*, *5*(3). https://doi.org/10.3390/jdb5030009

Tong, H., Yang, T., Xu, S., Li, X., Liu, L., Zhou, G., Yang, S., Yin, S., Li, X. J., & Li, S. (2024). Huntington's Disease: Complex Pathogenesis and Therapeutic Strategies. *Int J Mol Sci*, *25*(7). https://doi.org/10.3390/ijms25073845

Torres, E. M., & Dunnett, S. B. (2012). 6-OHDA Lesion Models of Parkinson's Disease in the Rat. In E. L. Lane & S. B. Dunnett (Eds.), *Animal Models of Movement Disorders: Volume I* (pp. 267-279). Humana Press. https://doi.org/10.1007/978-1-61779-298-4_13

Treisman, J. E. (1999). A conserved blueprint for the eye? *BioEssays*, *21*(10), 843-850. https://doi.org/10.1002/(sici)1521-1878(199910)21:10<843::Aid-bies6>3.0.Co;2-j

Treisman, J. E., & Heberlein, U. (1998). 4 Eye Development in Drosophila: Formation of the Eye Field and Control of Differentiation. In R. A. Pedersen & G. P. Schatten (Eds.), *Current Topics in Developmental Biology* (Vol. 39, pp. 119-158). Academic Press. https://doi.org/https://doi.org/10.1016/S0070-2153(08)60454-8

Tu, S., Akhtar, M. W., Escorihuela, R. M., Amador-Arjona, A., Swarup, V., Parker, J., Zaremba, J. D., Holland, T., Bansal, N., Holohan, D. R., Lopez, K., Ryan, S. D., Chan, S. F., Yan, L., Zhang, X., Huang, X., Sultan, A., McKercher, S. R., Ambasudhan, R., . . . Nakanishi, N. (2017). NitroSynapsin therapy for a mouse MEF2C haploinsufficiency model of human autism. *Nature Communications*, *8*(1), 1488. https://doi.org/10.1038/s41467-017-01563-8

Turner, K. M., Svegborn, A., Langguth, M., McKenzie, C., & Robbins, T. W. (2022). Opposing Roles of the Dorsolateral and Dorsomedial Striatum in the Acquisition of Skilled Action Sequencing in Rats. *The Journal of Neuroscience*, *42*(10), 2039-2051. https://doi.org/10.1523/jneurosci.1907-21.2022

Tuthill, J. C., Nern, A., Holtz, S. L., Rubin, G. M., & Reiser, M. B. (2013). Contributions of the 12 neuron classes in the fly lamina to motion vision. *Neuron*, *79*(1), 128-140. https://doi.org/10.1016/j.neuron.2013.05.024

Valjent, E., & Gangarossa, G. (2021). The Tail of the Striatum: From Anatomy to Connectivity and Function. *Trends Neurosci*, *44*(3), 203-214. https://doi.org/10.1016/j.tins.2020.10.016

van der Plas, E., Schultz, J. L., & Nopoulos, P. C. (2020). The Neurodevelopmental Hypothesis of Huntington's Disease. *J Huntingtons Dis*, *9*(3), 217-229. https://doi.org/10.3233/jhd-200394

Van Pelt, K. M., & Truttmann, M. C. (2020). Caenorhabditis elegans as a model system for studying aging-associated neurodegenerative diseases. *Translational Medicine of Aging*, *4*, 60-72. https://doi.org/https://doi.org/10.1016/j.tma.2020.05.001

Vatsavayai, S. C., Dallérac, G. M., Milnerwood, A. J., Cummings, D. M., Rezaie, P., Murphy, K. P. S. J., & Hirst, M. C. (2007). Progressive CAG expansion in the brain of a novel R6/1-89Q mouse model of Huntington's disease with delayed phenotypic onset. *Brain Research Bulletin*, *72*(2), 98-102. https://doi.org/https://doi.org/10.1016/j.brainresbull.2006.10.015

Verheyen, E. M. (2022). The power of Drosophila in modeling human disease mechanisms. *Dis Model Mech*, *15*(3). https://doi.org/10.1242/dmm.049549

Vernes, S. C., MacDermot, K. D., Monaco, A. P., & Fisher, S. E. (2009). Assessing the impact of FOXP1 mutations on developmental verbal dyspraxia. *Eur J Hum Genet*, *17*(10), 1354-1358. https://doi.org/10.1038/ejhg.2009.43

Vernizzi, L., Paiardi, C., Licata, G., Vitali, T., Santarelli, S., Raneli, M., Manelli, V., Rizzetto, M., Gioria, M., Pasini, M. E., Grifoni, D., Vanoni, M. A., Gellera, C., Taroni, F., & Bellosta, P. (2020). Glutamine Synthetase 1 Increases Autophagy Lysosomal Degradation of Mutant Huntingtin Aggregates in Neurons, Ameliorating Motility in a Drosophila Model for Huntington's Disease. *Cells*, *9*(1). https://doi.org/10.3390/cells9010196

Verzi, M. P., Agarwal, P., Brown, C., McCulley, D. J., Schwarz, J. J., & Black, B. L. (2007). The transcription factor MEF2C is required for craniofacial development. *Dev Cell*, *12*(4), 645-652. https://doi.org/10.1016/j.devcel.2007.03.007

Vidal-Sancho, L., Fernández-García, S., Solés-Tarrés, I., Alberch, J., & Xifró, X. (2020). Decreased Myocyte Enhancer Factor 2 Levels in the Hippocampus of Huntington's Disease Mice Are Related to Cognitive Dysfunction. *Mol Neurobiol*, *57*(11), 4549-4562. https://doi.org/10.1007/s12035-020-02041-x

Vieweg, S., Mahul-Mellier, A.-L., Ruggeri, F. S., Riguet, N., DeGuire, S. M., Chiki, A., Cendrowska, U., Dietler, G., & Lashuel, H. A. (2021). The Nt17 Domain and its Helical Conformation Regulate the Aggregation, Cellular Properties and Neurotoxicity of Mutant Huntingtin Exon 1. *Journal of Molecular Biology*, *433*(21), 167222. https://doi.org/https://doi.org/10.1016/j.jmb.2021.167222

Vizcaíno, C., Mansilla, S., & Portugal, J. (2015). Sp1 transcription factor: A long-standing target in cancer chemotherapy. *Pharmacology & Therapeutics*, *152*, 111-124. https://doi.org/https://doi.org/10.1016/j.pharmthera.2015.05.008

von Hörsten, S., Schmitt, I., Nguyen, H. P., Holzmann, C., Schmidt, T., Walther, T., Bader, M., Pabst, R., Kobbe, P., Krotova, J., Stiller, D., Kask, A., Vaarmann, A., Rathke-Hartlieb, S., Schulz, J. B., Grasshoff, U., Bauer, I., Vieira-Saecker, A. M. M., Paul, M., . . . Riess, O. (2003). Transgenic rat model of Huntington's disease. *Human Molecular Genetics*, *12*(6), 617-624. https://doi.org/10.1093/hmg/ddg075

Vrečar, I., Innes, J., Jones, E. A., Kingston, H., Reardon, W., Kerr, B., Clayton-Smith, J., & Douzgou, S. (2017). Further Clinical Delineation of the MEF2C Haploinsufficiency Syndrome: Report on New Cases and Literature Review of Severe Neurodevelopmental Disorders Presenting with Seizures, Absent Speech, and Involuntary Movements. *J Pediatr Genet*, *6*(3), 129-141. https://doi.org/10.1055/s-0037-1601335

Wagner, L. A., Menalled, L., Goumeniouk, A. D., Brunner, D., & Leavitt, B. R. (2008). CHAPTER 6 - Huntington Disease. In R. A. McArthur & F. Borsini (Eds.), *Animal and Translational Models for CNS Drug Discovery* (pp. 207-266). Academic Press. https://doi.org/https://doi.org/10.1016/B978-0-12-373861-5.00018-7

Wang, B., Lin, D., Li, C., & Tucker, P. (2003). Multiple domains define the expression and regulatory properties of Foxp1 forkhead transcriptional repressors. *J Biol Chem*, *278*(27), 24259-24268. https://doi.org/10.1074/jbc.M207174200

Wang, B., Weidenfeld, J., Lu, M. M., Maika, S., Kuziel, W. A., Morrisey, E. E., & Tucker, P. W. (2004). Foxp1 regulates cardiac outflow tract, endocardial cushion morphogenesis and myocyte proliferation and maturation. *Development*, *131*(18), 4477-4487. https://doi.org/10.1242/dev.01287

Wang, H., Lim, P. J., Yin, C., Rieckher, M., Vogel, B. E., & Monteiro, M. J. (2006). Suppression of polyglutamine-induced toxicity in cell and animal models of Huntington's disease by ubiquilin. *Hum Mol Genet*, *15*(6), 1025-1041. https://doi.org/10.1093/hmg/ddl017

Wang, N., Lu, X. H., Sandoval, S. V., & Yang, X. W. (2013). An independent study of the preclinical efficacy of C2-8 in the R6/2 transgenic mouse model of Huntington's disease. *J Huntingtons Dis*, *2*(4), 443-451. https://doi.org/10.3233/jhd-130074

Wanker, E. E., Ast, A., Schindler, F., Trepte, P., & Schnoegl, S. (2019). The pathobiology of perturbed mutant huntingtin protein–protein interactions in Huntington's disease. *Journal of Neurochemistry*, *151*(4), 507-519. https://doi.org/https://doi.org/10.1111/jnc.14853

Wankhede, N. L., Kale, M. B., Upaganlawar, A. B., Taksande, B. G., Umekar, M. J., Behl, T., Abdellatif, A. A. H., Bhaskaran, P. M., Dachani, S. R., Sehgal, A., Singh, S., Sharma, N., Makeen, H. A., Albratty, M., Dailah, H. G., Bhatia, S., Al-Harrasi, A., & Bungau, S. (2022). Involvement of molecular chaperone in protein-misfolding brain diseases. *Biomedicine & Pharmacotherapy*, *147*, 112647. https://doi.org/https://doi.org/10.1016/j.biopha.2022.112647

Warrick, J. M., Chan, H. Y., Gray-Board, G. L., Chai, Y., Paulson, H. L., & Bonini, N. M. (1999). Suppression of polyglutamine-mediated neurodegeneration in Drosophila by the molecular chaperone HSP70. *Nat Genet*, *23*(4), 425-428. https://doi.org/10.1038/70532

Weiss, A. R., Liguore, W. A., Brandon, K., Wang, X., Liu, Z., Domire, J. S., Button, D., Srinivasan, S., Kroenke, C. D., & McBride, J. L. (2022). A novel rhesus macaque model of Huntington's disease recapitulates key neuropathological changes along with motor and cognitive decline. *eLife*, *11*, e77568. https://doi.org/10.7554/eLife.77568

West, A. E., & Greenberg, M. E. (2011). Neuronal activity-regulated gene transcription in synapse development and cognitive function. *Cold Spring Harb Perspect Biol*, *3*(6). https://doi.org/10.1101/cshperspect.a005744

Wexler, A., Wild, E. J., & Tabrizi, S. J. (2016). George Huntington: a legacy of inquiry, empathy and hope. *Brain*, *139*(Pt 8), 2326-2333. https://doi.org/10.1093/brain/aww165

Wexler, N. S., Lorimer, J., Porter, J., Gomez, F., Moskowitz, C., Shackell, E., Marder, K., Penchaszadeh, G., Roberts, S. A., Gayán, J., Brocklebank, D., Cherny, S. S., Cardon, L. R., Gray, J., Dlouhy, S. R., Wiktorski, S., Hodes, M. E., Conneally, P. M., Penney, J. B., . . . Landwehrmeyer, B. (2004). Venezuelan kindreds reveal that genetic and environmental factors modulate Huntington's disease age of onset. *Proc Natl Acad Sci U S A*, *101*(10), 3498-3503. https://doi.org/10.1073/pnas.0308679101

William Yang, X., & Gray, M. (2011). Frontiers in Neuroscience. Mouse Models for Validating Preclinical Candidates for Huntington's Disease. In D. C. Lo & R. E. Hughes (Eds.), *Neurobiology of Huntington's Disease: Applications to Drug Discovery*. CRC Press/Taylor & Francis, Copyright © 2011 by Taylor and Francis Group, LLC.

Williamson, W. R., & Hiesinger, P. R. (2010). Preparation of developing and adult Drosophila brains and retinae for live imaging. *J Vis Exp*(37). https://doi.org/10.3791/1936

Wong, J. H., Alfatah, M., Sin, M. F., Sim, H. M., Verma, C. S., Lane, D. P., & Arumugam, P. (2017). A yeast two-hybrid system for the screening and characterization of small-molecule inhibitors of protein–protein interactions identifies a novel putative Mdm2-binding site in p53. *BMC Biology*, *15*(1), 108. https://doi.org/10.1186/s12915-017-0446-7

Wu, W., de Folter, S., Shen, X., Zhang, W., & Tao, S. (2011). Vertebrate paralogous MEF2 genes: origin, conservation, and evolution. *PLOS ONE*, *6*(3), e17334. https://doi.org/10.1371/journal.pone.0017334

Wu, Y., Dey, R., Han, A., Jayathilaka, N., Philips, M., Ye, J., & Chen, L. (2010). Structure of the MADS-box/MEF2 domain of MEF2A bound to DNA and its implication for myocardin recruitment. *J Mol Biol*, *397*(2), 520-533. https://doi.org/10.1016/j.jmb.2010.01.067

Xiong, Y., Wang, L., Jiang, W., Pang, L., Liu, W., Li, A., Zhong, Y., Ou, W., Liu, B., & Liu, S.-m. (2019). MEF2A alters the proliferation, inflammation-related gene expression profiles and its silencing induces cellular senescence in human coronary endothelial cells. *BMC Molecular Biology*, *20*(1), 8. https://doi.org/10.1186/s12867-019-0125-z

Yagi, R., Mabuchi, Y., Mizunami, M., & Tanaka, N. K. (2016). Convergence of multimodal sensory pathways to the mushroom body calyx in Drosophila melanogaster. *Scientific Reports*, *6*(1), 29481. https://doi.org/10.1038/srep29481

Yang, J. S., Nam, H. J., Seo, M., Han, S. K., Choi, Y., Nam, H. G., Lee, S. J., & Kim, S. (2011). OASIS: online application for the survival analysis of lifespan assays performed in aging research. *PLOS ONE*, *6*(8), e23525. https://doi.org/10.1371/journal.pone.0023525

Yhnell, E., Dunnett, S. B., & Brooks, S. P. (2016). A Longitudinal Motor Characterisation of the HdhQ111 Mouse Model of Huntington's Disease. *J Huntingtons Dis*, *5*(2), 149-161. https://doi.org/10.3233/jhd-160191

You, H., Wu, T., Du, G., Huang, Y., Zeng, Y., Lin, L., Chen, D., Wu, C., Li, X., Burgunder, J. M., & Pei, Z. (2021). Evaluation of Blood Glial Fibrillary Acidic Protein as a Potential Marker in Huntington's Disease. *Front Neurol*, *12*, 779890. https://doi.org/10.3389/fneur.2021.779890

Yu, Y. T., Breitbart, R. E., Smoot, L. B., Lee, Y., Mahdavi, V., & Nadal-Ginard, B. (1992). Human myocyte-specific enhancer factor 2 comprises a group of tissue-restricted MADS box transcription factors. *Genes Dev*, *6*(9), 1783-1798. https://doi.org/10.1101/gad.6.9.1783

Yu-Taeger, L., Petrasch-Parwez, E., Osmand, A. P., Redensek, A., Metzger, S., Clemens, L. E., Park, L., Howland, D., Calaminus, C., Gu, X., Pichler, B., Yang, X. W., Riess, O., & Nguyen, H. P. (2012). A novel BACHD transgenic rat exhibits characteristic neuropathological features of Huntington disease. *J Neurosci*, *32*(44), 15426-15438. https://doi.org/10.1523/jneurosci.1148-12.2012

Zasadzińska, E., Barnhart-Dailey, M. C., Kuich, P. H. J. L., & Foltz, D. R. (2013). Dimerization of the CENP-A assembly factor HJURP is required for centromeric nucleosome deposition. *The EMBO Journal*, *32*(15), 2113-2124. https://doi.org/https://doi.org/10.1038/emboj.2013.142

Zhang, M., Zhu, B., & Davie, J. (2015). Alternative splicing of MEF2C pre-mRNA controls its activity in normal myogenesis and promotes tumorigenicity in rhabdomyosarcoma cells. *J Biol Chem*, *290*(1), 310-324. https://doi.org/10.1074/jbc.M114.606277

Zhang, S., Binari, R., Zhou, R., & Perrimon, N. (2010). A genomewide RNA interference screen for modifiers of aggregates formation by mutant Huntingtin in Drosophila. *Genetics*, *184*(4), 1165-1179. https://doi.org/10.1534/genetics.109.112516

Zhang, S., Feany, M. B., Saraswati, S., Littleton, J. T., & Perrimon, N. (2009). Inactivation of Drosophila Huntingtin affects long-term adult functioning and the pathogenesis of a Huntington's disease model. *Dis Model Mech*, *2*(5-6), 247-266. https://doi.org/10.1242/dmm.000653

Zhang, X., Wan, J. Q., & Tong, X. P. (2018). Potassium channel dysfunction in neurons and astrocytes in Huntington's disease. *CNS Neurosci Ther*, *24*(4), 311-318. https://doi.org/10.1111/cns.12804

Zhang, Z., & Zhao, Y. (2022). Progress on the roles of MEF2C in neuropsychiatric diseases. *Molecular Brain*, *15*(1), 8. https://doi.org/10.1186/s13041-021-00892-6

Zhao, C. (2023). Cell culture: in vitro model system and a promising path to in vivo applications. *Journal of Histotechnology*, *46*(1), 1-4. https://doi.org/10.1080/01478885.2023.2170772

Zheng, L., de Polavieja, G. G., Wolfram, V., Asyali, M. H., Hardie, R. C., & Juusola, M. (2006). Feedback network controls photoreceptor output at the layer of first visual synapses in Drosophila. *J Gen Physiol*, *127*(5), 495-510. https://doi.org/10.1085/jgp.200509470

Zheng, Z., & Diamond, M. I. (2012). Chapter 6 - Huntington Disease and the Huntingtin Protein. In D. B. Teplow (Ed.), *Progress in Molecular Biology and Translational Science* (Vol. 107, pp. 189-214). Academic Press. https://doi.org/https://doi.org/10.1016/B978-0-12-385883-2.00010-2

Zheng, Z., & Diamond, M. I. (2012). Huntington disease and the huntingtin protein. *Prog Mol Biol Transl Sci*, *107*, 189-214. https://doi.org/10.1016/b978-0-12-385883-2.00010-2

Zhou, W. Z., Zhang, J., Li, Z., Lin, X., Li, J., Wang, S., Yang, C., Wu, Q., Ye, A. Y., Wang, M., Wang, D., Pu, T. Z., Wu, Y. Y., & Wei, L. (2019). Targeted resequencing of 358 candidate genes for autism spectrum disorder in a Chinese cohort reveals diagnostic potential and genotype-phenotype correlations. *Hum Mutat*, *40*(6), 801-815. https://doi.org/10.1002/humu.23724

Zhou, X., Feliciano, P., Shu, C., Wang, T., Astrovskaya, I., Hall, J. B., Obiajulu, J. U., Wright, J. R., Murali, S. C., Xu, S. X., Brueggeman, L., Thomas, T. R., Marchenko, O., Fleisch, C., Barns, S. D., Snyder, L. G., Han, B., Chang, T. S., Turner, T. N., . . . Chung, W. K. (2022). Integrating de novo and inherited variants in 42,607 autism cases identifies mutations in new moderate-risk genes. *Nat Genet*, *54*(9), 1305-1319. https://doi.org/10.1038/s41588-022-01148-2

Zhu, B., Ramachandran, B., & Gulick, T. (2005). Alternative pre-mRNA splicing governs expression of a conserved acidic transactivation domain in myocyte enhancer factor 2 factors of striated muscle and brain. *J Biol Chem*, *280*(31), 28749-28760. https://doi.org/10.1074/jbc.M502491200

Zuccato, C., Ciammola, A., Rigamonti, D., Leavitt, B. R., Goffredo, D., Conti, L., MacDonald, M. E., Friedlander, R. M., Silani, V., Hayden, M. R., Timmusk, T., Sipione, S., & Cattaneo, E. (2001). Loss of huntingtin-mediated BDNF gene transcription in Huntington's disease. *Science*, *293*(5529), 493-498. https://doi.org/10.1126/science.1059581

Zuccato, C., Marullo, M., Conforti, P., MacDonald, M. E., Tartari, M., & Cattaneo, E. (2008). Systematic assessment of BDNF and its receptor levels in human cortices affected by Huntington's disease. *Brain Pathol*, *18*(2), 225-238. https://doi.org/10.1111/j.1750-3639.2007.00111.x